CALIFORNIA INSTITUTE OF TECHNOLOGY

EARTHQUAKE ENGINEERING RESEARCH LABORATORY
Center for Research on the Prevention of Natural Disasters

DYNAMIC SOIL–STRUCTURE INTERACTION

Hung Leung Wong

EERL 75-01

A Report on Research Conducted under Grants
from the National Science Foundation

Pasadena, California
May 23, 1975

DYNAMIC SOIL-STRUCTURE INTERACTION

Thesis by

Hung Leung Wong

In Partial Fulfillment of the Requirements

for the Degree of

Doctor of Philosophy

California Institute of Technology

Pasadena, California

1975

(Submitted May 23, 1975)

ACKNOWLEDGMENTS

The author wishes to sincerely thank Professor M. D. Trifunac for his guidance and encouragement. He is grateful to his Advisor, P. C. Jennings, and Dr. J. E. Luco for their conscientious support and constructive criticism.

The author expresses gratitude to Ms. Sharon Vedrode for her expert typing and artistic decoration of this manuscript. Also, the polishing of the text made by his fiance', Erna Hsieh, requires special acknowledgment.

Financial aid received from the California Institute of Technology and the National Science Foundation during the tenure of the author's graduate study is greatly appreciated. The partial support of this investigation by the U. S. Geological Survey is also acknowledged.

Finally, to the prime motivators of his work, the author dedicates this dissertation to his parents.

ABSTRACT

The dynamic response of a structure placed on a deformable soil medium subjected to seismic excitation is studied. The basic phenomena of soil-structure interaction was investigated by several analytical models supplemented by experimental observations; a brief review of literature in this discipline is also included.

Among the physical phenomena investigated: the effects caused by local topography, the interaction with other structures, and the dissipation of dynamic energy through the soil medium were described by exact series solutions. Foundations of arbitrary shape, however, were modeled by using an approximate integral representation. This latter method utilizes the principle of superposition and provides flexibility in analyzing numerically the three-dimensional disc foundations placed on the soil surface. The results indicate that the detailed description for the shape of a rigid foundation placed on a deformable soil medium is not essential in the overall response of the superstructure, but the stress distribution under the disc foundation is quite sensitive to these changes in detail.

In this thesis, several methods for the calculation of foundation compliances for several types of foundation models were discussed, some of which have direct practical applications. The importance of the base input motion induced by incident seismic waves is also stressed, because the seismic input, along with the foundation compliances, are necessary for a complete analysis of this problem.

TABLE OF CONTENTS

TABLE OF CONTENTS (CONT.)

TABLE OF CONTENTS (CONT.)

CHAPTER I - INTRODUCTION

[1-1] GENERAL INTRODUCTION

The dynamic response of foundations placed on top of a semi-infinite medium is of considerable interest in the fields of applied mechanics, wave propagation, and in the design of machine bases. In earthquake engineering, when the soil medium is relatively soft, the dynamic interaction between the superstructure, its foundation, and the soil medium may become important.

During the shaking of an earthquake, seismic waves are transmitted through the soil from the fault rupture to a structure of interest. The wave motion of the soil excites the structure which in turn modifies the input motion by its movement relative to the ground. These interaction phenomena will be called "soil-foundation-superstructure interaction," or simply "soil-structure interaction."

Depending on the material properties of the soil medium, the source of dynamic excitation, and the particular type of foundation considered, the response of the structural system can be quite different from the case where the supporting system is rigid. This interaction effect may be especially significant in the frequency band near the resonant frequencies of the superstructure because the soft foundation can provide the means for energy absorption. Because of this, the interaction is generally considered to be favorable in earthquake engineering design.

In spite of its advantages, however, soil-structure interaction has also contributed additional complications to the analysis. It is characterized by many complex wave propagation phenomena that are otherwise omitted from the analysis. These phenomena may be briefly summarized as follows:

(1) The influences of non-vertically incident seismic waves. Complicated coupling phenomena may occur for non-vertically incident body waves or for surface waves, since those tend to cause rotation as well as translation. This rotation component is automatically neglected while studying translation if the base is assumed to be rigid.

(2) The overall dissipation of dynamic energy from the superstructure is quite important for characterizing its response. In the case when interaction is not neglected, the semi-infinite soil medium acts as a sink because the energy is dissipated by geometrical spreading of waves.

(3) The geometrical shape and the rigidity of the superstructure and its foundation can be important. For example, torsional vibration may be induced by horizontal excitation if the structure is not symmetrical.

(4) The influence of surrounding buildings may also be significant. The vibration of the nearby foundations can be thought of as additional wave sources. Therefore, in densely constructed metropolitan areas, motion of a particular foundation may be amplified or attenuated by the existence of neighboring structures. This

effect may be more dominant when the nearby structures are larger and heavier than the one considered.

(5) A flexible support may allow larger relative movements between the heavier structural frames which can cause higher localized stresses.

The objective of this study is to investigate and to analyze some of the phenomena mentioned above. To initiate this work with a "well-controlled" analysis, several simple two-dimensional models will be investigated. These models can be analyzed by exact series solutions; therefore, the dynamic characteristics of the interacting system can be considered in terms of just a few key parameters.

Using these two-dimensional models, the effect of embedment, shape of foundation, incident seismic waves, and interaction with other structures may be studied in detail. Also, simplified cases concerning the effect of soil damping and the local topography will be studied. Following this, the phenomena occurring in three dimensions will be discussed by using an approximate method which is based on the principle of superposition. This method can be applied to some realistic foundation models with the restriction that the foundation is flat. Nevertheless, such results seem to be of practical value. Finally, this three-dimensional theory will be used to interpret data gathered experimentally on the vibrations of a full-scale structure.

[1-2] THE STATE-OF-THE-ART IN SOIL-STRUCTURE INTERACTION

Since the paper by Sezawa and Kanai[A1] in 1935, numerous reports have been presented in the field of soil-structure interaction, most of which were published recently. A comprehensive bibliography is compiled in Appendix A on the subject of soil-structure interaction. The publications are ordered by the year in which they were published. The abbreviation for references cited in the text consists of a number following the letter A. These should not be confused with the general references, however, which are referred to by their authors' names followed by the year of publication in parentheses.

The present situation in soil-structure interaction research is that enough work, both theoretical and experimental, has been presented to allow a modest understanding of most engineering problems. However, as the number of high rise buildings and nuclear power plants increase, there still appears to exist a demand for more sophisticated methods of analysis and carefully controlled experiments.

Presently, there are mainly two methods for solving the interaction problem: The Finite Element Method and the Continuum Approach, Hadjian, et al. (1974). The Finite Element Method[A105] makes use of the variational principle to obtain an approximate solution to a particular governing equation and the prescribed boundary conditions. Since each particular model may be divided into many smaller elements, the geometrical configuration of the model does not present major difficulties. This method is

therefore capable of solving a large class of practical problems. The continuum approach, on the other hand, models the soil medium as a semi-infinite or layered half space, and the soil properties are limited to those of elastic or viscoelastic materials. The solutions obtained by the continuum approach are usually more direct and they can represent the real problem by the minimum number of pertinent parameters. The limitations of this approach, however, are caused by the limited number of geometrical configurations for which exact solutions of the elasto-dynamic equations can be obtained.

Ideally, if the two methods described above are formulated correctly, the solution obtained by either of these methods should yield similar results. However, recent comparisons show conflicting results.[A62, A79] In this section, a brief review of the literature for both methods will be made, and some of their advantages and disadvantages will be discussed.

Using the continuum approach, the model representing the system must be simplified somewhat from the viewpoint of geometrical shapes, whereas the material properties are presently limited to the elastic and viscoelastic materials. As will be shown in Section [2-1], the soil-structure interaction problem can be separated into three parts so that the compliance functions and the "driving forces" caused by seismic waves can be obtained independently. While the latter has only been studied briefly,[A52, A74] the impedance functions, or their reciprocals, the compliance functions, are available for a variety of foundation shapes and soil models.

The foundation shapes which are compatible with the cartesian or polar coordinates attracted several investigators. The infinitely long rigid strip foundation was investigated by Karasudhi, Keer, and Lee,[A157] Oien,[A159] and Luco and Westmann.[A160] The above authors considered the in-plane vertical, horizontal, and rocking motions. Hradilek[A156] presented a solution for the anti-plane motion. For the rigid circular disc foundation on an elastic half space, many pertinent results are available. Shah[A125] investigated the vertical resistance, while Luco and Westmann[A129] and Veletsos and Wei[A130, A131] investigated the horizontal and rocking motions by using the "relaxed" boundary conditions for which some of the boundary conditions are ignored. Bielak[A134] extended the solution for a rigid disc by solving the problem with "welded contact" in which all boundary conditions of the disc surface were satisfied. Later, Veletsos and Verbic[A145] extended the above solutions to include soil damping, and Luco[A142] investigated the effects caused by the reflections from a layer over an elastic half space. Other contributions made to the layered model were by Bycroft,[A135] Warburton,[A136] Kashio,[A139] and Wei.[A140]

Another simple foundation shape of much practical interest is the rectangle. Although it matches perfectly the cartesian coordinate system, no exact solutions for the rigid foundation are currently available. Kobori et al.[A162, A164, A167] and Sarrazin[A166] obtained the compliances for the rectangular foundation by assuming a stress distribution over the rectangular area and used the displacement at

the center as the foundation deflection. The result from the above assumption is a non-rigid foundation; the compliance is of a different nature from the one for a rigid foundation, especially when the width to length ratio is far from 1. Elorduy, Nieto, and Szekely[A163] used a point load influence surface formulation where the unknown traction at the foundation surface is obtained by applying the compatibility conditions to the displacements. This method can be applied to foundations with arbitrary shapes as well, but it encounters numerical difficulties because of the singularity directly under the point load.

The above summary deals only with flat foundations. A very limited amount of work, however, is available for embedded foundations because of the difficulty in mathematical solutions. Based on the simplifying assumption initiated by Baranov,[A177] Novak et al.[A182, A181, A183] obtained approximate results for various embedded foundation models. Earlier, Tajimi[A184] had suggested a foundation model in a single layer of soil. Although many two-dimensional foundation models are also available [Luco,[A168] Thau and Umek,[A171] Wong and Trifunac[A172]], the analysis for an embedded foundation using the continuum approach is still in its infancy.

Embedded foundations can be modeled by several types of finite elements: the three-dimensional elements,[A109] the axisymmetric elements,[A107] and, the most common, the two-dimensional plane strain elements.[A105] An advantage of the finite element analysis here is that some non-linearities and other types of

material behavior can also be included. These programs can readily pick up the details of the foundation shape.

Unfortunately, at this time the finite element method may not represent as powerful a tool as it is for most other dynamic analyses. For example, so far this approach does not provide the needed capability to model a soil medium adequately, because of its large dimensions and the limited storage space of the presently available computers. The consequence of this restriction is that a finite medium must be used, and, hence, some form of a reflection from the "artificial boundaries" is included. In a few studies, "quiet" or "transparent" boundaries have been incorporated.(A106, A110) To simulate the "radiation" damping, material damping is often introduced in the soil medium to dissipate some of the energy reflected from the outer boundaries. Hadjian, Luco, and Bos(A79) made a series of comparisons to indicate the marked differences between the two types of damping. A similar discussion on the same subject is also presented in Section [3.6] of this thesis.

Another difficulty encountered by the finite element method is the description of the incident waves. In most available solutions, the excitation is applied through the shaking of the "artificial" boundary which is totally in phase.(A111)

At the present time, the author feels that it is preferable to treat the soil-structure interaction problem by the continuum approach until the finite element methods reach the point where a large soil medium can be represented accurately.

[1-3] ORGANIZATION

The soil-structure interaction models studied in this thesis are within the framework of linear elasto-dynamic theory. From the organizational viewpoint, this thesis consists of four parts:

(1) In the first part, the linear soil-foundation superstructure interaction problem is first separated into three simpler problems, then the final results are obtained by superposition. These three problems deal with (i) the resistance of the soil on the foundation, (ii) the forces transmitted to the foundation from the given seismic excitation, and (iii) the forces and moments exerted on the foundation by the superstructure.

(2) In the second part, two-dimensional problems in soil-structure interaction are considered. Using the method of images, several exact solutions have been obtained by using the separation of variables approach. The effect of foundation embedment, interaction of many structures, and the effect of local topography have been studied for the simplified two-dimensional models. In addition, the effect of foundation shape has also been studied using an approximate method derived for solving the Weber's integral equation for two-dimensional scalar wave scattering. The purpose of of this part is to illustrate several important physical phenomena in the framework of simple analytical formulations. Though some of the results are not directly applicable to practical design problems, they can improve our understanding for these complicated phenomena in two dimensions. No doubt, some of these characteristics have an anology in three dimensions.

(3) The third part is devoted to the development and discussion of an approximate method using the superposition of influence functions. This method is capable of modeling three-dimensional flat foundations of arbitrary shape and flexibility.

(4) In the last part of this thesis, the method described in part (3) is used to interpret experimental data from full-scale testing of the Millikan Library at the California Institute of Technology. An investigation on the effect of flexible foundations has also been presented for the same experimental data.

CHAPTER II - SOIL-FOUNDATION-SUPERSTRUCTURE INTERACTION

[2-1] A GENERAL FORMULATION

The harmonic analysis of the soil-rigid foundation-superstructure problem can be separated into three parts. The first two parts involve only the interaction between the soil medium and the foundation, i.e., the motion of a rigid-massless foundation, while the third part considers the dynamics of the superstructure.

The analysis of the superstructure is usually considered to be easily solved by the finite element method or other numerical methods. There are also numerous reports describing the computational as well as experimental determinations of the dynamic response of typical structures. Thus, the problem in soil-structure interaction when using the continuum approach is practically reduced to the determination of the steady state motion of a rigid massless foundation subjected to the action of seismic waves and external forces. This procedure has the advantage that, once the solutions of the first two steps are obtained for a class of foundations, the results can be used to calculate the interaction response for a large variety of superstructures. This approach is, of course, applicable to linear problems only.

The motion of a rigid foundation may be described by defining six coordinates if the displacements remain small. These coordinates include two orthogonal horizontal translations, a vertical translation, two rotations about two mutually perpendicular horizontal axes, and a torsional rotation about the vertical axis.

Using the principle of superposition, the generalized displacement $\underline{u}\, e^{i\omega t}$ of the rigid foundation may be represented as

$$\underline{u} = \underline{u}^* + \underline{u}_o \tag{2-1.1}$$

where $\underline{u}^* e^{i\omega t}$ corresponds to the six components of translation and rotation of the rigid foundation under the action of seismic waves and in absence of external forces, while $\underline{u}_o e^{i\omega t}$ corresponds to the six components in which the foundation is under action of the external force without seismic excitations. In this thesis, the displacements $\underline{u}^*$ and $\underline{u}_o$ will be designated as "foundation input motion" and "relative displacement," respectively.

The relative displacement $\underline{u}_o e^{i\omega t}$ generated by the interaction forces $\underline{F}_s e^{i\omega t}$ that the foundation exerts on the ground may be expressed by means of the following linear relationship

$$\underline{u}_o = [C_s]\underline{F}_s \tag{2-1.2}$$

where $[C_s]$ is the compliance matrix for the rigid foundation. Conversely, the interaction forces may be expressed in terms of the relative displacement by

$$\underline{F}_s = [K_s]\underline{u}_o \tag{2-1.3}$$

where $[K_s] = [C_s]^{-1}$ is the impedance matrix for the rigid foundation.

The complex impedance and compliance matrices which describe the force-displacement relationship between the foundation and soil medium depend mainly on the frequency of harmonic

excitation, the material property of the soil medium, and the shape of the foundation. Physically, the impedance functions for a rigid foundation can be viewed as

$$[K_s] = [k_s] + i\omega[c_s] \qquad (2\text{-}1.4)$$

where $[k_s]$ and $[c_s]$ are real, frequency dependent matrices which represent the stiffness and damping contribution to $[K_s]$, respectively.

If the soil medium is assumed to be elastic, then no energy dissipating mechanism exists in the material itself. Therefore, the dissipating term of the impedance matrix arises solely from the radiation of wave energy into the half space. This damping term usually dominates the stiffness term in the high frequency range. The behavior of $[K_s]$ becomes more complicated if the underlying soil medium is layered, because a significant part of the radiated energy may be trapped in the "low-velocity" layers and scattered back towards the foundation.

Since the impedance matrix $[K_s]$ represents a force-displacement relationship for the rigid foundation and the soil medium, the "driving force," $\underline{F_s}^*$, of the seismic waves can be introduced as

$$\underline{F_s}^* = [K_s]\underline{u}^* \ . \qquad (2\text{-}1.5)$$

With the input motion $\underline{u}^*$ measured relative to an inertial frame, the "driving force," $\underline{F_s}^*$, corresponds to the forces caused by the seismic excitation while the foundation is kept fixed.

Using equation (2-1.2) and the inverse of (2-1.5), the displacement $\underline{u}$ of equation (2-1.1) can be expressed as

$$\underline{u} = [C_s]\underline{F_s} + [C_s]\underline{F_s^*} \ . \qquad (2\text{-}1.6)$$

Therefore, to solve the problem of the dynamic response of rigid foundations, it is possible to separate the problem in two parts: the first part corresponding to the determination of the restraining force, or, equivalently, the determination of the compliance (impedance) matrices; the second part being the evaluation of the driving forces F_s^*.

In the past, the case most commonly studied has been that of the vertically incident S-wave of a unit amplitude. The amplitude of the free-field motion at every point on the surface is then equal to two. In that case, no scattering occurs for a flat foundation, the "base input motion" is just two, and the driving forces $\underline{F_s^*}$ are equal to two times the impedance functions which are given by equation (2-1.5).

For non-vertically incident waves, the free-field motion is no longer constant everywhere on the free surface and, hence, wave scattering will occur. This effect becomes especially important when the incident wave's wavelength is comparable to the characteristic dimension of the foundation. Also, for embedded foundations, the "free-field" motion below the ground surface must also be taken into account. In that case, the scattering will occur even for vertically incident waves.

In previous research work dealing with soil-structure interaction, most of the effort has been devoted to the determination of the compliance matrix. On the other hand, the evaluation of driving forces has been neglected by most authors. It should be noted here that the driving forces are equally important because they contain the characteristics of the incident waves.

[2-2] SUPERPOSITION OF RESULTS

The principal unknown of the soil-foundation-superstructure interaction problem is the motion of the foundation. This motion is excited by seismic waves and the external forces exerted on the foundation by the superstructure. Resistance to this motion is offered by the soil and the inertia forces of the foundation. Once the displacement of the foundation is determined, all other quantities, such as the stress and deformation of the superstructure, can be obtained. If more than one structure is present, the scattered wave pattern outside the foundation must also be determined.

Next, one can derive the equations of motion for the foundation by using Newton's Law. First of all, the steady state motion of the foundation, $\underline{u}\, e^{i\omega t}$, can be expressed as the superposition of the "base input motion" $\underline{u}^*$ and the "relative motion" $\underline{u}_o$,

$$\underline{u} = \underline{u}^* + \underline{u}_o \,. \tag{2-2.1}$$

The relative displacements and rotations, $\underline{u}_o\, e^{i\omega t}$, are caused by forces and moments exerted on the foundation by the superstructure.

Multiplying equation (2-2.1) by the impedance matrix, using the relations (2-1.3) and (2-1.5),

$$[K_s]\,\underline{u} = \underline{F_s} + \underline{F_s}^* \tag{2-2.2}$$

in which $-\underline{F_s}$ is the total force that the ground exerts on the foundation, and knowing the mass matrix $[M_o]$ of the foundation, we can write the force balance equation as

$$[M_o]\frac{d^2}{dt^2}(\underline{u}e^{i\omega t}) = -\underline{F_s}e^{i\omega t} + \underline{F_e}e^{i\omega t} . \qquad (2\text{-}2.3)$$

Here, $\underline{F_e}e^{i\omega t}$ is the external force acting on the foundation and is caused by the superstructure.

Substituting (2-2.2) into (2-2.3) and using the definition (2-1.3), equation (2-2.3) becomes

$$\{-\omega^2[M_o] + i\omega[c_s] + [k_s]\}\underline{u} = \underline{F_s}^* + \underline{F_e} . \qquad (2\text{-}2.4)$$

Equation (2-2.4) corresponds to a general linear system which has frequency dependent damping and stiffness matrices. By manipulating (2-2.4), an equation for the relative motion can be written as

$$\{-\omega^2[M_o] + i\omega[c_s] + [k_s]\}\underline{u_o} = \omega^2[M_o]\underline{u}^* + \underline{F_e} . \qquad (2\text{-}2.5)$$

In both equations (2-2.4) and (2-2.5), the unknowns $\underline{u}$ or $\underline{u_o}$ can easily be calculated if the results for the three parts of the problem as described earlier are available.

The above procedure appears to be quite useful because it enables us to concentrate on a small segment of a problem and to use the available data from previous analyses. This approach can increase the efficiency of the analysis and avoid costly duplication of the available results.

CHAPTER III - LONG FOUNDATIONS SUBJECTED TO SH-WAVE EXCITATION

[3-1] THE APPLICATION OF THE METHOD OF IMAGES

Except for a limited amount of work done using the continuum approach,[A177, A182, A183] the analyses of embedded foundations are usually done by finite element computer codes. The finite element method gives only an approximate solution and its accuracy may depend greatly on the number and size of elements, as well as on the assumed displacement or stress variation in each element itself. Due to the approximate nature of this approach, the finite element solutions should be tested first by a comparison with a simple exact solution so that more complicated problems may be analyzed with confidence.

Unfortunately, exact solutions for wave scattering in the elastic half space are scarce. To obtain an exact solution of the wave equation with more than one space dimension, the physical boundary may have to coincide with one of the constant coordinate lines. For example, wave scattering from a sphere in an infinite elastic space will require the boundary conditions to be satisfied on the radial coordinate, $r = a$, the radius of the sphere. This procedure can be carried out methodically without difficulties. However, when the scattering of a semi-spherical body embedded in an elastic half space is considered, the boundary conditions must be matched using both radial and angular coordinates. Here, the radial coordinate is held constant to match the boundary condition at the spherical surface, while the two angular coordinates are held

constant for the free surface condition at the half space boundary. This procedure usually cannot be carried out effectively.

A simple idea of the method of images allows some cases of the two-dimensional half space problem to be solved. However, this method is presently limited only to the SH-wave problem because just one space derivative is required to satisfy stress compatibility conditions. For the in-plane SV- and P-wave motions, the second space derivatives of the potentials are also required.

To apply the method of image to the z-component of the displacement, w, consider the scattering object or foundation shown in Figure 3-1.1a. The wave motion located outside this object consists of incident waves and scattered waves. Now, if one chooses the object to be symmetrical about the x-axis and imposes an image of the incident wave about the same x-axis, then the condition $\frac{\partial w}{\partial y} = 0$ holds at y = 0 because of symmetry. Physically, this image wave is actually the reflected wave from the free surface. In linear elasticity, $\tau_{yz} = \mu_s \frac{\partial w}{\partial y}\Big|_{y=0}$ corresponds to the shear stress at the surface where y = 0; hence, the problem represented in Figure 3-1.1a is equivalent to that in Figure 3-1.1b. Of course, the scattered wave from the foundation must also be symmetrical about the x-axis.

In the following sections, several problems in foundation dynamics are solved exactly using this idea. As will be shown, certain aspects of soil-structure interaction can be understood and explained by using this approach.

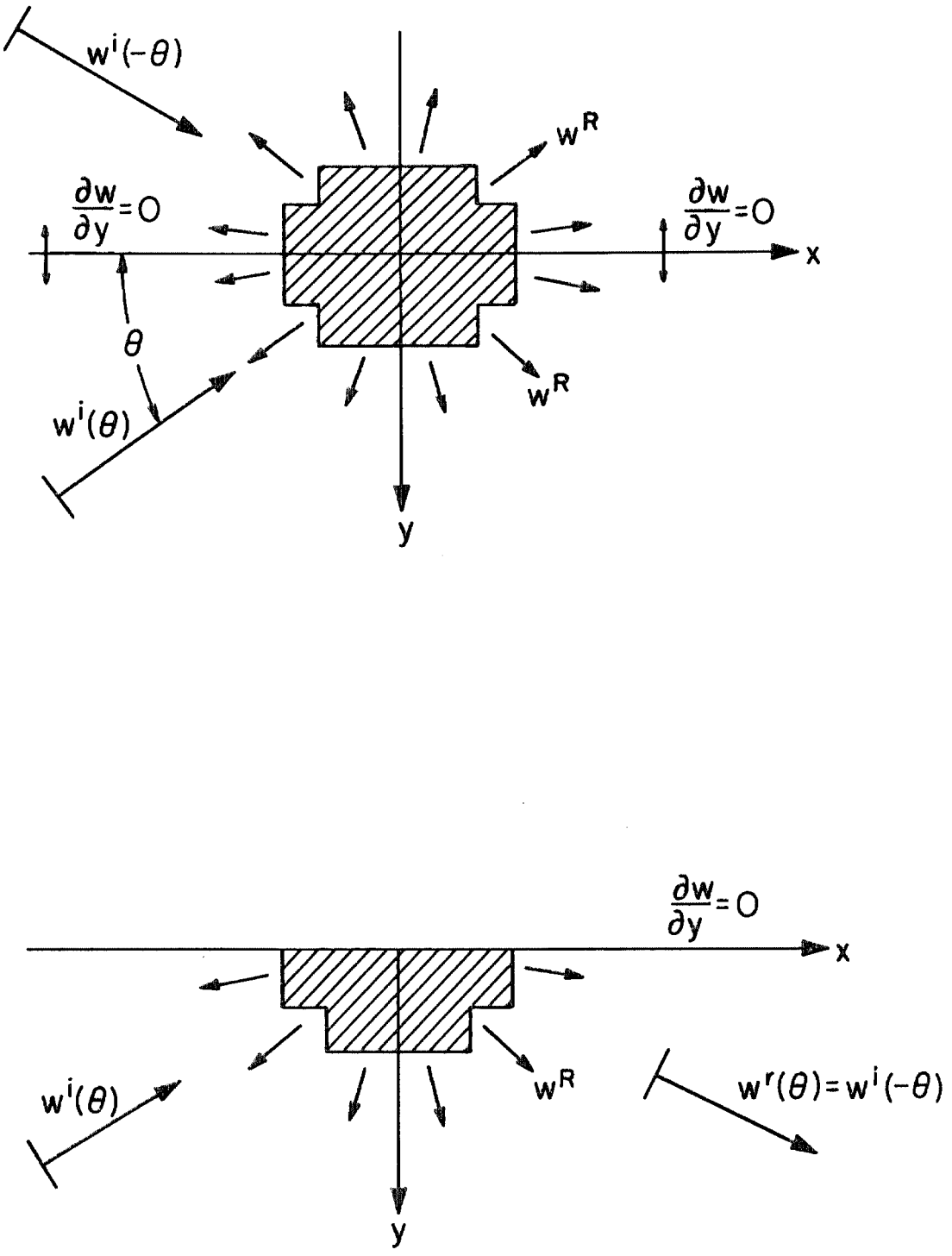

Figure 3-1.1 Symmetrical formulation of the image problem.

[3-2] THE EFFECT OF EMBEDMENT ON FOUNDATION RESPONSE

Even though the symmetry argument for the SH-wave problem allows us to obtain some simple solutions in the half space, there are only a few simple coordinate systems that allow an exact solution for the scalar wave equation. In two dimensions, the wave equation is separable in the cartesian, polar, elliptical, and parabolic coordinates, and infinite series solutions are possible. The cartesian coordinates perhaps best fit the shape of most common foundations, but the exterior wave scattering problem for a rectangular foundation is not yet solved because difficulties arise when the boundary condition has to be posed at both x and y coordinates.

Using polar coordinates, Luco(A168) investigated the semi-circular cylindrical foundation excited by a vertically incident S-wave. Trifunac(A169) generalized the results to include SH-waves with an arbitrary angle of incidence. Because a circle is symmetrical about its origin, it was found that the angle of incidence has no effect on the response of the foundation.

The disadvantage of the semi-circular foundation model from the point of view of analysis is that the embedment ratio of the foundation cannot be varied. The semi-elliptical shape of the foundation, on the other hand, has both the semi-circular and strip foundation(A156) as its limiting cases. The embedment ratio can be changed easily by varying the focal length of the ellipse.

Because a great deal of literature is available on the subject of an elliptical scatterer, it is not difficult to formulate the

SH-wave problem in the elliptical coordinates. In Mow and Pao (1971), the elliptical coordinates are defined as

$$\begin{aligned} x &= a \cosh\xi \cos\eta \qquad 0 \le \xi < \infty \\ y &= a \sinh\xi \sin\eta \qquad 0 \le \eta \le 2\pi \end{aligned} \tag{3-2.1}$$

where a is the focal length of the ellipse, while η and ξ are the angular and radial coordinates, respectively. Using the above coordinates, the integral solution of the two-dimensional scalar wave equation degenerates into an infinite series of Mathieu and Modified Mathieu functions. Though they are tedious to calculate, the general method to generate them is quite well developed (Abramowitz and Stegun, 1970).

To apply this two-dimensional wave solution to soil-structure interaction, the rigid foundation is assumed to be infinitely long and embedded in an elastic half space, Figure 3-2.1. The width and depth of the elliptical cross section are b and h, respectively. Because SH-wave is being studied, only the longitudinal component of the generalized vectors $\underline{u}$ and $\underline{F_s}$ of (2-1.1) are non-zero. Because of this simplification, the longitudinal element of the impedance matrix is independent from all other components.

To calculate the value of the impedance function K_s, the radiating wave w^R from the elliptical foundation was expanded into a generalized Fourier series of orthogonal Mathieu functions. The unknown coefficients in the expansion were then determined by the compatibility of displacements at the foundation surface,

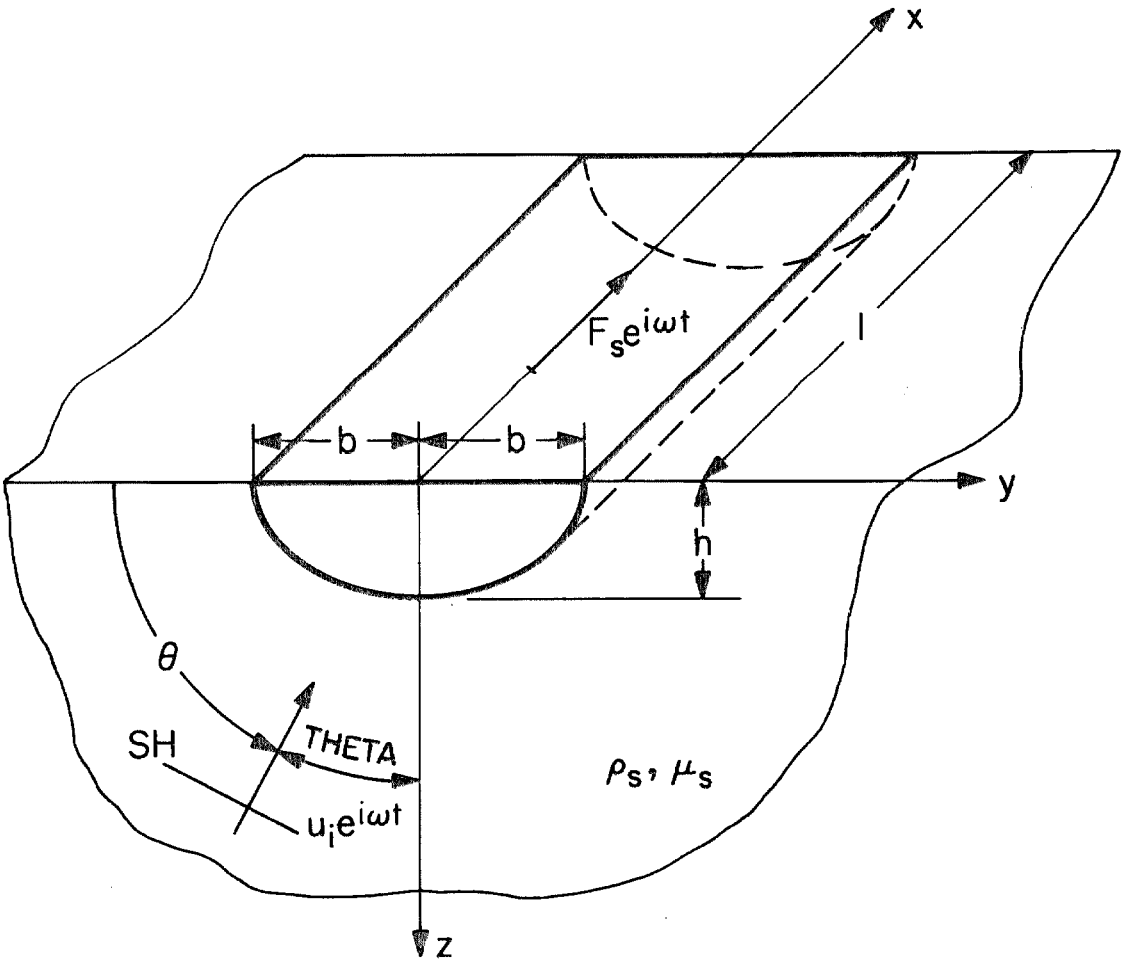

$$F_s = (K_s \Delta - F_s^*)$$

(Massless foundation)

Figure 3-2.1 Elliptical foundation model

$$w^R\Big|_{\xi=\xi_o} = 1\, e^{i\omega t} \; ; \qquad 0 \le \eta \le 2\pi \tag{3-2.2}$$

where ξ_o is the radial coordinate that matches the perimeter of the foundation.

While the foundation is subjected to a unit excitation, the surface boundary condition for the half space is automatically satisfied by symmetry if only even Mathieu functions are used. Therefore, the forces resisting the foundation can be obtained by integrating the shear stress $\sigma_{\xi z}$ over the surface area. For a unit displacement excitation, this force is the impedance function

$$K_s = -\int_s \sigma^R_{\xi z}\Big|_{\xi=\xi_o} ds = -\mu \int_{-\pi}^{\circ} \frac{\partial w^R}{\partial \xi}\Big|_{\xi=\xi_o} d\eta \; . \tag{3-2.3}$$

Further details of this derivation can be found in Wong and Trifunac.(A172)

The equivalent stiffness and damping coefficients associated with the real and imaginary parts of K_s are shown in Figure 3-2.2 for different embedment ratios h/b and for dimensionless frequencies $a_o = \omega b/\beta_s$ in the range from 0 to 4. These results indicate that both the equivalent stiffness and damping coefficients are fairly constant for values of the dimensionless frequency larger than 0.5. For low frequencies, the stiffness coefficient increases with the embedment ratio; for high frequencies, however, the value of the stiffness coefficient lies between the values corresponding to a strip foundation(A156) (h/b = 0) and a semi-circular foundation(A168, A169) (h/b = 1). This result is in agreement with the finding of Thau and

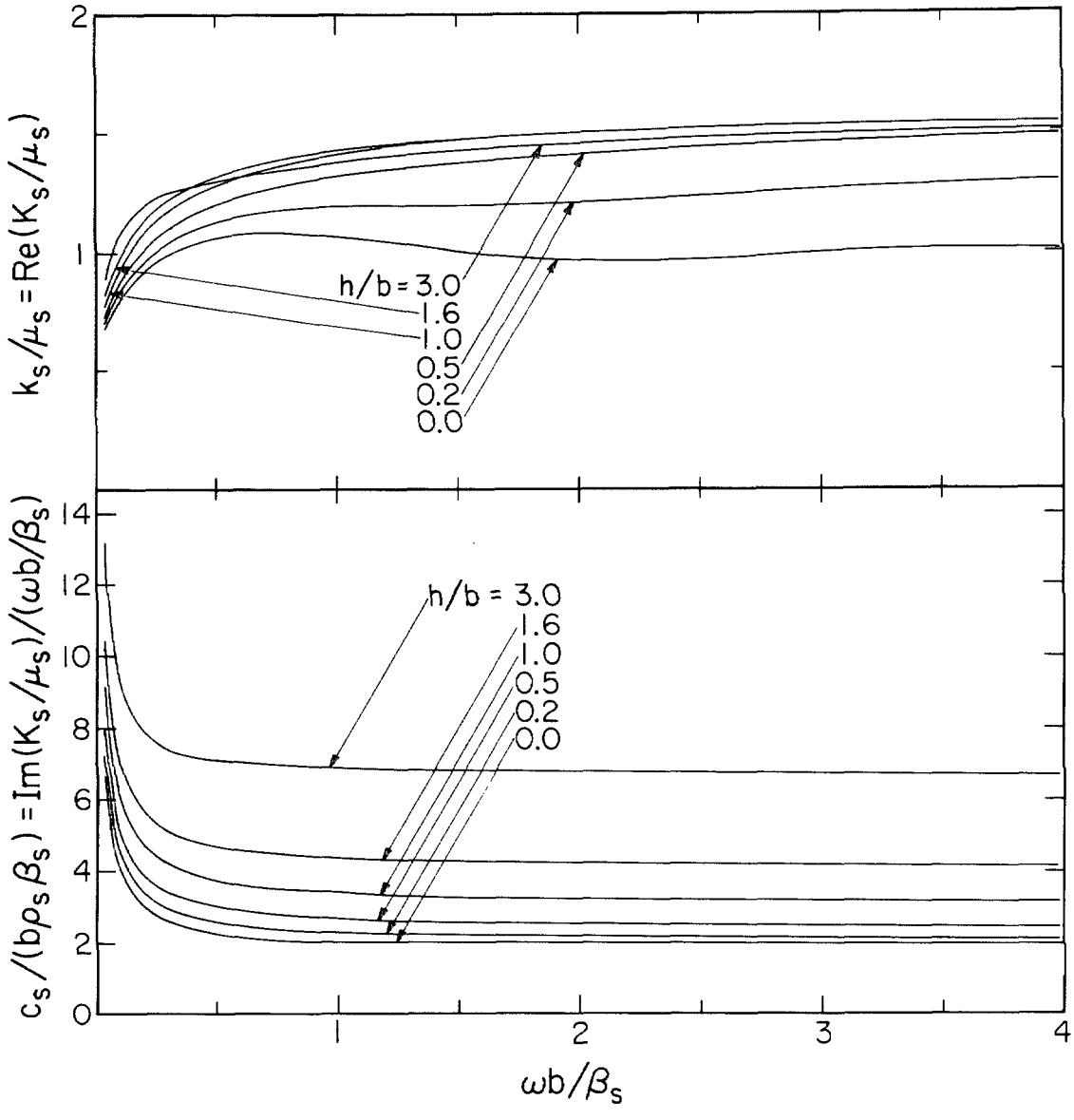

Figure 3-2.2 Real and Imaginary parts of the longitudinal impedance function.

Umek[A171] that the longitudinal stiffness coefficient for a rectangular embedded foundation at high frequencies is only 20 per cent larger than the corresponding stiffness for a flat foundation. Figure 3-2.2 also shows that the damping coefficient is highly dependent on the embedment ratio; the values for high frequencies being directly proportional to the contact area between the foundation and soil. This result is thus in agreement with one's intuitive expectation that the efficiency of energy loss through radiation of waves would be increased for larger foundations.

For a complete analysis of the foundation, it is necessary to calculate the longitudinal driving force, F_s^*, per unit length. For simplicity and clarity, plane SH-waves with incident angle θ and amplitude w^i may be assumed. For this wave scattering problem, assume an unknown scattered wave from the foundation to be $w^s e^{i\omega t}$. It must satisfy the "fixed" condition along with w^i and its reflection w^r from the half space boundary. The boundary condition is, therefore,

$$\left[w^s + w^i(\theta) + w^r(-\theta)\right]\Big|_{\xi=\xi_o} = 0 \; ; \qquad 0 \le \eta \le 2\pi \; . \tag{3-2.4}$$

and the longitudinal driving force per unit length is

$$F_s^* = -\int_s \sigma^s_{\xi z}\Big|_{\xi=\xi_o} ds = -\mu \int_{-\pi}^{0} \frac{\partial}{\partial \xi}\left(w^s + w^i + w^r\right)\Big|_{\xi=\xi_o} d\eta \; . \tag{3-2.5}$$

The real and imaginary parts of the longitudinal driving force, per unit length, F_s^* acting on the foundation are shown in

Figures 3-2.3a and 3-2.3b, respectively, for different angles of incidence and different embedment ratios. In particular, for a flat foundation (h/b = 0) and for vertical incidence (θ = 90 degrees), equation (2-1.5) indicates that $F_s^* = 2K_s u_i (u^* = 2u_i)$. For other embedment ratios and angles of incidence not equal to θ = 90 degrees, $F_s^* \neq 2K_s u_i$, as may be seen in Figure 3-2.3. The deviations from this simple case become more important for higher frequencies and for deeper embedments, indicating that the input motion $u^* = F_s^*/K_s$ may be quite different from the free-field motion $2u_i$. In general, these differences become apparent at values of $\omega b/\beta_s$ between 0.5 and 1 and correspond to wavelengths of the order of three to six times the total width of the foundation. The longitudinal impedance and driving forces shown in Figures 3-2.2 and 3-2.3 can be used, along with equation (2-2.4), to study soil-structure interaction.

An application of these results to an infinitely long shear wall was given by Wong and Trifunac.(A172) Described by the one-dimensional wave equation, the shear wall secures the "fixed-free" boundary condition while subjected to a base excitation of $\Delta e^{i\omega t}$, where Δ is the unknown displacement of the foundation to be determined.

The shear force which the wall exerts on the foundation is $F_e = \omega^2 M_b \left(\frac{\tan k_b H}{k_b H}\right) \Delta e^{i\omega t}$, where M_b and k_b are the mass and the wave number of the shear wall, respectively. Substituting F_e into equation (2-2.4) and rearranging, the solution is

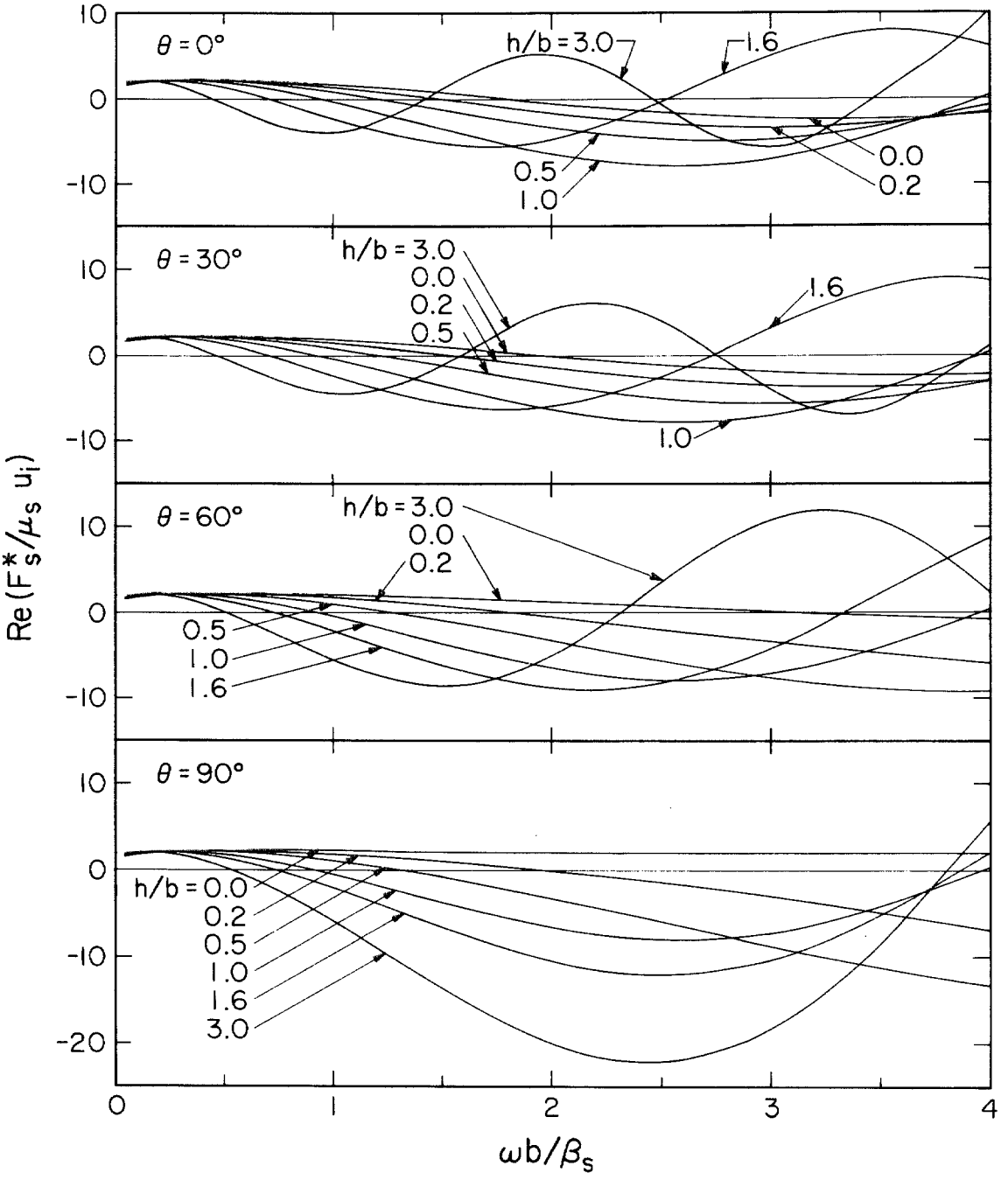

Figure 3-2.3a Real part of the longitudinal driving force.

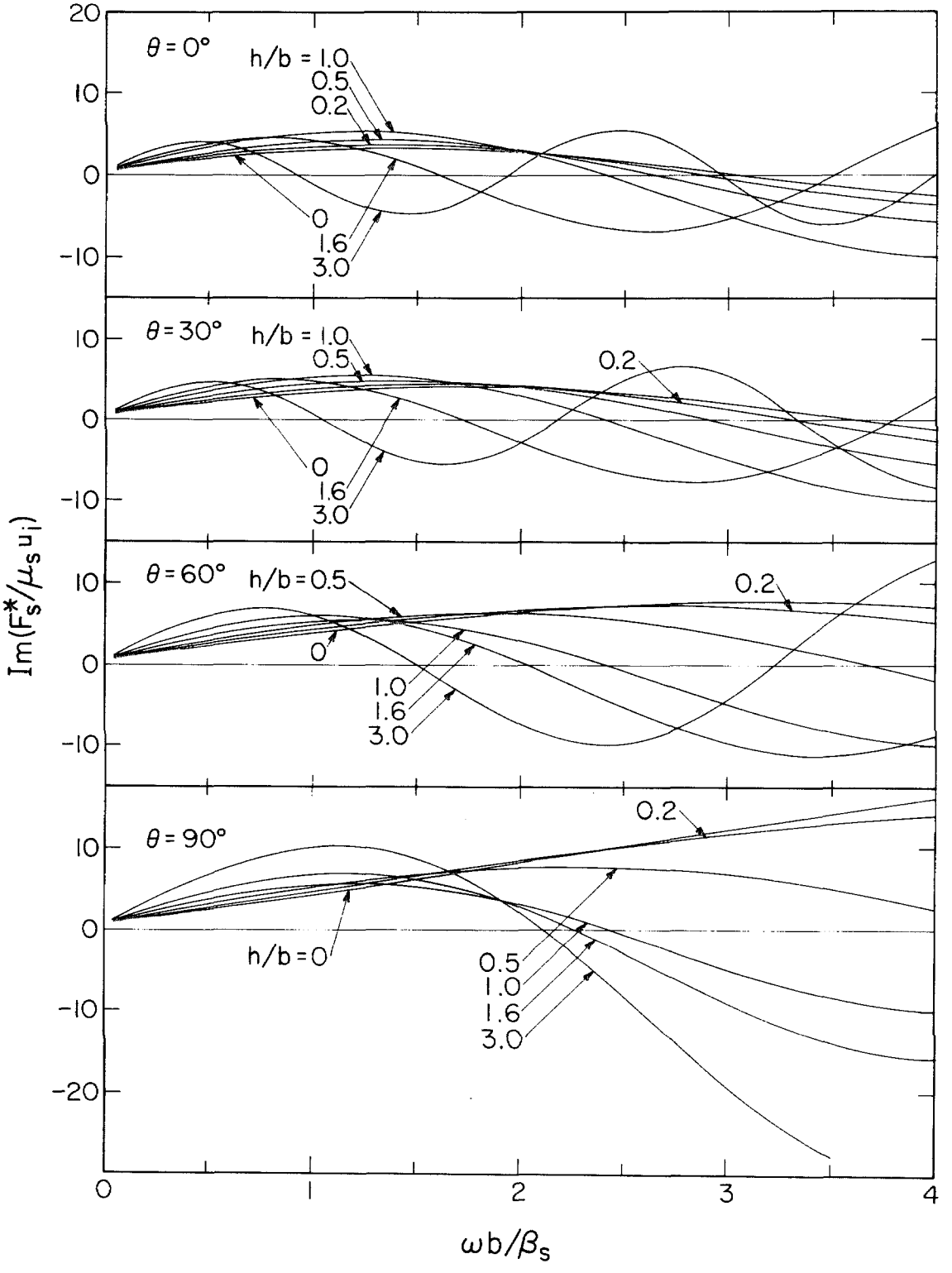

Figure 3-2.3b Imaginary part of the longitudinal driving force.

$$\Delta = F_s^* \left\{ k_s + i\omega C_s - \omega^2 \left[M_o + M_b \frac{\tan (k_b H)}{(k_b H)} \right] \right\}^{-1} . \qquad (3\text{-}2.6)$$

The unknown foundation motion $\Delta e^{i\omega t}$ is then completely determined by the results shown in Figures 3-2.2 and 3-2.3.

These results can be characterized by the following dimensionless parameters:

(1) $\omega A/\beta_s$, the dimensionless frequency, where A is the major axis of the ellipse;

(2) M_b/M_s, M_o/M_s, the ratio of the shearwall mass, M_b, and the foundation mass, M_o, to the mass of the soil replaced by the foundation, M_s;

(3) $\epsilon = k_b H/k_s A$, which involves the ratio of the wave numbers in the superstructure and in the soil medium;

(4) b/h, the embedment ratio of the foundation.

In Figures 3-2.4 and 3-2.5, the amplitude of the foundation motion $|\Delta|$ determined by equation (3-2.6) is plotted versus $\omega A/\beta_s$ for the angle of incidence SH-waves "THETA", where THETA is defined in Figure 2-2.1. It is seen that for $\omega A/\beta = 0$, all curves tend to 2 which is the amplification at the half space boundary. Each figure presents $|\Delta|$ for the four axis ratios b/A equal to 0.05, 0.30, 0.70, and 0.99. The small axis ratio represents either a shallow foundation or a very deep foundation, while the ratio b/A = 1 corresponds to the semi-circular cross section.

Since the values of THETA defined in Figure 3-2.1 are measured with respect to the vertical axis, i.e., THETA = $\frac{\pi}{2} - \theta$; the results for THETA = 0 in the case of the shallow foundation

Figure 3-2.4 Effect of interaction on the displacement amplitude $|\Delta|$ of a rigid foundation.

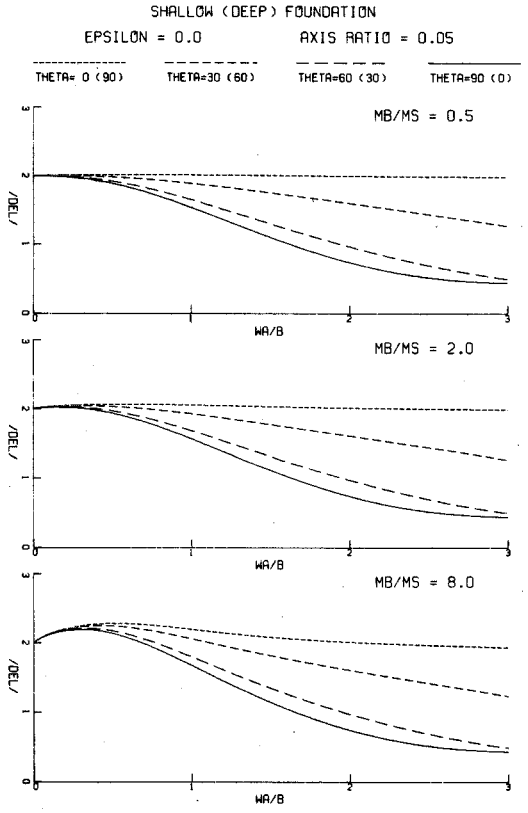
SHALLOW (DEEP) FOUNDATION
EPSILON = 0.0
AXIS RATIO = 0.05
THETA= 0 (90)
THETA=30 (60)
THETA=60 (30)
THETA=90 (0)
MB/MS = 0.5
MB/MS = 2.0
MB/MS = 8.0
/DEL/
WA/B

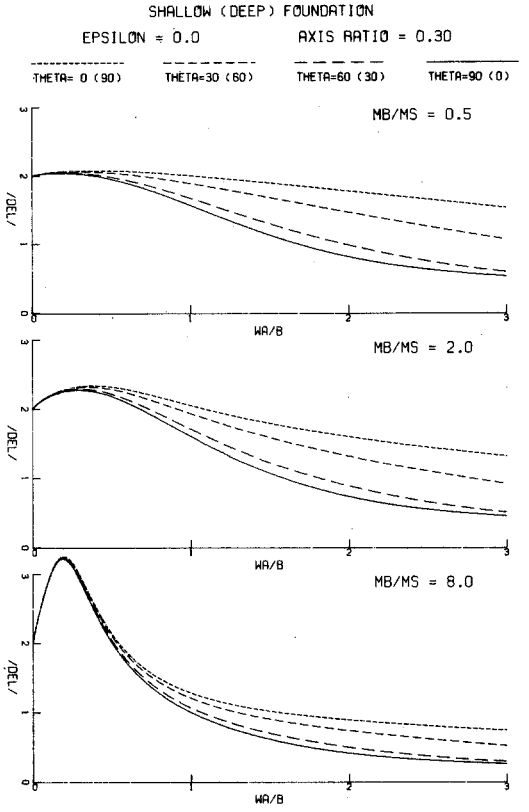
SHALLOW (DEEP) FOUNDATION
EPSILON = 0.0
AXIS RATIO = 0.30
THETA= 0 (90)
THETA=30 (60)
THETA=60 (30)
THETA=90 (0)
MB/MS = 0.5
MB/MS = 2.0
MB/MS = 8.0
/DEL/
WA/B

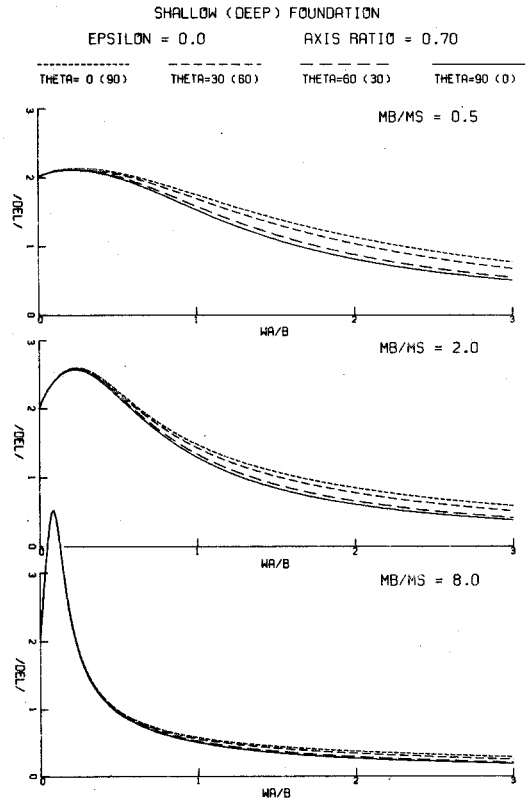
SHALLOW (DEEP) FOUNDATION
EPSILON = 0.0
AXIS RATIO = 0.70
THETA= 0 (90)
THETA=30 (60)
THETA=60 (30)
THETA=90 (0)
MB/MS = 0.5
MB/MS = 2.0
MB/MS = 8.0
/DEL/
WA/B

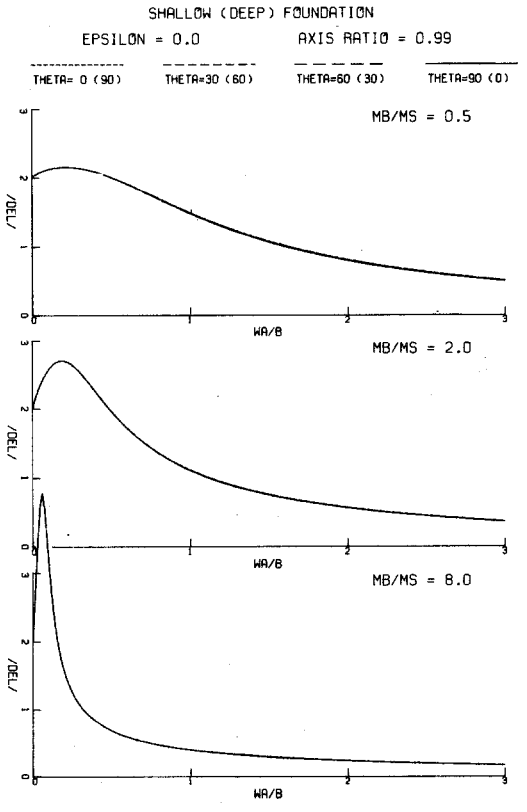
SHALLOW (DEEP) FOUNDATION
EPSILON = 0.0
AXIS RATIO = 0.99
THETA= 0 (90)
THETA=30 (60)
THETA=60 (30)
THETA=90 (0)
MB/MS = 0.5
MB/MS = 2.0
MB/MS = 8.0
/DEL/
WA/B

Figure 3-2.5 Effect of interaction on the displacement amplitude $|\Delta|$ of a rigid foundation

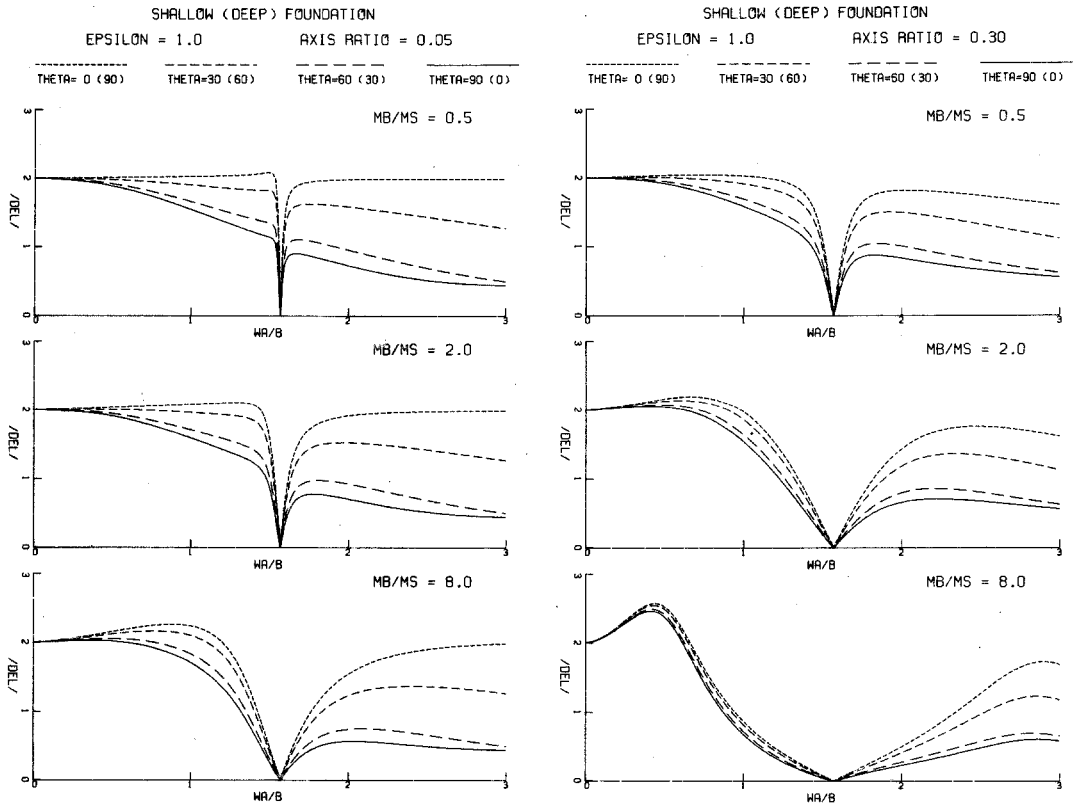
SHALLOW (DEEP) FOUNDATION
EPSILON = 1.0
AXIS RATIO = 0.05
THETA= 0 (90)
THETA=30 (60)
THETA=60 (30)
THETA=90 (0)
MB/MS = 0.5
MB/MS = 2.0
MB/MS = 8.0
/DEL/
WA/B
SHALLOW (DEEP) FOUNDATION
EPSILON = 1.0
AXIS RATIO = 0.30
THETA= 0 (90)
THETA=30 (60)
THETA=60 (30)
THETA=90 (0)
MB/MS = 0.5
MB/MS = 2.0
MB/MS = 8.0
/DEL/
WA/B

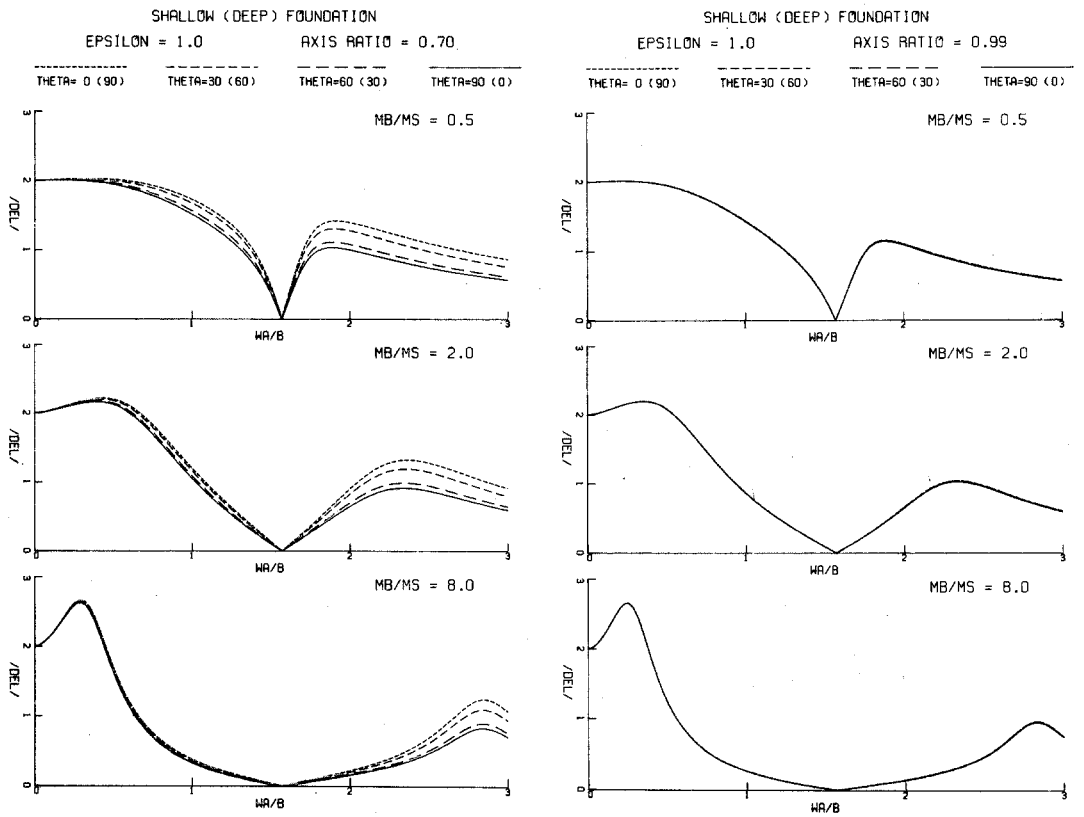
SHALLOW (DEEP) FOUNDATION
EPSILON = 1.0
AXIS RATIO = 0.70
THETA= 0 (90)
THETA=30 (60)
THETA=60 (30)
THETA=90 (0)
MB/MS = 0.5
MB/MS = 2.0
MB/MS = 8.0
/DEL/
WA/B
SHALLOW (DEEP) FOUNDATION
EPSILON = 1.0
AXIS RATIO = 0.99
THETA= 0 (90)
THETA=30 (60)
THETA=60 (30)
THETA=90 (0)
MB/MS = 0.5
MB/MS = 2.0
MB/MS = 8.0
/DEL/
WA/B

are the same as those for THETA = 90° for the deep foundation. All the curves in Figures 3-2.4, 3-2.5, and 3-2.6 are labeled first for "shallow" and then "deep" (in brackets) foundation cases. In each figure, the data are plotted for the same ϵ value and for three values of M_b/M_s = 0.5, 2.0, and 8.0. The value of M_o/M_s is set equal to 1 for all cases studied here.

Figure 3-2.4 presents the $\epsilon = 0$ case. From the definition of ϵ, this may be realized for a rigid wall ($\beta_b \to \infty$) or for a wall with mass concentrated at the base so that H = 0. In either case, there is no motion of the wall mass relative to the foundation, and, consequently, no structural resonances enter into the problem. As a result, Figure 3-2.4 has no zeroes in the $|\Delta|$ diagram, while Figure 3-2.5 with $\epsilon = 1.0$ has one zero. The zeroes in $|\Delta|$ curves correspond to the natural frequencies of the shear wall, at which the external force F_e on the right hand side of equation (3-2.6) becomes unbounded, and the foundation becomes a node in the half space. Since the fixed base resonance frequencies of a shear wall occur at $k_bH = (n + \frac{1}{2})\pi$, the zeroes of $|\Delta|$ will then appear at $\omega A/\beta = (n + \frac{1}{2})\pi/\epsilon$.

The $\epsilon = 0$ case in Figure 3-2.4 describes the case of a rigid mass $M = M_o + M_b$ forced to vibrate by the incident SH waves. It is seen from Figure 3-2.4 that for small axis ratios and small M_b/M_s ratio of 0.5, the dimensionless frequency band for $\omega A/\beta$ between 0 and 3, very shallow foundation and vertical-wave incidence, or for very deep foundation and horizontal incidence, the foundation moves essentially like the half space would move in the

absence of any foundation. In these two cases the "projection" of that part of the foundation mass which is in contact with the half space onto the normal of the plane-wave front is "small" relative to the cases of THETA = 90° incidence for shallow foundation and THETA = 0° incidence for deep foundations, so that the incident waves do not "see" the foundation very well. Consequently, the scattering and diffraction effects and interaction are therefore reduced. As the angle THETA increases toward 90° for the shallow foundation, or decreases toward 0° for the deep foundation, the size of the projection of the foundation onto the normal of the plane-wave front increases, the scattering and diffraction become more prominent, and $|\Delta|$ becomes more sentitive to changes of $\omega A/\beta$. This is best displayed in Figure 3-2.4 for $M_b/M_s = 0.5$ and axis ratio equal to 0.05. As the axis ratio increases toward 1, i.e., the elliptical cross section of the foundation tends toward a circular cross section, the size of the "projection" of the foundation onto the plane-wave front and the amplitude $|\Delta|$ become independent of the incidence angle THETA. For the axis ratio of 0.99 this dependence is already lost.

When M_b/M_s is small or zero, and since we take $M_o/M_s = 1$, Figure 3-2.4 reflects the consequences of assuming that the foundation medium is rigid. As M_b/M_s increases, the effective density of the foundation block increases relative to the density of the surrounding medium and the contribution of inertial forces becomes more prominent. The result of this is that the characteristics of a single-degree-of-freedom system represented by a spring, mass,

and a dash-pot emerge as representative of the $|\Delta|$ curves in Figure 3-2.4. Keeping the foundation shape constant in effect means that one keeps the equivalent elastic spring, k_s, and the equivalent dash-pot, C_s, of the impedance fixed, and then the increasing of M_b, which leads to the increase of $M = M_s + M_o + M_b$, results in the reduction of the equivalent natural frequency and the fraction of critical damping. This trend is clearly seen in Figure 3-2.4.

As ϵ increases, the zeroes of $|\Delta|$ at $\omega A/\beta_s = (n + \frac{1}{2})\pi/\epsilon$ become more densely distributed; the overall trends of $|\Delta|$ and the characteristic of the low-frequency peak, however, remain the same as the case where $\epsilon = 0$. While ϵ governs the position of zeroes in the $|\Delta|$ diagrams because of the definition of the dimensionless frequency, the width of the reduced $|\Delta|$ amplitudes centered around these zeroes increases with M_b/M_s. This behavior can be explained by equation (3-2.6); with larger M_b, the inertia force of the structure also becomes greater.

In the analysis and design of earthquake-resistant structures, it is necessary to know the maximum amplitudes of the displacement of the top of the superstructure relative to its foundation. From the maxima of these relative displacements, it may be possible to calculate the linear strain and therefore the maximum stresses experienced at any point in the superstructure.

For a shear wall, the displacement at its top is $\Delta/\cos(k_b H)$. Therefore, the relative response is

$$|R| = \left|\Delta\left[\frac{1}{\cos(k_b H)} - 1\right]\right| . \qquad (3\text{-}2.7)$$

At the "fixed base" natural frequencies of the wall, $k_b H = (n + \frac{1}{2})\pi$, $n = 1, 2, \ldots$, the relative response $|R|$ is infinite if the value of Δ is non-zero, as in the case of the rigid base. However, if the interaction is not neglected, Δ is equal to zero, and the relative response given by (3-2.7) is finite. Thus, the interaction plays a role similar to that of the damping mechanisms, which are used to model the energy dissipation in structural dynamics.

Figure 3-2.6 shows the relative response $|R|$ given by equation (3-2.7) for the same set of parameters used in describing $|\Delta|$ versus $\omega A/\beta_s$ as in Figure 3-2.5. The solid lines in these figures correspond to the response on a rigid base, and they tend to infinity for $\omega A/\beta_s = (n + \frac{1}{2})\pi/\epsilon$. The dashed lines correspond to $|R|$ and show the relative response for four typical incident angles THETA = 0°, 30°, 60°, and 90°. It is seen that the relative response is strongly dependent on the incidence angle of SH-waves when the axis ratio of the elliptical rigid foundation is small. When the axis ratio tends to one, i.e., when the cross section of a foundation becomes circular, the dependence on THETA disappears.

The ratio M_b/M_s has a pronounced effect on the relative response. As it increases, the overall amplitudes of the relative response $|R|$ decreases and the shape of the curves changes appreciably. This change is so pronounced for the larger values of M_b/M_s that the peaks at resonance are completely lost. This could, therefore, represent one possible mechanism that might

Figure 3-2.6 Effect of interaction on relative response.

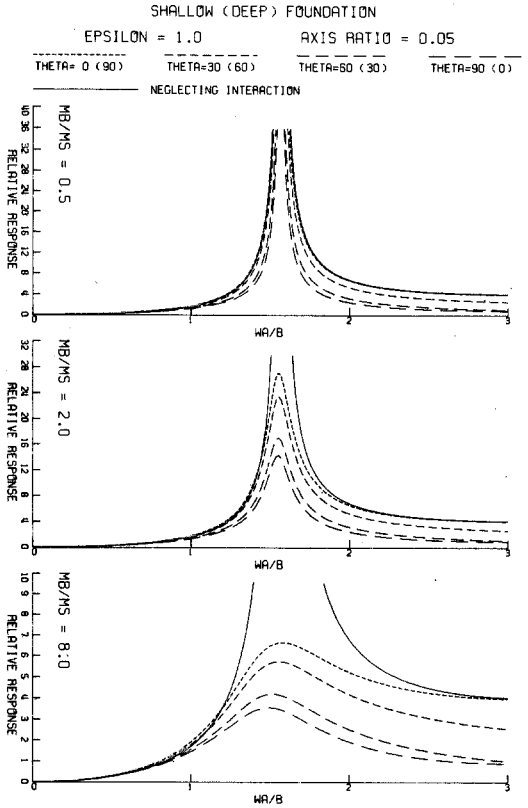
SHALLOW (DEEP) FOUNDATION
EPSILON = 1.0
AXIS RATIO = 0.05
THETA= 0 (90)
THETA=30 (60)
THETA=60 (30)
THETA=90 (0)
NEGLECTING INTERACTION
MB/MS = 0.5
MB/MS = 2.0
MB/MS = 8.0
RELATIVE RESPONSE
WA/B

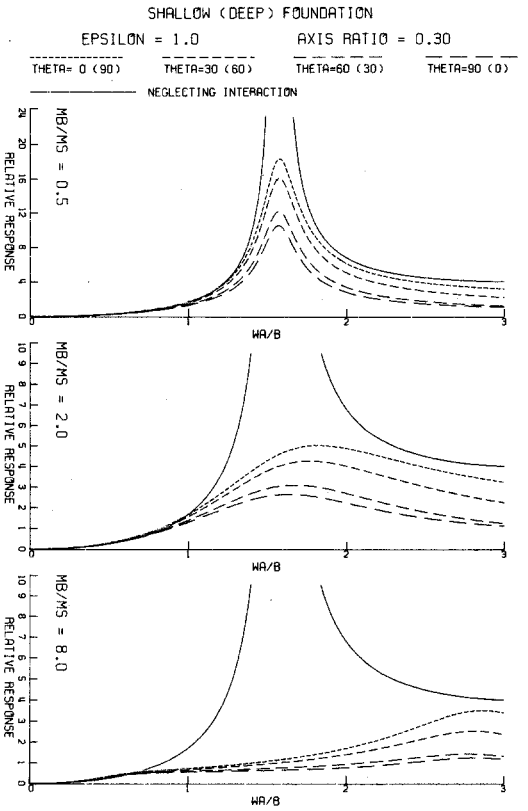
SHALLOW (DEEP) FOUNDATION
EPSILON = 1.0
AXIS RATIO = 0.30
THETA= 0 (90)
THETA=30 (60)
THETA=60 (30)
THETA=90 (0)
NEGLECTING INTERACTION
MB/MS = 0.5
MB/MS = 2.0
MB/MS = 8.0
RELATIVE RESPONSE
WA/B

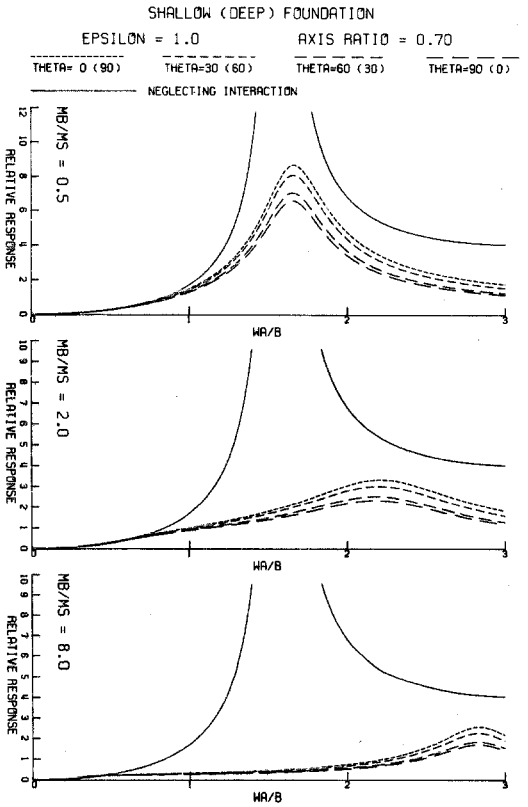
SHALLOW (DEEP) FOUNDATION
EPSILON = 1.0
AXIS RATIO = 0.70
THETA= 0 (90)
THETA=30 (60)
THETA=60 (30)
THETA=90 (0)
NEGLECTING INTERACTION
MB/MS = 0.5
MB/MS = 2.0
MB/MS = 8.0
RELATIVE RESPONSE
WA/B

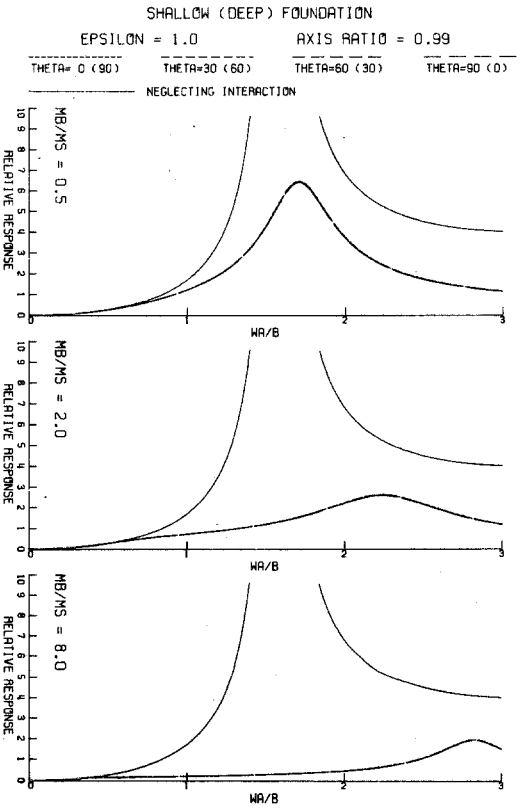
SHALLOW (DEEP) FOUNDATION
EPSILON = 1.0
AXIS RATIO = 0.99
THETA= 0 (90)
THETA=30 (60)
THETA=60 (30)
THETA=90 (0)
NEGLECTING INTERACTION
MB/MS = 0.5
MB/MS = 2.0
MB/MS = 8.0
RELATIVE RESPONSE
WA/B

explain the differences between calculated and measured natural frequencies for some full-scale structures.

[3-3] SHIELDING AND AMPLIFYING EFFECTS CAUSED BY LOCAL TOPOGRAPHY

In the quest for the safest locations for building important structures, the idea of shielding from seismic waves by use of trenches and canyons has often been proposed [Brown (1971), Lysmer and Waas (1972)]. However, the shielding characteristics of a trench are limited to very high frequencies only, not to mention the fact that an amplifying effect would occur if the incident waves were to come from the opposite direction. In this section, some of these topographic effects will be discussed by considering a simple two-dimensional model.

Consider the model shown in Figure 3-3.1. It consists of a semi-circular cylindrical foundation with radius a_2 which is placed to the right of a semi-circular canyon with radius a_1. Though the geometry illustrated is far too simple to qualify for practical applications, it simulates adequately a simple shielding problem.

Since the wave scattering objects are assumed to be of semi-circular cross sections, it is convenient to define two polar coordinates, (r_1, ϕ_1) and (r_2, ϕ_2), with their origins located at the centers of the canyon and the foundation, respectively. The two origins are separated by a distance D. The presence of the canyon will alter both the impedance functions and the driving forces derived in the previous section. To formulate this foundation interaction problem, we must be able to transform the scattered waves, w_1^R and w_2^R, and their expansions from one polar coordinate system to another so that all the boundary conditions can be satisfied.

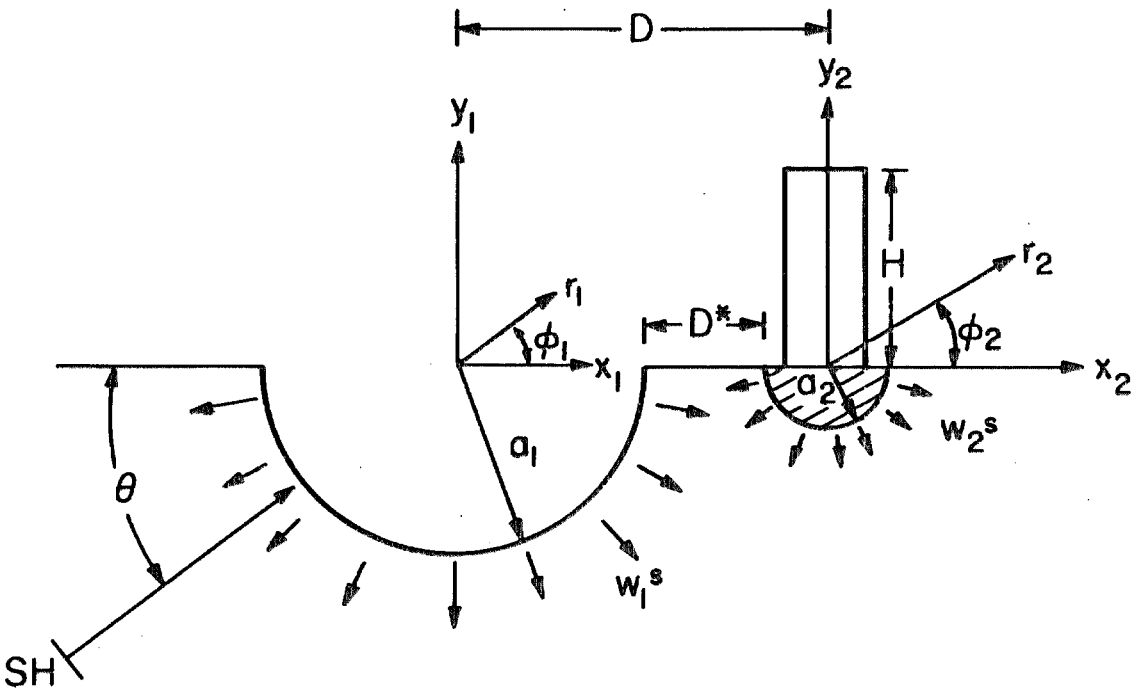

Figure 3-3.1 Canyon, Shear Wall, foundation, and soil.

In polar coordinates, the scattered waves from cylindrical objects are usually expressed in an infinite series of Hankel functions and harmonic functions. These series can be transformed from one coordinate system to another by applying the addition theorem [Abramowitz and Stegun (1971)]

$$H_n^{(2)}(kr_1)\cos n\phi_1 = \sum_{m=0}^{\infty} (-1)^m \frac{\varepsilon_m}{2} K_m^n(kD) J_m(kr_2)\cos m\phi_2$$

$$H_n^{(2)}(kr_2)\cos n\phi_2 = (-1)^n \sum_{m=0}^{\infty} \frac{\varepsilon_m}{2} K_m^n(kD) J_m(kr_1)\cos m\phi_1 \qquad (3\text{-}3.1)$$

where $K_m^n(kD) = H_{n+m}^{(2)}(kD) + (-1)^m H_{n-m}^{(2)}(kD)$ and $\varepsilon_0 = 1$, $\varepsilon_m = 2$ for $m \neq 1$.

The boundary conditions to be satisfied for the calculation of the impedances are

$$\mu \frac{\partial}{\partial r_1}\left[w_1^R(r_1,\phi_1) + w_2^R(r_1,\phi_1)\right]\Big|_{r_1=a_1} = 0 \qquad (3\text{-}3.2)$$

and

$$\left[w_1^R(r_2,\phi_2) + w_2^R(r_2,\phi_2)\right]\Big|_{r_2=a_2} = 1\, e^{i\omega t} . \qquad (3\text{-}3.3)$$

Equation (3-3.2) imposes conditions on the canyon so that the surface shear stresses are zero. The radiated wave from the foundation, w_2^R, originally expressed in coordinates (r_2,ϕ_2) as

$$w_2^R(r_2,\phi_2) = \sum_{n=0}^{\infty} a_n^{(2)} H_n(kr_2)\cos n\phi_2 \qquad (3\text{-}3.4)$$

can now be transformed to (r_1, ϕ_1) by (3-3.1). In (3-3.4), only the cosine functions were chosen because of the symmetry required to meet the boundary condition at the half space surface, $\sigma_{\theta z} = \mu \frac{\partial w}{\partial \theta} \Big|_{\theta=0, -\pi} = 0$. Similarly, the radiated waves from the canyon

$$w_1^R(r_1, \phi_1) = \sum_{n=0}^{\infty} a_n^{(1)} H_n(kr_1) \cos n\phi_1 \qquad (3\text{-}3.5)$$

are transformed to satisfy the displacement condition (3-3.3) at (r_2, ϕ_2) where a unit excitation is imposed. Because the Addition Theorem (3-3.1) involves infinite sums, the boundary conditions (3-3.2) and (3-3.3) will result in an infinite matrix equation for the unknown coefficients, $a_n^{(1)}$, $a_n^{(2)}$, $n = 0, 1, 2, \ldots$. Since it is not possible to invert an infinite matrix, the matrix is approximated by a finite one and is inverted numerically. Taking advantage of the descending behavior of the coefficients, this reduction of the matrix size can be used effectively because the higher order coefficients are small enough to be ignored. The numerical solution of the coefficients can be considered satisfactory if the results obtained by using N equations are sufficiently close to those obtained by using N+1 equations.

An analogous formulation applies to the calculations of the driving force. Together with the incident and reflected waves from the half space boundary, the scattered waves w_1^s and w_2^s must satisfy the following conditions,

$$\mu \frac{\partial}{\partial r_1} [w_1^s(r_1,\phi_1) + w_2^s(r_1,\phi_1) + w^i(r_1,\phi_1) + w^r(r_1,\phi_1)]\Big|_{r_1=a_1} = 0 \qquad (3\text{-}3.6)$$

$$[w_1^s(r_2,\phi_2) + w_2^s(r_2,\phi_2) + w^i(r_2,\phi_2) + w^r(r_2,\phi_2)]\Big|_{r_2=a_2} = 0 \ . \qquad (3\text{-}3.7)$$

Equations (3-3.6) and (3-3.7) represent the "free surface" condition at the canyon and the "fixed" condition at the foundation, respectively.

For non-vertically incident waves, the wave front arrives at the two coordinate systems at different instances. These arrivals are related by the phase relationship

$$[w^i(r_2,\phi_2) + w^r(r_2,\phi_2)] = e^{-i\frac{\omega}{\beta}D\cos\theta} [w^i(r_1,\phi_1) + w^r(r_1,\phi_1)] \qquad (3\text{-}3.8)$$

where θ is the angle of the incident wave. Because of this phase difference of the excitation, the solution can be quite different for various angles θ.

Because of the presence of the canyon, the driving force is dependent on the angle of incidence. For $\theta \leq \frac{\pi}{2}$, the incident waves approach from left to right in Figure 3-3.1 and the canyon acts as a shield for the foundation. For $\theta \geq \frac{\pi}{2}$, however, the canyon reflects the waves toward the foundation and thereby creates a standing wave pattern whose amplitudes at places may reach two times the amplitudes of "free field" motion.

To investigate the characteristics of the response of a rigid foundation and shear wall structure system, the amplitude of the foundation motion $|\Delta|$ is plotted versus the dimensionless

frequencies, $\omega a_1/\beta_s$ and $\omega a_2/\beta_s$. The shear wall studied here is identical to that of the previous section. Therefore, all parameters used there apply here. Without any loss of generality, the foundation radius a_2 is set equal to 1, while a_1 is varied to show the effects the canyon size may have on the response amplitudes. Since the presence of the canyon causes $|\Delta|$ to be θ-dependent, the five cases where $\theta = 0°$, 45°, 90°, 135°, and 180° have been studied.

Figures 3-3.2 and 3-3.3 illustrate the response of a rigid foundation without a superstructure; its density is set equal to that of the soil medium, i.e., $M_0/M_s = 1$. This arrangement was made so that the effect of the canyon can be studied without interaction with the superstructure. In each of these figures, the cases where $a_1 = 1, 3, 5$, and ∞ are shown in parts (a), (b), (c), and (d), respectively. Also plotted on these graphs, for comparison, is the case where $a_1 = 0$, i.e., the half space solution without a canyon. This response curve is represented by the dash-dot-dash line. Since different sizes of canyons are dealt with, it is convenient to select the distance so that $D^* = D - (a_1 + a_2)$ is a constant for all four parts. D^* is the distance between the two nearest edges of the foundation and the canyon. In Figure 3-3.2, $D^* = 1$; while in Figure 3-3.3, $D^* = 5$.

While examining Figures 3-3.2 and 3-3.3, the most important thing is to observe whether there are any significant shielding effects. Let us consider first the horizontally incident case, $\theta = 0°$; the foundation response $|\Delta|$ is represented by a fine dashed line. As shown, this response is very similar to that of the half space

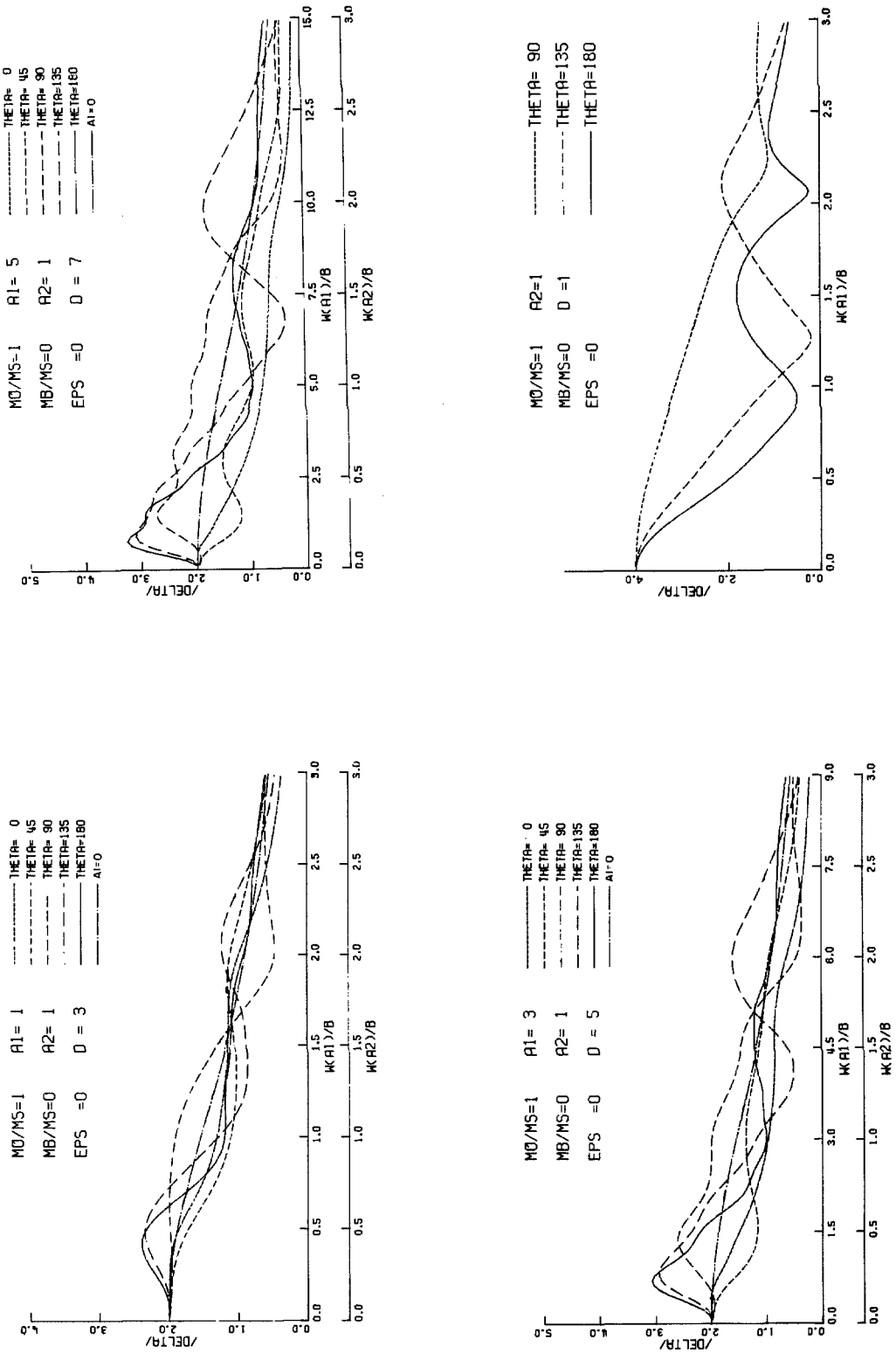

Figure 3-3.2 Displacement of a massless foundation subjected to plane SH-waves, $D^* = 1$.

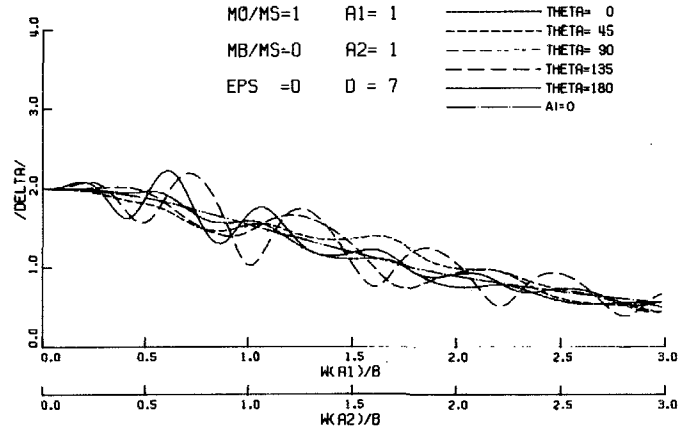

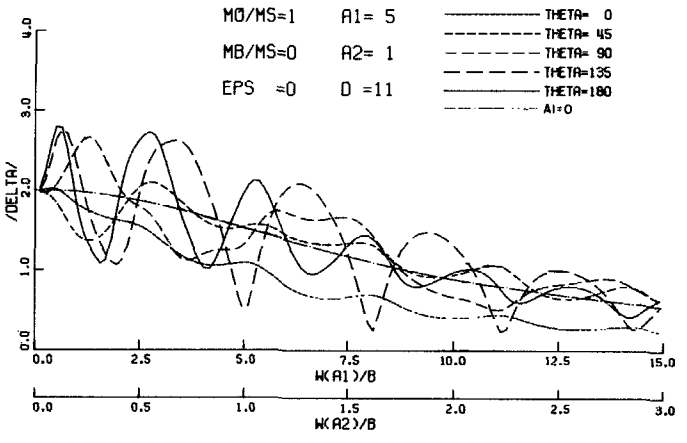

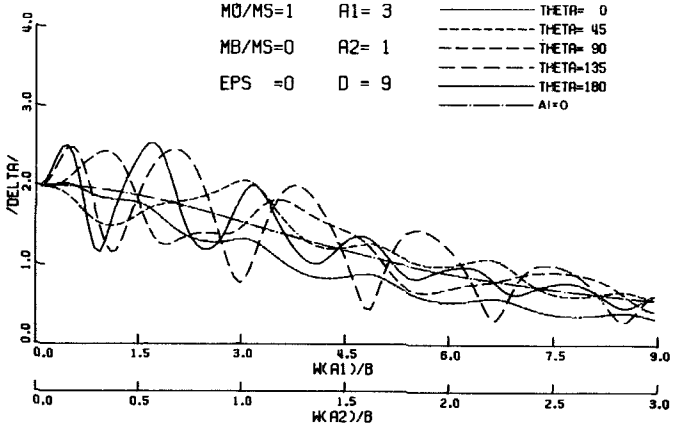

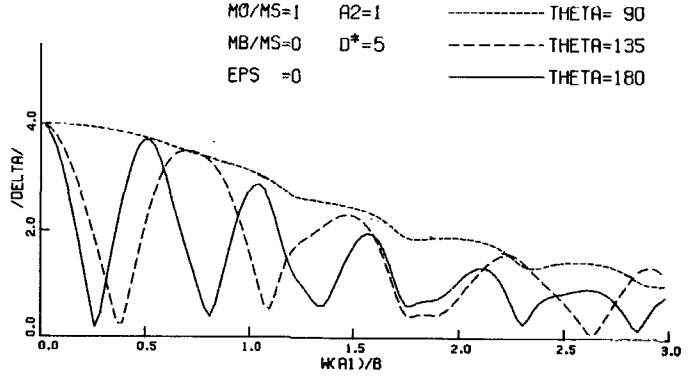

Figure 3-3.3 Displacement of a massless foundation subjected to plane SH-waves, $D^* = 5$.

solution when $a_1 = 1$. In fact, the results are nearly identical up to $\omega a_2/\beta_s = 0.5$. Physically, this means that the low frequency waves which have long wavelengths are not greatly altered by small scattering objects. To scatter away some of these longer waves, the size of the canyon must be increased as clearly shown by parts (b) and (c) in the figures. The shielding by the canyon with $a_1 = 5$ is effective for $\omega a_2/\beta_s$ down to 0.25; for $\omega a_2/\beta_s > 0.75$, the amplitude is reduced nearly 50%. Therefore, a canyon in front of a foundation does shield away part of the horizontally incident waves with wavelengths less than the width of the canyon. Whether this advantage can be used effectively is clearly a question for the designer and may depend on the problem at hand. However, some consequences caused by non-horizontally incident waves must also be considered carefully.

For incident waves with $\theta \neq 0°$, the shadow zone behind the canyon approximately extends up to its projection onto the half space surface. Therefore, the shielding diminishes if the structure is moved further away from the canyon. For example, consider the case when $\theta = 45°$ and $D^* = 1$ in Figure 3-3.2; the foundation is shielded for $a_1 = 3$ and 5, but the foundation is already out of the shadow area if $a_1 = 1$. If the distance D^* is increased to 5, the foundation is no longer protected for incident angles greater than 45°; in fact, the response amplitude may exceed that of the half space solution for certain frequencies because part of the energy is trapped in between the two scatterers.

This situation worsens as the incident angle increases; for $\theta > 90°$, the canyon plays the role of a wave source as part of the incident waves are reflected and focused back towards the foundation. As shown by Figures 3-3.2 and 3-3.3, the response amplitude can increase by more than 50% over the half space solution. Of course, this amplification is less pronounced if the canyon is further away, because the reflected wave diminishes as $1/\sqrt{D}$. Using the same reasoning as before, the longer waves are not reflected by the smaller canyon, therefore, the amplitude of response is near the static value of 2 for low frequencies. With the presence of a large canyon, the longer waves are also partially reflected, while all waves are reflected for the limiting case $a_1 = \infty$. For $a_1 = \infty$, the half space has become the quarter space, and the free surface amplitude becomes 4 for a unit input excitation.

In Figure 3-3.4, the interaction of a shear wall is also included. The structural response characteristics discussed in Section [3-2] also appear here, except for the minor changes caused by the canyon. The node in the response curve represents the resonance frequency of the shear wall. At this frequency, the base shear force directly cancels out the input driving force. Therefore, at the resonant frequency of the superstructure, $|\Delta|$ is not affected by the canyon, although the relative response is.

Judging from the discussion above, the canyon does provide some limited shielding for the structure. In the next section, a different type of shielding, that provided by local structures, will be discussed.

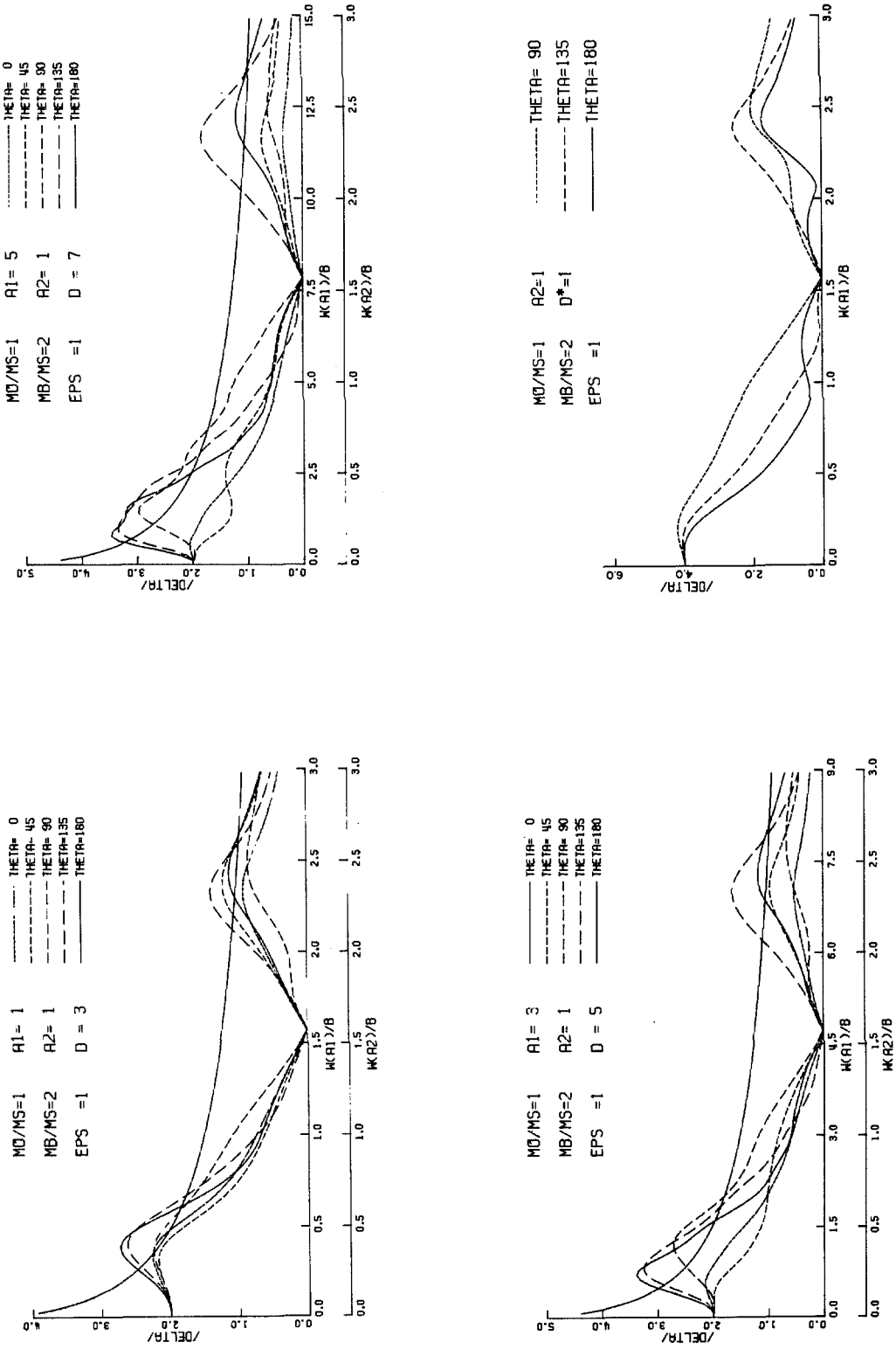

Figure 3-3.4 Displacement of a shear-wall-rigid foundation system subjected to plane SH-waves, $D^* = 1$.

[3-4] STRUCTURE-SOIL-STRUCTURE INTERACTION

This investigation will now focus on a more complex problem of structure-soil-structure interaction. In a set-up consisting of many structures, there are many possible arrangements of many structures, which make this problem difficult. Other than some two-dimensional finite element analyses, the interaction between two foundations has been explored analytically by Warburton et al.(A147) and experimentally by MacCalden and Mathieson.(A148) Their models consisted of two rigid circular foundations placed on top of an elastic half space. For anti-plane vibrations, Luco and Contesse(A170) studied the interaction of two embedded foundations with semi-circular cross sections excited by vertically incident harmonic SH-waves.

In the following analysis, a simple two-dimensional model is presented. Although, in this case, only one longitudinal component of the displacements remains, the mathematical manipulation becomes quite tedious. Nevertheless, the exact solution can explain some phenomena, which may be of fundamental importance for the understanding and interpretation of other, even more complicated three-dimensional models.

Using a procedure similar to that outlined in the previous section, the coordinate systems for the N buildings are defined in Figure 3-4.1. Contrary to the previous problems, the impedance function is now an $N \times N$ matrix, $K_{p\ell}$. Its elements depend on the frequency of excitation, the sizes and separations of all the

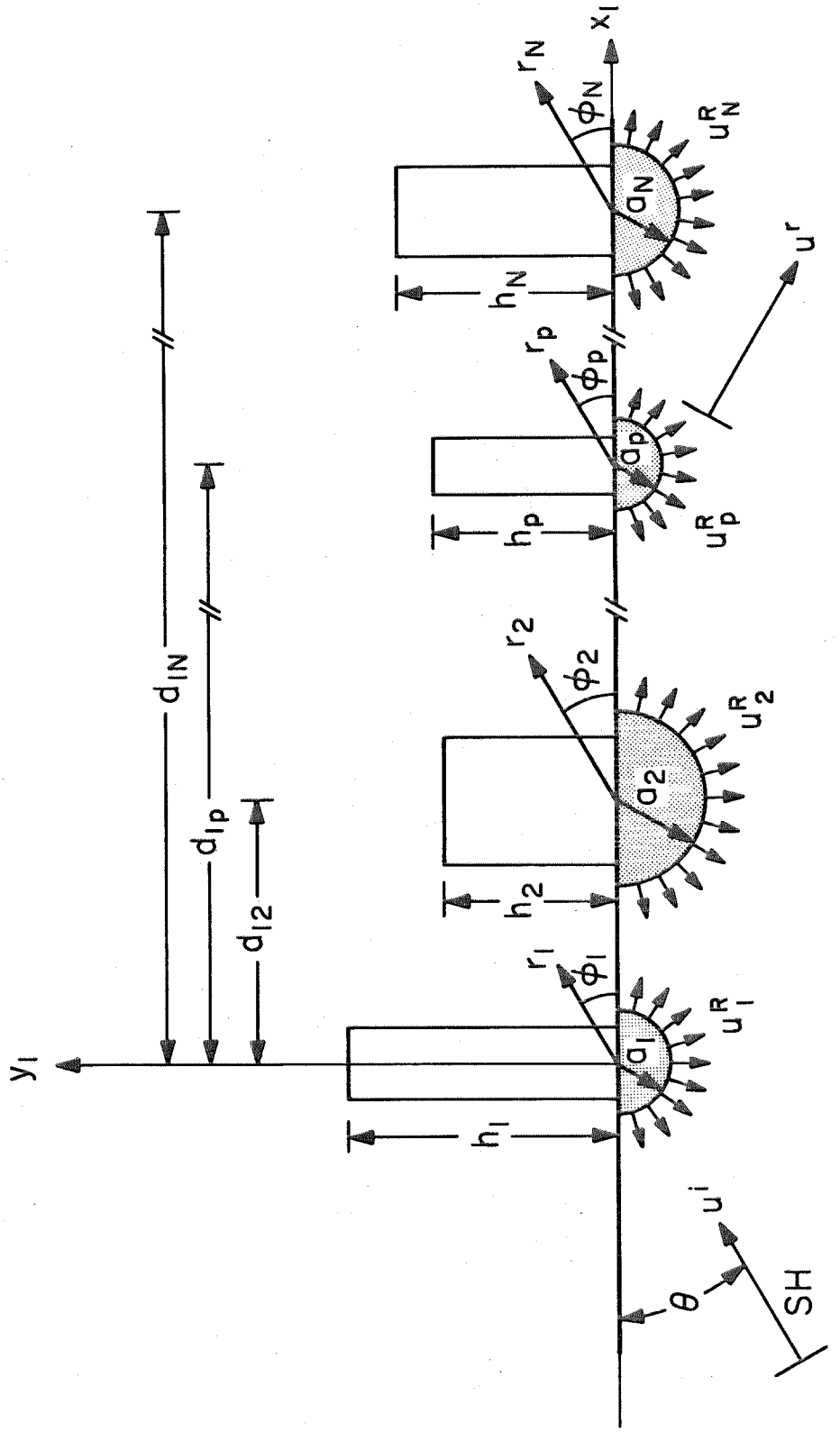

Figure 3-4.1 The arrangement of structures and the coordinate systems.

foundations, and the properties of the soil medium. Physically, $K_{p\ell}$ represents the force exerted on the pth foundation, while only the ℓth foundation is moved harmonically with a unit displacement.

To calculate the impedance matrix, $K_{p\ell}$, we assume that the radiating waves from the jth foundation have the form

$$w_j^{\ell}(r_j, \phi_j) = \sum_{n=0}^{N} C_n^{j,\ell} H_n^{(2)}(kr_j) \cos n\phi_j , \qquad j = 1, 2, \ldots, N . \qquad (3\text{-}4.1)$$

Then, the boundary condition $\mu \left.\frac{\partial w_j^{\ell}}{\partial y}\right|_{y=0} = 0$ is automatically satisfied at the half space boundary. But, in addition, the following boundary conditions must be specified,

$$\text{for } \ell = 1,2,\ldots,N; \quad \sum_{j=1}^{N} w_j^{\ell}(a_p, \phi_p) = \delta_{\ell p} e^{i\omega t} , \qquad p = 1,2,\ldots,N . \qquad (3\text{-}4.2)$$

Conditions (3-4.2) constrain the scattered waves so that only the ℓth foundation is moved by one unit. Along with equations (3-4.1) and (3-3.1), the boundary conditions (3-4.2) will again yield, for each ℓ, an infinite matrix for the unknown coefficients, $C_n^{j,\ell}$, $j = 1, 2, \ldots, N$; $n = 1, 2, 3, \ldots$.

After the unknown coefficients have been determined by numerical inversion of a finite matrix which closely approximates the original one, the impedances, $K_{p\ell}$, can be evaluated as

$$K_{p\ell} = -\int_{-\pi}^{\circ} \mu \frac{\partial}{\partial r_p} \left[\sum_{j=1}^{N} w_j^{\ell}(r_p, \phi_p) \right] \Big|_{r_p=a_p} a_p d\phi_p \qquad (3\text{-}4.3)$$

$$p = 1, 2, \ldots, N ; \qquad \ell = 1, 2, \ldots, N .$$

Now, in order to include the contributions from the incident wave, it is necessary to calculate the driving forces, S_p, $p = 1, 2, \ldots, N$. Physically, S_p represents the force which the soil exerts on the pth foundation while all foundations are kept fixed. By considering this as the (N+1)th problem, the scattered waves can be written in the same form as equation (3-4.1). The boundary conditions for zero displacements at the foundation surfaces are

$$\left[\sum_{j=1}^{N} w_j^{N+1}(a_p, \phi_p) + w^i(a_p, \phi_p) + w^r(a_p, \phi_p) \right] = 0 \qquad (3\text{-}4.4)$$

$$p = 1, 2, \ldots, N ,$$

where w^i and w^r are the incident and reflect waves, respectively. Equations (3-4.4) constitute an infinite system of simultaneous equations for the unknown coefficients, $C_n^{j,N+1}$, $j = 1, 2, \ldots, N$; $n = 1, 2, \ldots$. See Wong and Trifunac (A173) for the detailed derivation and numerical methods.

With the coefficients, $C_n^{j,N+1}$, calculated, the driving forces S_p can be determined by

$$S_p = -\int_{-\pi}^{\circ} \mu \frac{\partial}{\partial r_p} \left[\sum_{j=1}^{N} w_j^{N+1} + w^i + w^r \right] \Big|_{r_p=a_p} a_p d\phi_p . \qquad (3\text{-}4.5)$$

We next consider the superposition of the above results. The $N \times N$ matrix $[K_{p\ell}]$ and the "N" vector $\{S_p\}$ can now be used to analyze the interaction of N buildings as shown in Figure 3-4.1. The total force exerted on the pth foundation by the soil is by superposition

$$F_p^s = S_p + \sum_{\ell=1}^{N} K_{p\ell} \Delta_\ell \tag{3-4.6}$$

where Δ_ℓ, $\ell = 1, 2, \ldots, N$, are the unknown displacements of the N foundations. The total displacements outside the foundations are obtained likewise by superposition,

$$W = \sum_{j=1}^{N} \left[w_j^{N+1} + w^i + w^r + \sum_{\ell=1}^{N} w_j^\ell \Delta_\ell \right] . \tag{3-4.7}$$

Equation (3-4.7) now satisfies all the boundary conditions of the interaction problem as the displacement at the pth foundation is now set equal to Δ_p.

The determination of the unknowns, Δ_p, also depends on the external forces and, hence, the type of superstructures selected. For simplicity, the shear wall is again chosen for this analysis, and the excitation is assumed to consist of plane SH-waves with the angle of incidence θ.

The shear force at the base of the pth shear wall when it is subjected to the base excitation $\Delta_p e^{i\omega t}$ is

$$F_p^w = -\omega^2 (M_b)_p \left[\frac{\tan (k_b h)_p}{(k_b h)_p} \right] \Delta_p e^{i\omega t} , \qquad (3\text{-}4.8)$$

where $(M_b)_p$, $(k_b)_p$, and h_p are the mass, wave number, and height of the pth building, respectively. Since the motions of the N buildings are simultaneous, the displacement of one foundation will also depend on the displacement of another. Therefore, the N unknown displacements Δ_p, p = 1, 2, . . . , n= must be determined simultaneously through the N equations of motion written for the N foundations. These are of the form

$$\omega^2 \Delta_p (M_o)_p = -\omega^2 (M_b)_p \left[\frac{\tan (k_b h)_p}{(k_b h)_p} \right] \Delta_p + \left\{ S_p + \sum_{\ell=1}^{N} K_{p\ell} \Delta_\ell \right\} \qquad (3\text{-}4.9)$$

where $(M_o)_p$ is the mass of the pth foundation. Note, that the structure-soil-structure interaction effects are coupled through the terms $S_p + \sum_{\ell=1}^{N} K_{p\ell} \Delta_\ell$.

Dividing (3-4.9) by $\mu\pi k a_p$, and introducing the parameter $(M_s)_p = \frac{1}{2}\rho \pi a_p^2$, which is the mass per unit length of the soil replaced by the pth foundation, the equations of motion can be written in a dimensionless form as follows

$$\frac{(ka_p)^2}{2} \left[\left(\frac{M_o}{M_s} \right)_p + \left(\frac{M_b}{M_s} \right) \frac{\tan (k_b h)_p}{(k_b h)_p} \right] \Delta_p - \sum_{\ell=1}^{N} \left(\frac{K_{p\ell}}{\mu\pi} \right) \Delta_\ell = \left(\frac{S_p}{\mu\pi} \right) \qquad (3\text{-}4.10)$$

$$p = 1, 2, \ldots, N .$$

The Nature of the Interaction

The interaction of two or more structures are now considered by studying the numerical results presented in the figures which follow. The results shown in these figures depend mainly on the angle of the incident wave, θ, and four other dimensionless parameters:

(i) $\omega a_p/\beta = kA_p \equiv \eta_p$, the dimensionless frequency which compares the wavelength of the incident wave to the size of the pth foundation. To describe a system of foundations with different sizes, the maximum radius will be chosen as the reference, and the parameter $\omega a_{max}/\beta$ will be used in plotting the figures. (The notation of WA/B is used in place of $\omega a_{max}/\beta$ in the figures.)

(ii) $\frac{(M_o)_p}{(M_s)_p}$, the ratio of the mass of the foundation to the mass of the soil replaced by the foundation. For all the cases studied in this thesis, this ratio has been equated to 1.

(iii) $\frac{(M_b)_p}{(M_s)_p}$, the ratio of the mass of the pth shear wall to the mass of the soil replaced by the pth foundation.

(iv) $\epsilon_p = \frac{(k_b h)_p}{k a_p}$. This ratio describes the flexibility and the relative height of a shear wall. Larger values of ϵ indicate taller and/or more flexible walls,

while $\epsilon = 0$ implies a rigid structure or one with all its weight ($h_p = 0$) located at the base.

One of the interesting results that can be derived from the solution of equations (3-4.10) is represented by the displacements Δ_p of the foundations. In the figures that follow, amplitudes $|\Delta_p|$ have been plotted versus the dimensionless frequency WA/B ($A \equiv a_{max}$) and are identified by a dashed line or a solid line. All of these amplitudes approach the low frequency limit of $|\Delta_p| = 2$ (the displacement amplitude of the surface of half space due to an incident SH-wave with amplitude 1) as $WA/B \rightarrow 0$.

Another characteristic of the foundation displacement Δ_p is that it becomes zero when the flexible pth shear wall is being excited at its fixed-base natural frequencies, $(K_b h)_p = (2n+1)\pi/2$, $n = 0, 1, 2, \ldots$, or by using relation 3-4.10, Δ_p is zero at

$$\frac{\omega a_{max}}{\beta} = \frac{(2n+1)\pi}{2\epsilon_p}\left(\frac{a_{max}}{a_p}\right) \qquad (3\text{-}4.11)$$

Δ_p has no finite zeroes if $\epsilon_p = 0$. The occurrence of the zeroes of Δ_p has been explained by Luco[A168] and Trifunac.[A169] It is that during the steady excitation of incident plane SH-waves at the resonant frequencies of equation (3-4.11), the foundations behave as a node in a standing wave pattern.

The envelope of the response for a single wall placed on a half space, $|\Delta_e|_p$, is plotted on the same graph as the foundation displacements $|\Delta_p|$. This envelope, $|\Delta_e|_p$, provides an upper limit for the response of the pth foundation if it is the only structure on

the half space, therefore it may be used to indicate the strength of the additional interaction effects caused by the presence of other structures. These envelopes resemble a hyperbola and are described by the equation [Trifunac (A169)]:

$$|\Delta_e|_p = \left|\left[J_1(ka_p) - \frac{J_0(ka_p)H_1^{(2)}(ka_p)}{H_0^{(2)}(ka_p)}\right]\left[\frac{J_0^2(ka_p) + Y_0^2(ka_p)}{Y_0(ka_p)J_1(ka_p) - Y_1(ka_p)J_0(ka_p)}\right]\right|. \quad (3\text{-}4.12)$$

These envelopes have been plotted with the same type of lines as $|\Delta_p|$ in the subsequent figures.

Interaction of Two Walls

Displacements, Δ_p, during the steady interaction between the two walls have been illustrated in Figures 3-4.2, 3-4.3, and 3-4.4 and are designated by "DELTA." Each of these figures consists of parts (a), (b), and (c), which present the effects of different separation distances; each part also includes five graphs which correspond to the angles of incidence $\theta = 0°, 45°, 90°, 135°$, and $180°$. (Note: θ is written as THETA in these graphs.) These figures have been arranged so that the influence of the angle of incidence and the separation distance can be studied together.

For the two cases shown in Figures 3-4.2 and 3-4.3, the values of ϵ_p are taken to be zero so that the interaction effects of only the foundations can be more clearly shown. In this way the complications introduced by the vibrating walls are eliminated.

An interesting interaction phenomenon occurs when the incident wave travels with a shallow angle of incidence. The wall in front acts as a shield for the wall behind, but the latter may amplify the excitation for the former. This shielding effect is most evident in Figure 3-4.3 where the size of wall No. 1 is 5 times that of wall No. 2. (The numbering system used here is the same as that used in Figure 3-4.1)

For incident wave angles, THETA = 0° or 45°, and small wall separation distances, the smaller wall No. 2 moves with nearly the same displacement as the larger wall No. 1. The additional amplification effects caused by the smaller wall are negligible in this case because of the massiveness of the larger wall. The situation

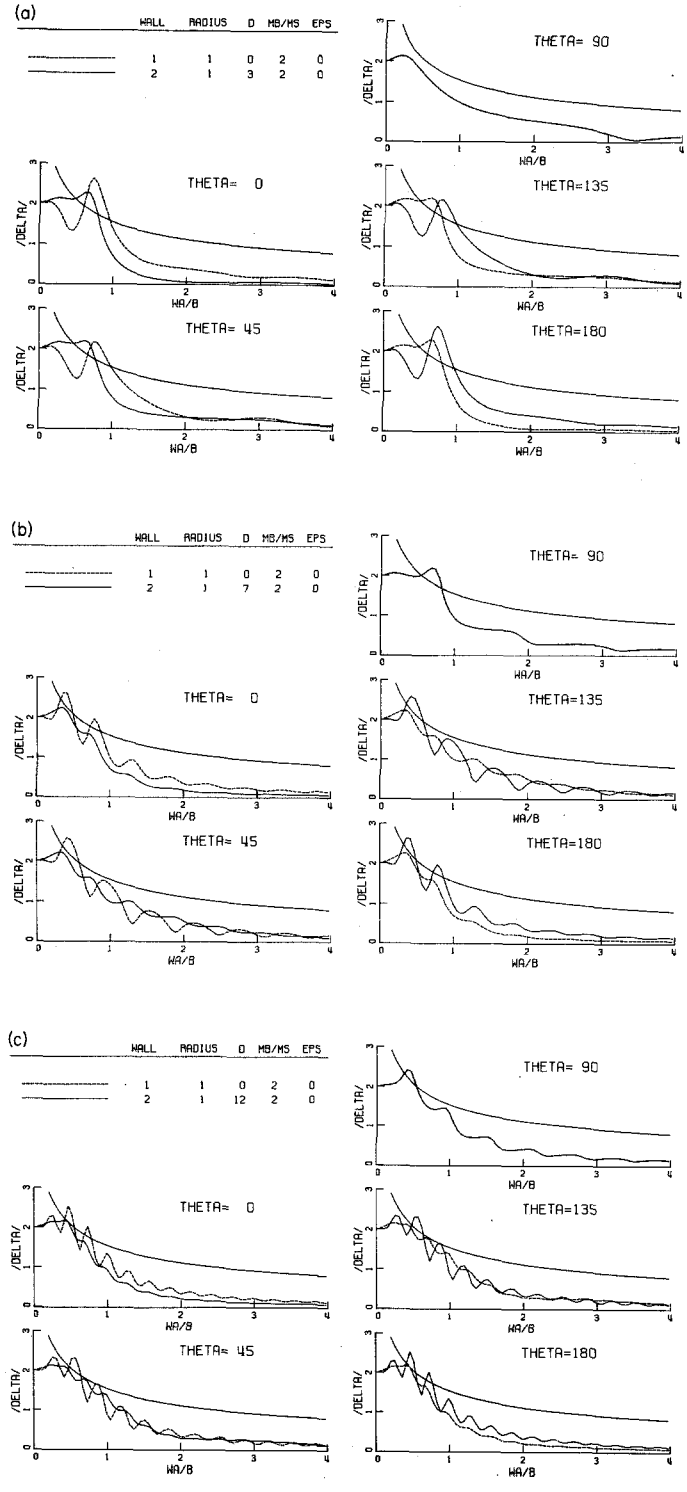

Figure 3-4.2 Foundation displacement for two identical structures.

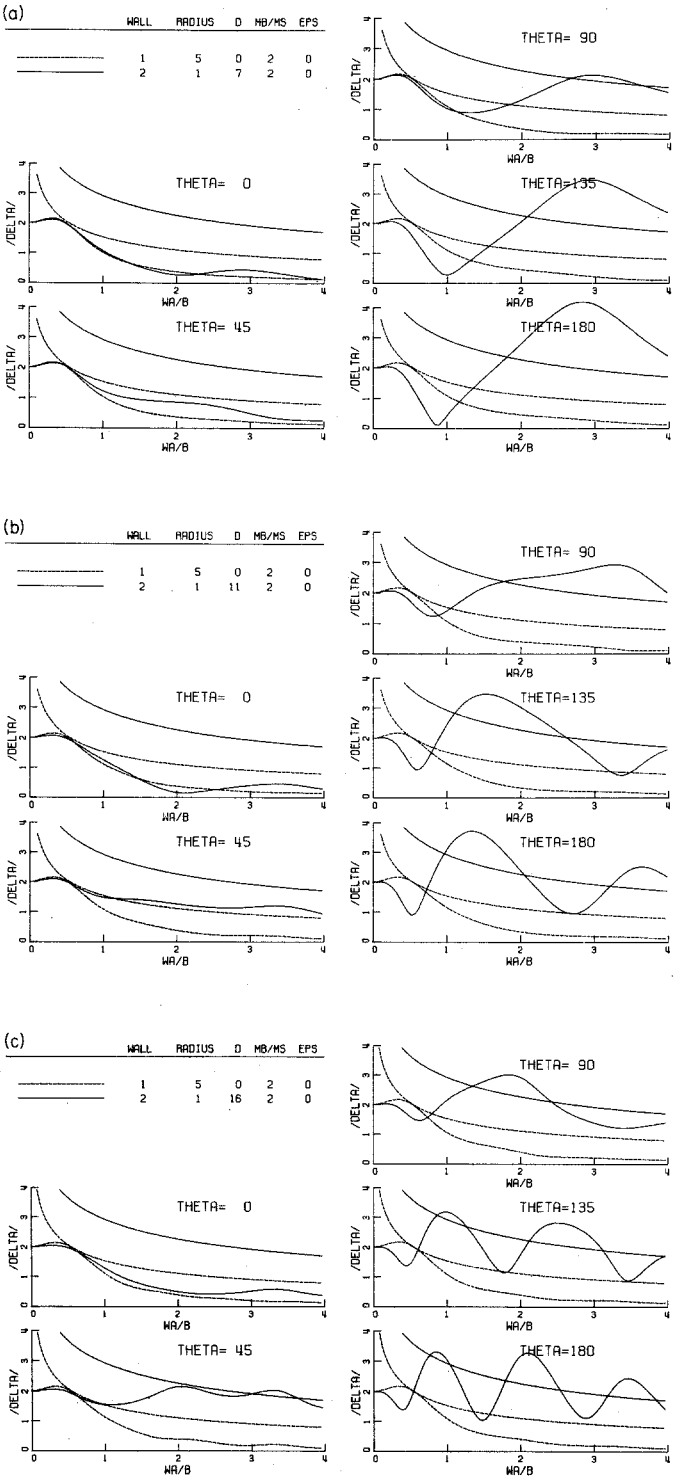

Figure 3-4.3 Foundation displacement for two structures with foundation size ratio of 5:1.

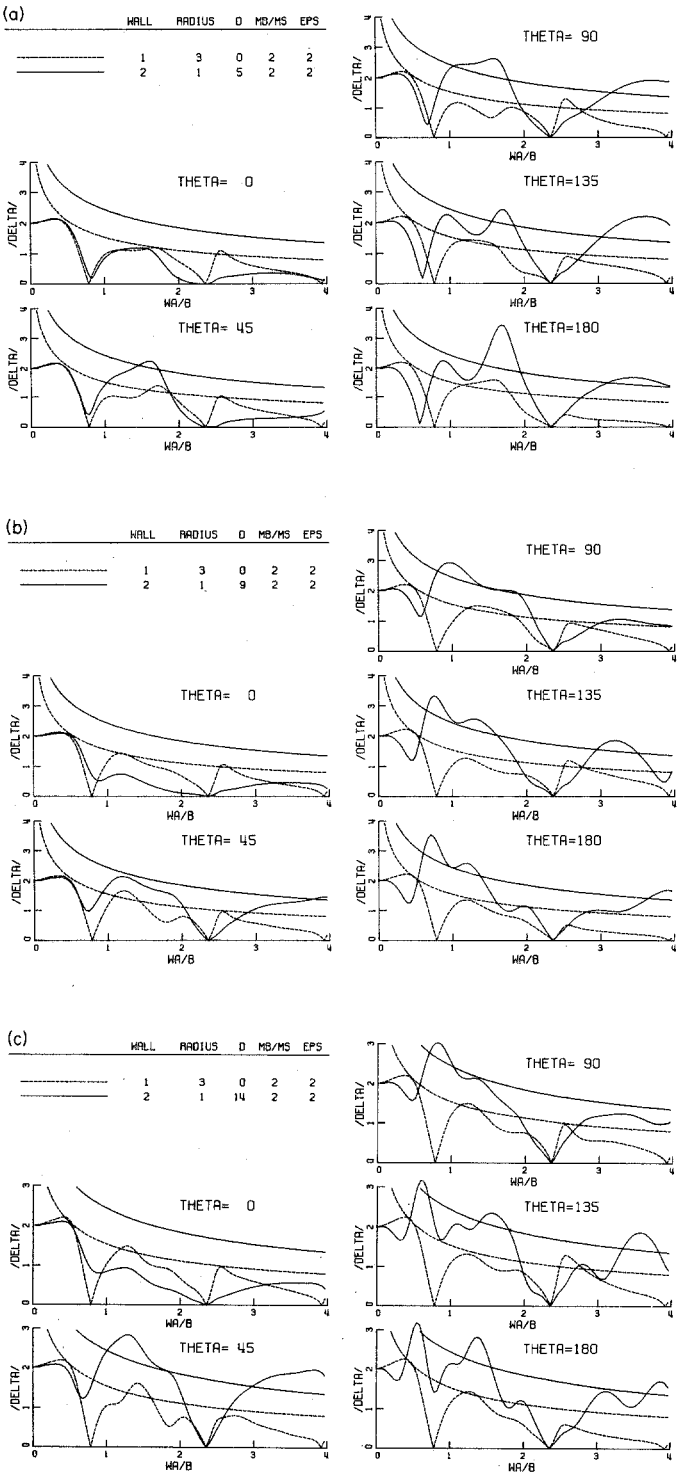

Figure 3-4.4 Foundation displacement for two structures with foundation size ratio of 3:1.

is reversed, however, when the waves are coming at an angle THETA = 135° or 180°. Now the "front wall" is much smaller than the "back wall"; here, the "front wall" meaning the first wall to be hit by the incident waves. In this case, the shielding effect provided by the "front wall" is negligible, while the amplifying effect caused by the "back wall" is overwhelming.

For the cases where the "front wall" is of comparable size or much smaller than the "back wall," the response of the front foundation dips down to a small value of Δ before it rises to a level exceeding the envelope curve of equation 3-4.12 at some higher frequency. This dip in foundation response amplitude for the front wall is greater when this foundation is smaller than the back foundation. The response is nearly zero at this point for the case described in Figure 3-4.3.

This phenomenon can be explained by the standing waves generated by the interference of the incident and the reflected wave from the larger back wall. For certain frequencies and/or distances, the smaller wall may be situated on a node and experience pure torsional excitation. This behavior can also be explained qualitatively by a vibration absorber example. Consider the following simplified model of the two foundation system. The spring constants k_1, k_2, and k_{12} depend upon the soil properties and, hence, are highly frequency dependent because of the geometrical configuration of the foundations. The displacements resulting from simple harmonic excitation are

$$\begin{cases} x_1 = \dfrac{k_1(k_2 + k_{12} - \omega^2 m_2)}{\Delta} e^{i\omega t} \\ x_2 = \dfrac{k_1 k_{12}}{\Delta} e^{i\omega t} \end{cases}$$

where

$$\Delta = (k_1 + k_{12} - \omega^2 m_1)(k_2 - \omega^2 m_2) - k_{12}^2 . \qquad (3\text{-}4.13)$$

Note that if $k_2 + k_{12} = \omega_*^2 m_1$ or $\omega_* = \sqrt{\dfrac{k_2 + k_{12}}{m_2}}$, the response of m_1, x_1 becomes zero and $x_2 = -\dfrac{k_1}{k_{12}} e^{i\omega t}$. Hence, m_1 is stationary at $\omega = \omega_*$, while m_2 is moving in an opposite direction from the excitation; so the forces on either side of m_1 eliminate each other, and m_1 is located on a node of a "standing wave" pattern. The system in Figure 3-4.5 is, of course, far too simplified to describe the phenomenon of the interactions in detail because the scattering from the foundations introduces "damping" into the system and the wave propagation is two dimensional. However, the intuitive physical explanation of this interaction problem is well represented by this model.

The spring constant k_{12} can be visualized as the soil joining the two foundations, so that as the separation becomes large, the interaction is weaker, and $k_{12} \to 0$ as $d_{12} \to \infty$. The frequency ω_* becomes smaller and the dip occurs at lower frequencies for larger separations.

The troughs and the crests in the response of Δ_p for the front foundation may be better visualized by studying Figures 3-4.6, 3-4.7, and 3-4.8, where the amplitudes of surface

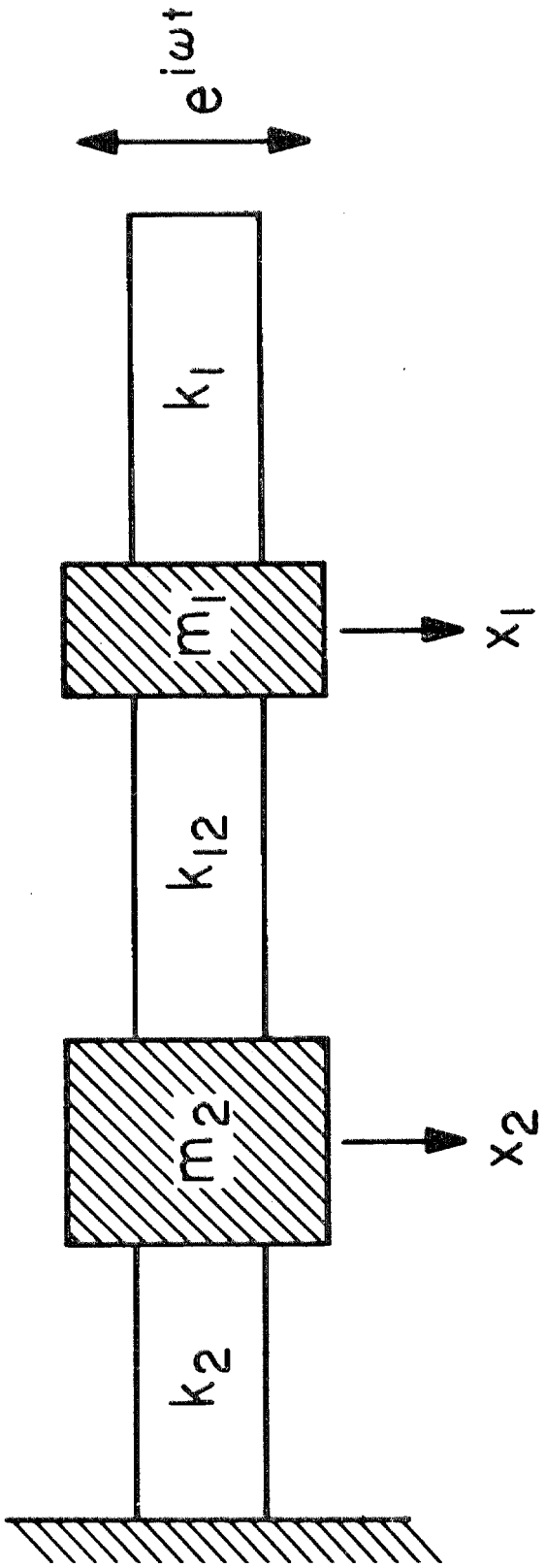

Figure 3-4.5 A simplified model of the two-structure system.

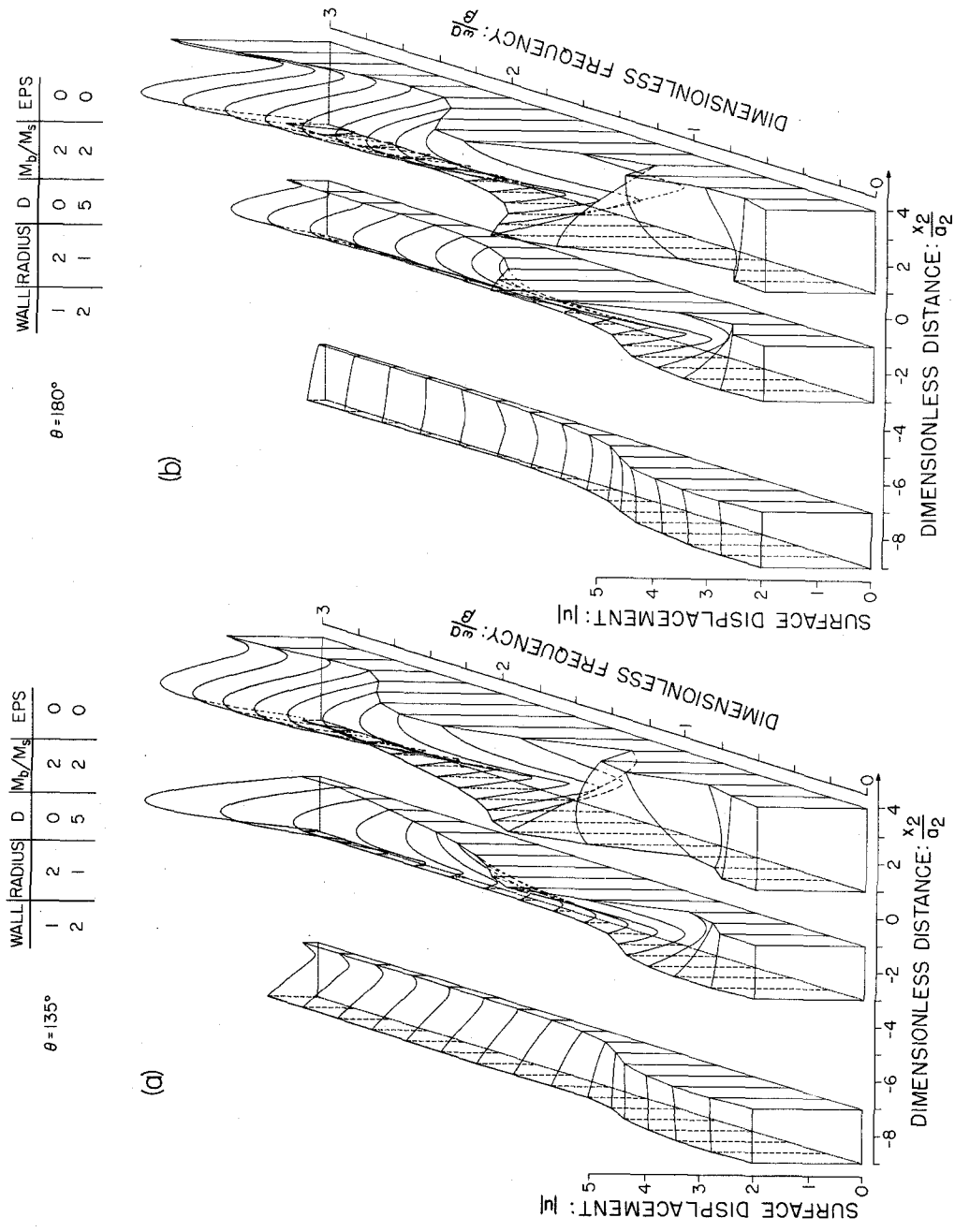

Figure 3-4.6 Ground surface displacement around two structures. Foundation size ratio is 2:1, separation distance is 5.

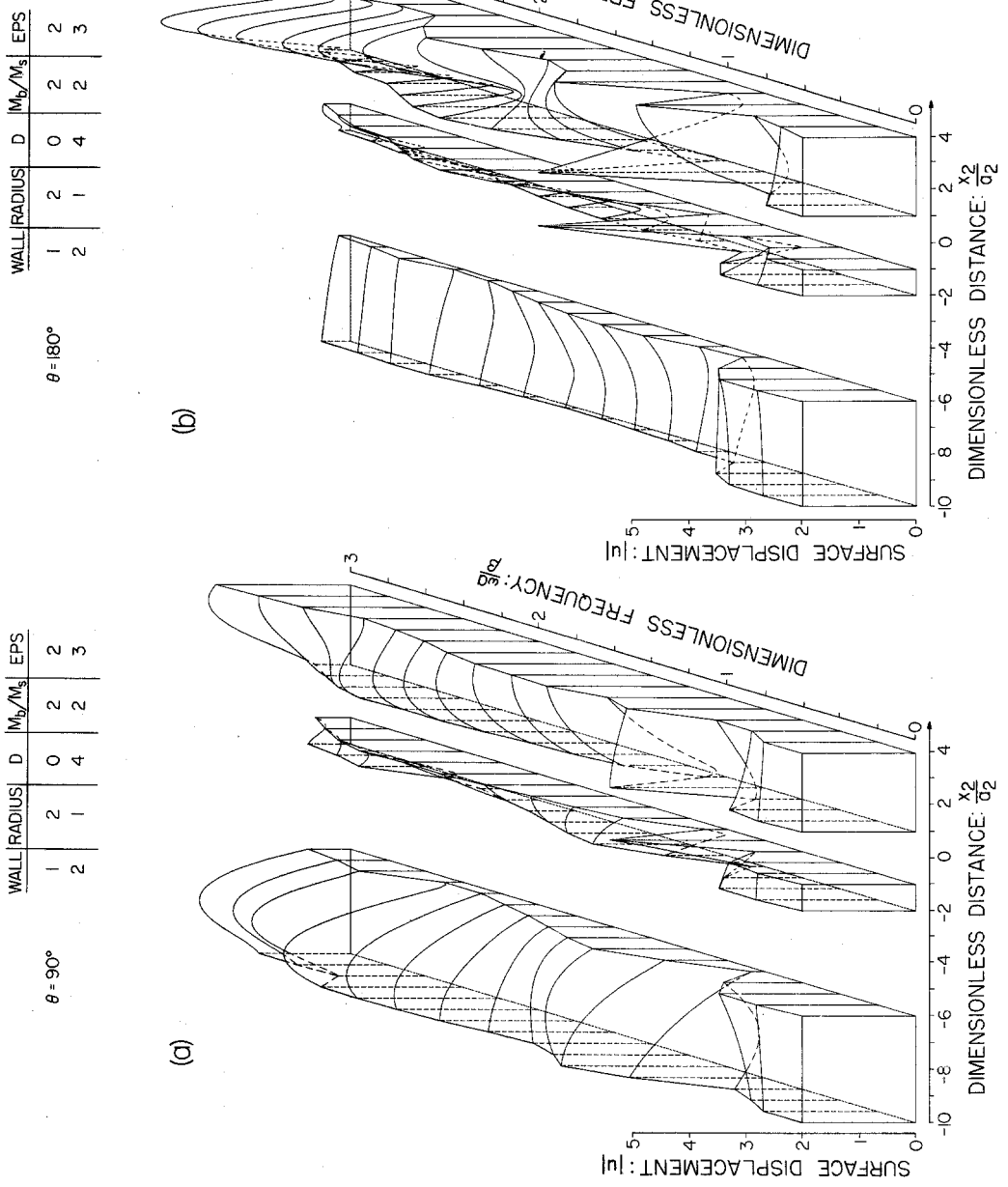

Figure 3-4.7 Ground surface displacement around two structures. Foundation size ratio is 2:1, separation distance is 4.

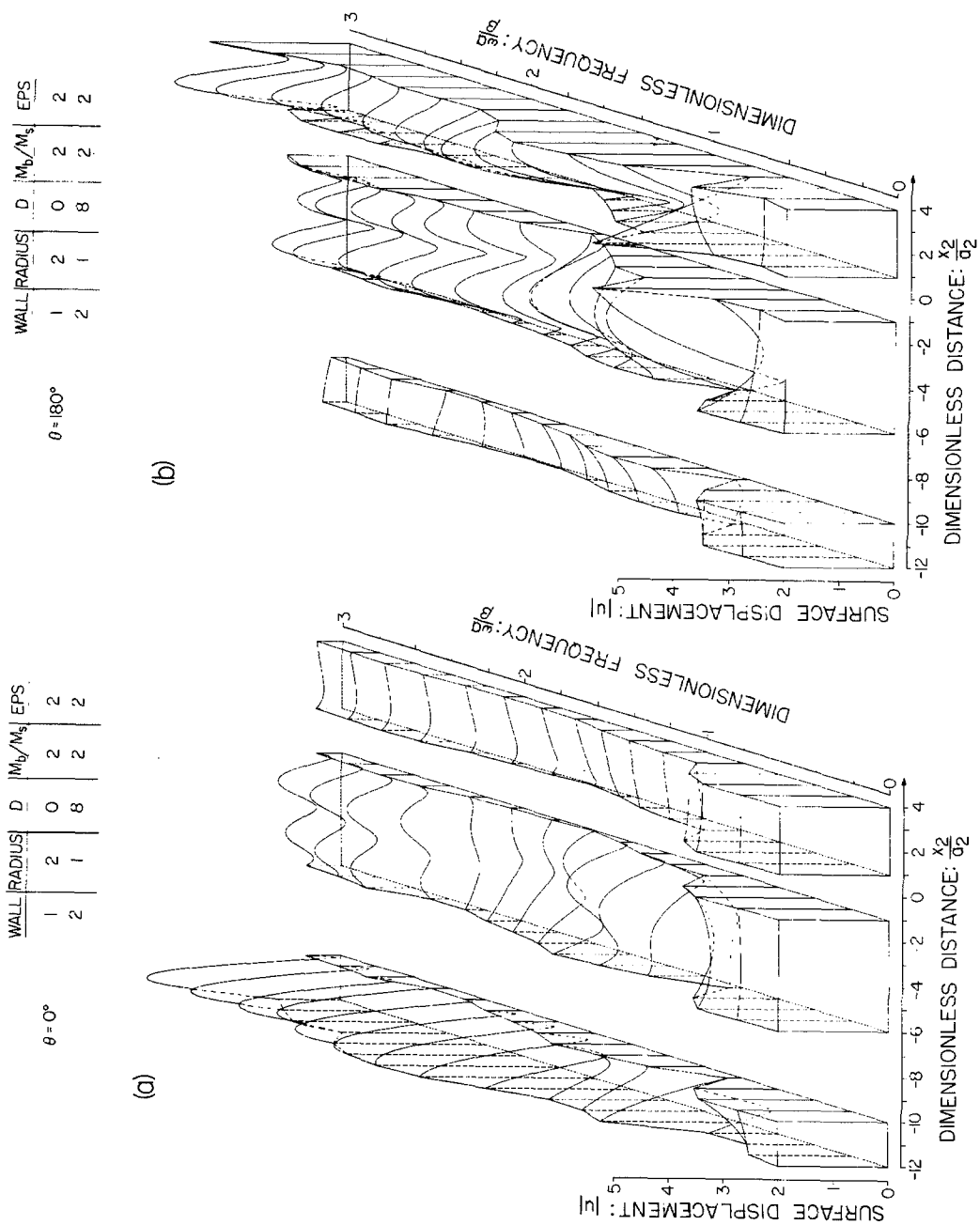

Figure 3-4.8 Ground surface displacement around two structures. Foundation size ratio is 2:1, separation distance is 8.

displacements in the vicinity of the two foundations are plotted against the dimensionless frequency, η, and the dimensionless distance $\frac{x}{a}$. The definition of dimensionless parameters used in these figures is identical to those discussed previously.

The foundation size ratio for all cases presented in Figures 3-4.6, 3-4.7, and 3-4.8 is 2 to 1. Figure 3-4.6 illustrates the scattered wave patterns around the two foundations for THETA = 135° and 180°, both of which have rigid walls, i.e., for $\epsilon = 0$. Figure 3-4.7 illustrates the effect of vertically incident waves in part (a) and the effect of horizontally incident waves in part (b); both shear walls considered here are flexible and tall. The surface displacement plots of Figure 3-4.8 show the weaker interaction with a larger separation distance.

In Figure 3-4.6b, the phenomenon described by a simple model in Figure 3-4.5 can be observed. The first trough of the response Δ_2 of the smaller foundation occurs at $\omega A/\beta \cong 0.4$. At that frequency, both foundations are moving in phase with foundation No. 1 and have large amplitudes. Not far to the right of foundation No. 2, there is a point with small displacement. This is where the displacements on either side change direction and, hence, the point pivots the movement of both walls. If the foundation size ratio is much greater than 2 to 1, e.g., 5 to 1, the presence of the smaller foundation can almost be ignored when studying the response of a large foundation. Also, for a certain wavelength of incident waves, the motion of the smaller foundation may be located on a node of a standing wave pattern and remain stationary.

The crest of the response Δ_2, which follows the trough, occurs at $\omega A/\beta \cong 1.0$ in Figure 3-4.6b and is created by the amplifying effect of wall No. 1. At this particular frequency, the two walls are nearly 180° out of phase and the "node" is now located between the two foundations. Because of the rapid change of phase in the vicinity of a "node," the ground motion at that point is essentially torsional. When the frequencies are higher than $\omega A/\beta \cong 1.5$, or when the wavelength of the incident wave becomes smaller than the separation distance, the interaction effects gradually disappear and the response of the foundations most likely does not exceed appreciably the envelopes for the response of a single foundation.

It is clear from the above discussion that the presence of two shear walls increases the complexity of response of each foundation and that the interference of waves scattered from the two foundations may lead to appreciable modification of their base motions, Δ_p. It is beyond the scope of this paper to analyze in detail these amplifications caused by the building-soil-building interaction effects, but the general trends may nevertheless be extracted from several cases considered. These amplifications determined for three foundation size ratios are presented in Figures 3-4.9 and are plotted versus the separation distance, d_{12}. Some of these results have been extracted from Figures 3-4.2 and 3-4.3.

The two sets of points in Figure 3-4.9 show the differences caused by the angle of incidence. Since wall No. 2 is smaller, the

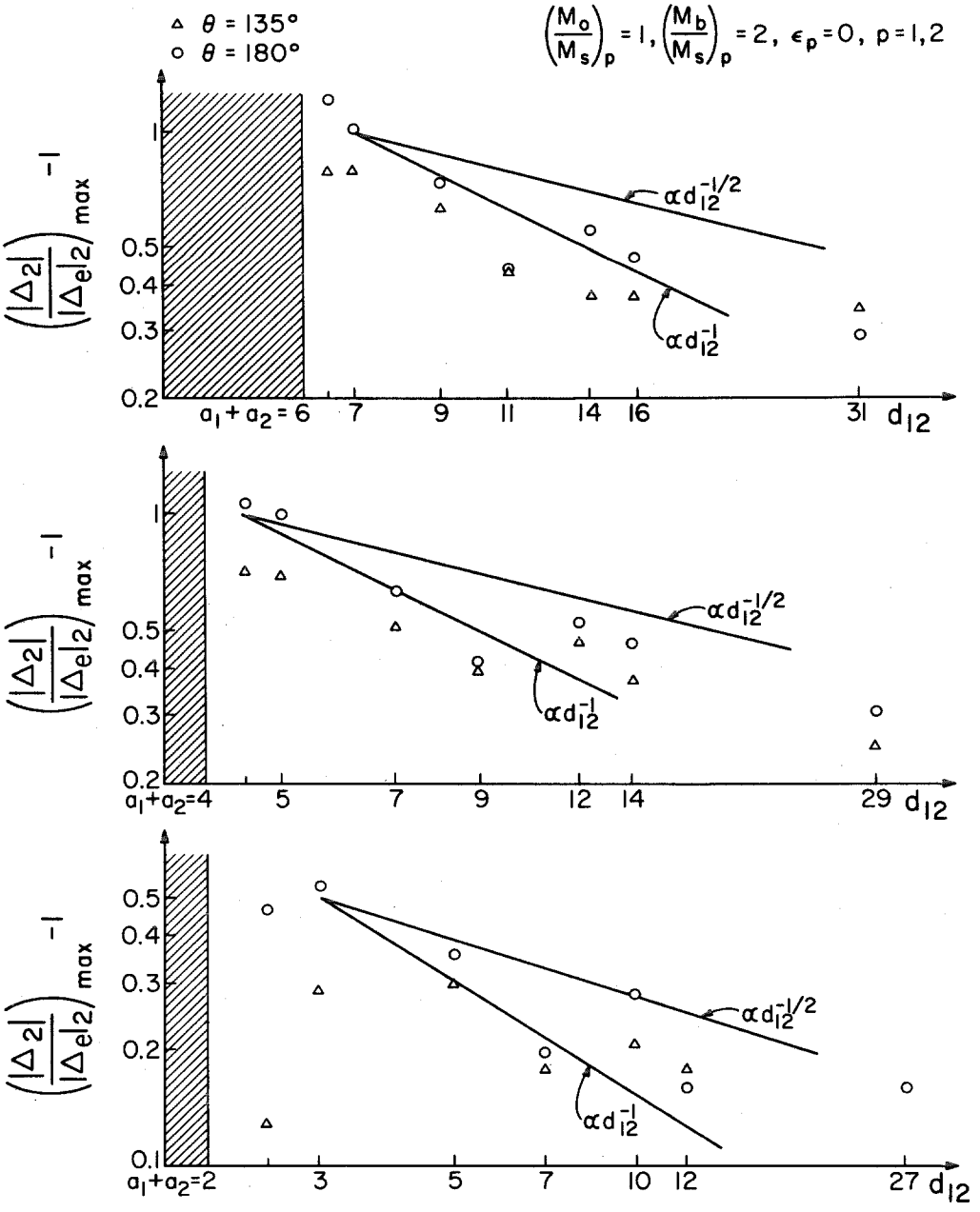

Figure 3-4.9 The effect of separation distance on the amplifying influence of other structures for interaction of two structures

amplifying effects occur for $\theta > 90°$, e.g., $\theta = 135°$ and $180°$. Because the waves scattered from the two foundations are of a cylindrical type, one would expect that the peak amplitude $|\Delta_2|$ of small foundations would be related to its envelope $|\Delta_e|$ by $(|\Delta_2| / |\Delta_e|)_{max} - 1 \approx \text{const.}/d_{12}^{\frac{1}{2}}$ when d_{12} is larger compared to $a_1 + a_2$. This is simply stating that $|\Delta_e|$ is entirely due to scattered, u^R, waves. Diffraction and interference effects for d_{12} small may alter this trend appreciably, and in the limit for $d_{12} \to a_1 + a_2$, we have $(|\Delta_2| / |\Delta_e|)_{max} - 1 \to 0$. It appears that the few points plotted in Figure 3-4.9 may be explained by these trends. It is clear, however, that the continuous representation of $(|\Delta_2| / |\Delta_e|)_{max} - 1$ versus d_{12} should have numerous peaks and troughs which are caused by the interference of scattered field with the incident plane SH-waves. It is this interference that causes the apparent scatter of the few randomly selected points in Figure 3-4.9.

Interaction of Many Walls

The interaction which involves many foundations clearly becomes more complex as the number of foundations increases, but the solution presented in this paper should provide a simplified two-dimensional picture of what might occur.

In Figures 3-4.10 and 3-4.11, foundation responses $|\Delta_p|$ for three foundations with rigid walls have been presented. Figure 3-4.10 shows a case where one small wall is placed between two larger walls of three times its size and $\epsilon_p = 0$ for all three walls.

For the foundation response shown in Figure 3-4.10a, the two large outside walls behave as if the smaller middle wall is absent. This conclusion results from comparison of $|\Delta_1|$ and $|\Delta_3|$ with $|\Delta_1|$ and $|\Delta_2|$ of Figure 3-4.2a, where the response of two identical walls has been presented. However, at $WA/B \cong 1.8$, Δ_1 and Δ_3 are slightly altered and the response of wall no. 2 is strongly excited for $d_{12} = 5$ and $d_{13} = 10$. In Figure 3-4.10b, the peak at $WA/B \cong 1.8$ has been translated to $WA/B \cong 0.85$, indicating that the "resonant frequency" of the small wall is highly dependent on the distance to the larger walls. For the case in Figure 3-4.10c, the separation distance is large, so that the building-soil-building interaction effects cease to be prominent.

The interaction of three walls as described above can again be visualized by using a simplified model of springs and masses. Since the relative motions of the large outside walls are relatively

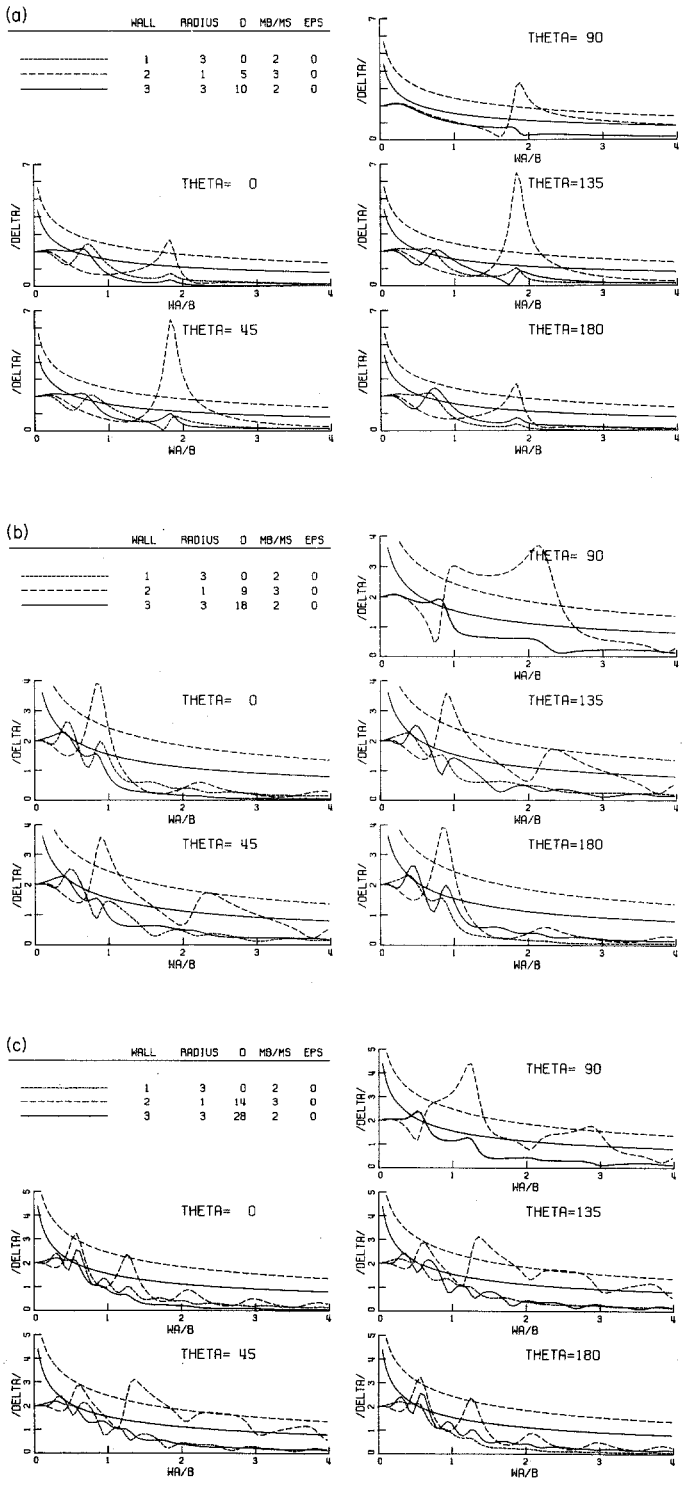

Figure 3-4.10 Foundation displacements of three structures with foundation size ratios of 3 : 1 : 3.

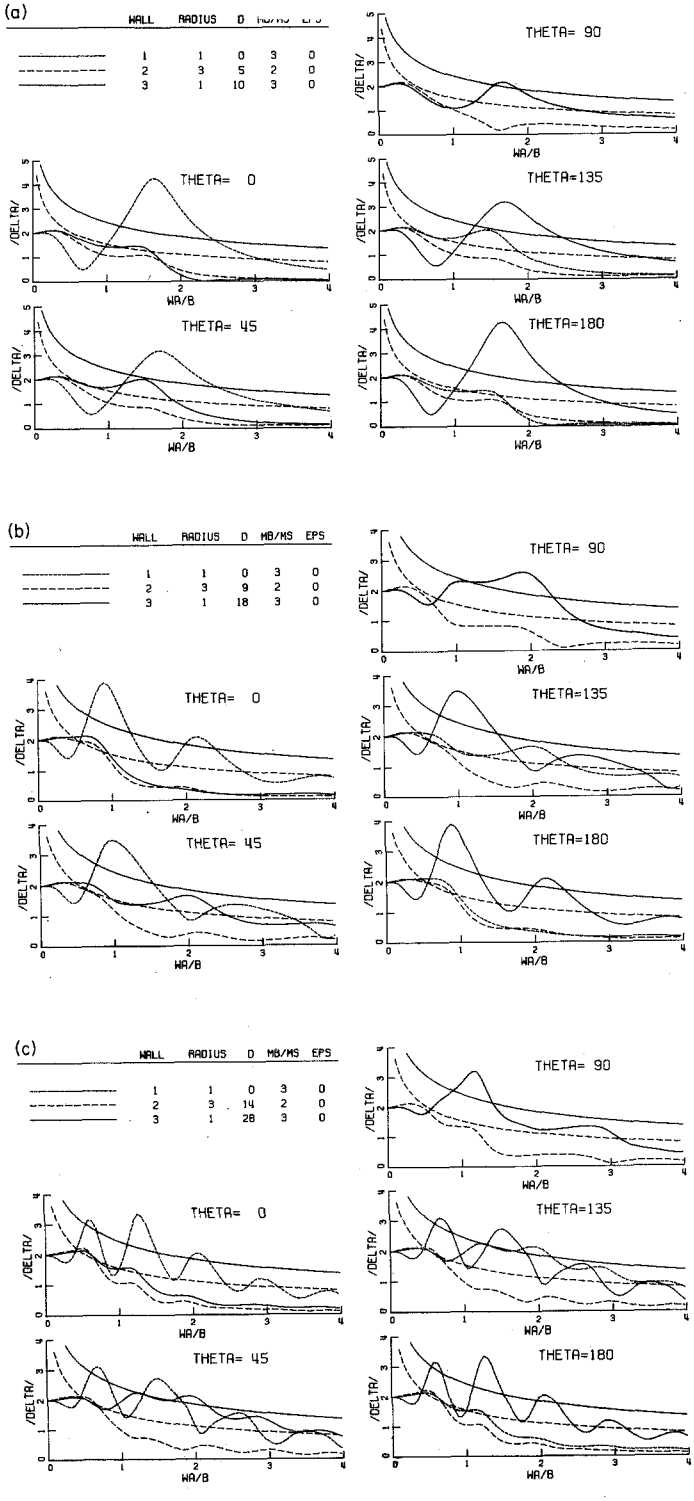

Figure 3-4.11 Foundation displacements of three structures with foundation size ratios of 1:3:1.

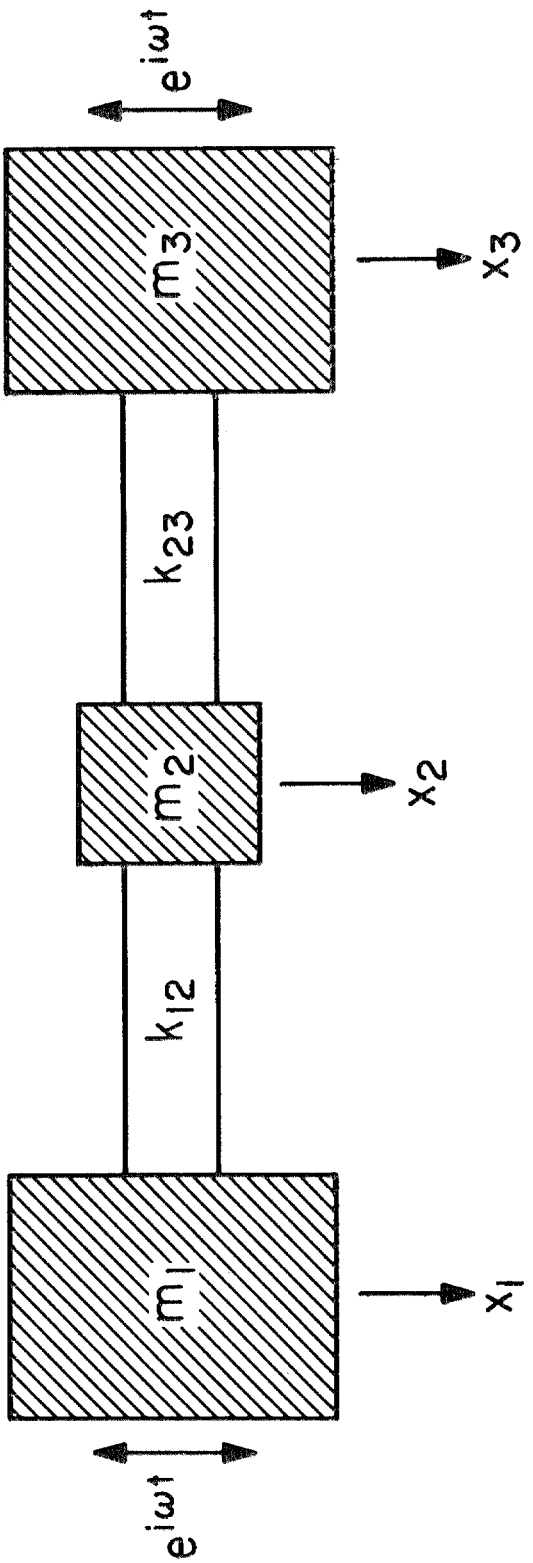

Figure 3-4.12 A simplified model of the three-structure system.

small, the excitation can be considered to be such that m_1 and m_3 are moving with displacement $e^{i\omega t}$ as shown in Figure 3-4.12. The "resonant frequency" of m_2 is therefore

$$\sqrt{\frac{k_{12} + k_{23}}{m_2}} \quad . \tag{3-4.14}$$

When excited at that particular frequency, the motion of m_2 would become unbounded. But again, in the two-dimensional model, scattering of waves from the semi-cylindrical foundations reduces the response amplitude. As the separation distances d_{12} and d_{13} increase, the "spring constants" k_{12} and k_{23} decrease, and by equation (3-4.14), the "resonant frequency" also decreases. Therefore, the simplified model shown in Figure 3-4.12 qualitatively explains the translation of the peaks shown in Figure 3-4.10a and 3-4.10b when d_{12} and d_{13} become large.

Another case of interest is when a large wall is surrounded by smaller walls. Figure 3-4.11 presents such an example for three walls with the middle wall three times larger than the two outside walls. The distances d_{12} and d_{13} are the same as those used in Figure 3-4.10. Now the middle wall "drives" the outside walls because of its weight and size, and a totally different situation arises. As may be seen in Figure 3-4.11, the response of the large middle wall is not greatly affected by the smaller outside walls. But the smaller walls behave as if they were interacting with the large wall alone, i.e., the small wall contributes very little to the behavior of the other small wall. For horizontally

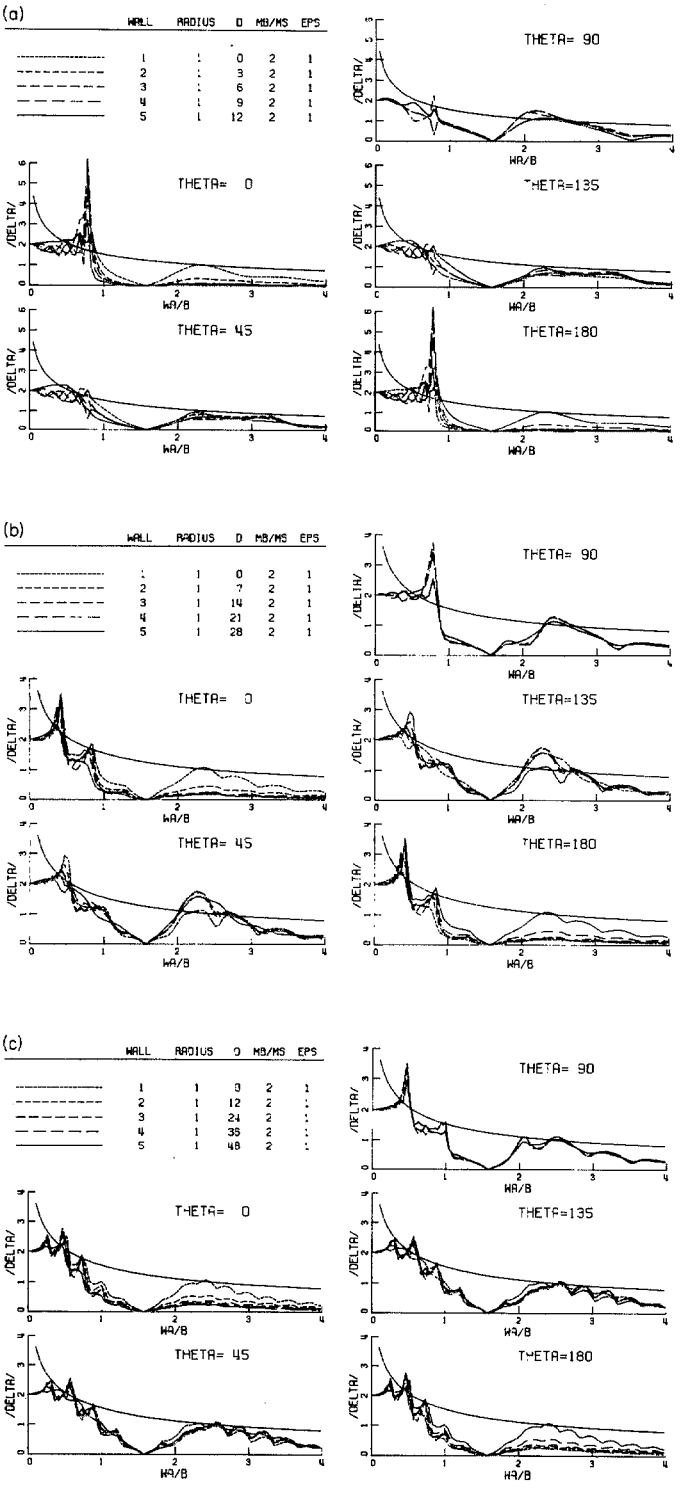

Figure 3-4.13 Foundation displacements of five identical and equally spaced structures.

incident waves, the response of the front wall is being amplified, while the back wall is being shielded. The large middle wall moves as if the other two are absent.

As indicated by the above analysis, the weight and size of the structure plays an important role in the interaction process. This suggests that there may be circumstances in which the smaller structures will receive the heavier "bombardment" of scattered waves from nearby larger buildings.

Large amplitudes of response can also arise when many buildings of comparable size are closely grouped. Figure 3-4.13 presents an arrangement of five identical foundations, all of which support a rigid wall. In this particular case, we find that the amplitude $|\Delta_p|$ can exceed the single foundation envelope given by equation (3-4.12) by more than 200%. We expect, however, that such building-to-building interaction effects will not be so prominent in three dimensions, because the geometrical radiative scattering of waves causes the "radiation damping" of the whole system to increase.

The Measurement of Earthquake Motions

In earthquake engineering the measurement of the base motion of structures as well as the free field motion is of interest. Considering the interaction effects discussed in the previous sections, the true measurement of the free field motions might be difficult to realize. As shown by the surface displacement plots (of Figures 3-4.6, 3-4.7, and 3-4.8), the amplitude of surface motion is greatly altered from the free field amplitude of 2. At some points, the displacements are near zero, while they are close to 4 at other locations. These rapid changes of displacement amplitudes are most evident for higher frequencies. The amplification of the surface displacement can be quite large even when caused by interaction at large distance, as shown, for example, in Figure 3-4.8.

An accelerogram recorded at the base of a structure may also be modified by the effects from neighboring large structures or structures of comparable size. As pointed out by Luco,[A168] such records may be filtered around the natural frequencies of the structure. From the discussion of the interaction of many foundations, it now appears that it is possible to have "resonant frequencies" caused by the specific arrangement of the surrounding buildings. This suggests that the "resonant frequency" of a large structure may also be recorded in surrounding smaller structures as it dominates the behavior of the others. This effect can be observed in Figure 3-4.4, where the parameters are $a_1 = 3$, $a_2 = 1$, $\epsilon_1 = 2$ and $\epsilon_2 = 2$. By using equation (3-4.11), the response curve $|\Delta_1|$ should go to zero at $\omega a_{max}/\beta = 3(2n+1)\pi/4$, $n = 0,1,2,\ldots$.

In Figures 3-4.4a and 3-4.4b, the curve $|\Delta_2|$ also dips down to an amplitude of almost zero at the resonant frequency of the wall No. 1. When the large structure acts as a shield for the small structure, as in the case of $\theta = 0°$ and 45° in Figure 3-4.4, the small structure moves with nearly the identical displacements as that of the large structure. Of course, this behavior begins to change when the wavelength of the incident wave is less than that of the separation distance. Therefore, from the above discussion, the effects caused by structure-soil-structure interaction may be quite important.

[3-5] THE EFFECT OF FOUNDATION SHAPE ON SOIL-STRUCTURE INTERACTION

The examples given in the previous sections have dealt with various effects on soil-structure interaction, all of which were represented by two-dimensional models compatible with circular or elliptical cylindrical coordinates. For more general foundation geometries, other than the ones described above, exact series solutions are either very difficult or intractable. In this section, in order to investigate further the effect of varying shapes, an approximate integral formulation is used.

For scattering of scalar waves in a homogeneous, isotropic medium, the scattered wave field, $w^{(s)}(\underset{\sim}{r})$, outside a surface can be obtained by superimposing the contribution from a distribution of wave sources located on the scatterer's outer surface. The integral representation of $w^{(s)}(\underset{\sim}{r})$ written in terms of the boundary sources, $w^{(s)}(\underset{\sim}{r}_o)$ and $\partial w^{(s)}(\underset{\sim}{r}_o)/\partial n_o$, is

$$w^{(s)}(\underset{\sim}{r}) = \iint_A \left[w^{(s)}(\underset{\sim}{r}_o) \frac{\partial G(\underset{\sim}{r}, \underset{\sim}{r}_o)}{\partial n_o} - G(\underset{\sim}{r}, r_o) \frac{\partial w^{(s)}(\underset{\sim}{r}_o)}{\partial n_o} \right] ds, \quad \underset{\sim}{r}_o \text{ on } A \qquad (3\text{-}5.1)$$

where $\underset{\sim}{r}_o$ on A implies that $\underset{\sim}{r}_o$ is the coordinate of the surface A [Mow and Pao (1971)]. In (3-5.1), $G(\underset{\sim}{r}, \underset{\sim}{r}_o)$ is the Green's function of the scalar wave equation and $\underset{\sim}{r}$ and $\underset{\sim}{r}_o$ are the observation and source points, respectively. Since the two-dimensional SH-waves satisfy the scalar wave equation, equation (3-5.1) applies directly to the two-dimensional anti-plane foundation model.

Because the boundary sources $w^{(s)}(\underset{\sim}{r}_o)$ and $\partial w^{(s)}(\underset{\sim}{r}_o)/\partial n_o$ are usually the unknowns, the unique solution is obtained by specifying the boundary values. In many applications, especially the ones considered in this chapter, the boundary conditions are prescribed to the total wave $w^{(t)} = w^{(s)} + w^{(i)}$, where $w^{(i)}$ is the incident wave. Therefore, it is convenient to add to (3-5.1) the integral representation of $w^{(i)}$,

$$\iint_A \left[G(\underset{\sim}{r}, \underset{\sim}{r}_o) \frac{\partial w^{(i)}(\underset{\sim}{r}_o)}{\partial n_o} - w^{(i)}(\underset{\sim}{r}_o) \frac{\partial G(\underset{\sim}{r}, \underset{\sim}{r}_o)}{\partial n_o} \right] ds_o = 0, \quad \underset{\sim}{r}_o \text{ on } A . \tag{3-5.2}$$

$w^{(i)}(\underset{\sim}{r}_o)$ satisfies the Helmholtz's first formula, equation (3-5.2), because it possesses no singularities inside the surface A. The addition of (3-5.2) to (3-5.1) yields the integral representation for $w^{(t)}$ as,

$$w^{(s)}(\underset{\sim}{r}) = \iint_A \left[G(\underset{\sim}{r}, \underset{\sim}{r}_o) \frac{\partial w^{(t)}(\underset{\sim}{r}_o)}{\partial n_o} - w^{(t)}(\underset{\sim}{r}_o) \frac{\partial G(\underset{\sim}{r}, \underset{\sim}{r}_o)}{\partial n_o} \right] ds . \tag{3-5.3}$$

Now, to obtain a solution for the boundary values, the observation point is made to approach the surface A, resulting in an integral equation for the unknown values, $w^{(t)}(\underset{\sim}{r}_o)$ and $\partial w^{(t)}(\underset{\sim}{r}_o)/\partial n_o$. Because $\partial G(\underset{\sim}{r}, \underset{\sim}{r}_o)/\partial n_o$ is discontinuous across the surface A, a limit must be taken as $\underset{\sim}{r} \to \underset{\sim}{r}_o$. For a smooth surface, equation (3-5.3) becomes the following as $\underset{\sim}{r} \to \underset{\sim}{r}_o$, [Mow and Pao (1971)],

$$\tfrac{1}{2}w^{(t)}(\underset{\sim}{r}) = w^{(i)}(\underset{\sim}{r}) + \iint_A \left[w^{(t)}(\underset{\sim}{r}_o) \frac{\partial G(\underset{\sim}{r}, \underset{\sim}{r}_o)}{\partial n_o} - G(\underset{\sim}{r}, \underset{\sim}{r}_o) \frac{\partial w^{(t)}(\underset{\sim}{r}_o)}{\partial n_o} \right] ds_o \quad \underset{\sim}{r} \text{ on } A \tag{3-5.4}$$

where $w^{(i)}(\underset{\sim}{r})$ is usually the known quantity.

The integral equation (3-5.4) can be solved exactly if the surface A is compatible with certain coordinate systems, such as the circular cylinder and elliptical cylinder. In these cases, the Green's function $G(\underset{\sim}{r}, \underset{\sim}{r}_o)$ can be expanded in series of orthogonal functions, such as Bessel function or Mathieu functions. Using the orthogonal properties of these special functions, the integral equation can be solved by the Hilbert-Schmidt method. The results are identical to those obtained by the method of separation of variables. However, the original difficulty concerning the geometry of the foundations is still not resolved; other means of solutions, such as various numerical methods, must now be employed.

Banaugh and Goldsmith (1963) obtained numerical solutions for wave scattering in an infinite medium by cylinders of arbitrary shape. Their approach was to replace the integrals of (3-5.4) by numerical quadrature formulas, so that they could be represented by a finite sum of discrete values of the integrand. The displacements $w^{(t)}(\underset{\sim}{r}_o)$ are then matched on a chosen number of points on the surface A, resulting in a set of simultaneous equations for the unknowns. These unknowns can usually be determined by conventional methods of numerical analysis.

Using the method of images as discussed in the beginning of this chapter, the scattering of scalar waves in the infinite space

can be adopted to analyze some problems in the semi-infinite space [Wong and Jennings (1975)]. Following the same analysis procedures as described in Chapter 2, i.e., by considering only the dynamics of the foundation, the boundary conditions for problems (i) and (ii) can be prescribed.

In determining the impedances of the foundations, the foundation is moved harmonically by one unit of displacement; in the absence of incident waves, therefore, the boundary conditions for the z-component of the displacement are

$$w_1^{(s)}(\underset{\sim}{r}_o) = w_1^{(t)}(\underset{\sim}{r}_o) = 1\, e^{i\omega t} \quad r_o \text{ on } A \tag{3-5.5a}$$

and

$$\left.\frac{\partial w_1^{(t)}(\underset{\sim}{r})}{\partial y}\right|_{y=0} = 0 \quad \underset{\sim}{r} \text{ on } c(A) \, . \tag{3-5.5b}$$

The latter condition is imposed for the free surface requirement of the half space, and it can be satisfied simply by taking $w_1^{(t)}(\underset{\sim}{r})$ to be symmetric about the x-axis. Using boundary condition (3-5.5a), the integral equation (3-5.4) for $\partial w_1^{(t)}(\underset{\sim}{r}_o)/\partial n_o$ simplifies to

$$\iint_A G(\underset{\sim}{r}, \underset{\sim}{r}_o) \frac{\partial w_1^{(t)}(\underset{\sim}{r}_o)}{\partial n_o} ds_o = \left[\iint \frac{\partial G(\underset{\sim}{r}, \underset{\sim}{r}_o)}{\partial n_o} ds_o - \tfrac{1}{2}\right], \quad \underset{\sim}{r} \text{ on } A \tag{3-5.6}$$

an integral equation for the unknown $\partial w_1^{(t)}(\underset{\sim}{r}_o)/\partial n_o$, which is proportional to the stress distribution over the surface A.

For the calculation of driving forces induced by the seismic excitation, the foundation is kept fixed while the incident wave is

included. Since the incident wave field $w^{(i)}$ in the half space consists of an incident wave plus a reflected wave, the free surface condition for the half space is automatically satisfied. Therefore, by assuming a distribution symmetric about the x-axis for the unknown $w_2^{(s)}(\underset{\sim}{r}_o)$, the only remaining boundary condition is at the foundation surface,

$$w_2^{(t)}(\underset{\sim}{r}_o) = w^{(i)}(\underset{\sim}{r}_o) + w_2^{(s)}(\underset{\sim}{r}_o) = 0, \quad \underset{\sim}{r}_o \text{ on } A . \tag{3-5.7}$$

To satisfy (3-5.7), $w_2^{(t)}$ is set to zero in equation (3-5.4), and an integral equation again results for the normal gradient $\partial w_2^{(t)}/\partial n_o$,

$$\iint_A G(\underset{\sim}{r}, \underset{\sim}{r}_o) \frac{\partial w_2^{(t)}(\underset{\sim}{r}_o)}{\partial n_o} ds = w^{(i)}(\underset{\sim}{r}), \quad \underset{\sim}{r} \text{ on } A . \tag{3-5.8}$$

After the solution of the stress distribution $\sigma_{nz} = \mu_s \frac{\partial w^{(t)}}{\partial n_o}$ on the surface of the foundation is available, the impedance and the driving force can be calculated from

$$\frac{K_s}{\mu_s} = -\tfrac{1}{2} \iint_A \frac{\partial w_1^{(t)}(\underset{\sim}{r}_o)}{\partial n_o} ds_o \tag{3-5.9}$$

$$\frac{F_s^*}{\mu_s} = -\tfrac{1}{2} \iint_A \frac{\partial w_2^{(t)}(\underset{\sim}{r}_o)}{\partial n_o} ds_o , \tag{3-5.10}$$

respectively. The factor of $\frac{1}{2}$ is used because the foundation surface covers only half the area of the mathematically symmetrical wave scatterer.

Proceeding with the analysis, the integral equations (3-5.6) and (3-5.8) can be solved by the point matching technique. Using this technique for an assumed distribution of $\partial w^{(t)}(\underset{\sim}{r}_o)/\partial n_o$, the integral is matched with the given condition on the right hand side for a selected number of points only. Of course, the solution becomes more accurate if the number of matched points increases.

To evaluate the integral, it is convenient to parameterize the coordinate system. For an infinitely long cylinder, the surface area per unit length can be described by just one parameter. By introducing the parameter ϕ such that

$$\begin{cases} x = x(\phi) \\ y = y(\phi) , \end{cases} \tag{3-5.11}$$

the element of surface area per unit length is

$$ds_o = \sqrt{\left(\frac{dx}{d\phi}\right)^2 + \left(\frac{dy}{d\phi}\right)^2}\, d\phi = S_\phi d\phi . \tag{3-5.12}$$

Since the Green's function $G(\underset{\sim}{r}, \underset{\sim}{r}_o)$ for the two-dimensional scalar wave equation is $\frac{i}{4} H_o^{(2)}(k|\underset{\sim}{r} - \underset{\sim}{r}_o|)$, the Hankel function of the second kind, the left hand side of the equations (3-5.6) and (3-5.8) can be replaced by

$$\iint_A G(\underset{\sim}{r}, \underset{\sim}{r}_o) \frac{\partial w^{(t)}(\underset{\sim}{r}_o)}{\partial n_o} ds_o = \frac{i}{4} \int_o^{2\pi} H_o^{(2)}(k|\underset{\sim}{r} - \underset{\sim}{r}_o|) \frac{\partial w^{(t)}(\phi)}{\partial n_o} S_\phi d\phi . \tag{3-5.13}$$

The new integral can be evaluated numerically if the distribution $\partial w^{(t)}(\underset{\sim}{r_o})/\partial n_o$ is assumed; also, the logarithmic singularity of the Green's Function as $\underset{\sim}{r} \rightarrow \underset{\sim}{r_o}$ must be evaluated by a special method discussed by Banaugh and Goldsmith (1963).

The function $\partial w^{(t)}/\partial n_o$ also possesses singularities if the wave scattering object has sharp corners, and the numerical solution may become very difficult. However, it was shown by Shafai (1971) that $\partial w^{(t)}(\phi)/\partial n_o$ would have a singularity of the type $1/S_\phi$. Therefore, the quantity $\left[\frac{\partial w^{(t)}(\phi)}{\partial n_o} S_\phi\right]$ is smooth and can be determined more easily. Hence, it is advantageous to consider $\left[\frac{\partial w^{(t)}(\phi)}{\partial n_o} S_\phi\right]$ as the unknown because K_s/μ_s and F_s^*/μ_s are also expressed by the integrals whose integrands represent the stress. Therefore, with this new variable one can write

$$\iint_A \frac{\partial w^{(t)}(\underset{\sim}{r_o})}{\partial n_o} ds = \int_o^{2\pi} \left[\frac{\partial w^{(t)}(\phi)}{\partial n_o} S_\phi\right] d\phi \qquad (3\text{-}5.14)$$

Equation (3-5.14) brings out the fact that the total forces on the foundation do not change appreciably if the shape of the foundation changes by a small degree. This is not true for the stress distribution $\mu\partial w^{(t)}(\phi)/\partial n$, however, because it is sensitive to the local change of slopes. In other words, the assumption that the foundation is rigid has effectively eliminated the influence of detailed geometries and acts as a smoothing operation.

To obtain numerical results, assume that the unknown variable can be expressed by a finite Fourier series as follows

$$\left[\frac{\partial w_{\ell}^{(t)}(\phi_j)}{\partial n_o}\right] S_{\phi} = \sum_{j=0}^{N} b_j^{\ell} \cos j\phi_o \qquad (3\text{-}5.15)$$

where b_j^{ℓ} ($\ell = 1, 2$) are unknown coefficients for the problems (i) and (ii). Here, the cosine functions have been chosen to satisfy the symmetry requirement. Using (3-5.13) and (3-5.15), the integral equations (3-5.6) and (3-5.8) become

$$\sum_{j=0}^{N} b_j^{\ell} \left\{ \int_o^{2\pi} H_0^{(2)}(k|r(\phi) - r(\phi_o|) \cos j\phi_o d\phi_o \right\}$$

$$= \begin{cases} \left[\int_o^{2\pi} \frac{ik}{4} H_1^{(2)}(k|r(\phi) - r(\phi_o)| \frac{\partial |w(\phi) - r(\phi_o)|}{\partial n_o} d\phi_o - \frac{1}{2} \right] & (3\text{-}5.16) \\ u^{(i)}(\phi) & (3\text{-}5.17) \end{cases}$$

respectively. For N chosen values of ϕ on the boundary, (3-5.16) and (3-5.17) constitute N equations for the N unknown Fourier coefficients b_j^{ℓ} for each $\ell = 1, 2$.

Since the variable $\left[\frac{\partial w^{(t)}(\phi_o)}{\partial n_o} S_{\phi}\right]$ is quite smooth, the Fourier coefficients b_j^{ℓ} diminish rapidly. Further consideration of (3-5.14) and (3-5.15) shows that

$$-\frac{1}{2} \int_o^{2\pi} \left[\frac{\partial w^{(t)}(\phi_o)}{\partial n_o} S_{\phi}\right] d\phi_o = -\pi b_o \qquad (3\text{-}5.18)$$

because all higher harmonics integrate to zero. Equation (3-5.18) again indicates the smoothing effect of a rigid foundation, because

the contribution of the zeroth harmonic is smaller for higher frequencies. Therefore, the coefficients b_0^{ℓ} would be smaller due to the fact that most of the energy is radiated away.

The Influence of Small Differences of Foundation Geometry on Its Interaction with the Soil

We now consider the rectangular foundation. Although its geometry fits nicely with the cartesian coordinates, the exterior wave scattering problem cannot be solved exactly because the boundary conditions involve both independent variables x and y. However, the numerical values for the compliances and driving forces can be obtained readily by the method described above. They should be interesting to compare with the elliptical foundation because of the similarity in the overall dimensions. In Section [3.2], it was noted that the "radiation" damping is directly proportional to the area of the scattering surface. Therefore, the comparison of these two cases has been performed by equating the perimeter of the two cross sections.

The special case of the semi-circular foundation and the rectangular foundation with a height to width ratio of $\frac{1}{2}$ has been compared first. The numerical results for both foundation shapes are tabulated in Table 3-5.1a. The format of the numbers tabulated is (REAL PART, IMAGINARY PART). The imaginary part compares well, within a few percent, as would be expected, because the two surface areas are identical. Thus, the "smoothing" effect of the rigid foundation is displayed clearly, and the detailed foundation shape apparently does not affect the total force appreciably. The real part of the two cases deviates at higher frequencies. This is possibly due to the numerical errors created while the complex matrix equation is solved numerically. The numerical errors are

TABLE 3-5.1a

COMPARISON OF IMPEDANCE FUNCTIONS

$\omega A/B$	Exact Solution Semi-Circle	Appr. Solution Half-Square
0.20	(1.08, .931)	(1.06, .885)
0.40	(1.24, 1.55)	(1.20, 1.47)
0.80	(1.38, 2.76)	(1.30, 2.62)
1.20	(1.45, 3.98)	(1.31, 3.80)
1.60	(1.48, 5.21)	(1.24, 5.02)
2.00	(1.51, 6.44)	(1.15, 6.35)
2.40	(1.52, 7.68)	(1.17, 7.59)
2.80	(1.53, 8.90)	(1.18, 8.90)
3.20	(1.54, 10.2)	(1.22, 10.1)
4.00	(1.55, 12.7)	(1.26, 12.7)

TABLE 3-5.1b

COMPARISON OF THE DRIVING FORCES

$\frac{\omega\alpha}{\beta}$	Circle (EXACT) All Angles	$\theta = 0°$	$\theta = 30°$	$\theta = 60°$	$\theta = 90°$
0.2	(2.01, 1.84)	(2.00, 1.75)	(2.00, 1.75)	(2.00, 1.75)	(2.00, 1.75)
0.4	(1.88, 2.98)	(1.93, 2.84)	(1.93, 2.84)	(1.93, 2.84)	(1.93, 2.84)
0.8	(0.48, 4.68)	(0.74, 4.51)	(0.75, 4.51)	(0.75, 4.51)	(0.74, +4.50)
1.2	(-1.82, 5.34)	(-1.30, 5.35)	(-1.28, 5.40)	(-1.29, 5.37)	(-1.32, +5.30)
1.6	(-4.38, 4.74)	(-3.76, 5.04)	(-3.71, 5.23)	(-3.69, 5.17)	(-3.72, 4.41)
2.0	(-6.57, 2.88)	(-5.96, 3.45)	(-5.99, 4.12)	(-5.97, 4.06)	(-5.93, 3.33)
2.4	(-7.84, 0.0385)	(-7.85, 0.926)	(-7.60, 2.01)	(-7.56, 1.90)	(-7.75, 0.721)
2.8	(-7.78, -3.30)	(-8.67, -2.25)	(-8.29, -2.520)	(-8.21, -0.690)	(-8.50, -2.50)
3.2	(-6.24, -6.51)	(-8.02, -6.41)	(-7.58, -3.20)	(-7.46, -3.31)	(-7.76, -6.57)
3.6	(-3.37, -8.94)	(-6.11, -10.1)	(-6.07, -5.55)	(-5.90, -5.64)	(-5.74, -10.2)
4.0	(0.429, -10.1)	(-2.82, -13.0)	(-3.68, -7.12)	(-3.46, -7.19)	(-2.37, -12.9)

usually accumulated in the real part as the imaginary part becomes an order of magnitude larger.

Our attention is next turned to the comparison of the driving force induced by seismic excitation on a rectangular foundation and a semi-circular foundation. The exact solutions of the semi-circular foundation presented by Luco[A168] and Trifunac[A169] are both for the plane wave excitation. Therefore, to draw an analogy, a plane SH-wave with an angle of incidence θ is again assumed. The total incident wave motion $w^{(i)}(\underset{\sim}{r})$ in the half space is then

$$w^{(i)}[x(\phi), y(\phi)] = 2u_o \ell^{i\frac{\omega}{\beta}x(\phi)\cos\theta} \cos\left[\frac{\omega}{\beta} y(\phi) \sin\theta\right] , \quad (3\text{-}5.19)$$

and it makes up the right hand side of equation (3-5.8). The driving forces were calculated for four angles of incidence, $\theta = 0°$, $30°, 60°$, and $90°$, and are tabulated in Table 3-5.1b. Also tabulated in the second column of Table 3-5.1b is the driving force on the semi-circular foundation, which was shown by Trifunac[A169] to be independent of the angle of incidence. The differences in this case are again negligible for dimensionless frequencies of less than about two. The numerical error is not important in this case because both the real and imaginary parts are of the same order.

Another case of interest is when the height to width ratio is 3/2. Though the perimeter is again equated to yield the same surface area, the differences in geometry and slopes become more distinct than for the previous comparison. Impedances and driving

forces for these two foundation shapes are plotted in Figures 3-5.1 and 3-5.2, respectively.

The difference between the two cases for the driving forces becomes noticeable, especially at higher frequencies where the deviation is great. This can be explained by the greater sensitivity of waves to the geometries when the wavelength is of a comparable size with the foundation. Since the dimensionless frequencies are based on the width of the foundation, the frequencies considered here are actually higher than the case tabulated in Table 3.1. Figure 3-5.2 also shows that driving forces for a rectangular foundation are dependent on the angle of incidence θ. The vertically incident wave, for example, resulted in the greatest scattering because it arrived in the direction of the major axis.

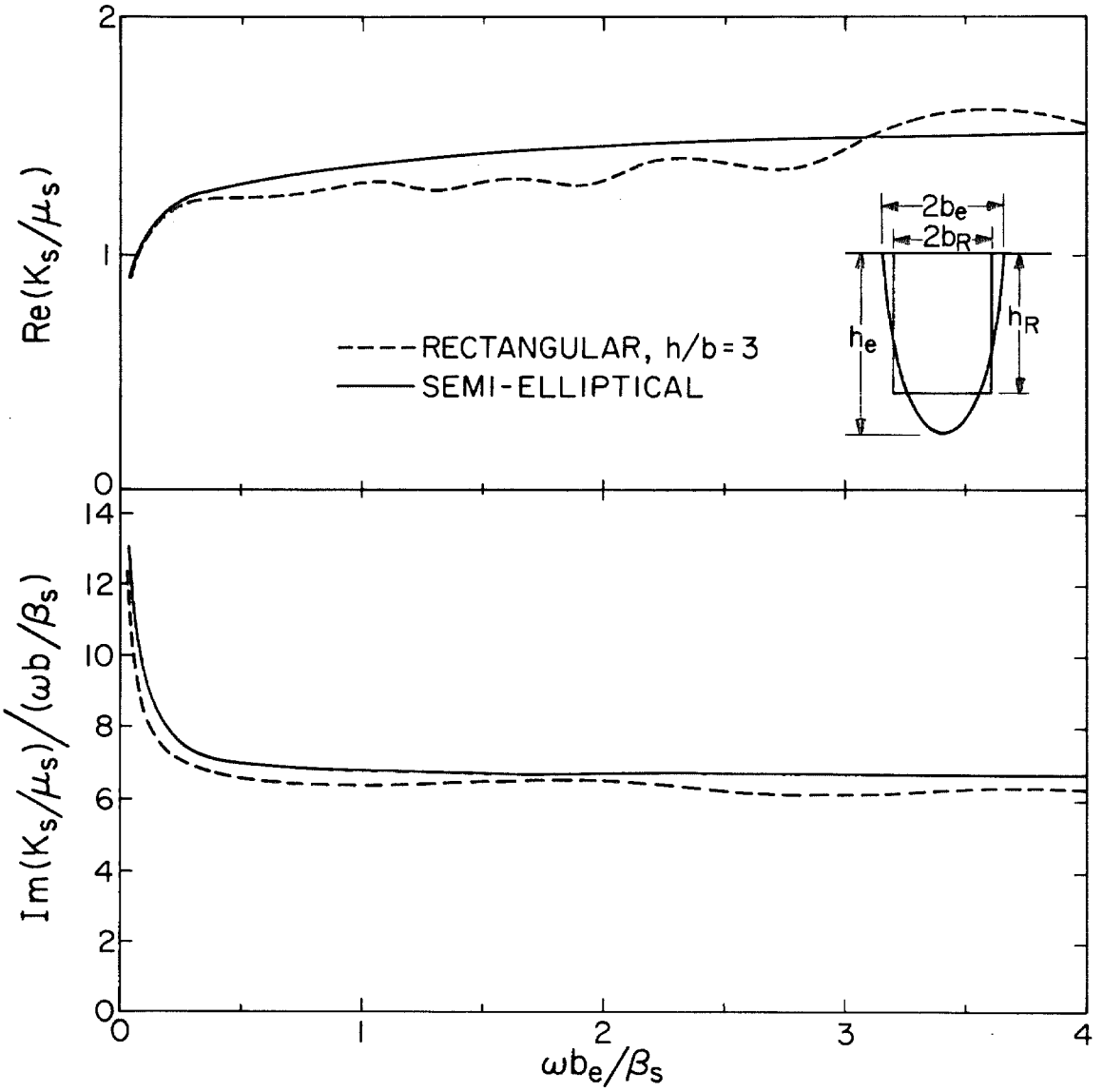

Figure 3-5.1 Comparison of the longitudinal impedance functions for a rectangular foundation and its equivalent elliptical foundation.

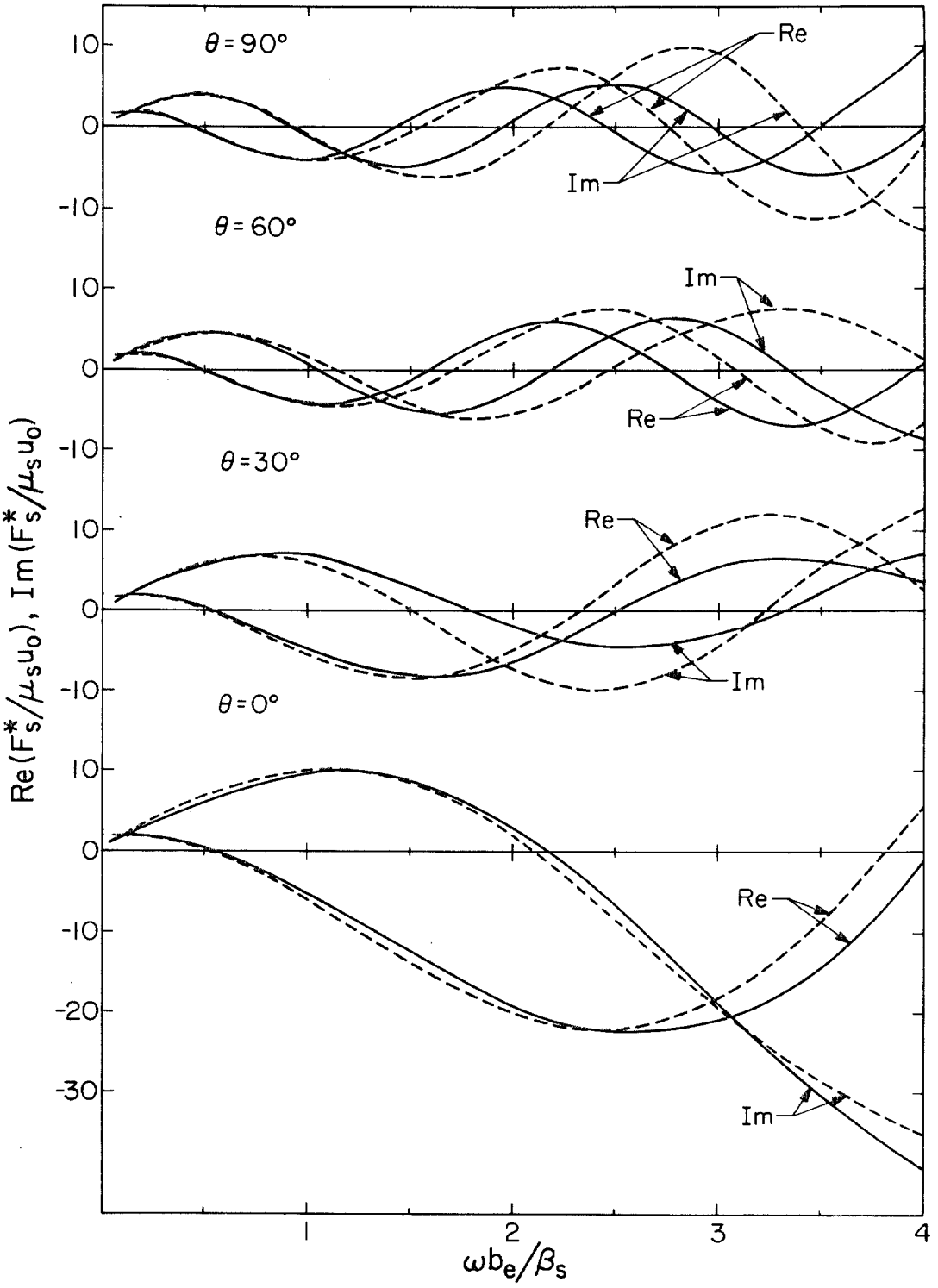

Figure 3-5.2 Comparison of the longitudinal driving forces for a rectangular foundation and its equivalent elliptical foundation.

[3-6] THE EFFECTS CAUSED BY AN ENCLOSED SOIL MEDIUM

As discussed previously in Section [1-2], most finite element programs for soil-structure interaction consist of a layered or homogeneous medium enclosed by an arbitrary boundary. The input of seismic excitation is made through the shaking of the outer boundary. This set-up can introduce into the analysis some unwanted reflections and standing wave patterns. Since all of the energy is trapped in the enclosed medium, the "radiation" type of damping cannot be accounted for. Therefore, artificial material damping is usually introduced into the finite element models to dissipate this trapped energy and, thus, hopefully to model approximately the semi-infinite medium.

Luco, Hadjian and Bos[A79] investigated this problem by comparing the exact solution of a rigid strip foundation to an approximate solution obtained by finite elements. The two-dimensional finite element model consisted of a rigid strip over an enclosed rectangular box. The size of the box was also varied to gain additional insight into the problem. The results they presented indicated that the modeling by a finite medium possesses characteristics which are entirely different from those of the half space, and that the difference is most pronounced for the symmetric vertical excitation. The unfortunate consequence of these approximations is the overestimation of the effective soil stiffness, which leads to the underestimation of response. Therefore, the solution which is based on a bounded finite element approach may not yield a conservative response estimate.

In this section, the characteristics of the foundation impedances for an enclosed medium are investigated by using an exact solution, so that various approximations made by the finite element approach can be eliminated.

We consider the anti-plane model illustrated in Figure 3-6.1. It consists of an infinitely long foundation with a semi-circular cross section of radius a_1. This foundation is embedded in a soil medium bounded by a rigid circular boundary of radius a_2. This configuration allows a simple exact solution for the longitudinal displacements.

Since the longitudinal displacement w satisfies the two-dimensional wave equation in polar coordinates, the harmonic displacement field in the soil medium has the form:

$$w(r, \phi) = \sum_{n=0}^{\infty} [a_n J_n(kr) + b_n Y_n(kr)][\cos n\phi + c_n \sin n\phi] \quad (3\text{-}6.1)$$

where k is the wave number in the soil and J_n and Y_n are Bessel functions of the 1st and 2nd kind, respectively. To calculate the impedance function for this foundation, we impose the following boundary conditions:

(i) the "free"condition for the soil surface:

$$\frac{\partial w}{\partial \phi}\Big|_{\phi=0,\pi} = 0 \quad (3\text{-}6.2)$$

(ii) a unit amplitude excitation by the foundation:

$$w(a_1, \phi) = 1e^{i\omega t} \quad (3\text{-}6.3)$$

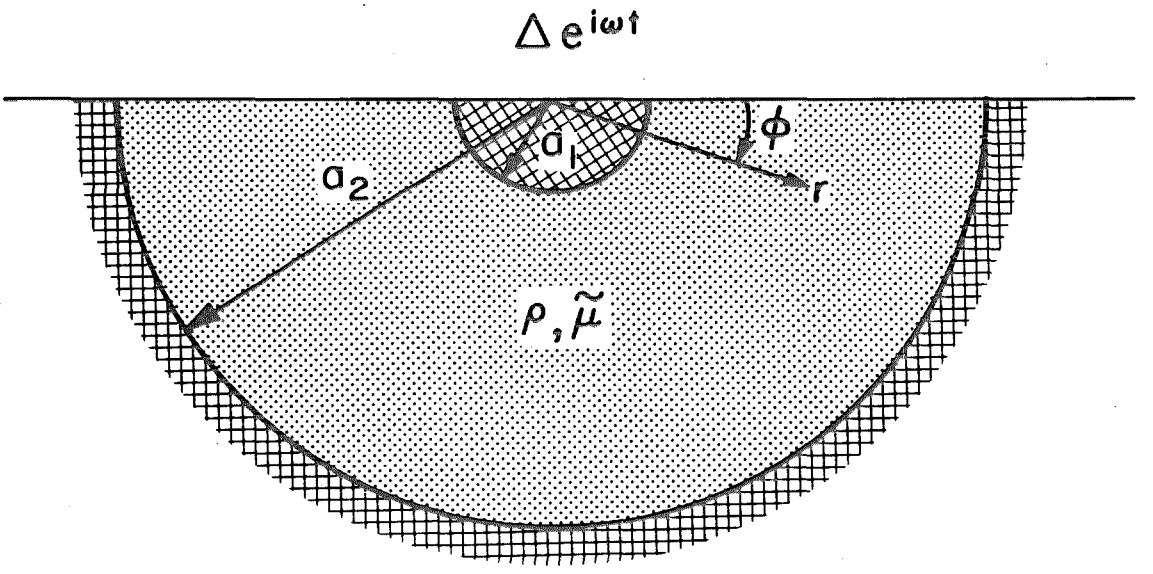

Figure 3-6.1 Circular foundation placed on a bounded soil medium.

(iii) the "fixed" condition at outer boundary:

$$w(a_2, \phi) = 0 \ . \tag{3-6.4}$$

Boundary condition (i) eliminated the unknown constants, $c_n = 0$, $n = 1, 2, \ldots$. Boundary conditions (ii) and (iii) lead to a solution for the coefficients, a_n, b_n, which are given by

$$a_0 = Y_0(ka_2)/D \ ; \qquad a_n = 0 \ , \qquad n = 1, 2, \ldots \tag{3-6.5}$$

$$b_0 = -J_0(ka_2)/D; \qquad b_n = 0 \ , \qquad n = 1, 2, \ldots \tag{3-6.6}$$

where

$$D = J_0(ka_1)\,Y_0(ka_2) - J_0(ka_2)\,Y_0(ka_1) \ .$$

Therefore, all harmonics drop out except for the zeroth. The displacement in the soil medium is then

$$w(r, \phi) = \frac{Y_0(ka_2)\,J_0(kr) - J_0(ka_2)\,Y_0(kr)}{D} \ , \tag{3-6.7}$$

and the impedance K^B is just the force exerted on the foundation by the soil,

$$K^B = -\int_{-\pi}^{\circ} \mu \frac{\partial w}{\partial r}\Big|_{r=a_1} a_1 d\phi = \mu\pi k a_1 [Y_0(ka_2)J_1(ka_1) - J_0(ka_2)Y_1(ka_1)]/D \tag{3-6.8}$$

For comparison with (3-6.8), the solution for the half space problem is

$$K^{HS} = \mu\pi k a_1 \frac{H_1^{(2)}(ka_1)}{H_0^{(2)}(ka_1)} \tag{3-6.9}$$

where $H_n^{(2)} = J_n - iY_n$ is the Hankel's function of the second kind, which represents diverging waves.

An immediate comparison of these results is that K^B is real, while K^{HS} is complex. Since the imaginary part of the impedance represents the energy dissipation, there exists no damping for the former case, because all of the radiated energy is totally reflected back from $r = a_2$. It should be pointed out that the amount of this reflected energy does not depend on the size of the enclosed medium, a_2.

The asymptotic amplitude of the Bessel functions for large arguments r decays as $1/\sqrt{r}$ [Abramowitz and Stegun (1971)], therefore, the corresponding wave energy is proportional to $1/r$ as $r \to \infty$. However, the total reflected energy at the outer boundary is

$$E^T \propto \int_0^{2\pi} \left(\frac{1}{\sqrt{a_2}}\right)^2 a_2 d\phi = \text{constant} , \qquad (3\text{-}6.10)$$

and thus is not dependent on the distance of the outer boundary a_2. Therefore, no energy dissipation is possible and, as a result, the converging waves from the outer boundary cause constructuve or destructive interference with the diverging waves from the foundation. The constructive interference will cause resonance within the soil medium, which can result in large amplitudes for low level excitation. The destructive interference, however, will tend to overestimate the stiffness of the soil medium if the foundation lies near a node in the standing wave pattern.

One possible way of introducing the damping into the bounded soil medium is to assume the soil to be viscoelastic. Following Veletsos and Verbic,[A145] the shear modulus $\tilde{\mu}$ of a viscoelastic material may be expressed as a complex quantity in terms of the real shear modulus and a damping coefficient. There are also several types of viscoelastic materials. For a viscous solid, $\tilde{\mu}_1 = \mu(1 + i\delta)$, while for a Voigt solid, $\tilde{\mu}_2 = \mu(1 + ia_0\xi)$, where $a_0 = ka_1 = \omega a_1/\beta$ is the dimensionless frequency; δ and ξ are damping coefficients.

The two types of viscoelastic materials defined above will now be used for the investigation of the material's dissipation of energy. Since the shear wave velocity is related to the shear modulus as $\tilde{\beta} = \sqrt{\tilde{\mu}/\rho}$, the dimensionless frequency can be expressed as

$$\tilde{a}_0^1 = \tilde{k}_1 a_1 = \frac{a_0}{\sqrt{1 + i\delta}} \quad \text{for viscous solid} \qquad (3\text{-}6.11)$$

and as

$$\tilde{a}_0^2 = \tilde{k}_2 a_1 = \frac{a_0}{\sqrt{1 + ia_0\xi}} \qquad (3\text{-}6.12)$$

for the Voigt solid. Substituting the complex frequency $\tilde{a}_0^1$ into equation (3-6.8), the value of K^B is now complex because the Bessel functions have complex arguments.

To compare these different phenomena caused by the material damping to those of radiative damping, the impedance functions are plotted versus the real dimensionless frequency, a_0, in Figures 3-6.2 for a viscous solid and in Figure 3-6.3 for a Voigt solid.

Each figure includes the ratios, $a_2/a_1 = 5$ and 10, so that the effect of the medium size can be studied. Also, five values of damping, δ or ξ equal to 0, 0.1, 0.25, 0.5, and 1, are shown, each one distinguished by a different dashed line.

Comparing these results, it is seen that the characteristics of K^B are far from those of K^{HS}, especially at low frequencies. The static impedance of the enclosed medium is always larger because of the additional restraint nearby. This restraint relaxes as a_2/a_1 becomes larger, as shown in Figures 3-6.2 and 3-6.3. For the dynamic impedances, K^B is generally oscillatory. The number of oscillations increases as a_2/a_1 increases. Therefore, as the outer boundary moves further away, the order of the mode shapes in the enclosed medium becomes higher for the same a_0.

Let us consider the undamped cases, i.e., ξ or $\delta = 0$. The impedance function has unbounded amplitudes at certain frequencies, while at some other frequencies its value is equal to zero. For the former case, the foundation lies on a node of the standing wave pattern where the resistance of the soil medium is equal in magnitude but opposite in direction to the input force; hence, the foundation has infinite rigidity and the motion is zero. For the latter case, the resistance is zero; therefore, the motion is undefined at these resonant frequencies as the waves constructively combine.

The introduction of damping into the material smooths out the large amplitude oscillation and contributes to the imaginary part of the impedance. However, the general characteristic is still far from that for the half space solution, even for large values of

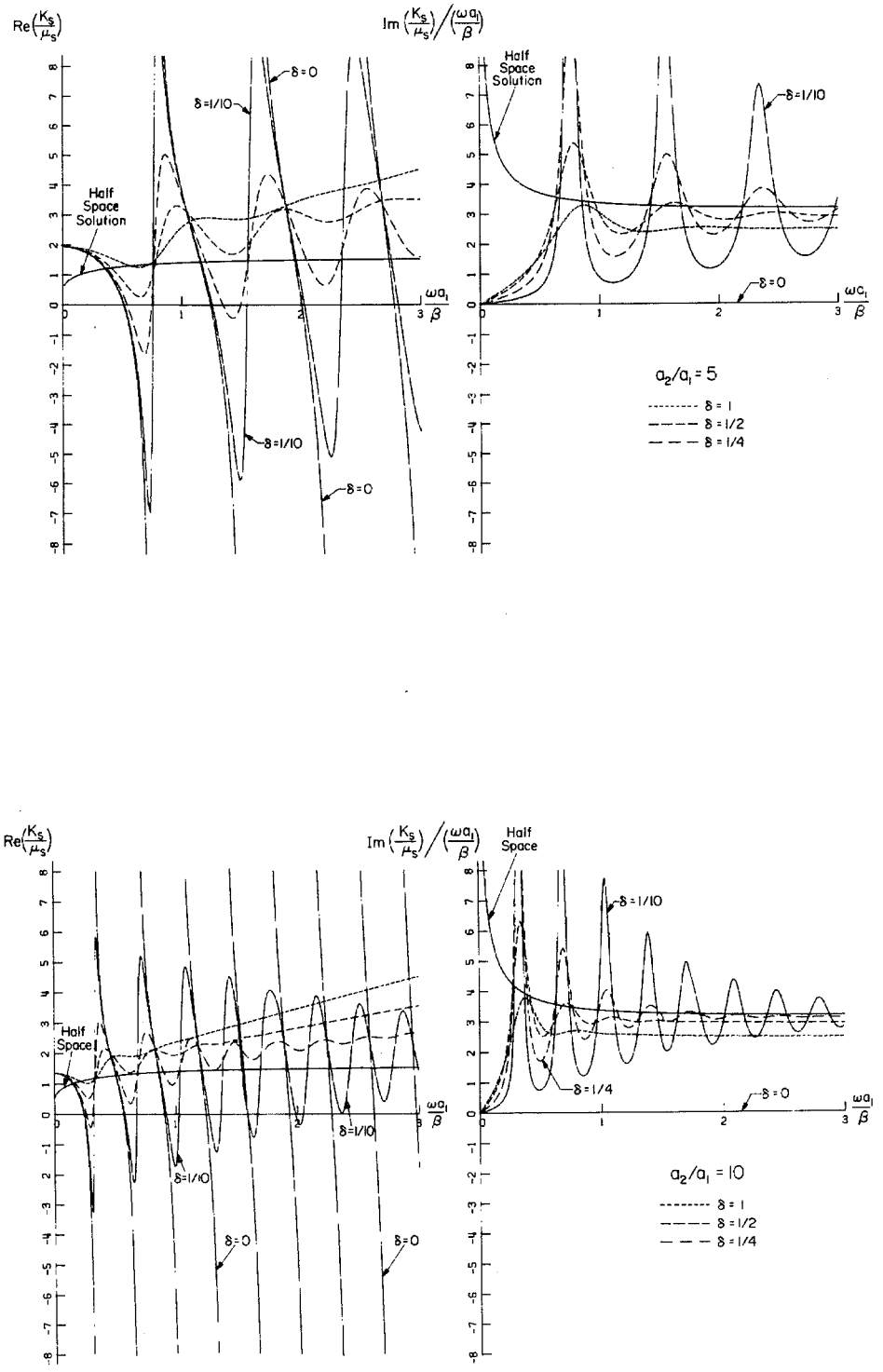

Figure 3-6.2 Comparison of the longitudinal impedance functions: Viscous soil model.

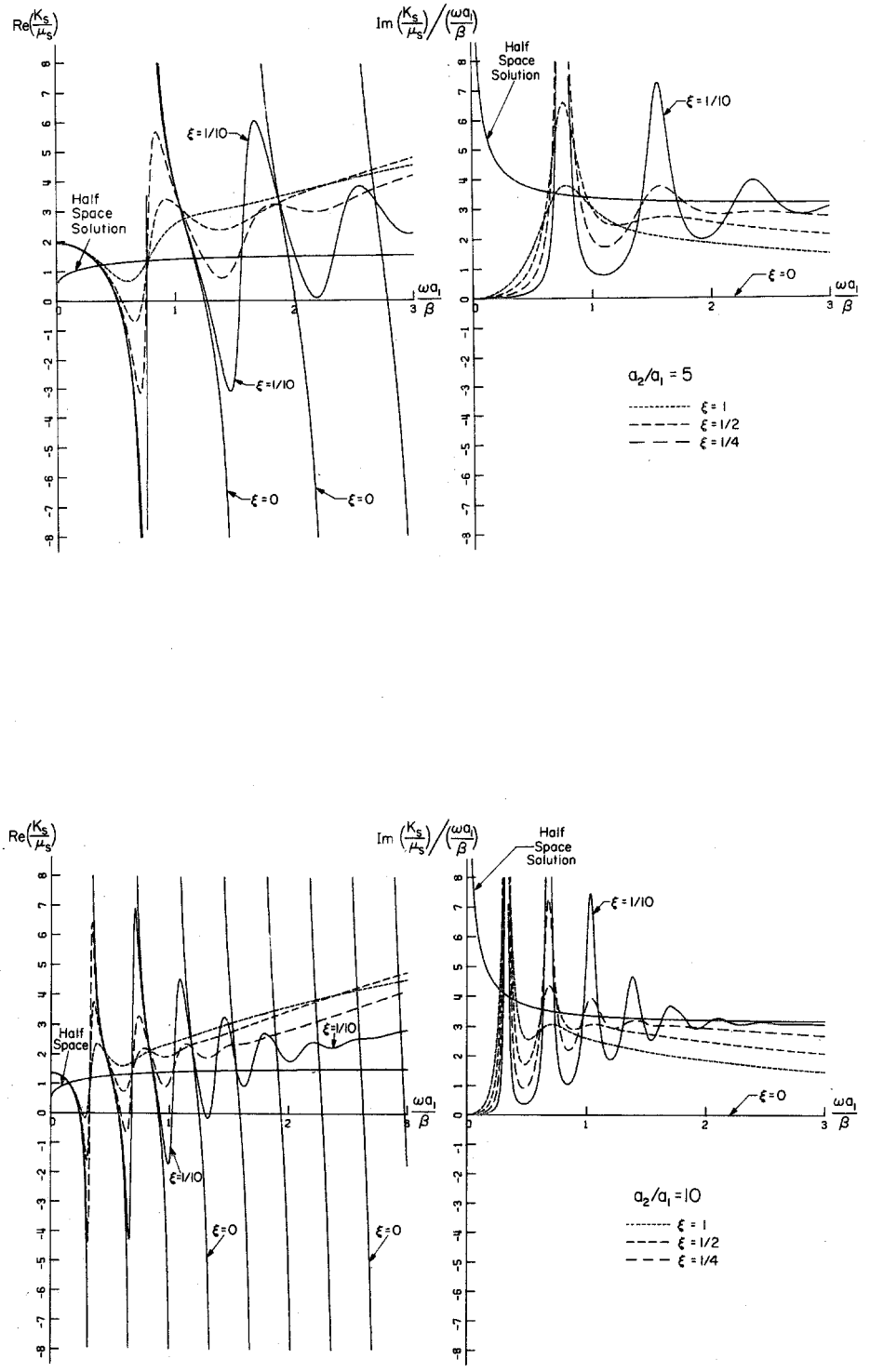

Figure 3-6.3 Comparison of the longitudinal impedance functions: Voigt soil model.

damping. There are no simple trends that explain the effect of the different types of material damping except that the oscillation is smoothed out much quicker for the Voigt solid as a_o increases.

For the lower frequency range which is of special importance for earthquake engineering, the imaginary part of the impedance is near zero, contrary to the large values of the half space solution. The Voigt solid model uses a shear modulus that depends on frequencies, but this helps only to damp out the oscillation of the impedance curve more at high frequencies. Otherwise, there is not much difference when it is compared with the viscous solid. Therefore, one might conclude that the harmonic behavior of a bounded medium is not the same as that of the semi-infinite medium because the waves cannot propagate outwards. This feature has a marked influence with steady state response to harmonic excitation.

CHAPTER IV - THREE-DIMENSIONAL FOUNDATION MODELS

[4-1] AN INTEGRAL FORMULATION FOR THE MIXED BOUNDARY VALUE PROBLEM

The nature of soil-structure interaction phenomena in two dimensions was discussed in Chapter III. The results indicate that soil-structure interaction may have important effects on the computation of complete structural response. Experimental evidence of these phenomena has been presented by Foutch et al. (1975). The full scale testing of a nine-story building has indicated that interaction contributed to at least 30% of the total deflection at the roof of the structure. Therefore, the design and analysis of important structures should not disregard the aspect of soil-structure interaction.

However, for the introduction of the soil-structure interaction computations into engineering design, three-dimensional models must be developed, because of the limitations of two-dimensional approximations [Luco and Hadjian (A78)].

But, as described in Section [3-1], the solution of this boundary value problem in the half space is difficult to obtain due to the conversion of longitudinal and shear wave modes. Since the boundary conditions are usually prescribed on the second space derivative of the potentials, the method of images cannot be applied here. As a result, only a few three-dimensional models have been successfully analyzed, most of which were reviewed in Section [1-2].

Because of the practical importance of the three-dimensional soil-foundation interaction, this chapter is devoted to the development of a general method which is capable of numerically calculating the impedances and "driving forces" for a flat foundation of an arbitrary shape. This method is a direct analog to the two-dimensional scheme discussed in Section [3-5].

In constructing a mathematical model for a three-dimensional foundation placed on top or within a half space, a mixed boundary value problem results. The half space surface outside the foundation is considered to be "traction free," while the compatibility of displacements is prescribed under the foundation. If this problem is posed in the framework of linear theory, the principle of superposition can be used effectively. Utilizing the Green's function on the surface of the half space, the displacements everywhere can be expressed in terms of the unknown traction via an integral formula. This representation thus results in an integral equation for the unknown surface tractions.

Superposition of Point Loads

Consider now a harmonic point load, $\underset{\sim}{P} = [P_1, P_2, P_3]e^{i\omega t}$, acting on the free surface of a half space which is composed of linear materials. The notation is such that P_3 is the normal component, while P_1 and P_2 are the tangential components in the x_1 and x_2 directions, respectively. Using a Green's function matrix, $\underset{\approx}{G}$, the resulting displacement, $\underset{\sim}{u}$, at $\underset{\sim}{x}$ is related to the exciting force $\underset{\sim}{P}$ at $\underset{\sim}{x}_0$ by

$$\underset{\sim}{u}(\underset{\sim}{x})\, e^{i\omega t} = \underset{\approx}{G}(\omega, \underset{\sim}{x} - \underset{\sim}{x}_0)\underset{\sim}{P}(\underset{\sim}{x}_0)\, e^{i\omega t} \qquad (4\text{-}1.1)$$

The elements of the matrix $\underset{\approx}{G}$, $g_{\ell m}(\omega, \underset{\sim}{x} - \underset{\sim}{x}_0)$, relate the ℓth component, u_ℓ, of the displacement and the mth component, P_m, of the point force. Applying the Maxwell reciprocity relation, the functions, $g_{\ell m}$, have the property

$$g_{12} = g_{21}, \quad g_{13} = -g_{31}, \quad \text{and} \quad g_{23} = -g_{32} \qquad (4\text{-}1.2)$$

Therefore, the matrix $\underset{\approx}{G}$ has actually only six independent elements.

By superimposing many of these point loads, the displacement, $\underset{\sim}{u}$, at $\underset{\sim}{x}$, caused by the traction, $\underset{\sim}{T}(\underset{\sim}{x}_0)$, over an area, A, is

$$\underset{\sim}{u}(\underset{\sim}{x}) = \iint_A \underset{\approx}{G}(\omega, \underset{\sim}{x} - \underset{\sim}{x}_0)\underset{\sim}{T}(\underset{\sim}{x}_0)\, dS_0, \qquad \underset{\sim}{x}_0 \text{ on } A. \qquad (4\text{-}1.3)$$

If the surface tractions, $T(\underset{\sim}{x}_0)$, in equation (4-1.3) are known or prescribed, the displacement, $\underset{\sim}{u}(\underset{\sim}{x})$, can be obtained by direct integration over the loaded area, A. However, for many practical

problems, the displacement, $\underset{\sim}{u}(\underset{\sim}{x})$, is prescribed over the foundation surface. Therefore, the values of $T(\underset{\sim}{x}_o)$ must be determined by solving the integral equation (4-1.3).

Because of the complexity of the kernel, $\underline{\underline{G}}(\omega, \underset{\sim}{x} - \underset{\sim}{x}_o)$, only very special geometries such as a circle or a strip are amenable to an exact solution. For many foundation shapes of practical importance, the exact solution of (4-1.3) appears either too complex to handle or impossible to obtain. Therefore, analogous to the two-dimensional problem, an effort is made here to solve the integral equation numerically.

The results presented in Section [3-5] indicated that the stress distribution is quite sensitive to the exact shape of the foundation while the integrals of the stresses, i.e., impedances and driving forces, are not. Therefore, if only the impedance and driving force are needed, the area, A, can be approximately represented by an area over which the integration over dS_o can be performed easily. In the following sections, two different numerical approaches will be discussed.

[4-2] METHOD I - PARTITIONING THE FOUNDATION AREA INTO SMALLER SUBREGIONS

The standard procedure for obtaining the numerical solution of an integral equation is to degenerate the continuous integral formulation into a set of discrete algebraic equations which can be solved numerically. To accomplish this, the integral on the right hand side of (4-1.3) is replaced by a sum over the yet unknown integrand, $\underline{\underline{G}}\,\underline{T}$. This sum may be weighted differently depending on the type of integration rules used. For complicated foundation shapes, numerical integration rules are not available. However, the foundation area can first be partitioned into many smaller areas of a fundamental shape for the purpose of integration. The integral in (4-1.3) can then be expressed approximately as

$$\iint_A \underline{\underline{G}}(\omega, \underline{x} - \underline{x}_o)\,\underline{T}(\underline{x}_o)\,dS_o \cong \sum_{j=1}^{N} \iint_{A_j} \underline{\underline{G}}(\omega, \underline{x} - \underline{x}_o)\,\underline{T}_j(\underline{x}_o)\,dS_o \quad (4\text{-}2.1)$$

where A_j is the area of the jth foundation element.

An attempt was made by Elorduy, Nieto, and Szekely[A163] to represent the total traction in an area A_j by a point load $\underline{P}_j^*$, where each element is taken to be a square. The integral equation (4-1.3) is then replaced by the set of $3N \times 3N$ simultaneous equations for the unknown point loads $\underline{P}_j^*$:

$$\underline{u}(\underline{x}_i) \cong \sum_{j=1}^{N} \underline{\underline{G}}(\omega, \underline{x}_i - \underline{x}_j)\,\underline{P}_j^* \; ; \qquad i, j = 1, 2, \ldots, N$$

where $\underset{\sim}{x}_i$ and $\underset{\sim}{x}_j$ are the observation and source points, respectively. However, the difficulty of this approach arises in the numerical evaluation of the Green's function $g_{\ell\ell}$, which has a singularity of the type $1/|(\underset{\sim}{x}_i - \underset{\sim}{x}_j)|$ when $\underset{\sim}{x}_i = \underset{\sim}{x}_j$ or $i = j$. Hence, the contribution to the diagonal terms of the algebraic equations is unbounded. To avoid this singularity, Elorduy *et al.*(A163) kept the source points at the center of the square elements while the observation points were shifted to an arbitrary corner of the element. This special scheme tends to introduce a bias into the equation because the diagonal terms, where $i = j$, are dominant.

In this section, a more rigorous approach is taken, in which the singularity of the Green's functions is properly accounted for. The traction, $\underset{\sim}{T}_j(\underset{\sim}{x}_o)$, in equation (4-2.1) is first expanded in a Taylor series about a point $\underset{\sim}{x}_j$ inside A_j as follows

$$\underset{\sim}{T}_j(\underset{\sim}{x}_o) = \underset{\sim}{T}_j(\underset{\sim}{x}_j) + \nabla\underset{\sim}{T}_j(\underset{\sim}{x}_j)\cdot(\underset{\sim}{x}_o - \underset{\sim}{x}_j) + \frac{1}{2!}(\underset{\sim}{x}_o - \underset{\sim}{x}_j)^T[H(\underset{\sim}{x}_j)](\underset{\sim}{x}_o - \underset{\sim}{x}_j) + \ldots \tag{4-2.2}$$

where $[H(\underset{\sim}{x}_j)]$, the Hessian matrix, consists of the second partial derivatives of $\underset{\sim}{T}_j$ at $\underset{\sim}{x}_j$. Since the values of the expansion coefficients $\underset{\sim}{T}_j(\underset{\sim}{x}_j)$, $\nabla\underset{\sim}{T}_j(\underset{\sim}{x}_j)$, $[H(\underset{\sim}{x}_j)], \ldots$, etc., are unknown, they must be determined by the compatibility conditions on the displacements. By substituting (4-2.2) into the right hand side of (4-2.1) and performing the integration over A_j, the resulting discrete sum will depend on the unknown Taylor expansion coefficients. By prescribing the displacements and their derivatives on the left hand side of (4-1.3) at the same location, $\underset{\sim}{x}_i$, a set of simultaneous

equations for the unknowns is obtained

$$\left\{\begin{Bmatrix} \underset{\sim}{u}_1 \\ \nabla\underset{\sim}{u}_1 \\ \vdots \end{Bmatrix} \begin{Bmatrix} \underset{\sim}{u}_2 \\ \nabla\underset{\sim}{u}_2 \\ \vdots \end{Bmatrix} \begin{matrix} \\ \vdots \end{matrix}\right\} = \left[\; M \;\right] \left\{\begin{Bmatrix} \underset{\sim}{T}_1 \\ \nabla\underset{\sim}{T}_1 \\ \vdots \end{Bmatrix} \begin{Bmatrix} \underset{\sim}{T}_2 \\ \nabla\underset{\sim}{T}_2 \\ \vdots \end{Bmatrix} \begin{matrix} \\ \vdots \end{matrix}\right\} \qquad (4\text{-}2.3)$$

Theoretically, the representation of $\underset{\sim}{T}_j$ in (4-2.2) improves as the number of terms is increased; however, only a few terms are necessary if the function $\underset{\sim}{T}_j(\underset{\sim}{x}_o)$ is well behaved inside the area A_j. From the exact solution of the circular disc [Bielak[A134]], the stress distribution under the disc was noted to be quite smooth except at the edge, where the stress is infinite. Since this singularity is quite easily integrable, an elaborate expression of (4-2.2) is not needed if only the integral of the stresses is wanted.

The limiting factor for the numerical solution of (4-2.3) is the number of equations allowed. Since the matrix, M, is a full matrix, the numerical round off errors, accumulated by computers during the inversion process, can cause the solution to be unstable. The maximum order of the matrix should be kept under about 500 even when double precision calculation is performed. With the maximum order of M fixed, the choice is either to have

many smaller areas, A_j, with a low order Taylor expansion, or to have fewer areas, A_j, with a higher order expansion for the traction. Of course, a hybrid of the two can be used effectively as well.

In the applications presented in this section, the former approach is taken because the integral of the lower order functions, $(\underset{\sim}{x} - \underset{\sim}{x}_j)^n$, over the area, A_j, can be carried out with less difficulty. Some examples of the actual calculations will be shown next using small rectangular elements and a zeroth order expansion of $\underset{\sim}{T}_j$.

An Application Using Rectangular Subregions

Using an appropriate number of rectangular areas, many foundation shapes can be modeled adequately as shown in Figure 4-2.1. Matching only the displacement compatibility and the zeroth order term of the traction at the center of each of the rectangular elements, $\underset{\sim}{x}_j$, equation (4-1.3) simplifies to

$$\underset{\sim}{u}(\underset{\sim}{x}_i) \cong \sum_{j=1}^{N} \iint_{A_j} \underline{\underline{G}}(\omega, \underset{\sim}{x}_i - \underset{\sim}{x}_o)\, \underset{\sim}{T}_j(\underset{\sim}{x}_j)\, dS_o \; ; \quad i,j = 1,2,\ldots,N \; . \tag{4-2.4}$$

Since $\underset{\sim}{T}_j(\underset{\sim}{x}_j)$ is actually a uniform load over the area A_j, it is convenient to introduce a total force over the whole area as $\underset{\sim}{P}^*_j(\underset{\sim}{x}_j) = \underset{\sim}{T}_j(\underset{\sim}{x}_j)[4b_jc_j]$, where $2b_j$ and $2c_j$ are the side dimensions of a rectangular element. Equation (4-2.4) can then be rewritten as

$$\underset{\sim}{u}(\underset{\sim}{x}_i) \cong \sum_{j=1}^{N} \left[\frac{1}{\mu c_j} \underline{\underline{\Phi}}\left(\frac{\omega b_j}{\beta_s}, \frac{(\underset{\sim}{x}_1)_i - (x_1)_j}{b_j}, \frac{(x_2)_i - (x_2)_j}{c_j} \right) \right] \underset{\sim}{P}^*_j(\underset{\sim}{x})_j \; ; \; i,j = 1,2,\ldots,N \tag{4-2.5}$$

where μ and β_s are the shear modulus and the shear wave velocity, respectively. The "influence coefficients," $\underline{\underline{\Phi}}$, are defined as follows:

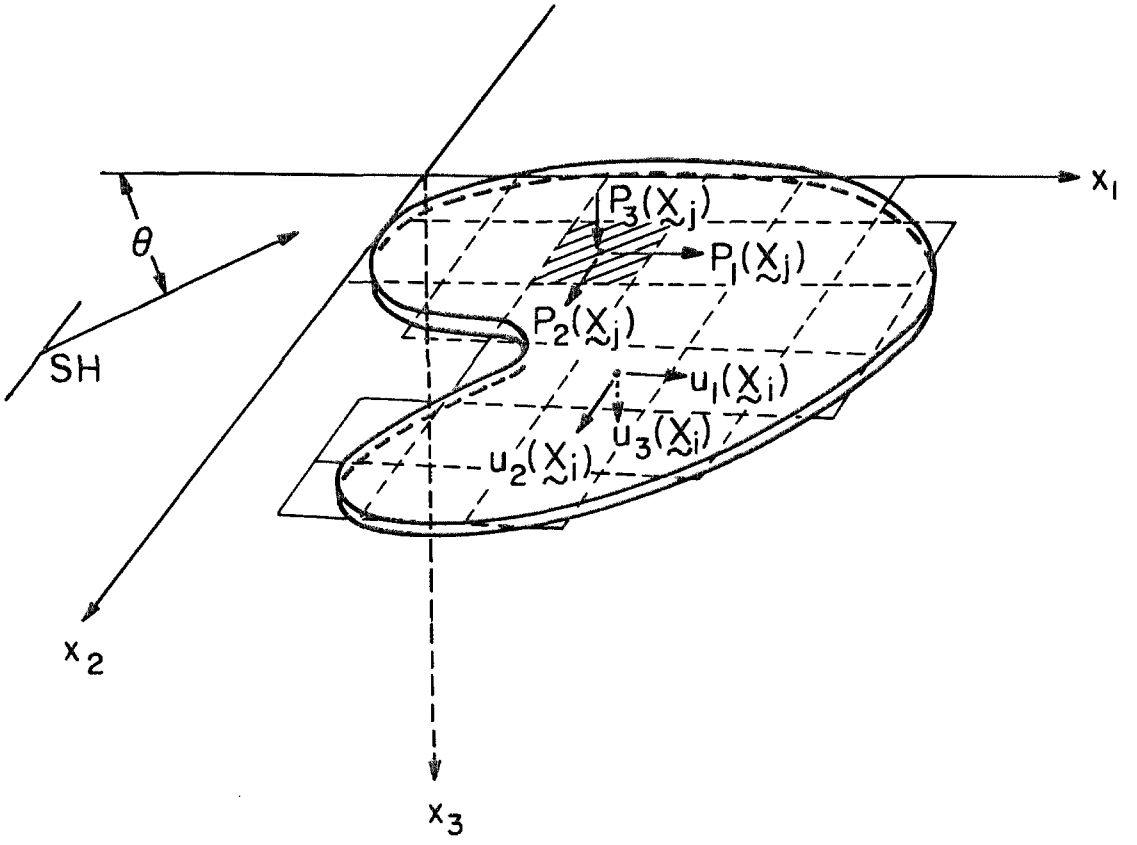

Figure 4-2.1 An approximation to a foundation of arbitrary shape.

$$\underline{\underline{\Phi}}\left(\frac{\omega b_j}{\beta_s}, \frac{(x_1)_i - (x_1)_j}{b_j}, \frac{(x_2)_i - (x_2)_j}{c_j}\right) = \begin{bmatrix} \phi_{11} & \phi_{12} & \phi_{13} \\ \phi_{21} & \phi_{22} & \phi_{23} \\ \phi_{31} & \phi_{32} & \phi_{33} \end{bmatrix}$$

$$= \int_{(x_2)_j - c_j}^{(x_2)_j + c_j} \int_{(x_1)_j - b_j}^{(x_1)_j + b_j} \frac{\mu}{4b_j} \left\{ \begin{bmatrix} g_{11} & g_{12} & g_{13} \\ g_{21} & g_{22} & g_{23} \\ g_{31} & g_{32} & g_{33} \end{bmatrix} (\omega, \underset{\sim}{x}_i - \underset{\sim}{x}_j) \right\} d\xi_1 d\xi_2 \ . \tag{4-2.6}$$

where $\phi_{\ell m}$; ℓ,m = 1, 2, 3; are complex quantities.

After the double integration, the influence functions become finite even when $\underset{\sim}{x}_i = \underset{\sim}{x}_j$. In fact, $\phi_{ii}\left(\frac{\omega b_i}{\beta_s}, \underset{\sim}{0}\right)$ are actually the compliance functions for the uniformly loaded area, A_i, normalized with respect to the deflection at the center [Kobori et al.(A164)]. The expression for the point load on the surface of the half space is quite lengthy and complicated [Ewing, Jardetsky, and Press (1957)]; therefore, the actual integration over the area, A_j, is difficult. An alternate approach, using two-dimensional Fourier Transforms, is taken since the definition of $\underline{\underline{\Phi}}$ in (4-2.6) physically represents the case where the rectangular element is uniformly loaded. Thomson and Kobori(A162) have derived the formulae for $\phi_{ii}\left(\frac{\omega b_i}{\beta_s}, \underset{\sim}{0}\right)$. The off-diagonal terms $\phi_{\ell m}\left(\frac{\omega b_j}{\beta_s}, \underset{\sim}{x}_i - \underset{\sim}{x}_j\right)$ can be derived similarly. The mathematical derivation of the above can be found in Appendix B. The formulae, after simplification, are

$$\phi_{11}\left(kb,\frac{x_1}{b},\frac{x_2}{c}\right) = \frac{1}{\pi^2 kb}\int_0^{\frac{\pi}{2}}\int_0^{\infty}\left[\frac{\sin^2\theta}{z\sqrt{z^2-1}} - \frac{\sqrt{z^2-1}\cos^2\theta}{z\,F(z)}\right]\Psi\,\frac{\cos(zkx_1\cos\theta)\cos(zkx_2\sin\theta)}{\sin\theta\cos\theta}\,dzd\theta \qquad (4\text{-}2.7a)$$

$$\phi_{21}\left(kb,\frac{x_1}{b},\frac{x_2}{c}\right) = \frac{1}{\pi^2 kb}\int_0^{\frac{\pi}{2}}\int_0^{\infty}\left[\frac{1}{z\sqrt{z^2-1}} + \frac{\sqrt{z^2-1}}{z\,F(z)}\right]\Psi\,\sin(zkx_1\cos\theta)\sin(zkx_2\sin\theta)\,dzd\theta \qquad (4\text{-}2.7b)$$

$$\phi_{31}\left(kb,\frac{x_1}{b},\frac{x_2}{c}\right) = -\frac{1}{\pi^2 kb}\int_0^{\frac{\pi}{2}}\int_0^{\infty}\frac{\left[(2z^2-1)-2\sqrt{(z^2-1)(z^2-n^2)}\right]}{F(z)\sin\theta}\Psi\,\sin(zkx_1\cos\theta)\cos(zkx_2\sin\theta)\,dzd\theta \qquad (4\text{-}2.7c)$$

$$\phi_{22}\left(kb,\frac{x_1}{b},\frac{x_2}{c}\right) = \frac{1}{\pi^2 kb}\int_0^{\frac{\pi}{2}}\int_0^{\infty}\left[\frac{\cos^2\theta}{z\sqrt{z^2-1}} - \frac{\sqrt{z^2-1}\sin^2\theta}{z\,F(z)}\right]\Psi\,\frac{\cos(zkx_1\cos\theta)\cos(zkx_2\sin\theta)}{\sin\theta\cos\theta}\,dzd\theta \qquad (4\text{-}2.7d)$$

$$\phi_{32}\left(kb,\frac{x_1}{b},\frac{x_2}{c}\right) = -\frac{1}{\pi^2 kb}\int_0^{\frac{\pi}{2}}\int_0^{\infty}\frac{\left[(2z^2-1)-2\sqrt{(z^2-n^2)(z^2-1)}\right]}{F(z)\cos\theta}\cos(zkx_1\cos\theta)\sin(zkx_2\sin\theta)\Psi\,dzd\theta \qquad (4\text{-}2.7e)$$

$$\phi_{33}\left(kb,\frac{x_1}{b},\frac{x_2}{c}\right) = -\frac{1}{\pi^2 kb}\int_0^{\frac{\pi}{2}}\int_0^{\infty}\frac{\sqrt{z^2-n^2}}{z\,F(z)}\Psi\,\frac{\cos(zkx_1\cos\theta)\cos(zkx_2\sin\theta)}{\sin\theta\cos\theta}\,dzd\theta \qquad (4\text{-}2.7f)$$

where $F(z) = (2z^2-1)^2 - 4z^2\sqrt{(z^2-1)(z^2-n^2)}$, $\Psi = \sin(zkb\cos\theta)\sin(zkc\sin\theta)$, $k = \omega/\beta_s$, and

$n = \beta_s/\alpha_s$ = shear wave velocity/longitudinal wave velocity.

Since $\underline{\underline{\Phi}}$, the integral of $\underline{\underline{G}}$, also satisfies the relation (4-1.2), only six independent components need to be evaluated.

As the frequency of excitation approaches zero, the formulae of (4-2.7) become the static solutions which can be obtained by superimposing the solution for a point load given by Love (1927),

$$\phi_{11}\left(0,\frac{x_1}{b},\frac{x_2}{c}\right) = \frac{1}{16\pi}\left(\frac{c}{b}\right)\int_{-1}^{1}\int_{-1}^{1}\left[\left(\frac{1-2n^2}{1-n^2}\right)\frac{\left(\frac{x_1-x_1'}{b}\right)}{R^3}+\frac{1}{(1-n^2)}\frac{1}{R}\right]d\left(\frac{x_1'}{b}\right)d\left(\frac{x_2}{c}\right) \qquad (4\text{-}2.8a)$$

$$\phi_{21}\left(0,\frac{x_1}{b},\frac{x_2}{c}\right) = \frac{1}{16\pi}\left(\frac{c}{b}\right)^2\int_{-1}^{1}\int_{-1}^{1}\left[\frac{(1-2n^2)}{(1-n^2)}\frac{\left(\frac{x_1-x_1'}{b}\right)\left(\frac{x_2^2-x_2'}{c}\right)}{R^3}\right]d\left(\frac{x_1'}{b}\right)d\left(\frac{x_2'}{c}\right) \qquad (4\text{-}2.8b)$$

$$\phi_{31}\left(0,\frac{x_1}{b},\frac{x_2}{c}\right) = \frac{1}{16\pi}\left(\frac{c}{b}\right)\left(\frac{n^2}{1-n^2}\right)\int_{-1}^{1}\int_{-1}^{1}\frac{\left(\frac{x_1-x_1'}{b}\right)}{R^2}d\left(\frac{x_1'}{b}\right)d\left(\frac{x_2'}{c}\right) \qquad (4\text{-}2.8c)$$

$$\phi_{22}\left(0,\frac{x_1}{b},\frac{x_2}{c}\right) = \frac{1}{16\pi}\int_{-1}^{1}\int_{-1}^{1}\left[\left(\frac{c}{b}\right)^3\left(\frac{1-2n^2}{1-n^2}\right)\frac{\left(\frac{x_2-x_2'}{c}\right)}{R^3}+\left(\frac{c}{b}\right)\frac{1}{(1-n^2)}\frac{1}{R}\right]d\left(\frac{x_1'}{b}\right)d\left(\frac{x_2'}{c}\right) \qquad (4\text{-}2.8d)$$

$$\phi_{32}\left(0,\frac{x_1}{b},\frac{x_2}{c}\right) = \frac{1}{16\pi}\left(\frac{c}{b}\right)^2\left(\frac{n^2}{1-n^2}\right)\int_{-1}^{1}\int_{-1}^{1}\frac{\left(\frac{x_2-x_2'}{c}\right)}{R^2}d\left(\frac{x_1'}{b}\right)d\left(\frac{x_2'}{c}\right) \qquad (4\text{-}2.8e)$$

$$\phi_{33}\left(0,\frac{x_1}{b},\frac{x_2}{c}\right) = \frac{1}{16\pi}\left(\frac{c}{b}\right)\frac{1}{(1-n^2)}\int_{-1}^{1}\int_{-1}^{1}\frac{1}{R}\,d\left(\frac{x_1'}{b}\right)d\left(\frac{x_2'}{c}\right) \qquad (4\text{-}2.8f)$$

where $R = \sqrt{\left(\frac{x_1-x_1'}{b}\right)^2+\left(\frac{c}{b}\right)^2\left(\frac{x_2-x_2'}{c}\right)^2}$

In the formulae above, the functions, ϕ_{ij}, are finite and well behaved. The algebraic equations (4-2.5) can then be rearranged

in matrix form

$$\begin{Bmatrix} \underset{\sim}{u}_1 \\ \underset{\sim}{u}_2 \\ \vdots \\ \underset{\sim}{u}_N \end{Bmatrix} = \frac{1}{\mu} \begin{bmatrix} \underline{\underline{\Phi}}(kb_1, 0) & \underline{\underline{\Phi}}(kb_2, \underset{\sim}{x}_1 - \underset{\sim}{x}_2) & \cdots & \underline{\underline{\Phi}}(kb_N, \underset{\sim}{x}_1 - \underset{\sim}{x}_N) \\ \underline{\underline{\Phi}}(kb_1, \underset{\sim}{x}_2 - \underset{\sim}{x}_1) & \underline{\underline{\Phi}}(kb_2, 0) & \cdots & \underline{\underline{\Phi}}(kb_N, \underset{\sim}{x}_2 - \underset{\sim}{x}_N) \\ \vdots & \vdots & & \vdots \\ \underline{\underline{\Phi}}(kb_1, \underset{\sim}{x}_N - \underset{\sim}{x}_1) & \underline{\underline{\Phi}}(kb_2, \underset{\sim}{x}_N - \underset{\sim}{x}_2) & \cdots & \underline{\underline{\Phi}}(kb_N, 0) \end{bmatrix} \begin{bmatrix} \underset{\sim}{P}_1^*/c_1 \\ \underset{\sim}{P}_2^*/c_2 \\ \vdots \\ P_N^*/c_N \end{bmatrix} \tag{4-2.9}$$

Numerical Evaluation of the Integrals

The double integrals appearing in equation (4-2.7) cannot easily be evaluated analytically or numerically. The infinite integral is convergent, since, when $z \to \infty$, the non-oscillatory part of the integrand for ϕ_{ij} approaches zero as $1/z^2$; but the denominator, $F(z)$, has a simple pole at s, where s is a root of $F(s) = 0$. One way to eliminate this simple pole is to use the method discussed by I. M. Longman (1958) in which the integrand was separated into an even part and an odd part. Since the odd part, which possesses the singularity, integrates to zero, the remaining even part is integrable. The results obtained by this method are actually the principal value of the integral; to avoid standing waves, one half of the residue of the "Rayleigh Pole" must be subtracted from it.

In the current application, contour integration over the complex plane is used to include the contribution from the Rayleigh pole and the branch cuts associated with $\sqrt{z^2-n^2}$ and $\sqrt{z^2-1}$. The contours used here are similar to those employed by Ewing et al. (1957). The process of contour integration has eliminated all non-integrable singularities and reduced the infinite integral over z for the diagonal terms, ϕ_{ii} to a residue plus two finite integrals with limits of $0 \leq z \leq n$ and $0 \leq z \leq 1$. This reduction was possible because the integrand is analytic everywhere except at the branch cuts and at the Rayleigh Pole.

After contour integration, the resulting integrals are still too complicated to be evaluated analytically; therefore, a numerical solution is necessary. With the aid of high speed digital computers,

numerical integration would appear to be an easy task, but for large values of k, x_1, and x_2, the integrand becomes highly oscillatory and standard quadrature formulae such as Simpson's rule are not efficient.

For an oscillatory integrand with sine and cosine functions, i.e.,

$$\int_a^b f(z)\begin{Bmatrix}\sin pz\\ \cos pz\end{Bmatrix} dz \ , \qquad (4\text{-}2.10)$$

the numerical calculation can be treated efficiently with the Filon's method [Abramowitz and Stegun (1971)]. This approximates the non-oscillatory function f(z) by intervals of parabolae as used in the Simpson's rule. These parabolae are then integrated exactly along with the sine or cosine dependent on the value of p, but only on the way f(z) is approximated. Another advantage of this approach is that f(z) in the integrand of (4-2.10) remains the same for all k, x_1, and x_2. Therefore, it can be stored to avoid repetitive calculations.
fore, it can be stored to avoid repetitive calculations.

Since the calculation of the influence functions $\underline{\underline{\Phi}}$ requires considerable effort, it is therefore wise to store the results for future usage. In the examples given in this Chapter, the foundation surfaces are formed using square elements; so square grids for the influence function were calculated and stored before the actual application. For the frequency band of interest, a square grid of 8×8 was calculated for the dimensionless frequencies $\omega b^*/\beta_s$ ranging from 0.05 to 0.50 in an increment of 0.05, and 4×4 grids were

calculated for $\omega b^*/\beta_s$ from 0.60 to 1.00 in an increment of 0.10. The influence functions also have symmetrical properties so that they only have to be calculated in one quadrant of the x_1x_2-plane for horizontal vibrations and in one octant for vertical vibrations. By taking advantage of all these properties, the calculation of the final results can be performed economically.

Reduction to the Relaxed Boundary Value Problem

Thus far the formulation in Section [4-2] has been concerned with the solution of equation (4-1.3), which is a set of three coupled integral equations involving the tractions in the x_1, x_2, and x_3 directions. Their unique solutions are to be determined by the compatibility conditions of the three components of displacement on the foundation surface. However, these coupled integral equations associated with the "welded-contact" problem are difficult to solve.

For numerous applications in soil-structure interaction, only an approximate answer is necessary. In these cases, it is worthwhile to ignore some of the less important boundary conditions which may uncouple part of the integral equations. The solution obtained by disregarding some boundary conditions is called a "relaxed" solution.

The relaxed boundary conditions can be based on different assumptions, and their justification is necessary. In this chapter, the following relaxed conditions will be used:

(1) Vertical Vibrations: The boundary conditions are such that the vertical displacement $u_3(x_1, x_2, 0)$ on the foundation surface is prescribed while the horizontal displacements are left unrestricted. In other words, the foundation surface is assumed to be frictionless in the horizontal directions. By ignoring the tangential stresses, equation (4-1.3) can be reduced to just one independent integral equation for the unknown normal stresses.

(2) Horizontal Vibrations: In this case, the horizontal displacement in one direction is prescribed while its complemental

components are not resisted. Once again, equation (4-1.3) reduces to an independent integral equation for the tangential stresses in the direction of the applied load. It should be noted, however, in some cases only the vertical component is relaxed [Luco and Westmann[A129]].

(3) Rocking Vibrations: The boundary conditions are similar to those of the vertical problem, except for the vertical displacement which now follows a rigid body rotation. The horizontal components for this case are assumed to be unimportant.

(4) Torsional Vibrations: The horizontal displacements are prescribed for torsional motion while no resistance is placed on the vertical displacement. In this case, the uncoupling of the two horizontal components is not possible because the interaction between the two is significant.

These "relaxed boundary conditions" listed above are quite commonly used,[A129, A130] and they are generally accepted to be adequate for engineering applications.

Compliances for Rigid Foundations

When the foundation is assumed to be rigid, the method of superposition which was discussed in Chapter II can be applied. For the calculation of the vertical compliance, C_{vv}, and the horizontal compliance, C_{hh}, the displacements must satisfy the rigid body translation conditions. But for the evaluation of the rocking compliances, C_{mm}, and for the torsion compliance, C_{tt}, rigid body rotation is imposed. The following examples illustrate the set-up of the algebraic equations; square elements with sides of $2b^*$ are used because of their simplicity.

(1) Vertical Compliance: Using the relaxed conditions described above, the compatibility conditions for the vertical displacement, under the constraint of rigid body translation, are

$$u_3(\underset{\sim}{x}) = \Delta_v , \qquad \underset{\sim}{x} \text{ on } A , \tag{4-2.11}$$

with $u_1(\underset{\sim}{x})$ and $u_2(\underset{\sim}{x})$ unrestricted. By ignoring the tangential stresses, equation (4-2.9) uncouples, and the set of algebraic equations for the normal loads $(P_3^*)_j$ are

$$\Delta_v \begin{Bmatrix} 1 \\ 1 \\ \vdots \\ 1 \end{Bmatrix} = \frac{1}{\mu b^*} \begin{bmatrix} \phi_{33}(kb^*, 0) & \phi_{33}(kb^*, \underset{\sim}{x}_1-\underset{\sim}{x}_2) & \cdots & \phi_{33}(kb^*, \underset{\sim}{x}_1-\underset{\sim}{x}_N) \\ \phi_{33}(kb^*, \underset{\sim}{x}_2-\underset{\sim}{x}_1) & \phi_{33}(kb^*, 0) & \cdots & \phi_{33}(kb^*, \underset{\sim}{x}_2-\underset{\sim}{x}_N) \\ \vdots & \vdots & & \vdots \\ \phi_{33}(kb^*, \underset{\sim}{x}_N-\underset{\sim}{x}_1) & \phi_{33}(kb^*, \underset{\sim}{x}_N-\underset{\sim}{x}_2) & \cdots & \phi_{33}(kb^*, 0) \end{bmatrix} \begin{Bmatrix} (P_3^*)_1 \\ (P_3^*)_2 \\ \vdots \\ (P_3^*)_N \end{Bmatrix} \tag{4-2.12}$$

Since the influence coefficients, ϕ_{33}, are calculated for the dimensionless frequency, $\omega b^*/\beta_s$, the dimensionless frequency, a_o, based on the characteristic length of the foundation, b, will actually be a factor of b/b^* higher. Using the numerical solution for the unknowns, $(P_3^*)_j/\mu b^* \Delta_v$, the dimensionless vertical compliance, $C_{vv}(a_o)$, can be defined by

$$C_{vv}\left[\left(\frac{b}{b^*}\right)\left(\frac{\omega b^*}{\beta_s}\right)\right] = \frac{\mu b \Delta_v}{Q_3} = \frac{b}{b^*}\left\{\sum_{j=1}^{N} \frac{(P_3^*)_j}{\mu b^* \Delta_v}\right\}^{-1} \qquad (4\text{-}2.13)$$

where $Q_3 e^{i\omega t}$ is the vertical load required to move the rigid foundation vertically with displacement, $\Delta_v e^{i\omega t}$.

Theoretically, the compliance thus evaluated will approach the exact value as the number of square elements used is increased. This trend is best illustrated by Figure 4-2.2, in which the results obtained for a square foundation by using 1, 4, 16 and 64 elements are plotted versus a_o, the dimensionless frequency. The Poisson ratio of the soil is assumed to be $\frac{1}{3}$, so the ratio of S wave to P wave velocity in the soil is $\frac{1}{2}$. When just one element is used, the foundation surface is under a uniform load; therefore, it does not actually represent a rigid foundation. This solution was originally presented by Thomson and Kobori.(A162) If the number of elements is increased to four, the stress distribution is still uniform because all four elements must be identical for symmetric loading. But the foundation deflection, Δ_v, is now prescribed at the points, $\left(\pm\frac{b}{2}, \pm\frac{b}{2}\right)$, rather than at the center; hence, Δ_v is equivalent to

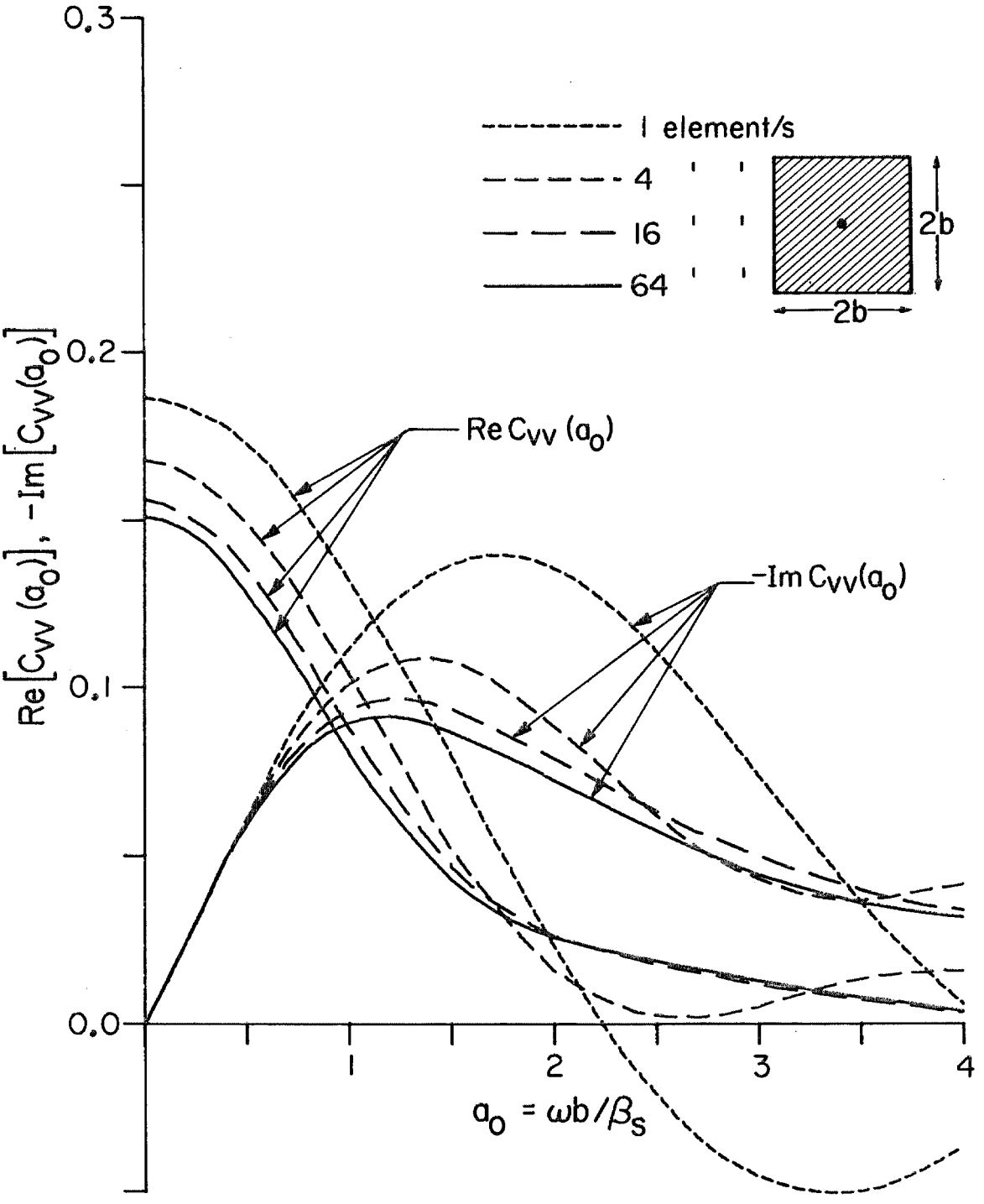

Figure 4-2.2 Effect of the number of subregions on the vertical compliance for a rigid square foundation ($\nu = \frac{1}{3}$).

an average of all displacements under the uniform load. When 16 or 64 elements are used, the stress distribution under the foundation is no longer uniform (the approximate static solution is shown in Figure 4-2.3; since the stress distribution is symmetrical about the x_1-axis and the x_2-axis, only the first quadrant of the stresses is shown in the figure). The loading at the corners and at the edges is higher than at the areas near the center of the foundation as is espected because of stress concentrations. Though the stress distribution of the two cases shown are quite different, the values of the compliances are remarkably close, indicating that the compliance is not as sensitive as the stress distribution is to the number of elements used.

(2) Horizontal Compliance: A similar set up can be made for horizontal excitations. First of all, the displacement conditions for the rigid body motion in the x_1 direction are

$$u_1(\underset{\sim}{x}) = \Delta_{H_1} \qquad \underset{\sim}{x} \text{ on } A \ , \tag{4-2.14}$$

with $u_2(\underset{\sim}{x})$ and $u_3(\underset{\sim}{x})$ unrestricted. Hence, the matrix equation for the unknown tangential loads, $(P_1^*)_j$, is

$$\Delta_{H_1}\begin{Bmatrix} 1 \\ 1 \\ \vdots \\ 1 \end{Bmatrix} = \frac{1}{\mu b^*}\begin{bmatrix} \phi_{11}(kb^*, \underset{\sim}{0}) & \phi_{11}(kb^*, \underset{\sim}{x}_1-\underset{\sim}{x}_2) & \cdots & \phi_{11}(kb^*, \underset{\sim}{x}_1-\underset{\sim}{x}_N) \\ \phi_{11}(kb^*, \underset{\sim}{x}_2-\underset{\sim}{x}_1) & \phi_{11}(kb^*, \underset{\sim}{0}) & \cdots & \phi_{11}(kb^*, \underset{\sim}{x}_2-\underset{\sim}{x}_N) \\ \vdots & \vdots & & \vdots \\ \phi_{11}(kb^*, \underset{\sim}{x}_N-\underset{\sim}{x}_1) & \phi_{11}(kb^*, \underset{\sim}{x}_N-\underset{\sim}{x}_2) & \cdots & \phi_{11}(kb^*, \underset{\sim}{0}) \end{bmatrix}\begin{Bmatrix} (P_1^*)_1 \\ (P_1^*)_2 \\ \vdots \\ (P_1^*)_N \end{Bmatrix} \tag{4-2.15}$$

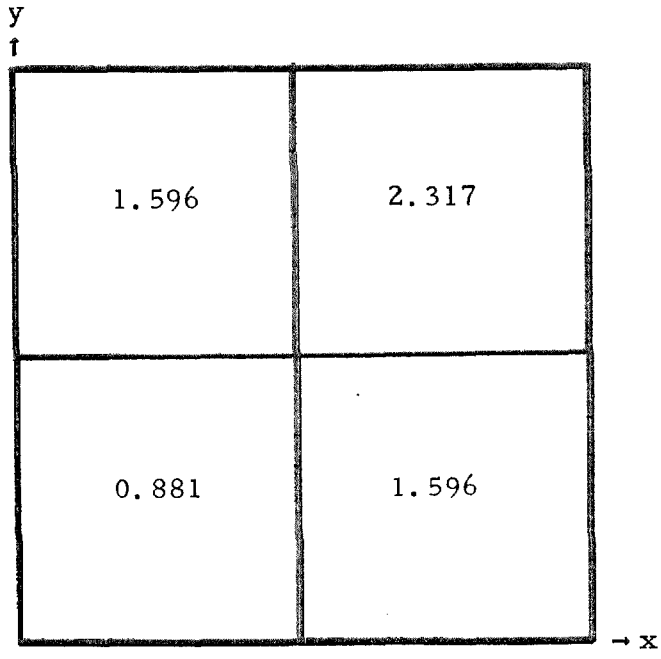

(a) N = 4 × 4

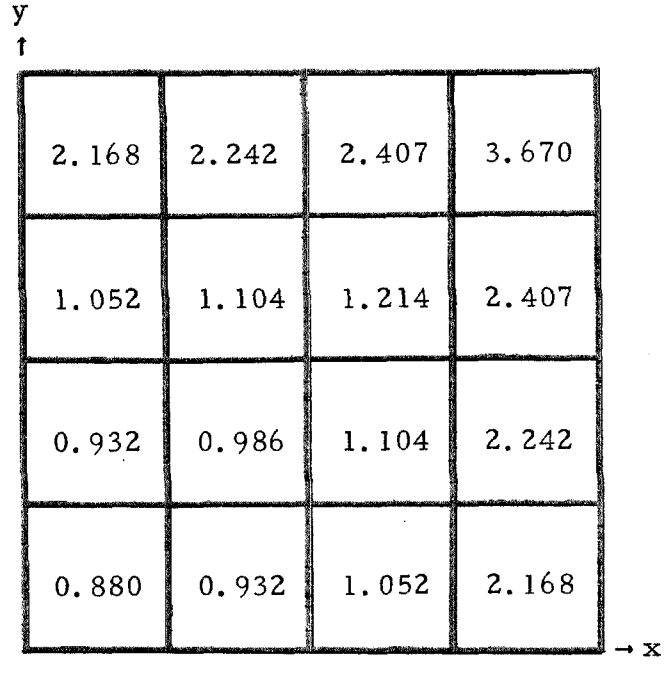

(b) N = 8 × 8

Figure 4-2.3 Approximate stress distribution under the first quadrant of a square foundation for vertical loading.

The numerical solution of $(P_1^*)_j/\mu b^* \Delta_{H_1}$ can now be superimposed to yield $C_{hh_1}(a_o)$ in the x_1 direction,

$$C_{hh_1}(a_o) = \frac{\mu b \Delta_{H_1}}{Q_1} = \left(\frac{b}{b^*}\right)\left|\sum_{j=1}^{N} \frac{(P_1^*)_j}{\mu b^* \Delta_{H_1}}\right|^{-1}$$

where $Q_1 e^{i\omega t}$ is the total horizontal force required to cause a foundation deflection of $\Delta_{H_1} e^{i\omega t}$. The horizontal compliance in the x_2 direction can be obtained by following the same procedure.

For a rectangular foundation, the horizontal compliance can be calculated readily by using square elements. Results for the cases in which the ratio of the sides c/b are equal to $\frac{1}{2}$, 1, and 2 are plotted in Figure 4-2.4 versus a_o. In these cases, the side b was chosen to be the characteristic dimension of the rectangular foundation, and the surface area depends only on the ratio c/b. As shown by Figure 4-2.4, $C_{hh_1}(a_o)$ is largest for $c/b = \frac{1}{2}$ because the area, $A = \frac{1}{2}b^2$, is the smallest of the three cases studied. When the area, hence, the resistance to the load Q_1, is smaller, the deflection, Δ_{H_1}, and also $C_{hh_1}(a_o)$ are larger. Therefore, the force, Q_1, and the displacement, Δ_{H_1}, are related through the size of the foundation area.

Since the surface area, A, when $c/b = 2$, is $2b^2$, which is four times larger than the case where $c/b = \frac{1}{2}$, one might expect that the ratio of their compliances should be 4. This is not true, however, because the resistance of a rectangular foundation when $c/b \neq 1$ is dependent on the direction in which the load is applied. Hence, when

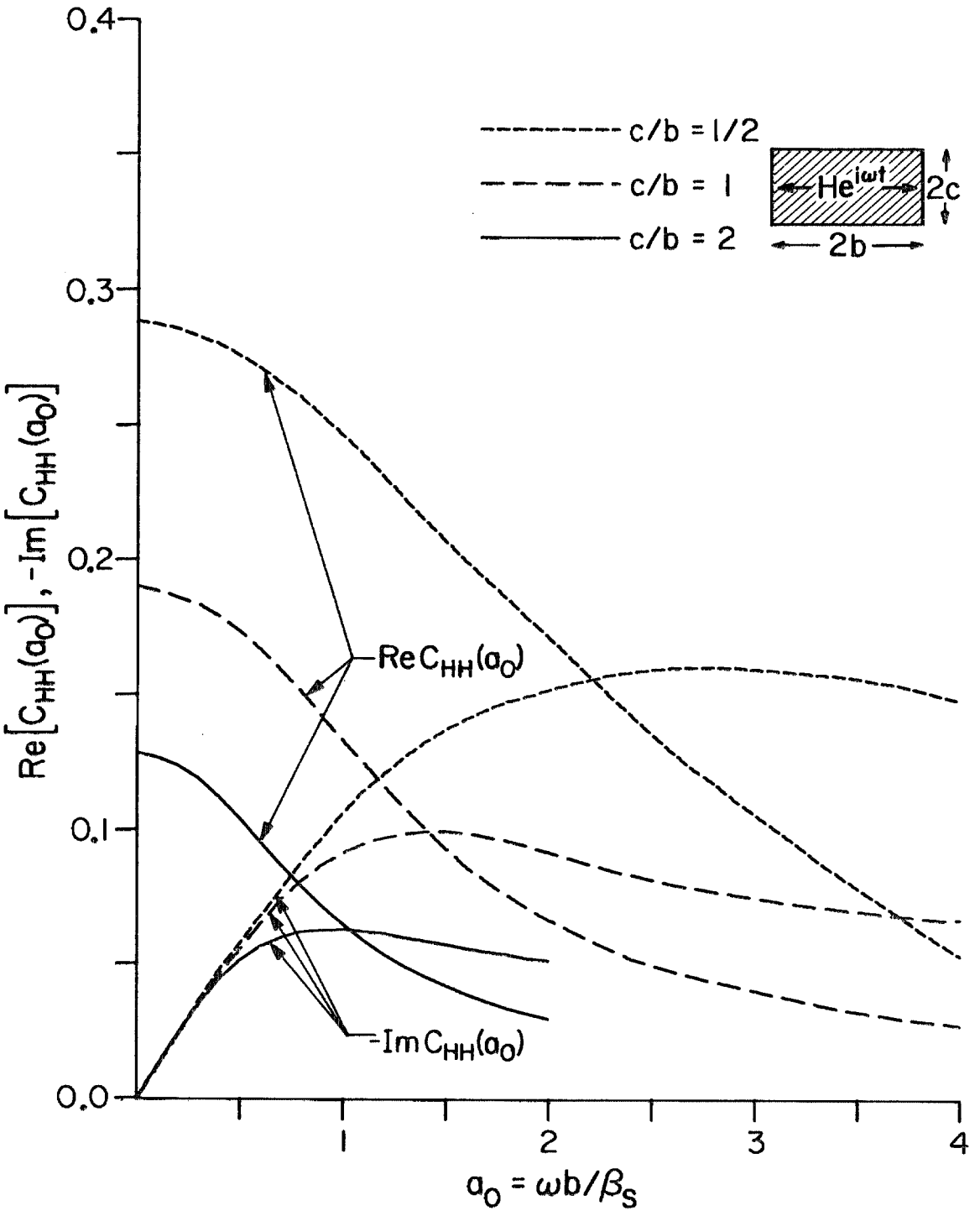

Figure 4-2.4 Horizontal compliance for rigid rectangular foundations ($\nu = \frac{1}{3}$).

$c/b = \frac{1}{2}$, the force is applied parallel to the direction of the "long side" b; while when $c/b = 2$, the force is applied parallel to the direction of the "short side" b. For the latter case, b is less than c. The resistance is thus greater in the direction parallel to the short side.

An analogous analysis was made for the rectangular foundation subjected to vertical excitation. The cases with $c/b = \frac{1}{4}$, $\frac{1}{2}$, and 1 are plotted versus a_0 in Figure 4-2.5. Since the rectangular foundation is symmetric about its center, the compliance for the case where $c/b = \frac{1}{4}$ would be just 16 times that for the case where $c/b = 4$. Note: for the two approximate solutions above, the element size was chosen such that $b^* = b/8$.

(3) Rocking Compliance: Consider next the rocking characteristics of a rigid rectangular foundation. The boundary conditions must now satisfy rigid body rotation. For rocking about the x_2-axis, the relaxed displacement conditions are

$$u_3(\underset{\sim}{x}) = \phi(x_1 - x_1^o) , \qquad \underset{\sim}{x} \text{ on } A , \tag{4-2.17}$$

with $u_1(\underset{\sim}{x})$ and $u_2(\underset{\sim}{x})$ unrestricted. x_1^o and ϕ in equation (4-2.17) are the center of moment of the area A and the angle of rotation about the x_2-axis, respectively.

One can define the dimensionless distance, $d_i^* = (x_i - x_1^o)/b$, as the moment arm measured from x_1^o perpendicular to the x_2-axis. Then the matrix equation for the normal loads, ignoring the tangential contribution, is,

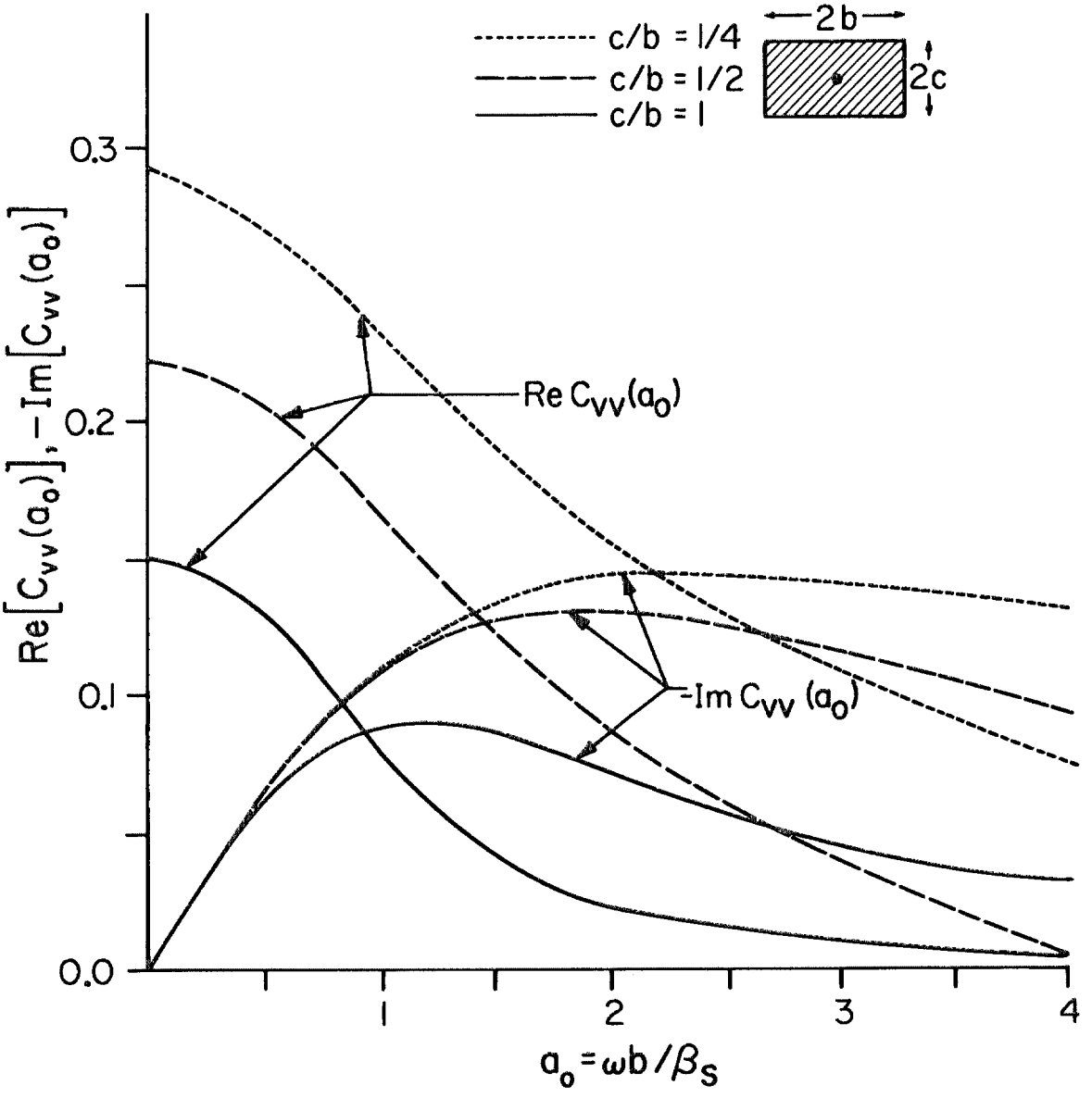

Figure 4-2.5 Vertical compliance for rigid rectangular foundations ($\nu = \frac{1}{3}$).

$$b\phi \begin{Bmatrix} d_1^* \\ d_2^* \\ \vdots \\ d_N^* \end{Bmatrix} = \frac{1}{\mu b^*} \begin{bmatrix} \phi_{33}(kb^*, \underset{\sim}{0}) & \phi_{33}(kb^*, \underset{\sim}{x_1}-\underset{\sim}{x_2}) & \cdots & \phi_{33}(kb^*, \underset{\sim}{x_1}-\underset{\sim}{x_N}) \\ \phi_{33}(kb^*, \underset{\sim}{x_2}-\underset{\sim}{x_1}) & \phi_{33}(kb^*, 0) & \cdots & \phi_{33}(kb^*, \underset{\sim}{x_2}-\underset{\sim}{x_N}) \\ \vdots & \vdots & & \vdots \\ \phi_{33}(kb^*, \underset{\sim}{x_N}-\underset{\sim}{x_1}) & \phi_{33}(kb^*, \underset{\sim}{x_N}-\underset{\sim}{x_2}) & \cdots & \phi_{33}(kb^*, 0) \end{bmatrix} \begin{Bmatrix} (P_3^*)_1 \\ (P_3^*)_2 \\ \vdots \\ (P_3^*)_N \end{Bmatrix} \tag{4-2.18}$$

Comparing (4-2.18) with (4-2.12), the two matrices are identical. The only difference between these two quantities is in the displacement compatibility conditions. For vertical excitation, u_3 is constant over the foundation surface; while for rocking excitation, u_3 varies linearly over the surface.

To superimpose the numerical results for $C_{mm}(a_o)$, the dimensionless moment is obtained by summing the dimensionless forces, $(P_3^*)_j/\mu bb^*\phi$, after having multiplied by the moment arm, $d_i b$,

$$C_{mm}(a_o) = \left\{ \sum_{j=1}^{N} \left[\frac{(P_3^*)_j}{\mu b^2} \right] \left(\frac{b}{b^*} \right) d_j \right\}^{-1} = \frac{\mu b^3 \phi}{M} . \tag{4-2.19}$$

As indicated by (4-2.18) and (4-2.19), $C_{mm}(a_o)$ is sensitive to the moment arm, $d_i b$; therefore, the contribution from the outer edges is more prominent than that of the inner areas.

Numerical results for a rectangular foundation are shown in Figure 4-2.6. The rocking compliance about the x_2-axis, for ratios $c/b = \frac{1}{2}$, 1, and 2, are plotted versus the dimensionless frequency, a_o. The rocking compliance is shown to be directional if

the foundation is not circular; the difference is greater in different directions if the foundation shape is elongated, and the resistance is related to the moment of inertia about the axis. Comparing the cases where $c/b = \frac{1}{2}$ and 2 in Figure 4-2.6, the former has an area 4 times less than that of the latter, but the rocking of the former is with respect to the shorter axis. By normalizing both cases to the same area, the compliance for the rectangular foundation with $c/b = 2$ is 50% higher than when $c/b = \frac{1}{2}$; hence, less resistance is encountered due to the smaller moment arms.

(4) Torsional Compliance: Similar to the rocking motion, the torsional excitation causes the horizontal displacements to vary linearly with respect to the center of torsional moment.

An example is shown in Figure 4-2.7 for a rectangular foundation with the ratio of its sides, c/b, equal to $\frac{1}{2}$ and 1. The relaxed boundary conditions used here are perhaps over-simplified because the transverse horizontal displacement caused by an applied load is neglected. These assumptions can be justified in a crude way because the transverse displacement is usually of an order of magnitude less than the longitudinal component of the horizontal displacement. As shown by Figure 4-2.7, the torsional resistance is greater for the elongated foundations if the area is held constant during the comparison because the moment depends on the leverage of the loads.

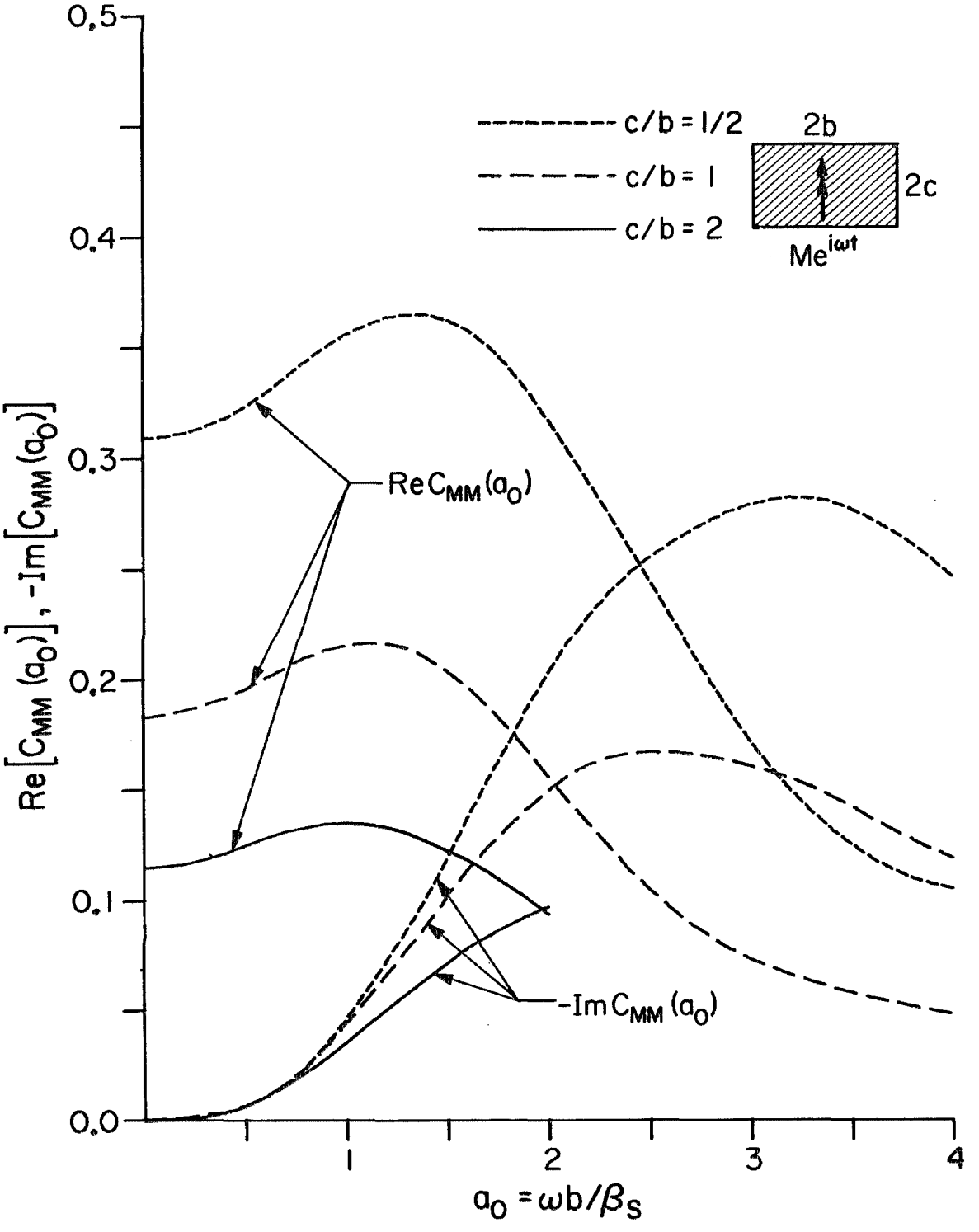

Figure 4-2.6 Rocking compliance for rigid rectangular foundations ($\nu = \frac{1}{3}$).

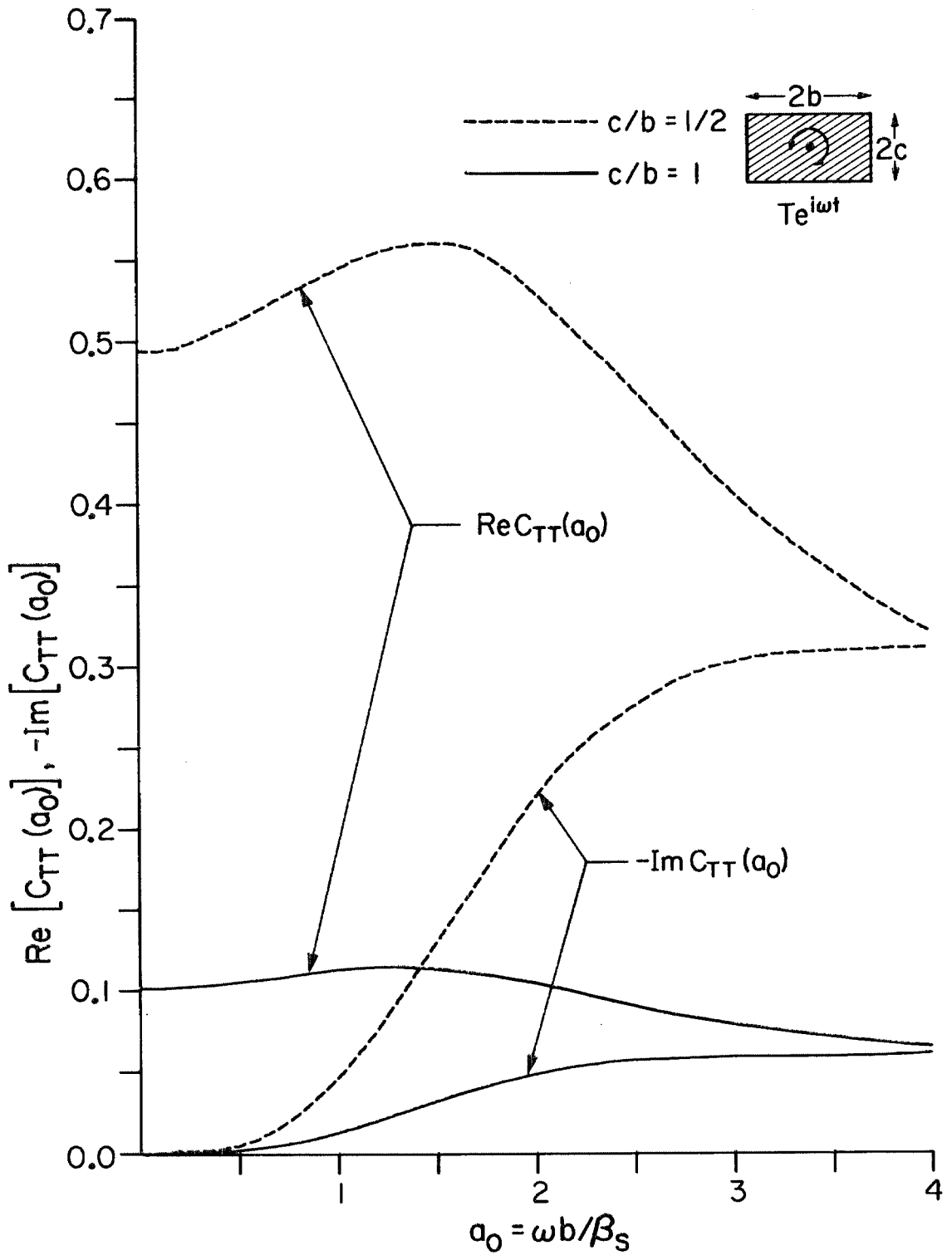

Figure 4-2.7 Torsional compliance for rigid rectangular foundations ($\nu = \frac{1}{3}$).

The Effect of Foundation Shape

The results of Section [3-5] indicated that fine details of the foundation do not affect the compliances appreciably at a low frequency; therefore, a circular foundation may be approximated by using square elements as well. In Table 4-2.1, the approximate vertical compliances for a circular disc foundation, obtained by using 52 square elements, is compared with the exact solution [Luco and Westmann[A129]]. Both of the above analyses have used the relaxed boundary conditions of equation (4-2.11) for vertical excitation. Besides the shape effect, Table 4-2.1 also demonstrates the accuracy of the numerical method; up to $a_0 = 2$, the error for the modulus of the compliance is still less than 5%. Since the important frequencies of most structures are well represented by the frequency band $0 \leq a_0 \leq 2$, the error created by using this approximate approach will usually be negligible.

Another type of foundation which may often occur in application is that with a hole. Likewise, ring type foundations are common in Nuclear Power Plant structures.

From studies of simply connected foundations, it is known that the stress is usually concentrated at the outer edges of the foundation [Veletsos and Wei[A130]]. Therefore, the contribution of the forces on the inside part to the total compliance is not great, and the presence of a hole inside the foundation might not cause significant changes unless the length of the radiated waves in the half space is comparable to the foundation dimensions.

TABLE 4-2.1

VERTICAL COMPLIANCES

$a_0 = \omega b/\beta$	Circular Foundation (Luco & Westmann)	Approximate Circular Foundation
0	(0.167 , 0.000)	(0.166 , 0.000)
0.4	(0.154 , -0.0495)	(0.154 , -0.0491)
0.8	(0.121 , -0.0846)	(0.122 , -0.0856)
1.2	(0.0815, -0.0978)	(0.0824, -0.102)
1.6	(0.0488, -0.0922)	(0.0495, -0.0967)
2.0	(0.0286, -0.0796)	(0.0291, -0.0888)

In Figure 4-2.8, a (2b × 2b) square foundation with a (2d × 2d) square hole is shown. The ratios of d/b equal to 0.75, 0.50, and 0 were studied. The case shown with d/b = 0 is identical to the example presented in Figure 4-2.2 using 64 elements. Comparing the results for d/b = 0 and 0.50, a large deviation does not occur until a_0 is equal to 2 for the real part and 1 for the imaginary part. This indicates that the compliances remain practically the same even when 25% of the foundation area is removed. Comparison of the cases d/b = 0 and 0.75 shows a consistent 15% difference even for the static solution, because more than one half of the area was removed. As indicated by Figure 4-2.8, the large hole causes some oscillatory behavior at higher frequencies. This is caused by wave interferences inside the foundation.

As illustrated by the above examples, the conclusion about the shape effect is again consistent with that of Section [3-5]. The compliance functions are insensitive to the small changes in foundation shape, and the main resistance is contributed by the high stresses near the edges. Since the soil medium cannot resist infinite stresses, the load distribution under a rigid foundation is always finite; thus, the compliance estimated by mathematical models may actually be lower than indicated by the analysis.

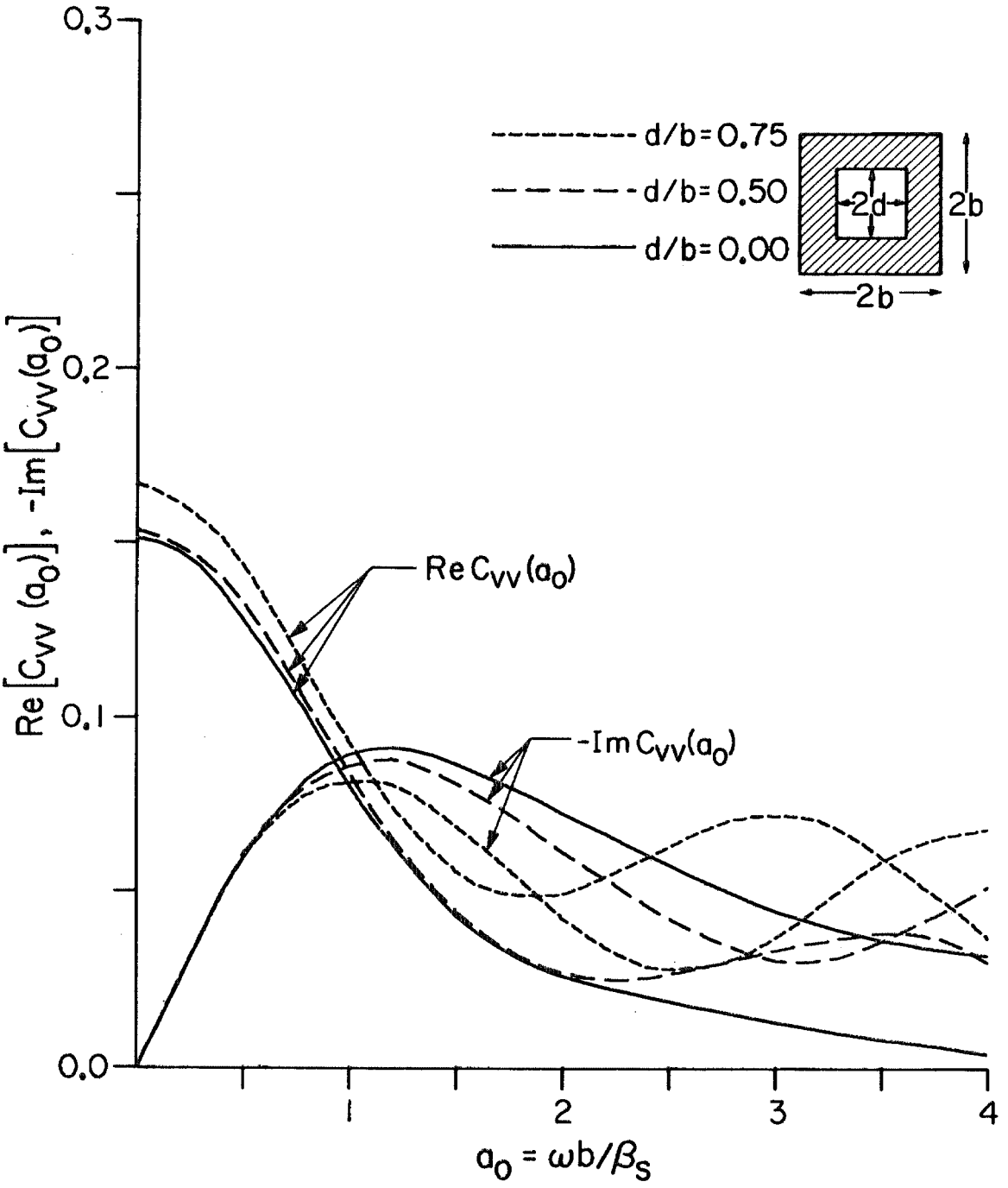

Figure 4-2.8 Vertical compliance for a rigid square foundation with an internal hole ($\nu = \frac{1}{3}$).

Calculation of the Driving Forces and Moments

To complement the compliances (or impedances) already obtained, the driving forces, $\underset{\sim}{F}_s^*$, as defined in Section [2-2] must be evaluated. To illustrate the rotational effects caused by a non-vertical incident wave, for example, a plane harmonic SH-wave is used. The normal of the plane wave is taken to lie in the x_1x_3-plane at an angle θ with the x_1-axis (Figure 4-2.1). The unit harmonic wave can be expressed as

$$u_2^i(x_1, x_2, x_3) = e^{-i\frac{\omega}{\beta}(x_1\cos\theta - x_3\sin\theta)} e^{i\omega t}. \qquad (4\text{-}2.20)$$

Superposed with the reflected wave from the half space boundary, the free field displacement at the surface is

$$u_2^i + u_2^r(x_1, x_2, 0) = 2e^{i\frac{\omega}{\beta}(-x_1\cos\theta)} e^{i\omega t}, \qquad (4\text{-}2.21)$$

which is independent of x_2.

The "fixed" boundary conditions required for calculation of the driving force and torque for the incident plane SH-wave, are then

$$u_2(x_1, x_2, 0) = -2e^{i\frac{\omega}{\beta}(-x_1\cos\theta)} \qquad (4\text{-}2.22)$$

with $u_1(x_1, x_2, 0)$ and $u_3(x_1, x_2, 0)$ unrestricted. The conditions imposed by equation (4-2.22) will directly cancel out with the incident wave motion (4-2.21) at the foundation surface, so that the displacement is zero as required by the "fixed" condition. Substituting (4-2.22)

into the left hand side of (4-2.15), the approximate surface stress distribution can be obtained by inverting the matrix equation.

An SH-wave with $\theta \neq 90°$ causes a translational force in the x_2-direction and a torque about the vertical axis x_3. If the "bonded" boundary conditions are used, all components of the displacement must be compatible. As a result, small rocking and vertical components are also present.

Figure 4-2.9 shows the driving force and torque on a square foundation with the incident wave angle $\theta = 0°$, 45°, and 90°. For $\theta = 90°$, which is the usual assumption made in soil-structure interaction [Jennings and Bielak[A68]], the field displacements in equation (4-2.21) become constant, 2, over the free surface; hence, no torsional motion is possible. The driving force for this case is equal to the impedance function multiplied by a factor of -2; therefore, no scattering of waves occur if $\theta = 90°$.

For angles other than vertical, the wave scattering becomes noticeable for the translation component when $a_0 > 1.0$. For the torsional component, it becomes important at $a_0 \cong 0.5$. Referring to Section [3-2], the wave scattering for embedded foundations is clearly more prominent.

To illustrate the differences created by the geometrical shape of the foundation, consider a square foundation with a hole within it. The size of the hole is such that $d/b = 0.75$ (Figure 4-2.10). The difference shown between its driving force and that of the square foundation is again not great for low frequencies, similar to the behavior of the compliances (Figure 4-2.8). The difference

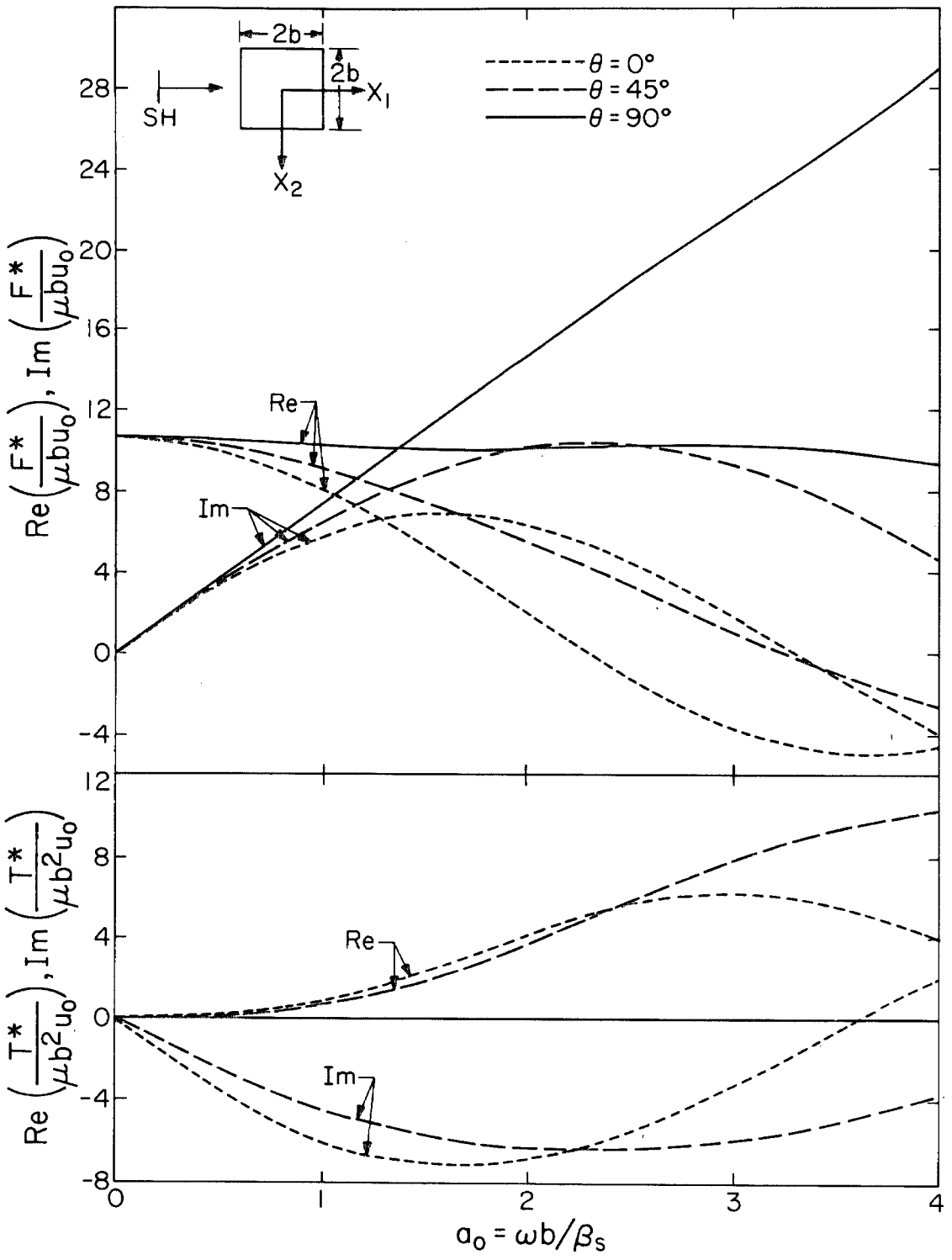

Figure 4-2.9 Transverse driving force and driving torque for a rigid square foundation subjected to incident plane SH-waves.

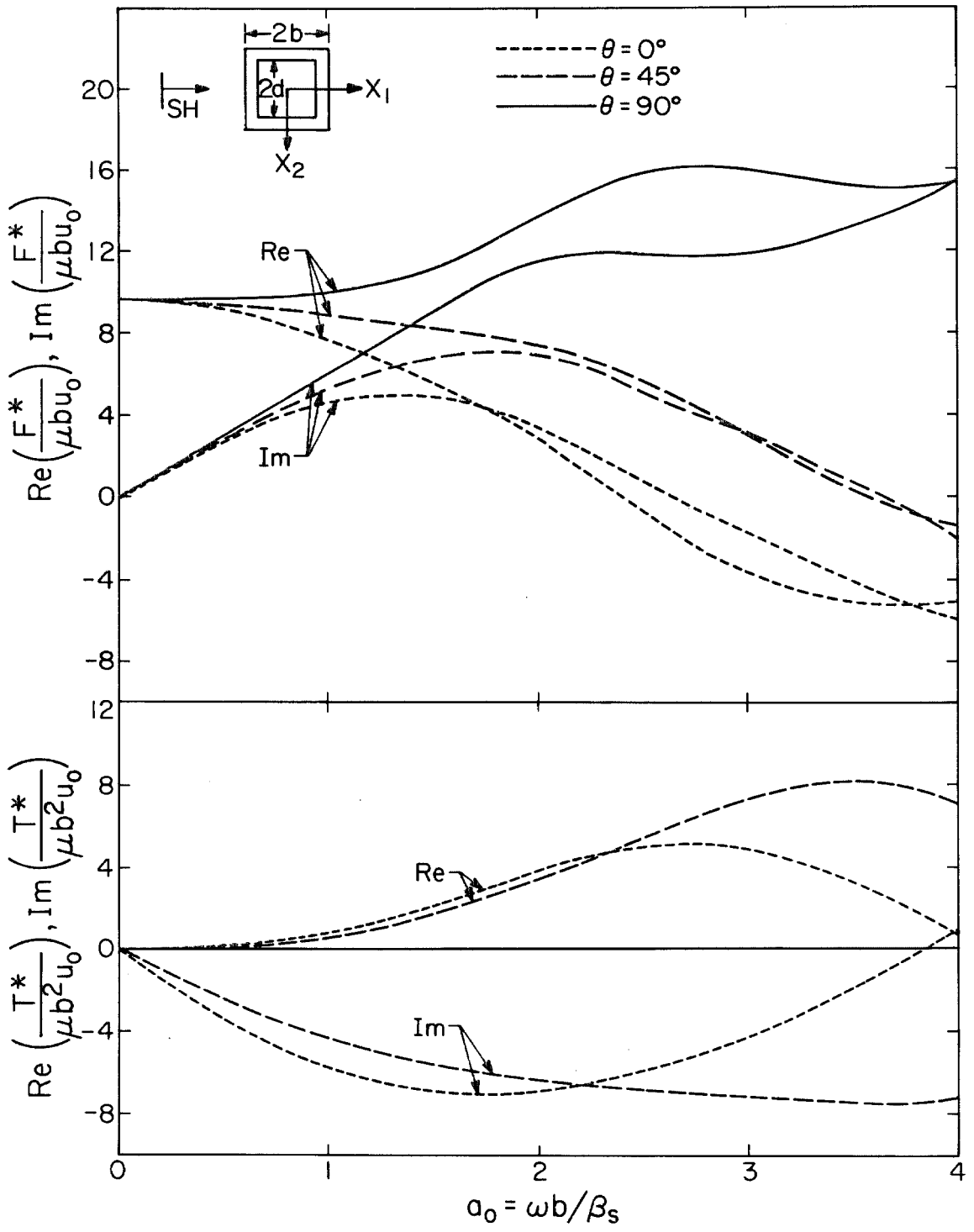

Figure 4-2.10 Transverse driving force and driving torque for a square foundation with a hole subjected to incident plane SH-waves.

in the induced torques for the two cases, however, is even smaller because the stresses are concentrated at the outer edges where the moment arm is the greatest. Therefore, the removal of the inner part has nearly no effect on the torsional characteristics of the foundation, for the torsional compliance function is analogous to the moment of inertia.

The above examples were used to bring out some of the fundamental phenomena of rigid foundation interaction with the soil. It is worthwhile to note, however, that the rigid foundation assumption may not be applicable for higher frequency waves unless its stiffness is much greater than that of the soil medium. If such is the case, the concept of using superposition of the impedance and driving forces must be modified; in general, the problem of soil-structure interaction must be analyzed as a whole without partitioning. An application of the above integral formulation, which can be extended to flexible foundation analyses, will be made in Chapter V.

[4-3] METHOD II - REPLACING THE CONTINUOUS INTEGRAL BY A DISCRETE SUM

Continuing in the search for an approximate solution of the integral equation (4-1.3), the conventional method for solving integral equations will be used. The double integral on the right hand side of (4-1.3) is first evaluated numerically with respect to its unknown integrand, $\underline{\underline{G}}\,\underset{\sim}{T}$, so that the continuous integral can be approximated by a discrete sum

$$\iint_A \underline{\underline{G}}(\omega, \underset{\sim}{x}-\underset{\sim}{x}_0)\underset{\sim}{T}(\underset{\sim}{x}_0)dS_0 \cong \sum_{m=1}^{M}\sum_{n=1}^{N} \alpha_n\alpha_m \underline{\underline{G}}[\omega, x_1-(x_1)_m, x_2-(x_2)_n]\underset{\sim}{T}[(x_1)_m, (x_2)_n] \tag{4-3.1}$$

where α_m and α_n are the weighting constants for the numerical integration in the x_1 and x_2 directions, respectively. The value of these weighting constants usually depends on the type of integration rules used. For the trapezoidal rule with a step size of h, α is equal to h except on the ends of the integration interval where it is equal to h/2.

The procedure for degeneration of equation (4-3.1) requires that the surface area, A, be suitable for simple cartesian integration; otherwise, the discrete sum may be difficult to define. However, if the foundation area, A, is irregular, it can again be broken into smaller elements as in Section (4-2) before the numerical integration is applied. Therefore, the basic approach of Method I and II is the same except for the approximation which follows.

Using the approximation of (4-3.1), the integral equation (4-1.3) can be degenerated into a set of simultaneous equations for

discrete values of the unknowns, $\underset{\sim}{T}$, by matching the displacement to the boundary conditions at the points where the numerical integration is sampled. The algebraic equation taken at the observation point, $[(x_1)_i, (x_2)_j]$, is

$$\underset{\sim}{u}_{ij} = \sum_{n=1}^{N} \sum_{m=1}^{M} \alpha_n \alpha_m \underline{\underline{G}}[\omega, (x_1)_i - (x_1)_m, (x_2)_j - (x_2)_n] \underset{\sim}{T}_{mn} , \qquad (4\text{-}3.2)$$

where $\underset{\sim}{u}_{ij}$ is the displacement at the observation point and $\underset{\sim}{T}_{mn}$ is the value of the traction at the source point. Equation (4-3.2) is similar to the formulation proposed by Elorduy *et al.*[A163] except for the weighting factor, α; therefore, the problem with singularity of the Green's function matrix $\underline{\underline{G}}$, when $(x_1)_i = (x_1)_m$ and $(x_2)_j = (x_2)_n$, remains.

In the present approach, the integrable singularity will be accounted for by exact integration over a small area surrounding the observation point. This approximation is analogous to the method by which Banaugh and Goldsmith (1963) handled the logarithmic singularity for a single integral. We first divide the surface area, A, into two parts: a small area, A_{ij}, surrounding the observation point, $[(x_1)_i, (x_2)_j]$, and the complementary area, $A^c = A - A_{ij}$. For integration over the surface A^c, the Green's function is well behaved and the numerical integration rule of equation (4-3.2) can be used effectively. For the surface area, A_{ij}, the integrand $\underline{\underline{G}}\,\underset{\sim}{T}$ can be integrated exactly to eliminate the singularity of $\underline{\underline{G}}$; the approach used in Method I will be applied here. By expanding $\underset{\sim}{T}$ in a Taylor Series about the observation point and taking only the zeroth order

term, $\underset{\sim}{T}_{ij}(\underset{\sim}{x}_{ij})$, the integral over A_{ij} can be reduced to $4\frac{b^*}{\mu}\Phi(kb^*, 0)\,\underset{\sim}{T}_{ij}$, where b^* is the characteristic dimension of the area A_{ij}. The dimension, b^*, of A_{ij} should be chosen so that it is compatible with the numerical integration grid. For example, when using a square grid network with step size of h, the area A_{ij} should be chosen so that it is an $(h \times h)$ square, centered at the point $[(x_1)_i, (x_2)_j]$.

With the above modification, (4-3.2) can be rewritten as

$$\underset{\sim}{u}_{ij} = \sum_{n=1}^{N}\sum_{\substack{m=1 \\ (m,n)\neq(i,j)}}^{M} \alpha_n\alpha_m G_{ijmn}\underset{\sim}{T}_{mn} + \alpha_i\alpha_j\left\{\frac{2h}{\mu}\Phi\left[k\left(\frac{h}{2}\right), 0\right]\underset{\sim}{T}_{ij}\right\} \qquad (4\text{-}3.3)$$

if the trapezoidal rule is used. The weighting factor $\alpha_i\alpha_j$ for this particular rule is $\frac{1}{4}h_nh_m$ at the corners $\frac{1}{2}h_nh_m$ at the sides, and h_nh_m at the interior of the grid network. The weights $\alpha_i\alpha_j$ can also be applied on the second term of the right hand side if the symmetric vertical or horizontal cases are considered, because the area A_{ij} is only $\frac{1}{4}(h_i \times h_j)$ at the corners and $\frac{1}{2}(h_i \times h_j)$ on the sides.

The unknowns, $\underset{\sim}{T}_{mn}$, can now be solved for by numerically inverting the matrix equation (4-3.3). The actual value of $\underset{\sim}{T}$ at the corners and sides is, of course, infinite; but using this approximate method, only finite values will be obtained. The numerical values of $\underset{\sim}{T}$ can then be used for the determination of the impedance and the "driving force" depending on the type of displacement compatibility imposed.

Circular "Ring-Shaped" Foundations, Vertical Excitation

Using Method II, the circular "ring-shaped" foundation can be analyzed by using the polar coordinate system, (r, θ). The ring-shaped foundation is also practical for many circular-cylindrically shaped structures such as liquid storage tanks, towers, etc., but an analytical solution for the dynamic problem is not yet available because of its complexity. Also, since the ring surface is multiply connected, triple integral equations will result for the mixed boundary value problem; therefore, the analytical solution is considerably more tedious than that of the circular disc foundation.

We now apply Method II by taking advantage of the simplicity of the polar coordinates. Equation (4-1.3) can be rewritten as

$$\begin{bmatrix} u_z(r,\theta) \\ u_r(r,\theta) \\ u_\theta(r,\theta) \end{bmatrix} = \int_0^{2\pi} \int_{r_i}^{r_o} G(\omega, |\underset{\sim}{r} - \underset{\sim}{r}^*|) \begin{bmatrix} T_z(r^*,\theta_o) \\ T_r(r^*,\theta_o) \\ T_\theta(r^*,\theta_o) \end{bmatrix} r^* dr^* d\theta_o \quad (4\text{-}3.6)$$

where r_i and r_o are the inner and outer radii of the ring, respectively. The integral equation (4-3.6) can then determine the traction, $\underset{\sim}{T}$, according to the displacement compatibilities on the left hand side. For the special case with vertical excitation, the condition of symmetry about the center of the ring can simplify the calculations even further because u_z and u_r are independent of the angular coordinate, θ, and u_θ is zero. In addition, if the relaxed boundary conditions are used, i.e., the horizontal component u_r is ignored, equation (4-3.6) can be reduced to a single integral

equation for the vertical component, u_z,

$$u_z(r) = \int_{r_i}^{r_o} T_z(r^*)\, r^* dr^* \int_0^{2\pi} g_{33}(\omega, |\underset{\sim}{r} - \underset{\sim}{r}^*|)\, d\theta_o \qquad (4\text{-}3.7)$$

where the distance, $|\underset{\sim}{r} - \underset{\sim}{r}^*|$, is $\sqrt{r^2 + (r^*)^2 - 2rr^* \cos\theta_o}$, by the cosine law.

For the present analysis, only the axisymmetric Green's function g_{33} is needed. From Love (1927), the static value for g_{33} is

$$g_{33}(0, r) = \frac{1}{4\mu\pi(1-n^2)\, r} = \frac{f_{33}(0)}{\mu r} \qquad (4\text{-}3.8)$$

and for the harmonic point load excitation [Ewing et al. (1957)],

$$g_{33}(\omega, r) = -\frac{a_o}{2\pi\mu r} \int_0^{\infty} \frac{\sqrt{z^2 - n^2}\; z\, J_0(a_o z)}{(2z^2-1)^2 - 4z^2\sqrt{(z^2-1)(z^2-n^2)}}\, dz = \frac{f_{33}(a_o)}{\mu r} \qquad (4\text{-}3.9)$$

where $a_o = \omega r/\beta_s$.

The above expressions are much simpler than the one defined for the influence coefficient, ϕ_{33}, in equation (4-2.7f); therefore, the numerical evaluation of (4-3.9) is not difficult.

To obtain a numerical solution of equation (4-3.7), we shall approximate the integration over the independent variable r* by the trapezoidal rule

$$\int_{r_i}^{r_o} T_z\, r^* \frac{f_{33}\left(\frac{\omega}{\beta_s}|\underset{\sim}{r} - \underset{\sim}{r}^*|\right)}{\mu|\underset{\sim}{r} - \underset{\sim}{r}^*|} dr^* \cong h \sum_{j=1}^{N} \left(\frac{\alpha_j}{h}\right) T_z(r_j) \frac{f_{33}\left(\frac{\omega}{\beta_s}|\underset{\sim}{r} - \underset{\sim}{r}|\right)}{\mu|\underset{\sim}{r} - \underset{\sim}{r}_j|}\, r_j \qquad (4\text{-}3.10)$$

where $h = \frac{(r_o - r_i)}{(N-1)}$ is the step size used for numerical integration. The two-dimensional integral formula is hence reduced to one with one dimension by analyzing the foundation surface in discrete ring elements.

Matching the boundary conditions for the displacements at the center point, r_ℓ, of the ring, the discrete form of equation (4-3.7) becomes

$$u_z(r_\ell) = \sum_{\substack{j=1 \\ j\neq\ell}}^{N} \alpha_j \frac{T_z^i r_j}{\mu} \int_o^{2\pi} \frac{d\theta_o f\left(\frac{\omega}{\beta_s} R\right)}{R} + \frac{\alpha_\ell T_z^\ell}{\mu} \frac{1}{h} \left\{ \int_{r_\ell - h/2}^{r_\ell + h/2} \int_{-h/2r_\ell}^{h/2r_\ell} \frac{d\theta_o r^* dr^* f_{33}\left(\frac{\omega}{\beta_s} R\right)}{\mu R} + r_\ell \int_{h/2r_\ell}^{2\pi - h/2r_\ell} \frac{d\theta_o f_{33}\left(\frac{\omega}{\beta_s} r_\ell \sqrt{2(1-\cos\theta_o)}\right)}{\mu\left(r_\ell \sqrt{2(1-\cos\theta_o)}\right)} \right\} \qquad (4\text{-}3.11)$$

where $R = \sqrt{r_\ell^2 + r_j^2 - 2r_\ell r_j \cos\theta_o}$. The double integral on the right hand side now represents the contribution from the small area surrounding the singularity at $r_\ell = r_j$; the limits of the $d\theta_o$ integral were chosen to be $\pm \frac{h}{2} / r_\ell$ so that this area is nearly a square except for a slight curvature. Also, if the step size, h, of the numerical integration is made small enough, the double integral over a slightly curved area can be performed in cartesian coordinates with only a small difference in value; and it is actually

$\frac{1}{\mu \frac{h}{2}} \phi_{33}\left[k\left(\frac{h}{2}\right), 0, 0\right]$. The remaining part of the ring centered at r_1 can now be approximated by assuming that the integrand is independent of r*; this assumption is an excellent one if the discrete rings are very thin, i.e., h is small.

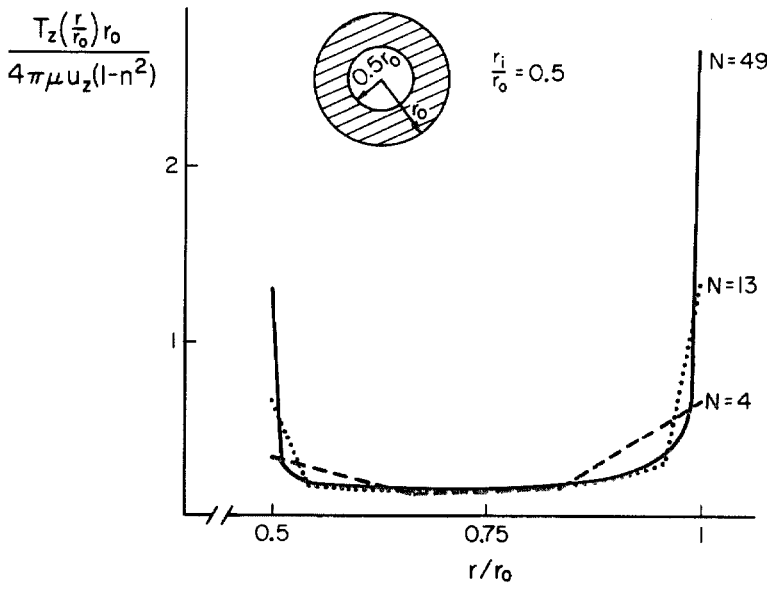

Figure 4-3. 1a Approximate distribution of vertical stress under a rigid ring for N = 4, 13, or 49.

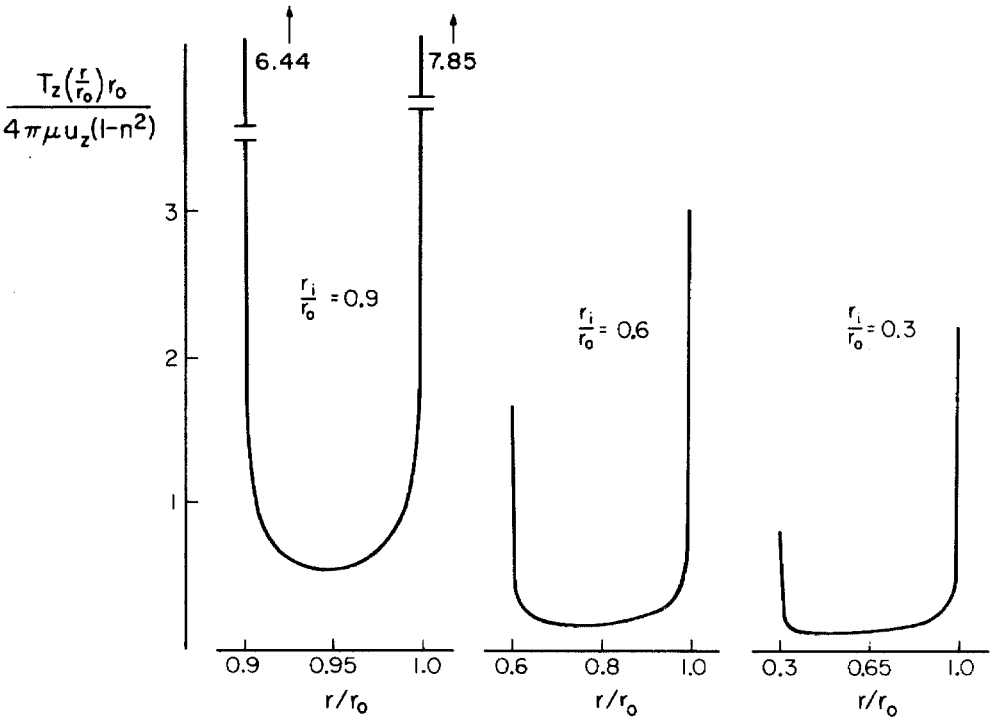

Figure 4-3. 1b Vertical stress distribution under rigid rings with r_i/r_o = 0. 9, 0. 6, and 0. 3 (N = 49).

Vertical Stress Distribution under the Ring Foundation

By numerically inverting the matrix equation (4-3.9), the unknown stress, T_z, at the discrete locations, r_j, $j = 1, 2, \ldots, N$, can readily be obtained. But for a ring foundation, the stress is infinite at both the inside and outside edges; therefore, the numerical approximation cannot equal the exact solution at the two edges. However, the stresses within the ring area can be estimated quite easily because they are usually quite regular.

In Figure 4-3.1a, the static stress distribution under a ring with an inner to outer radii ratio, r_i/r_o, of 0.5 is presented. Since the stress distribution is sensitive to the step size, h, of the numerical integration procedure, the results obtained by using 4, 13, and 49 discrete points were plotted for comparison. As indicated by the dimensionless stresses, the results for the two cases using $N = 13$ and $N = 49$ are nearly identical for most of the area inside the foundation except for a small portion near the outer edges. However, using $N = 4$, the results become quite coarse and do not match well with the results obtained by using $N = 49$, which are approaching those of the exact solution.

Although the exact stress distribution under the ring foundation cannot be approached asymptotically, the impedance of the rigid foundation, however, can approach the exact value quickly by using just a rough approximation. This fact was also indicated by the two-dimensional model in Section [3-5] and by the square plate foundation in Section [4-2]. To illustrate the rate of convergence, the value of the static compliance was calculated for ring

foundations by using different grid sizes and was tabulated in Table 4-3.1. The numerical examples where N = 3, 4, 7, 13, 25, and 49 were chosen for rings with radii ratio of 0.5 and 0.90. As indicated by the tabulated values, the compliance obtained by using 13 grid points is within 2% of that obtained by using 49 grid points. This quick convergence is caused by the smoothing process during the double integration of the stress distribution over the foundation area. This is an obvious advantage of the rigid foundation assumption.

TABLE 4-3.1

APPROXIMATE STATIC COMPLIANCES FOR A CIRCULAR RING FOUNDATION ($v = \frac{1}{3}$)

	$r_i/r_o = 0.5$		$r_i/r_o = 0.9$	
N	$C_{vv}(0)$	% Error	$C_{vv}(0)$	% Error
3	0.1545	9.5	0.1927	5.1
4	0.1594	6.1	0.1958	3.4
7	0.1645	2.9	0.1992	1.7
13	0.1671	1.3	0.2011	0.7
25	0.1685	0.4	0.2020	0.2
49	0.1692	---	0.2025	---

The Influence of the Hole in the Ring Foundation

Recalling the effects caused by a square hole in the square foundation {Section [4-2]}, a similar analysis can be made for the circular ring. The size of the hole, in this case, can be varied by changing the ratio of inner to outer radii, r_i/r_o. The basic phenomena are identical to those of the square foundation; the effect of the hole is not obvious until the ratio, r_i/r_o, is such that more than half of the area is removed.

Since the resistance of the foundation is nearly the same for many different r_i/r_o ratios, the static compliances are tabulated in Table 4-3.2 for comparison. Since the exact vertical static compliance of a circular disc is 0.1667 for a Poisson ratio of $\frac{1}{3}$ [Shah$^{(A125)}$], the values shown in Table 4-3.2 are probably within 1% of the exact compliance of the ring foundation. Tabulated to the right of $C_{vv}(0)$ are the ratios of the ring compliances to the compliance of the circular disc foundation; the trend of these ratios is that no noticeable differences occur until r_i/r_o is greater than 0.5. This is again evidence of the stress concentration occurring at the outer edge of the ring foundation. The stresses are so distributed that when half of the foundation surface is removed, i.e., r_i/r_o = 0.707, the compliance is only 7% higher than that of the circular disc. Therefore, the influence of the hole on the compliances is not significant until it is quite large.

The accuracy of the numerical values given in Table 4-3.2 can be checked in another way because the axisymmetric vertical

TABLE 4-3.2

VERTICAL STATIC COMPLIANCES FOR A RING

r_i/r_o	C_{vv}(ring)	C_{vv}(ring)/C_{vv}(disc)
0.10	0.1656	1.00
0.20	0.1659	1.00
0.30	0.1664	1.00
0.40	0.1674	1.01
0.50	0.1692	1.02
0.60	0.1720	1.04
0.70	0.1768	1.07
0.80	0.1851	1.12
0.90	0.2025	1.22
0.95	0.2223	1.34
0.99	0.2730	1.65

vibration of a ring foundation corresponds directly to an electrostatic problem in which the annular disc is electrified. The solution of this electrostatic problem was obtained by using triple integral equations, some numerical results were presented by Symthe (1951) and Sneddon (1966). The difference between their results and those presented in Table 4-3.2 is less than one percent.

Although the compliances are relatively insensitive to the width of the ring, the stress distribution under the ring, on the other hand, is quite different for all ratios of r_i/r_o. Shown in Figure 4-3.1b are the vertical dimensionless stress distributions under the ring foundations with ratios r_i/r_o = 0.30, 0.60, and 0.90. Other than the well known stress singularity at the inner and outer edges, the stresses within the ring are clearly higher for the case with r_i/r_o = 0.90 than the other two cases. This, perhaps, is accountable for the high load resistances of a thin ring. Note, however, that all of the above solutions are made within the framework of linear elasticity; therefore, the high stresses are a purely mathematical expression for stress concentration. In reality, these high stresses near the edges would cause soil failure; thus, the load resistance of a thin ring may be overestimated if the level of excitation is high enough for the soil to be in the inelastic range.

[4-4] FURTHER APPLICATIONS OF METHODS I AND II

As illustrated by the examples in Sections [4-2] and [4-3], Methods I and II can be used to analyze the vibration of foundations with arbitrary shapes. The power of these integral formulations does not end there, however. They can be extended to analyze many other important problems concerning the dynamics of foundations which can be considered to be flat. For example, the flexible foundation can readily be analyzed so that local stresses and deformations of the foundation as well as the superstructure can be estimated approximately. By knowing the location of large deformations, it is then possible to provide adequate reinforcement.

Another challenging problem is that of multi-structure interaction. By employing Methods I or II, the interactions between a reasonable number of foundations can be investigated. From the results of Section [3-4], the physical phenomena of this multi-structure interaction problem change according to the arrangement of the structures. Since there are infinitely many combinations of interest, there is no general solution for this problem. By physical intuition, one can imagine the complexity of this problem, because one component of force excitation can result in six components of motion for all the structures in the area. For example, the translation of one structure can cause translations in three directions plus rocking and torsional motions for a nearby structure. Of course, the relative sizes of the structures are also important.

From the derivations above, reasonably complex soil-structure interaction problems can be solved along with good engineering judgment. Although the above methods are not capable of handling very deep foundations or foundations on piles, they serve as an improvement over the existing methods for certain types of foundations.

An interesting comparison of the numerical results presented indicates that method I overestimates the exact value of the compliance while method II underestimates it. This trend is clearly shown in Figure 4-4.1, where the static vertical compliance $C_{vv}(0)$ for a square foundation calculated by the two methods is plotted versus N. For method I, $N \times N$ is the number of square subregions used to represent the square foundation, while for method II, $N \times N$ is the number of grid points used for the numerical integration.

From Figure 4-4.1, method I appears to converge to the exact value faster than method II, because the integration procedure, by using influence functions, is of a higher order than the trapezoidal rule. By using N = 25, the difference between the two numerical solutions is 4.5%. This may imply that the approximate solutions are less than 3% from the exact value. Applying the Romberg extrapolation, however, a fair approximation can be obtained by extrapolating and averaging the results given by the lower order approximations. Another modification that may also improve the numerical results is to use subregions of different sizes. This allows the areas with high stress concentrations to be covered by a denser mesh of smaller elementary areas.

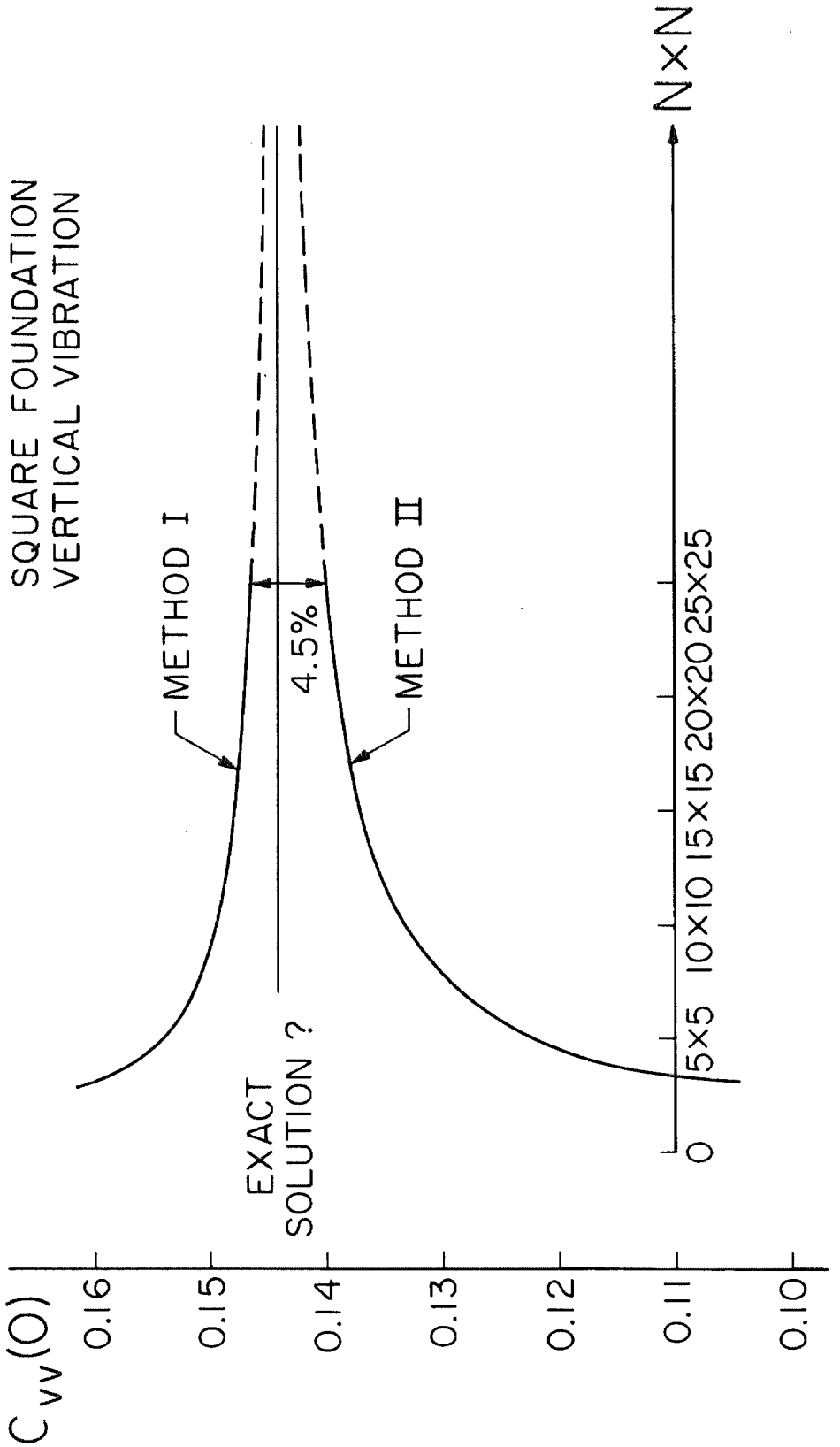

Figure 4-4.1 The rates of convergence for methods I and II.

To interpret physically the converging trends shown in Figure 4-4.1, consider the following explanations:

Method I: The observation points for this method were placed at the center of the rectangular subregions, hence, the displacement compatibilities are matched at points within the rigid foundation rather than on the outside edges. Therefore, the remaining edges of the approximate rigid foundation are "softer" so that the force required to displace it one unit is less than that of a totally rigid foundation. As a result, the compliance, which is inversely proportional to the total force, becomes an upper bound to the exact value.

Method II: The observation points for this method are sampled at the nodes of the grid network. Some of these nodes are located at the edges of the rigid foundation. Theoretically, the stresses are infinite at the sharp edges of the rigid foundation, but finite stresses were obtained numerically due to the approximate nature of the formulation. Nevertheless, the stresses at the edges are far higher than those at the interior nodes, and they contribute heavily to the total force. For this particular case, the weighting factors, α, of the trapezoidal rule overestimate the total force, which in turn underestimates the compliances.

Thus, these two methods appear to yield upper and lower bounds to the exact value; this characteristic can be used effectively in many situations. Comparing these two appraches, method I allows a faster rate of convergence, but method II is somewhat more convenient to apply. The author feels that the former is superior for

a detailed analysis of a single foundation, while the latter can be used more effectively for studies of interaction between many foundations. Of course, either method can be used to obtain results of acceptable accuracy.

CHAPTER V - AN EXPERIMENTAL OBSERVATION OF SOIL-STRUCTURE INTERACTION

[5-1] DEFORMATION OF A FLEXIBLE FOUNDATION

Several facets of soil-structure interaction have been investigated in previous chapters by using idealized two-dimensional or three-dimensional theoretical models. To simplify the realistic problem to a mathematically manageable one, numerous details of the prototype had to be sacrificed, because even the most sophisticated mathematical solutions cannot represent the true behavior of soil-structure interaction. In this chapter, some experimental observations will be discussed to complement the theoretical observations made in previous chapters so that a better understanding of the problem will be possible.

Since 1966, numerous experiments have been performed on the Robert A. Millikan Memorial Library at the California Institute of Technology by the personnel of the Earthquake Engineering Research Laboratory. As a result, the building characteristics, such as the mode shapes and mode frequencies, are well documented [e.g., Kuroiwa (A20), Trifunac (1972)]. Recently, an experiment designed to study the soil-structure interaction and the resulting wave propagation in the nearby soil was performed on the nine-story library by Luco et al. (1975). The vibration induced into the soil during the test was measured over a radius of several miles around the library, consistent with observations made by Jennings (1970), who

had concluded that a building excited at one of its resonant frequencies could become a very efficient wave generator.

In the analysis which follows, simple wave propagation theories discussed in previous chapters will be used in an attempt to correlate the experimental data with theoretical calculations. These data, presented by Luco et al. (1975), have been sampled at 50 locations in the basement of the library and also at 100 locations outside the library (Figures 5-1.1, 5-1.2, and 5-1.3).

We begin by examining the foundation plan of the Millikan Library as shown in Figure 5-1.4. Its dimensions are: 69 feet in the N-S direction, 75 feet in the E-W direction, and approximately 23 feet into the ground. The supporting system of the library consists of a central pad 32 feet wide and 4 feet deep which runs in the E-W direction connecting the two 12-inch thick shear walls on the east and west ends of the building. These shear walls provide the lateral strength to the building for the N-S deformations. The central pad also supports the smaller 12-inch thick reinforced concrete walls of the central core, which serve as an elevator shaft as well as strengthening the building for the E-W deformations. The vertical columns on the north and south ends of the building are supported on two independent beams, each 10 feet wide and 2 feet deep (Figure 5-1.4).

From the above brief description of the foundation plan, one can see that the foundation system of the Millikan Library is flexible and can be deformed by the forces exerted on it by the superstructure. Of course, this deformation of the foundation slabs

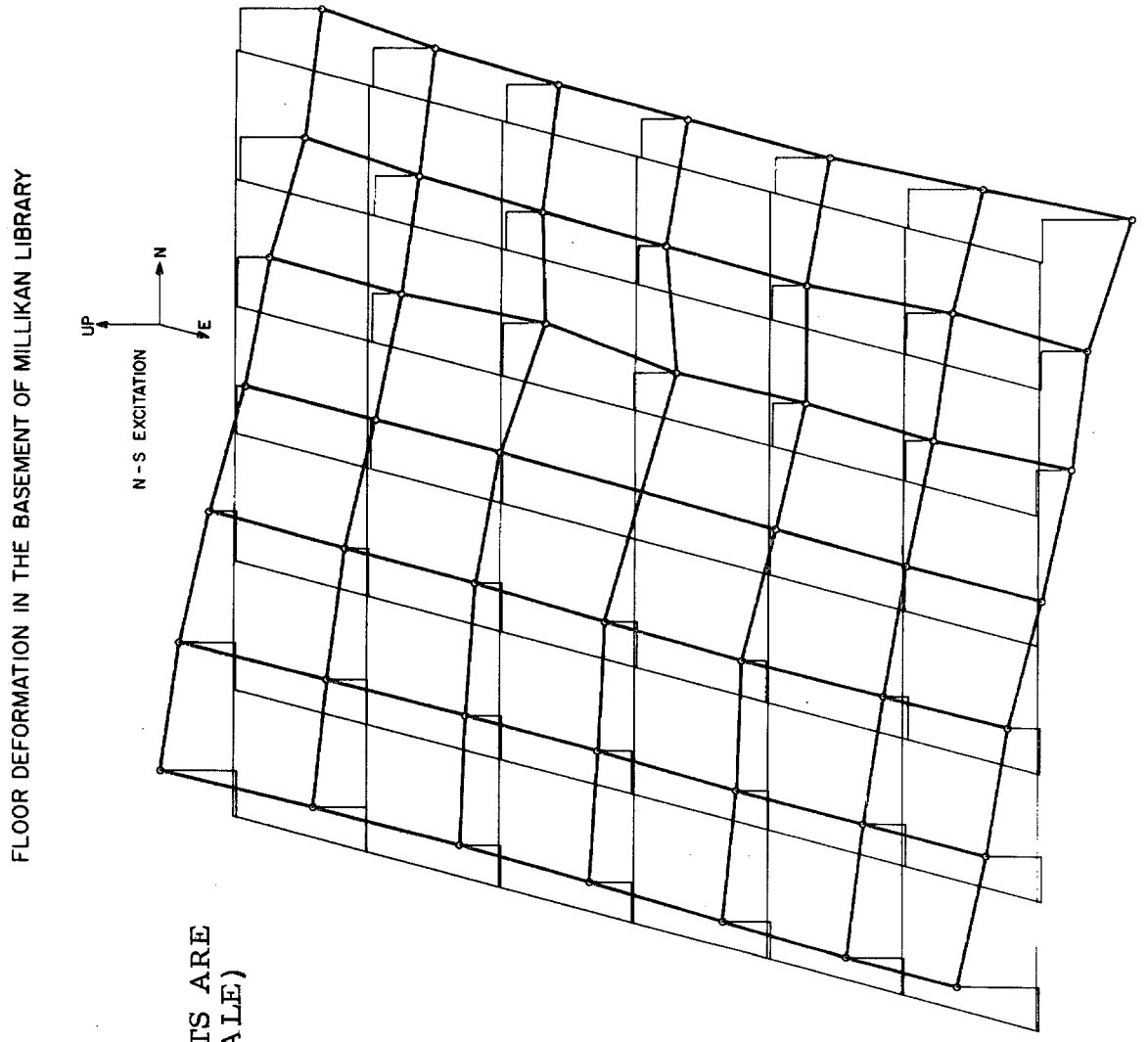
FLOOR DEFORMATION IN THE BASEMENT OF MILLIKAN LIBRARY
UP
N
E
N-S EXCITATION
(DISPLACEMENTS ARE
NOT TO SCALE)

Figure 5-1.1

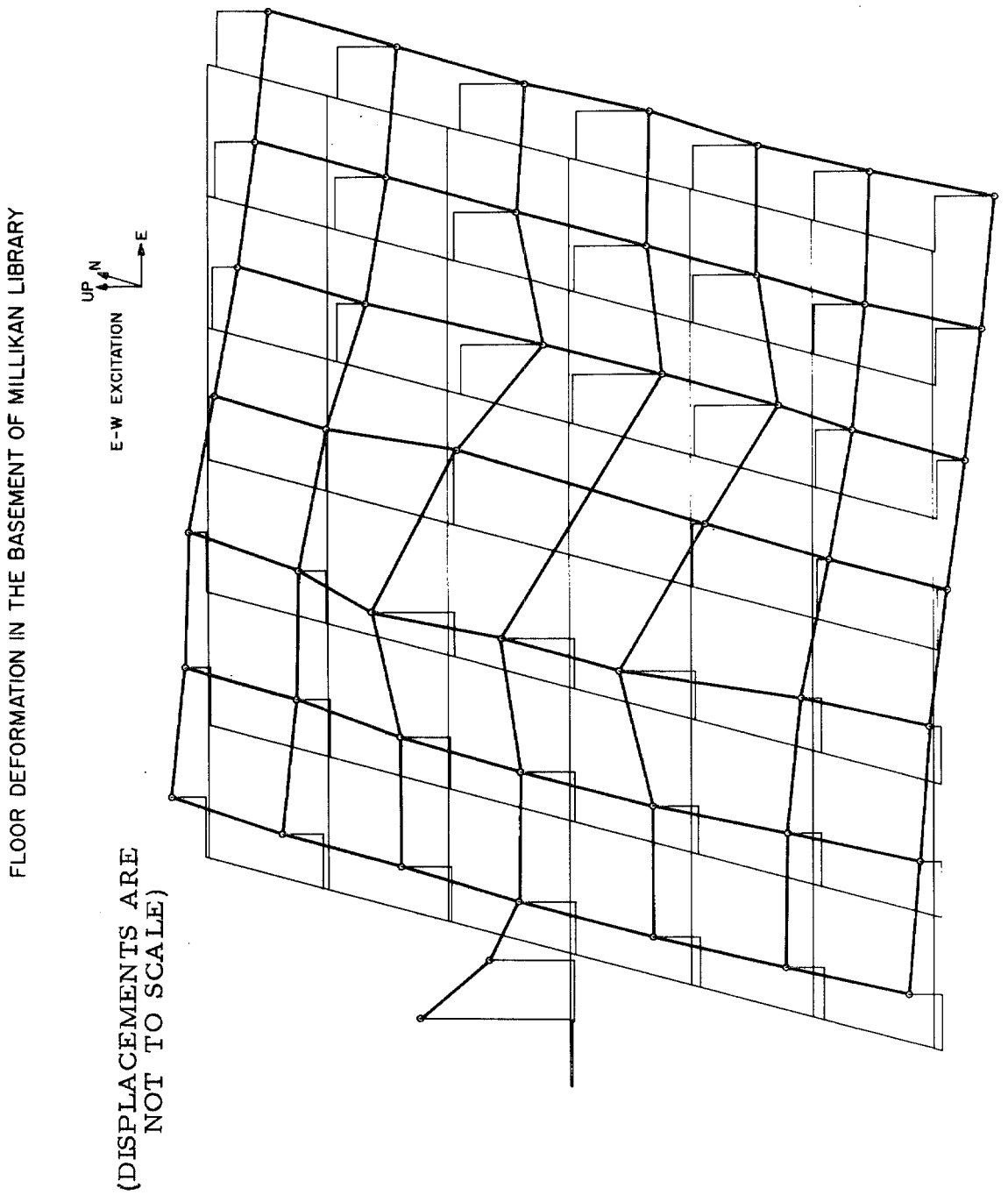
FLOOR DEFORMATION IN THE BASEMENT OF MILLIKAN LIBRARY
UP
N
E
E-W EXCITATION
(DISPLACEMENTS ARE
NOT TO SCALE)

Figure 5-1.2

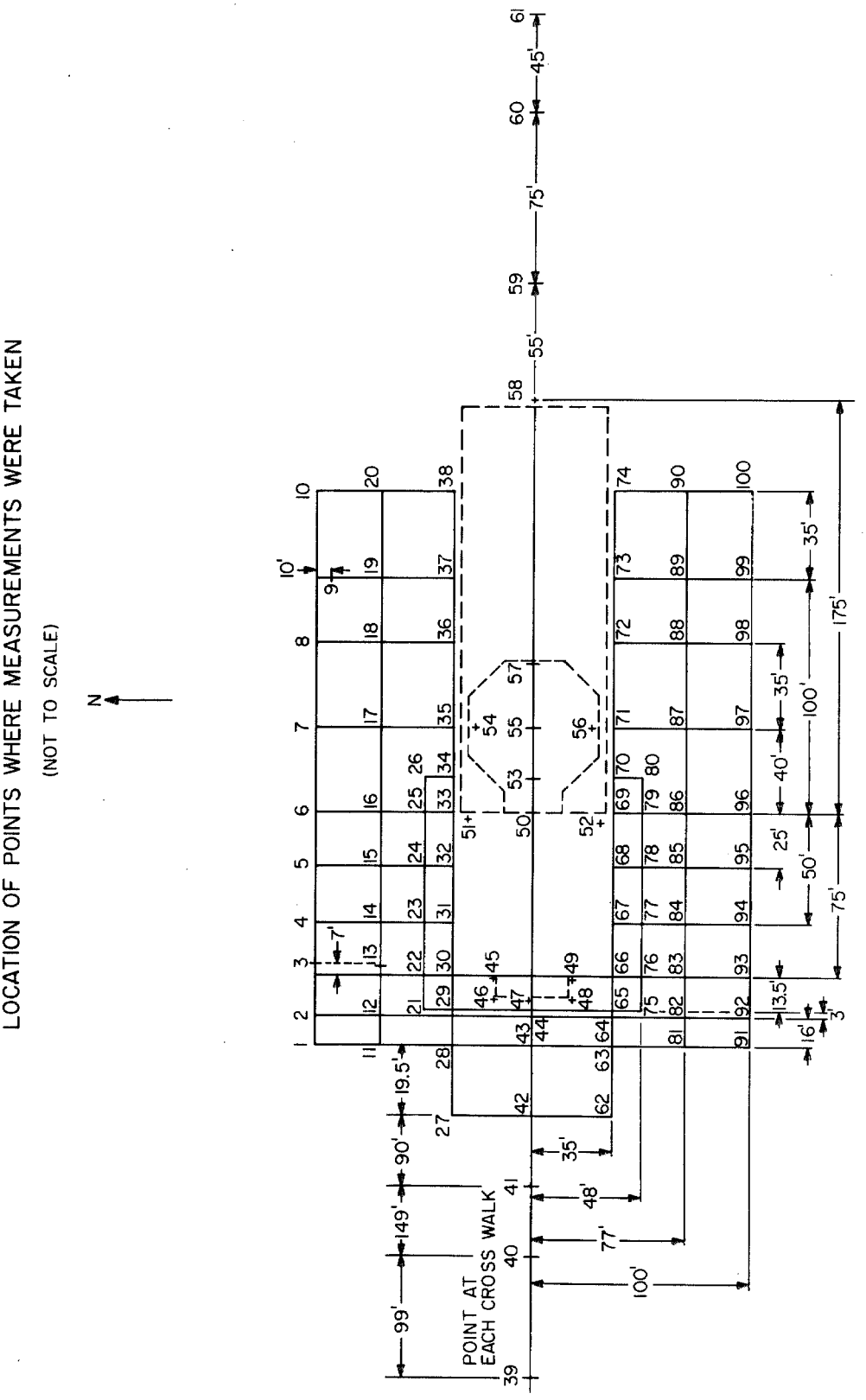
LOCATION OF POINTS WHERE MEASUREMENTS WERE TAKEN
(NOT TO SCALE)
N
POINT AT EACH CROSS WALK

Figure 5-1.3

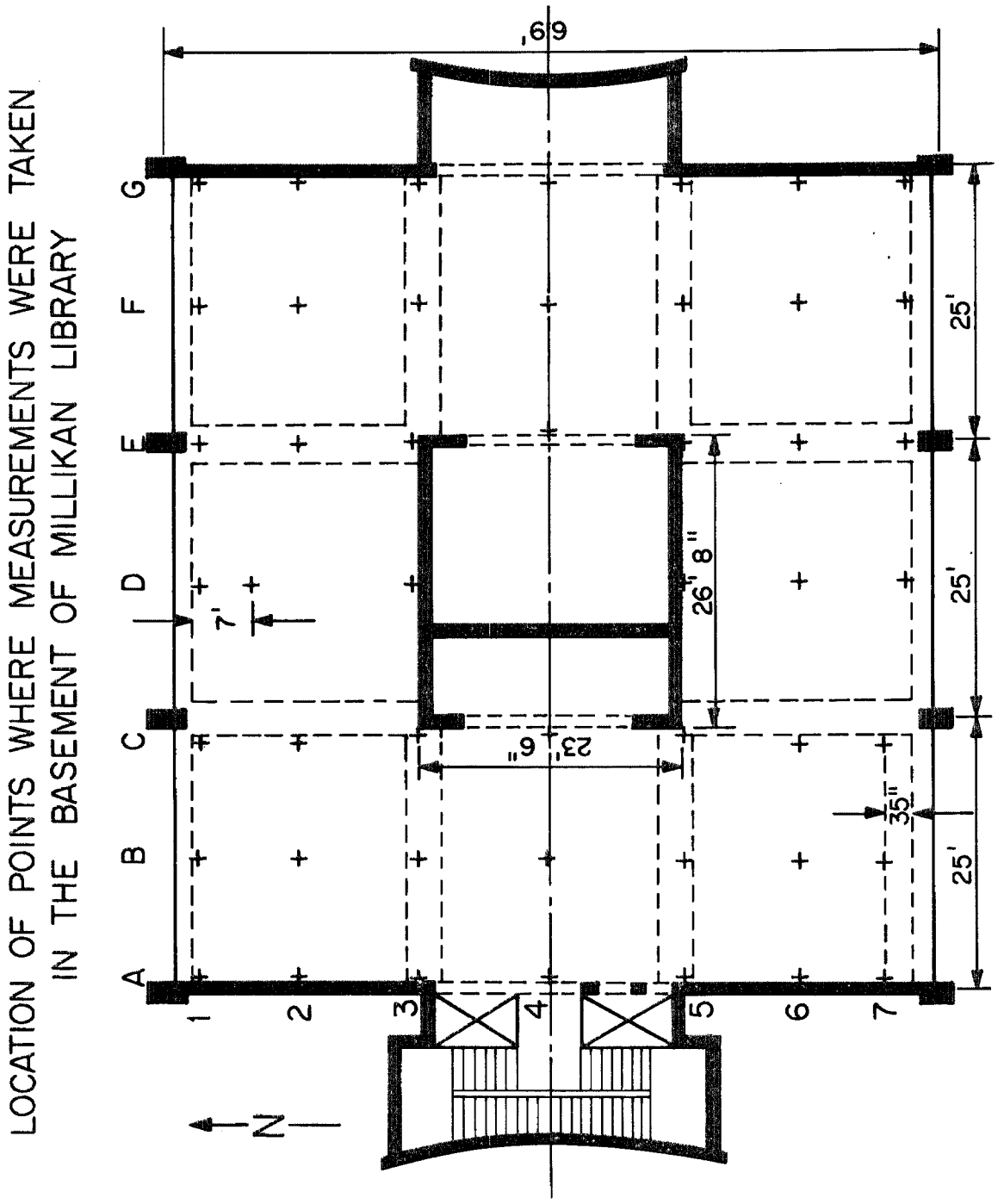
LOCATION OF POINTS WHERE MEASUREMENTS WERE TAKEN
IN THE BASEMENT OF MILLIKAN LIBRARY
69'
G
F
E
D
C
B
A
1
2
3
4
5
6
7
25'
25'
25'
26' 8"
7'
23' 6"
35"
N

Figure 5-1.4

depends on the relative movement of the structural members above it. For instance, the deformation pattern in the basement floor is not even similar for the E-W and N-S vibrations (Figures 5-1.1 and 5-1.2), indicating significant differences between the lateral stiffness provided by the shear walls (N-S) and by the central core (E-W). The investigation carried out by Foutch et al. (1975) also emphasized some of these characteristics. When the library building was excited at its fundamental mode in the N-S direction, the stiff shear walls on the east and west ends of the building caused the entire structure to translate and rotate in a way similar to that of a rigid body (see the basement deformation patterns illustrated in Figure 5-1.2). Though the motion of the foundation is quite uniform, the large shear walls and the central core walls cause the underlying foundation beams to deform like a beam on a soft foundation, as indicated by the type of curvatures that can be seen in this figure. For the E-W shaking, however, the central core walls, rather than the outside shear walls, are providing the main resistance to lateral motions. Hence, this results in a twist in the center of the foundation where the core wall is jointed to the central foundation slab (Figure 5-1.4). As shown by Figure 5-1.3, the basement floor plane is so distorted that the rigid foundation assumption may become questionable.

From the deformation patterns shown in Figures 5-1.1 and 5-1.2, it appears that a flexible foundation may experience larger local deformations than a rigid foundation. Therefore, the non-linear response or failure of the soil underneath the foundation,

or the nonlinear response of the superstructure, becomes more likely during high level excitations.

By using the displacement data of the basement floor presented in Figures 5-1.1 and 5-1.2, the approximate stress distribution impressed on the soil can be estimated by using the integral formulation derived in Section [4-2], because this method does not require the foundation to be rigid. However, one of the more serious restrictions is that the foundation model be flat. In the particular case of the library, however, the embedment to width ratio, h/b, is approximately 23 feet/75 feet; hence, in view of the results of Section [3-2], there may be some justification in making the flat foundation assumption. Also, because the excitation level of the test was low [Luco et al. (1975)], the linear theory can be used effectively here.

For the present analysis, the measured displacements will be imposed as the displacement compatibility conditions for the mixed boundary value problem. The various dimensionless parameters used will be based on the actual value of the structural system. The values of the dimensionless frequency, a_0, for example, are determined as in Table 5-1.1. The values calculated are approximately equal to 0.2, which is quite a low value for the dimensionless frequency a_0. Judging from the results presented in Chapter IV, the values of the compliances at such low frequencies are nearly equal to those for the static solution. Because of this, the simplified calculations of the following analysis will be made by using the static assumption.

TABLE 5-1.1

PROPERTIES OF THE FOUNDATION SYSTEM

	NS Direction	EW Direction
Shear Wave Velocity in Soil:	1300 ft/sec $< \beta_s <$ 2000 ft/sec	1300 ft/sec $< \beta_s <$ 2000 ft/sec
Fundamental Resonance Frequency:	f ~ 1.8 Hz	f ~ 1.3 Hz
Characteristic Dimension:	b = $\frac{1}{2}$ (69 feet)	b = $\frac{1}{2}$ (75 feet)
Dimensionless Frequency:	$0.19 < a_o < 0.29$	$0.14 < a_o < 0.22$

Shown in Figure 5-1.5 is a quantization of the basement floor plan using 50 rectangular elements. Admittedly, this may be rather crude, but further refinements are beyond the scope of this thesis, which is being focused on the first order effects. This particular arrangement was chosen so that the experimentally measured points (indicated by asterisks) are as close to the centers of the elements as possible. Also, to emphasize the loading of some of the heavier structural members, different sizes of elements were taken to model the stress distribution more closely.

This discrete flat foundation model shown in Figure 5-1.5 has been employed to obtain the resulting stresses by using the integral formulation presented in Section [4-2]. The results obtained for the N-S vibration and normalized to the highest value are tabulated in Table 5-1.2 under the heading "flexible foundation." The stresses for the E-W vibration are shown in Table 5-1.3. The numbering system of the elements used in these tables is defined in Figure 5-1.5. For both Tables 5-1.2 and 5-1.3, parts (a) and (b) display the vertical and the horizontal stresses, respectively.

The stress distributions tabulated in these tables show that the larger stresses in the soil usually occur under the heavier structural members, such as the shear walls and the central core, indicating that the largest soil deformations caused by the lateral and rocking motions of the building are underneath these members. Therefore, the flexible foundation, unlike the rigid foundation, may concentrate the loading on certain localized regions of the foundation.

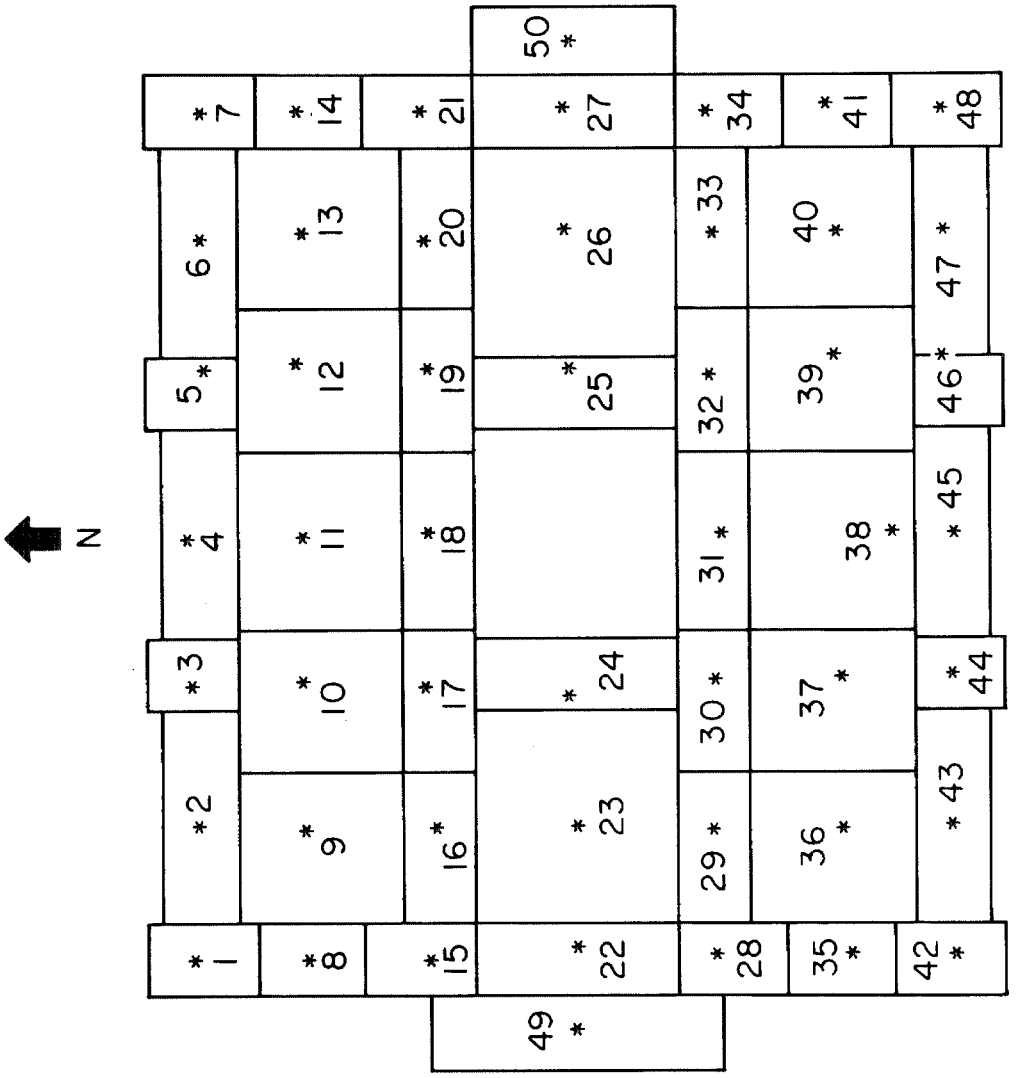

Figure 5-1.5 An approximation for the Millikan Library foundation plan in terms of non-uniform rectangular subregions.

TABLE 5-1.2(a)

NORTH-SOUTH VIBRATION
NORMALIZED VERTICAL STRESSES

Element	Flexible Foundation	Rigid Foundation	Element	Flexible Foundation	Rigid Foundation
1	0.871	0.607	26	-0.001	-0.000
2	0.370	0.445	27	0.051	-0.000
3	0.286	0.441	28	-0.185	-0.147
4	0.212	0.424	29	-0.095	-0.072
5	0.251	0.441	30	-0.120	-0.056
6	0.596	0.445	31	-0.273	-0.057
7	1.000	0.612	32	-0.139	-0.056
8	0.500	0.284	33	-0.100	-0.071
9	0.097	0.143	34	-0.234	-0.148
10	0.021	0.124	35	-0.503	-0.284
11	0.047	0.125	36	-0.119	-0.143
12	0.019	0.124	37	-0.107	-0.124
13	0.114	0.142	38	-0.091	-0.125
14	0.151	0.290	39	-0.047	-0.124
15	0.133	0.147	40	-0.115	-0.142
16	0.045	0.072	41	-0.427	-0.290
17	0.372	0.056	42	-0.827	-0.607
18	0.343	0.057	43	-0.330	-0.445
19	0.174	0.056	44	-0.145	-0.441
20	0.095	0.071	45	-0.190	-0.424
21	0.229	0.148	46	-0.262	-0.441
22	0.060	-0.000	47	-0.400	-0.445
23	0.007	-0.000	48	-0.917	-0.612
24	-0.094	-0.000	49	0.060	0.000
25	0.029	-0.000	50	-0.007	0.000

TABLE 5-1.2(b)

NORTH-SOUTH VIBRATION
NORMALIZED HORIZONTAL STRESSES (N-S COMPONENT)

Element	Flexible Foundation	Rigid Foundation	Element	Flexible Foundation	Rigid Foundation
1	0.914	0.860	26	0.110	0.061
2	0.487	0.701	27	0.116	0.194
3	0.410	0.615	28	0.283	0.222
4	0.404	0.617	29	0.085	0.021
5	0.323	0.615	30	0.136	0.023
6	0.513	0.702	31	0.229	0.051
7	0.962	0.867	32	-0.028	0.024
8	0.175	0.318	33	-0.005	0.022
9	-0.015	0.125	34	0.270	0.253
10	-0.022	0.124	35	0.358	0.318
11	0.089	0.104	36	0.100	0.125
12	-0.074	0.125	37	0.164	0.124
13	0.117	0.126	38	0.158	0.104
14	0.097	0.328	39	0.047	0.125
15	0.504	0.222	40	0.155	0.126
16	0.245	0.021	41	0.428	0.328
17	0.590	0.024	42	1.000	0.860
18	-0.106	0.051	43	0.676	0.701
19	0.282	0.024	44	0.498	0.615
20	-0.059	0.022	45	0.431	0.617
21	0.429	0.253	46	0.391	0.615
22	0.258	0.178	47	0.409	0.702
23	0.147	0.060	48	0.921	0.867
24	0.296	0.076	49	0.509	0.397
25	0.209	0.076	50	0.888	0.437

TABLE 5-1.3(a)

EAST-WEST VIBRATION
NORMALIZED VERTICAL STRESSES

Element	Flexible Foundation	Rigid Foundation	Element	Flexible Foundation	Rigid Foundation
1	-0.098	-0.360	26	0.119	0.065
2	-0.050	-0.155	27	0.140	0.145
3	-0.082	-0.072	28	0.113	-0.191
4	0.022	0.000	29	-0.037	-0.077
5	0.074	0.073	30	-0.472	-0.030
6	0.109	0.157	31	0.057	0.000
7	0.201	0.363	32	0.399	0.031
8	-0.051	-0.251	33	0.084	0.079
9	-0.005	-0.083	34	0.161	0.222
10	-0.019	-0.034	35	-0.041	-0.251
11	-0.020	0.000	36	-0.031	-0.083
12	-0.015	0.034	37	-0.003	0.034
13	0.060	0.085	38	0.027	0.000
14	0.184	0.259	39	0.015	0.034
15	0.073	-0.191	40	0.050	0.085
16	-0.077	-0.077	41	0.133	0.259
17	-0.514	-0.030	42	-0.107	-0.360
18	0.008	0.000	43	-0.025	-0.155
19	0.423	0.031	44	-0.055	-0.072
20	0.099	0.079	45	0.035	0.000
21	0.174	0.222	46	-0.055	0.073
22	0.079	-0.132	47	0.140	0.157
23	-0.061	-0.063	48	0.278	0.363
24	-0.421	-0.028	49	-1.000	-0.309
25	0.466	0.028	50	0.256	0.332

TABLE 5-1.3(b)

EAST-WEST VIBRATION
NORMALIZED HORIZONTAL STRESSES (E-W COMPONENT)

Element	Flexible Foundation	Rigid Foundation	Element	Flexible Foundation	Rigid Foundation
1	0.781	0.786	26	0.054	0.097
2	0.457	0.332	27	-0.002	0.201
3	0.411	0.220	28	0.120	0.395
4	0.460	0.277	29	0.071	0.109
5	0.411	0.219	30	-0.104	0.067
6	0.392	0.328	31	0.246	0.093
7	0.780	0.799	32	-0.032	0.068
8	0.370	0.561	33	0.096	0.117
9	0.290	0.147	34	0.297	0.491
10	-0.025	0.078	35	0.410	0.561
11	0.104	0.054	36	0.170	0.147
12	0.132	0.078	37	0.083	0.078
13	0.133	0.146	38	0.093	0.054
14	0.404	0.567	39	0.175	0.079
15	0.187	0.395	40	0.089	0.146
16	0.089	0.109	41	0.454	0.567
17	-0.296	0.067	42	0.687	0.786
18	0.629	0.093	43	0.396	0.332
19	-0.153	0.068	44	0.333	0.220
20	0.0968	0.117	45	0.420	0.277
21	0.307	0.063	46	0.289	0.219
22	0.126	0.200	47	0.408	0.328
23	0.043	0.092	48	0.841	0.799
24	-0.211	0.201	49	0.989	0.589
25	-0.264	0.063	50	1.000	0.634

To estimate the degree by which the calculated stresses exceed those of a rigid foundation having the same shape, a study was made of an equivalent rigid foundation. Since the displacement pattern under the flexible foundation is different from that which would be caused by a rigid foundation, an equivalent horizontal displacement, Δ_H, and an equivalent rocking angle, ϕ, were defined for the rigid foundation so that the horizontal load and rocking moment induced would be equal to those calculated for the flexible foundation. It was found that the horizontal displacement is approximately the average of the displacements, i.e., $\Delta_H \simeq \frac{1}{N} \sum_{j=1}^{N} u_1^j$; while the equivalent angle of rotation is subjected to a "moment" type of normalization: $\phi \approx \frac{\sum_{j=1}^{N} d_j u_3^j}{\sum_{j=1}^{N} d_j^2}$, where d_j is the moment arm of the jth element.

The stress distribution of the equivalent rigid foundation is also tabulated in Tables 5-1.2 and 5-1.3. It can be seen to be more uniform than that of the flexible foundation, but, as would be expected, the higher stresses are concentrated at the outside portions of the plan.

Comparing these two models, one can easily distinguish their principal areas of load resistance, especially for the E-W motions. As indicated earlier, the reinforcements in the E-W direction are

partly provided by the central elevator core, e.g., elements #17, 18, 19, 30, 31, and 32. Thus, a significant part of the rocking moment is counteracted by the reaction moments created by the vertical stresses on elements #17, 19, 30, and 32. This is indicated by their higher stress levels when compared to the neighboring elements.

The equivalent rigid foundation, on the other hand, makes no distinction for the locations of the load carrying members because it translates and rotates as a rigid plate. The load resisting reactions are mainly provided by the outer edges; the vertical stresses at the central core area are then more than an order of magnitude lower (Table 5-1.3a). Hence, there is an obvious difference in the emphasis on the support.

The fundamental differences of these two foundation models may also be detected in the superstructure. For a rigid foundation, there is little relative deformation between the major structural members, such as the Millikan Library excited in the N-S direction. But for a flexible foundation, such as the Millikan Library excited in the E-W direction, the relative movement between the central core and the two large shear walls can result in larger deformations in the floor slabs on the higher levels [Foutch et al. (1975)]. Hence, in several aspects of design, a rigid foundation plan may be more desirable.

[5-2] RECORDED GROUND MOTIONS IN THE IMMEDIATE VICINITY OF THE MILLIKAN LIBRARY

From the point of view of the overall soil deformation, the motion outside the library is of special interest. Detailed studies of the data recorded outside the Millikan Library can reveal whether the effect of embedment has important contributions to the "near field" term or to what extent the body and surface waves contribute to the recorded motions. For distant measurements, of course, the library resembles a point source [Luco et al. (1975)], and the details of the foundation plan are not important. But the shape as well as the flexibility of the foundation plays a major role in the vibrations in the immediate vicinity of the building. It is therefore useful to analyze the "near field" data by using the displacement measurements made inside the library.

The "near field" experimental data obtained from Luco et al. (1975) covered an area extending 400 feet from the library in both the east and the west directions and 100 feet in the north and the south directions. Three components were available for each of the 100 locations shown in Figure 5-1.3, all of which are within the campus of the California Institute of Technology.

The surrounding area of the Millikan Library cannot easily be considered as a simple elastic half space. For example, the recordings at stations 40-43 (Figure 5-1.3) were made on pavement, while stations 33-38 and 69-74 (Figure 5-1.3) were placed on the side of a fountain. Also, stations 1-10 and 91-100 were placed along the arcades of the surrounding buildings. Nevertheless, the

displacement pattern for the network of recorded motions in Figure 5-1.3 will be analyzed by using the same integral formulations as in Section [5-1] and by neglecting the adverse effects that may be created by the nearby buildings.

Since the approximate stresses under the library foundation have been calculated in the previous section, the model no longer represents a "mixed boundary value problem." By superimposing the known stresses, the displacement on the surface of the half space can be obtained. Doing so for the stations where the field measurements were taken, the theoretical results can be compared with the measurements as in Figure 5-2.1 for the N-S vibration and in Figure 5-2.2 for the E-W vibration.

In these figures, x is defined to be positive in the east direction, while positive y points in the north direction. Each of the figures consists of part a through i, displaying the vertical and horizontal components of the displacement at the longitude lines where y = 0, ±35, ±48, ±77, and ±100 feet. Included are the experimental points and theoretical curves for both the flexible (solid lines) and the equivalent rigid foundation (dotted lines). The notation used is such that "FH" and "FV" represent the horizontal and vertical motions for the "flexible" foundation, while "RH" and "RV" represent the horizontal and vertical motions for the equivalent "rigid" foundation.

The amplitude of the displacements plotted on the vertical scales in Figures 5-2.1 and 5-2.2 were normalized to match the measurements inside the library at the basement so that a direct

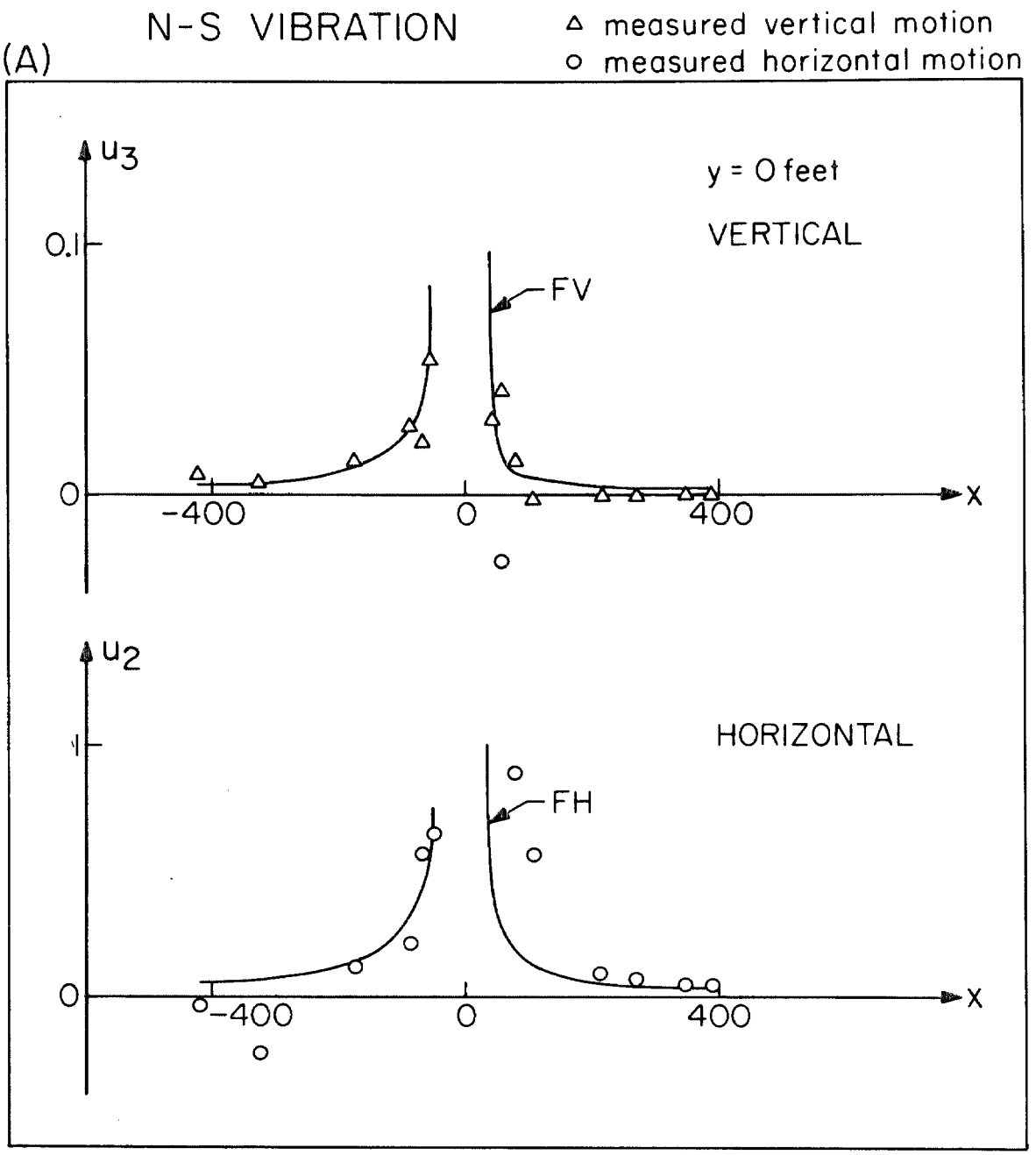

Figure 5-2.1(A) Ground displacements near the Millikan Library during its excitation in the N-S direction, y = 0.

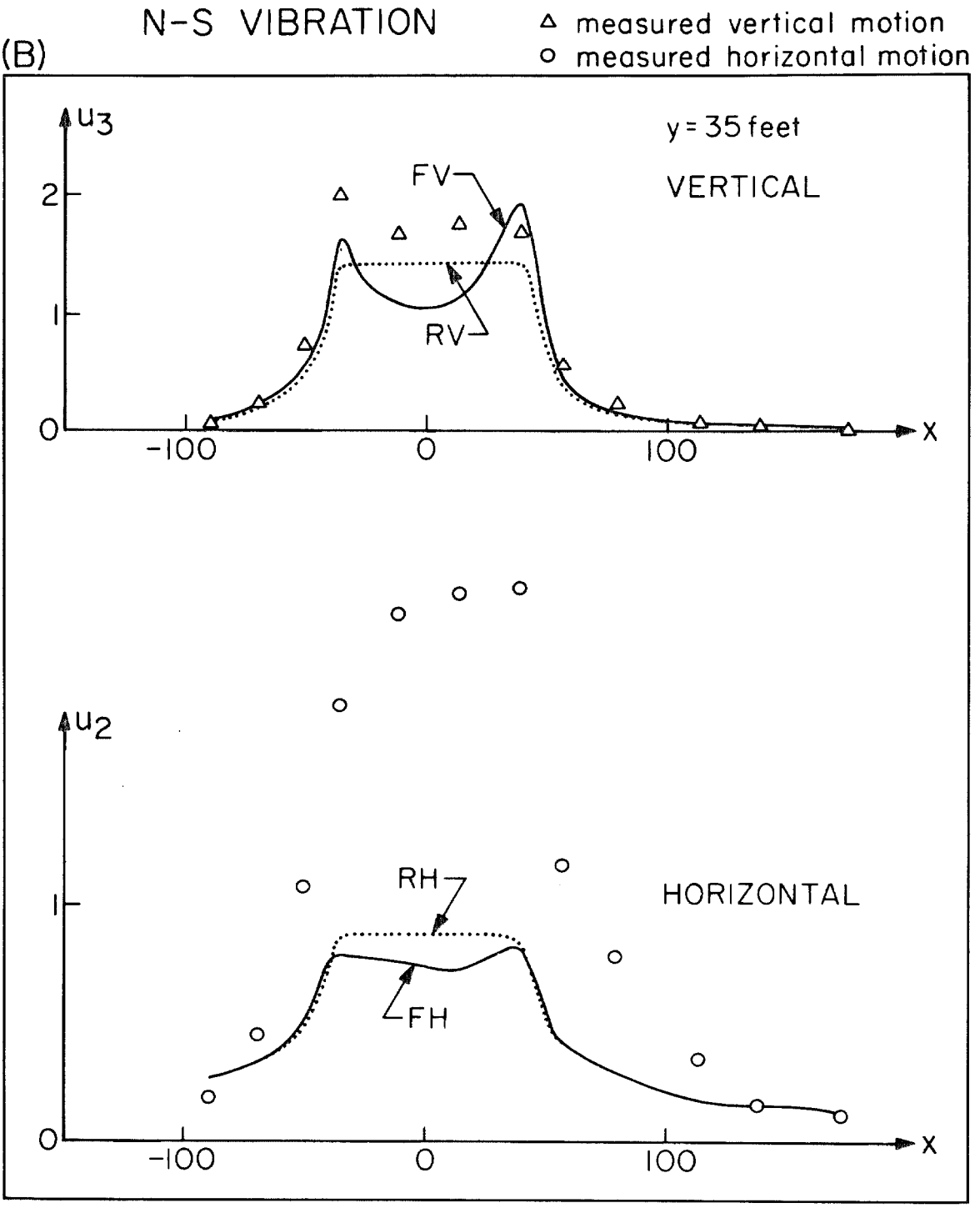

Figure 5-2.1(B) Ground displacements near the Millikan Library during its excitation in the N-S direction, y = 35 feet.

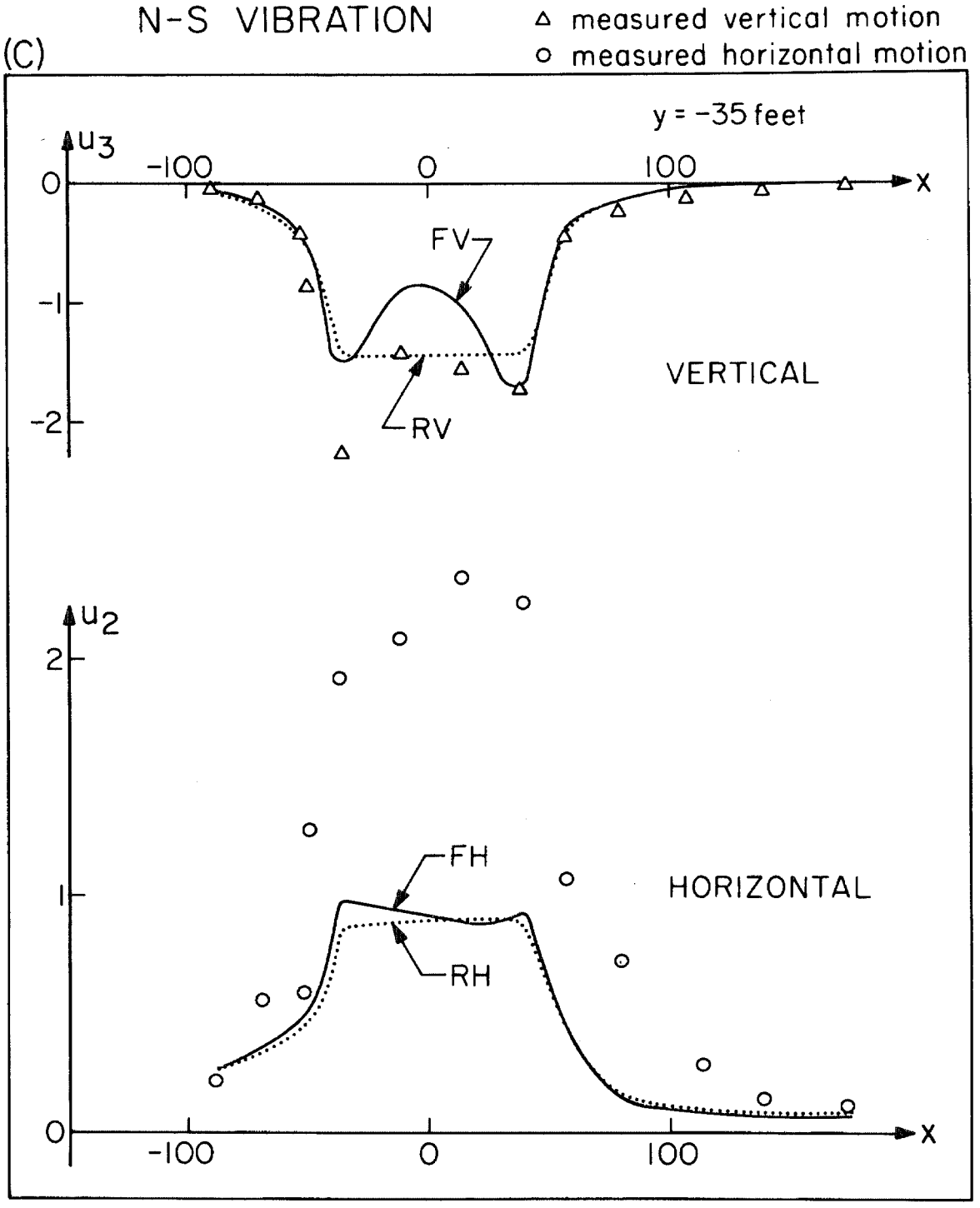

Figure 5-2.1(C) Ground displacements near the Millikan Library during its excitation in the N-S direction, y = -35 feet.

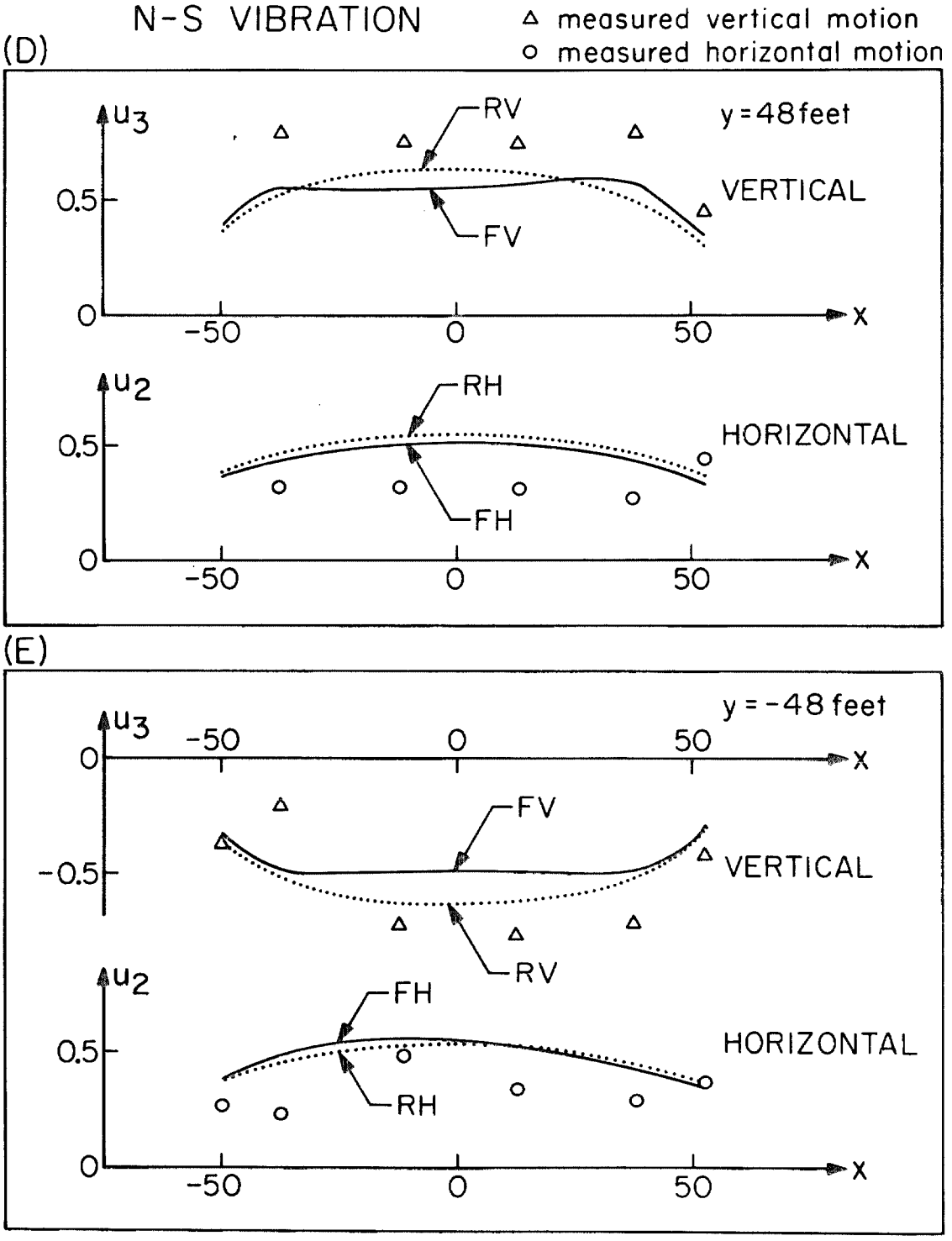

Figure 5-2.1(D) and (E) Ground displacements near the Millikan Library during its excitation in the N-S direction, y = 48 feet and y = -48 feet, respectively.

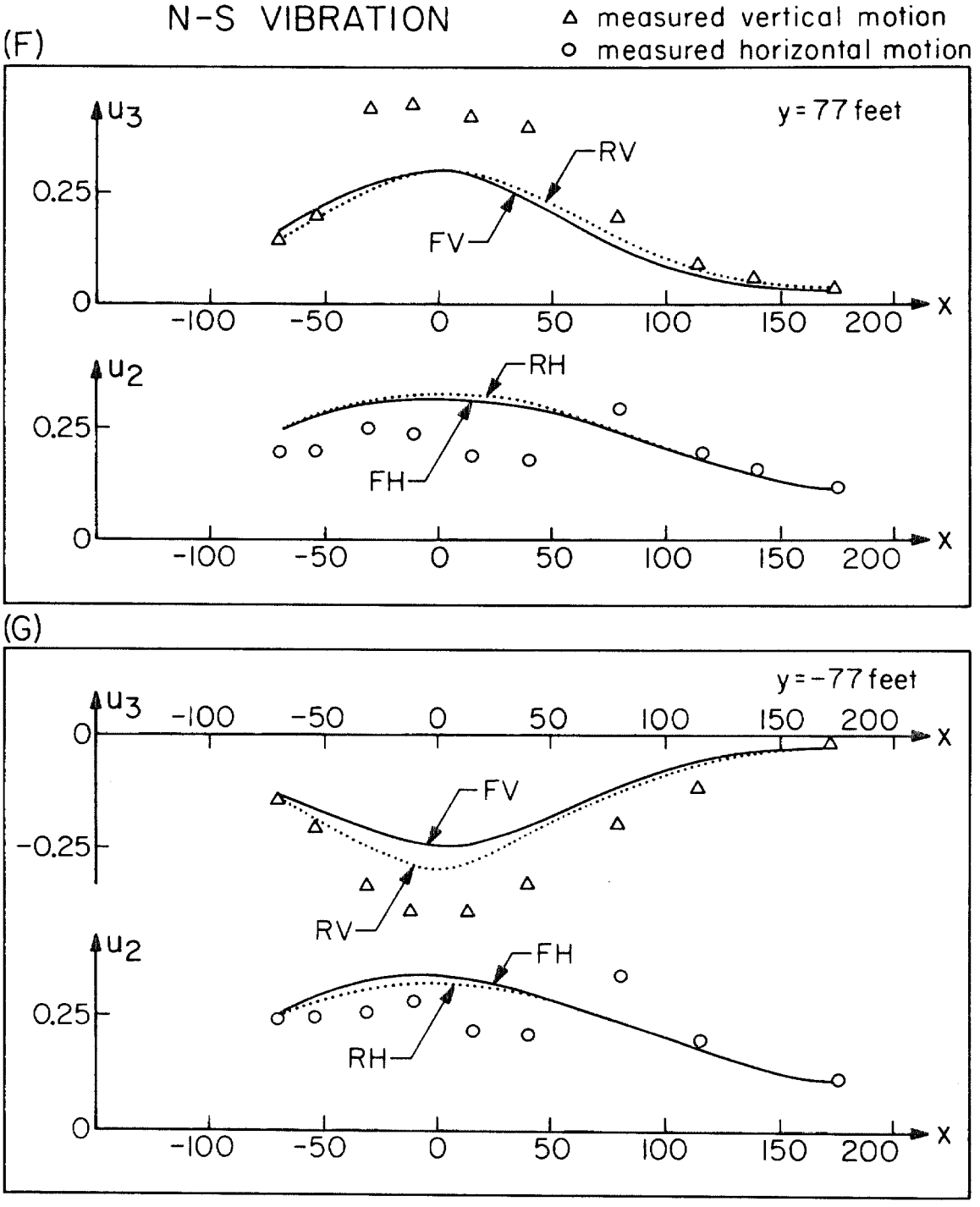

Figure 5-2.1(F) and (G) Ground displacements near the Millikan Library during its excitation in the N-S direction, y = 77 feet and y = -77 feet, respectively.

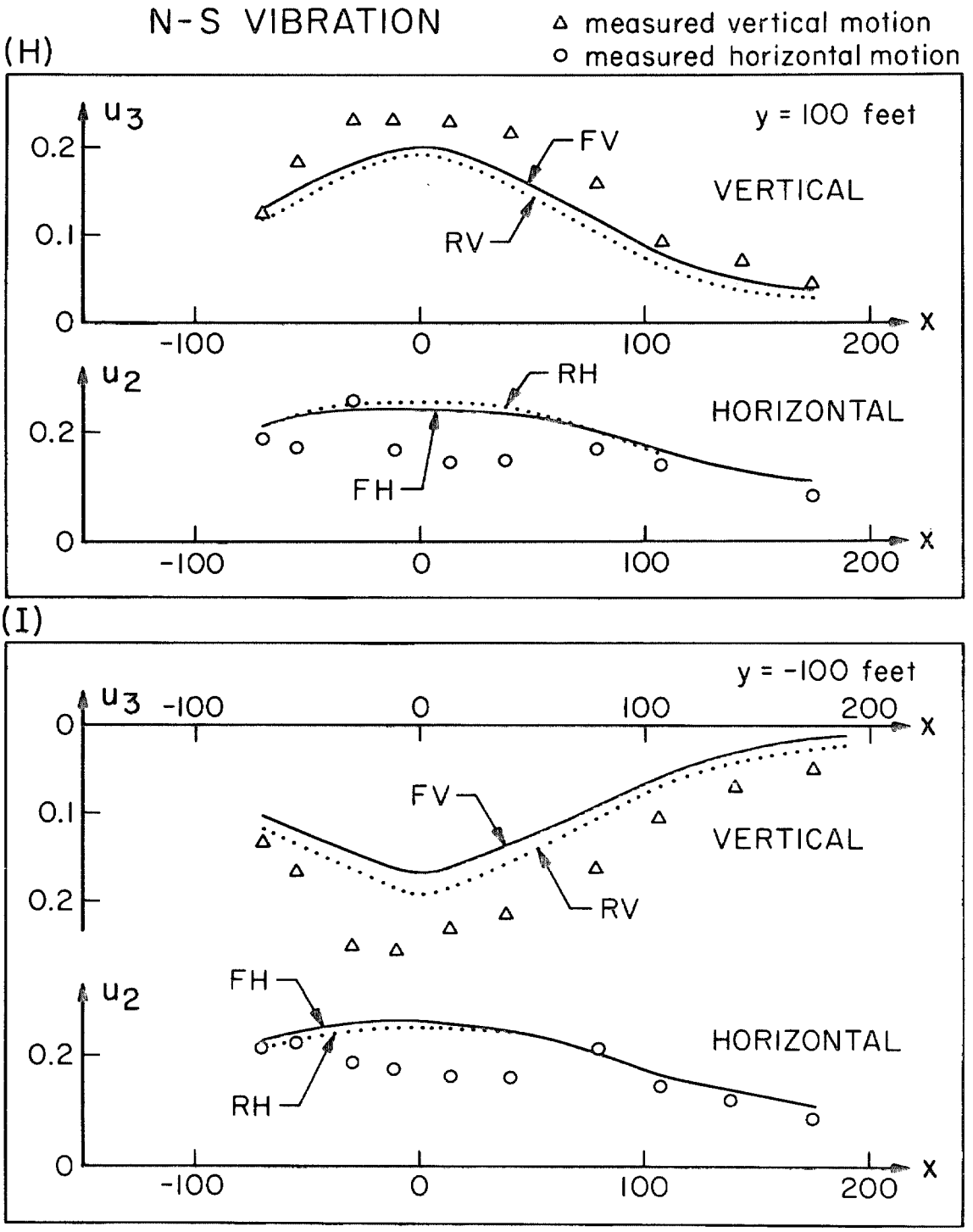

Figure 5-2.1(H) and (I) Ground displacements near the Millikan Library during its excitation in the N-S direction, y = 100 feet and y = -100 feet, respectively.

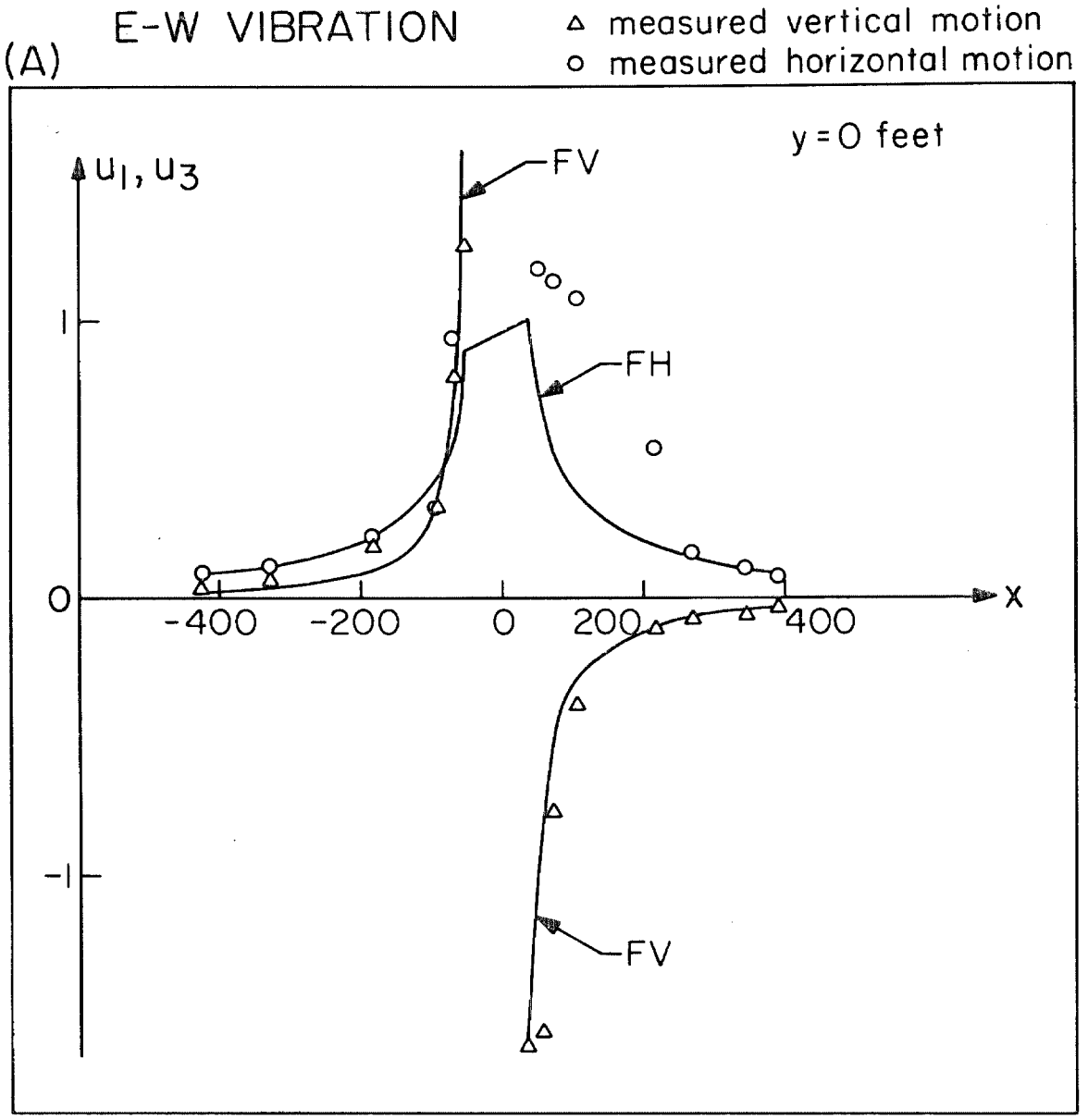

Figure 5-2.2(A) Ground displacements near the Millikan Library during its excitation in the E-W direction, y = 0.

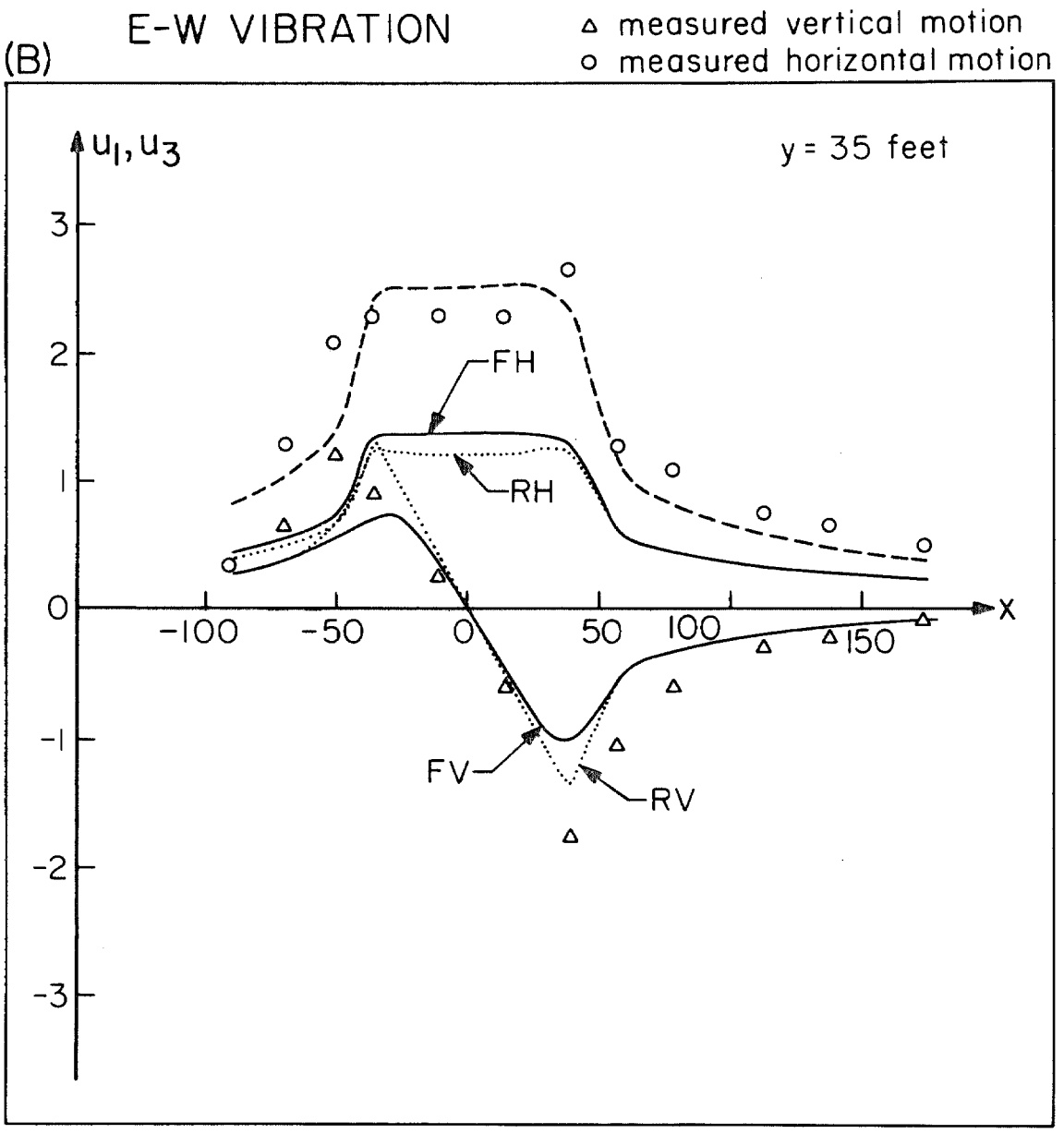

Figure 5-2.2(B) Ground displacements near the Millikan Library during its excitation in the E-W direction, y = 35 feet.

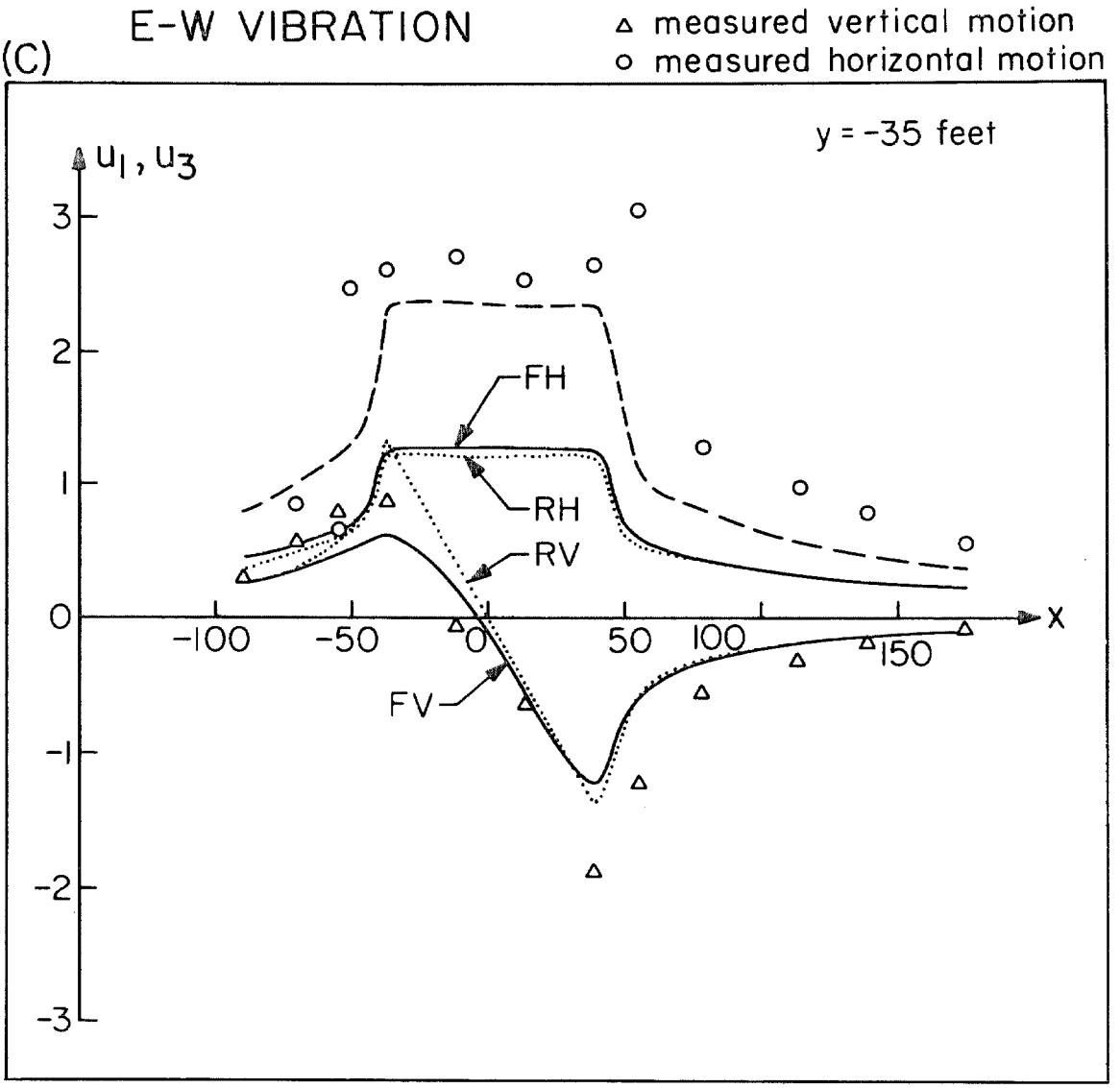

Figure 5-2.2(C) Ground displacements near the Millikan Library during its excitation in the E-W direction, y = -35 feet.

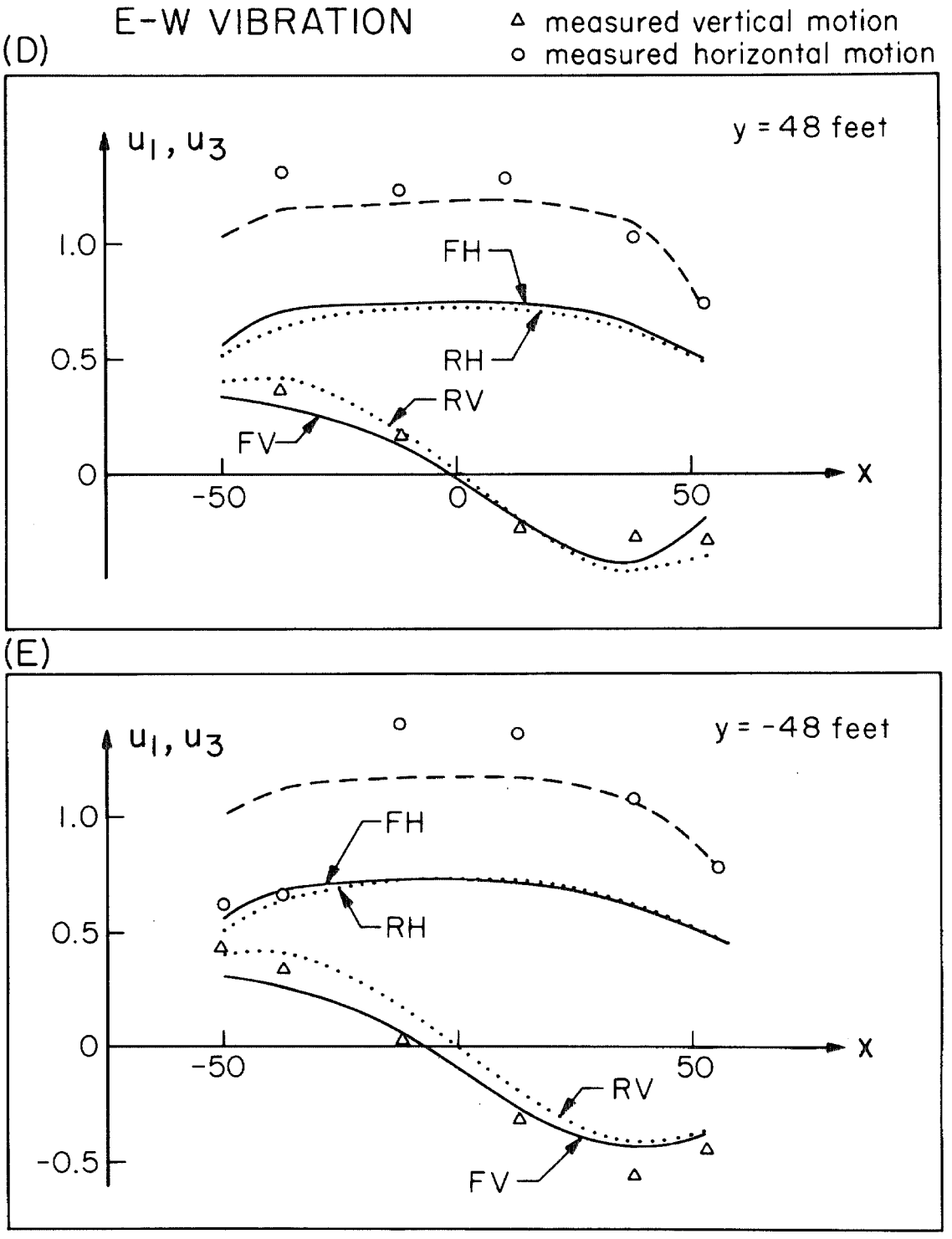

Figure 5-2.2(D) and (E) Ground displacements near the Millikan Library during its excitation in the E-W direction, y = 48 feet and y = -48 feet, respectively.

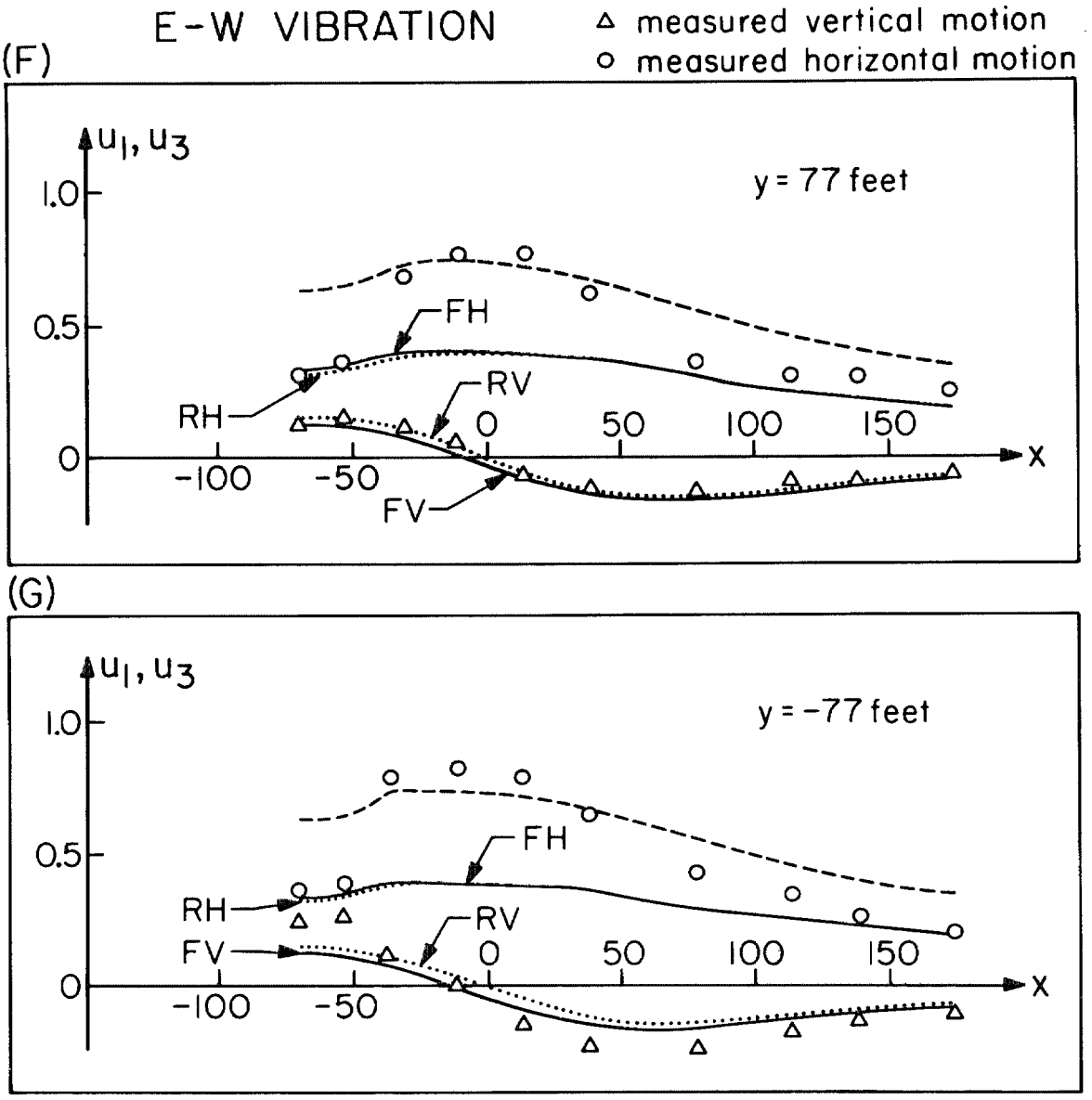

Figure 5-2.2(F) and (G) Ground displacements near the Millikan Library during its excitation in the E-W direction, y = 77 feet and y = -77 feet, respectively.

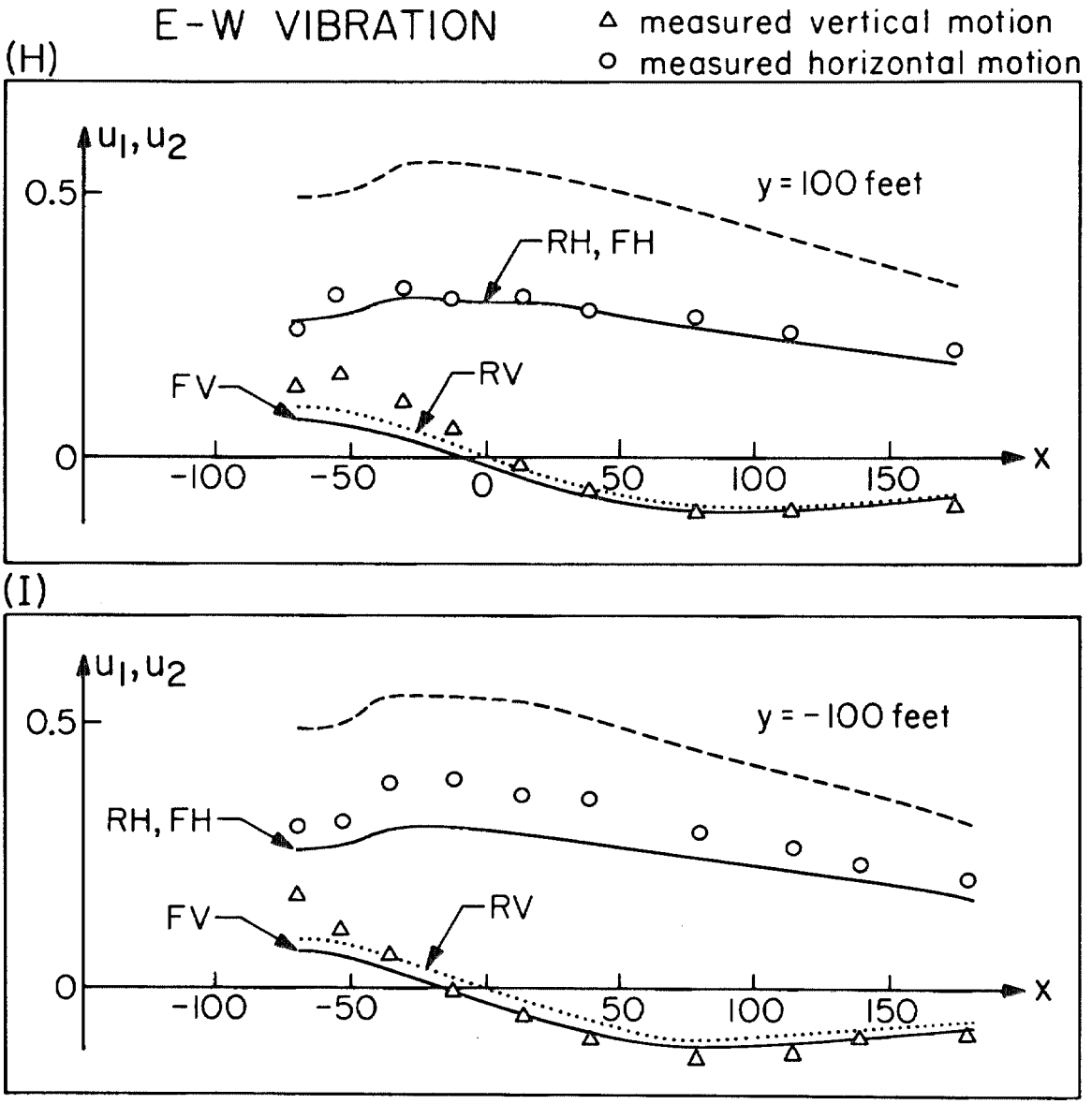

Figure 5-2.2(H) and (I) Ground displacements near the Millikan Library during its excitation in the E-W direction, y = 100 feet and y = -100 feet, respectively.

comparison could be made. The N-S data were based on the N-S component of the measurement made at element #18 in Figure 5-1.5 and those for E-W vibration were based on the E-W value at element #25. Also, because of the way in which the measuring stations are arranged in Figure 5-1.3, e.g., some lines have more stations than others, the horizontal axes are labelled differently and, hence, are not uniform in all figures.

The comparison of the computed and the measured motions in these figures has indicated that the agreement for the vertical component of displacement is quite good, while the horizontal displacements show a difference of about two times in amplitude. An explanation for this deviation is that the experimental data for the deformation of the basement floor discussed in Section [5-1] have been measured at a depth of 14 feet below the ground surface, while most of the data outside the library have been measured on the ground surface. Since the building has a large rocking component during steady state excitation at the fundamental mode frequency [Foutch et al. (1975)], the horizontal data recorded at the soil surface, which approximately coincides with the first floor, have an extra rotational term that should be added to the motion at the basement. If one assumes that the library rotates as a rigid body between the basement and the first floor, the two horizontal displacements should be related as

$$u(\text{first floor}) \cong u(\text{basement}) + h\phi \qquad (5\text{-}2.1)$$

where ϕ is the rocking angle of the basement floor and h is the

difference in height between the two levels. Applying this simple correction to the computed E-W horizontal motions in Figures 5-2.2, which amounts to an increase of approximately 75%, the measured and theoretical data are then in better agreement as indicated by the dashed lines in the plots. Obviously, a similar correction can be applied to the N-S horizontal displacement, but the necessity of a correction suggests that a more complete analysis including the embedment of the foundation may be necessary before the better theoretical fit of data is possible.

The comparison of the vertical data is encouraging, however, especially at larger distances. The good fit of the data away from the library indicates that the effect of embedment decreases rapidly with distance. The large displacement amplitude near the library may also be influenced by other unknown factors, because the setting of the library in the midst of the nearby buildings may affect the simple half space assumption in a complicated way. The presence of the other buildings can affect the deformation of the soil as measured at stations 1-10 and 91-100 shown in parts h and i of Figures 5-2.1 and 5-2.2. The horizontal displacements for this data set appears to be a factor of nearly two lower than the others. This might be caused by the arcades there.

Recalling the assumptions made in the last section, this analysis is actually a static solution of the problem. The static assumption was made because the dimensionless frequency of the building vibration is low (about 0.2) and the compliance at this frequency is near that of the static compliance. In this section, it has been

assumed that the "near field" motions can also be analyzed by a static solution, although, clearly, the "far field" motion, which is dominated by surface waves, cannot be assumed static. At the present time, the static solution provides an adequate model for deformation outside a vibrating building at low frequencies, which has special significances if the relative displacement of the building and the ground is important. A better dynamic analysis of the Millikan Library can clearly improve the correlation of the theoretical and experimental data, but its effect is probably of second order to the complexity of the half space.

The deformations caused by the actual flexible foundation and the equivalent rigid foundation were also compared. The differences between the two are significant only at locations nearest to the building. From the results shown in Figures 5-2.1b and 5-2.1c for the N-S vibration, the vertical indentation on the soil caused by the two shear walls at $x = \pm 38$ feet is obvious, because the middle of the building is supported by small columns. However, at $y = \pm 48$ feet (parts d and e of the figures), the difference between the two cases has diminished. The results are practically identical at $y = \pm 100$ feet, as shown in parts h and i of Figures 5-2.1 and 5-2.2. Note, in part h and i, the vertical component of the two cases differs by a small constant factor. This is due to the fact that the library was vibrating in the vertical direction as well. Although the equivalent rigid foundation matches the horizontal load and rocking moment to the flexible foundation, it did not include the small vertical vibrations.

In the light of the fair correlations between the simple theoretical computations and the experimental measurements shown in Figure 5-2.1 and Figure 5-2.2, it appears that it may be possible to apply the simple theory above to roughly determine the deformation in the vicinity of a vibrating building. Despite the simplification required for the above analysis, a general trend of the deformation can be determined. It appears, however, that the experimental data could be better matched by employing a foundation model which includes the effect of embedment, but this improvement is presently beyond the scope of this effort.

CHAPTER VI - SUMMARY

In this thesis, a class of problems in soil-structure interaction has been investigated in the framework of linear theory of wave propagation. In some portions of this work, the emphasis has been directed towards the development of theoretical methods which can be applied to many simplified soil-structure interaction analyses in engineering applications. In other parts of this thesis, the thrust of the investigation has been focused on the physical phenomena which accompany the interaction process. Though the former may be more useful for applications in designs and analysis, the latter provides a good basic knowledge of the problem so that more difficult problems can be understood.

From the results given in Section [3-5] and Chapter IV, it is clear that the theory of potentials, which has been applied frequently in other disciplines, can be applied advantageously in soil-structure interaction as well. The integral equation with a singular kernel, which results from the superposition of point sources on the foundation surface, can be approximately represented by a set of algebraic equations with the singular part handled by special methods. Two methods have been presented, and each has been shown to converge towards the "exact solution" of the integral equation as the number of simultaneous equations increases; the rate of convergence has been shown to be fast enough to be practical. Method I yields an upper bound to the "exact" compliance, while method II presents a lower bound; hence, a good approximate answer can be obtained by extrapolation and averaging.

Using this integral formulation, which is not limited to flat foundations only, many problems in linear wave propagation can be solved numerically. The advantage of this numerical method is that the shape of the foundation model can be quite arbitrary. This approach appears to be especially effective when the size of the soil medium is large compared to the foundation and the material properties are relatively uniform so that it can be considered as a homogeneous or layered half space. An additional feature of this integral formulation is that flexible foundations may be analyzed without difficulties; the much needed analysis of multi-structure-soil interaction is also possible. The development of these numerical methods has thus expanded our capability to apply the continuum approach to solve problems that cannot be solved analytically.

The analyses made in the previous chapters dealt mainly with the structures placed on top of a homogeneous half space, but the method used can easily be extended to the analysis involving elastic or viscoelastic strata. As a general rule, however, the difficulty of the analysis increases as the details and sophistication of the model increase. Therefore, the optimal selection of an adequate analytical model must be made by using good engineering judgment and experience.

From the experimental and theoretical observations given in this text, some conclusions can be made that might be helpful for further investigation of phenomena in soil-structure interaction. These can be summarized as follows:

(1) In Section [3-2], the characteristics of an isolated structure placed on a homogeneous half space have been investigated. The interaction with the soil usually becomes important if the ratio of the elastic wave speed in the superstructure and in the soil medium is increased, i.e., the structure is stiffer than the soil. Also, the mass of the entire structure plays an important role during interaction because a massive structure on soft soil can cause a large reduction in the fundamental "fixed base" resonant frequency. This might be one possible explanation for the fact that the measured resonant frequency is often lower than the theoretically predicted one. The radiation damping of the soil medium may also be included as part of the measured modal damping when interpretations are made on the observed responses, hence, the actual damping in the superstructure may be overestimated. In many cases, the radiation damping for small foundations can be ignored; it increases, however, as the surface area of the foundation increases. Therefore, the energy dissipation by geometrical spreading of waves can become significant if the foundation is large and embedded into the soil.

(2) The effects caused by incident waves on the response of the structure require special attention, especially for embedded foundations. Large rotational characteristics accompanying the translational motions can be induced by non-vertically incident waves for both the embedded and flat foundations. The rotational components are usually amplified, while the translational components are reduced as the wavelength of the incident wave increases.

(3) For the analysis of rigid foundations, the concept of superimposing the impedance and the driving forces is often used, and the characteristics of the incident wave motion are usually included in the latter. The "driving forces" induced by various types of seismic waves act as the complement to the impedance; both of these are essential for a complete analysis of the interaction problem. The only exception is perhaps that of the flat foundation subjected to vertically incident waves; then, only the impedances are necessary.

(4) As the complexity of the local geology and topography increase, the determination of both the impedances and the driving forces become more difficult. Here, the topographical effects on the incident waves, as well as the change in impedances due to reflection from layers, have to be accounted for. Shielding and focusing are now more likely to occur because of the constructive and destructive interferences of the incident and refracted waves. Although the shielding properties of the geological and topographical features may eventually be used advantageously in some future applications, the nature of seismic waves is still too unpredictable for practical use of these shielding phenomena.

(5) Another possibly important characteristic for structures located in densely constructed areas is the interaction of many structures with the soil. A general conclusion which can be drawn from the simple analysis in Section [3-4] is that lighter and smaller structures might be excited by more energy than that provided by the incident waves alone unless they are placed in the

shadow zone of the larger structures. From a physical point of view, the motion of the neighboring structures can be considered to represent wave sources which can be constructively combined with the incident waves to amplify the ground motion for a particular structure. The motion created by smaller structures usually cannot generate enough energy to disturb their larger neighbors, but the opposite is true for larger structures.

The phenomena of multi-structure-soil interaction are analogous to those of "spring-mass-dash pot" systems. The mass can represent the structure, the spring can represent the interrelation through the soil, and the dash pots can approximately model the radiative damping. This analogy extends further to the phenomena of mode vibrations of the entire system; e.g., a certain arrangement of the structures can result in resonances which are not directly related to the properties of the structures but the spacing between them. These effects are, of course, most prominent when the spacings are small and the number of structures is large. For the two-dimensional cases investigated in this thesis, the radiated waves from each foundation decays as $1/\sqrt{d}$, where d is the distance from the foundation. A much faster decay is expected for a three-dimensional model; therefore, the interaction between typical structures will not be as strong as the two-dimensional case studied here.

(6) Development of the most general analysis which includes all of the above mentioned phenomena quickly becomes difficult to handle and therefore some details must be sacrificed. It was

shown in Section [3-5] and Chapter IV, for example, that the effect of foundation shape is not important for the overall response of rigid foundations for intermediate or long incident waves. Using this result, the foundation of an arbitrary shape can be replaced by one of similar but simpler shape so that the analysis can be simplified, e. g., a rectangular foundation with a reasonably small hole can be replaced by a rectangular foundation without a hole. The above simplification is, of course, not adequate for the stress analysis of the structure or foundation, because the stress distribution is very sensitive to the details of the foundation shape. In addition, the foundation cannot always be considered as rigid as indicated by the data shown in Chapter V. In the case of a flexible foundation, the localized stresses and deformations usually exceed those of an equivalent rigid foundation. Considering the particular case of the Millikan Library, for example, the local stresses under the foundation can be as much as $2\frac{1}{2}$ times those for the equivalent rigid foundation. Therefore, depending on the type of analysis which is made, the assumption of rigid foundation may not always be an acceptable one.

This thesis has been motivated by a need to provide a review of the "state-of-the-art" in soil-structure interaction, as well as to present some new applications using potential theories and the method of separation of variables. The intent of the analyses has been to lean towards the basic phenomena, in hopes that this may expand our understanding of these problems. For more sophisticated analysis involving soil-structure interaction, in the case of the

deeply imbedded pile foundation, for example, the theory is still in its infancy. Thus, continual and conscientious effort will clearly be necessary before we can develop adequate methods which may become applicable to a broad class of applied engineering problems.

GENERAL REFERENCES

1. Abramowitz, M.A., and I.A. Stegun (1970). " Handbook of Mathematical Functions," Dover 0-486-61272-4, New York.

2. Banaugh, R.P., and W. Goldsmith (1963). " Diffraction of Steady Acoustic Waves by Surfaces of Arbitrary Shape," Journal of Acoust. Soc. of Amer., Vol. 35, No. 10, 1590.

3. Brown, C.B. (1971). " Seismic Energy Transmission to Deep-Founded Structures," Bull. Seism. Soc. Amer., Vol. 61, No. 3, pp. 781-788.

4. Ewing, W.M., W.S. Jardetsky, and F. Press (1957). " Elastic Waves in Layered Media," McGraw-Hill Book Company, Inc., New York.

5. Foutch, D.A., J.E. Luco, M.D. Trifunac, and F.E. Udwadia, (1975). " Full Scale, Three-Dimensional Tests of Structural Deformations during Forced Excitation of a Nine-Story Reinforced Concrete Building," Proc., U.S. Nat. Conf. on Earthquake Engrg., Ann Arbor, Michigan.

6. Hadjian, A.H., J.E. Luco, and N.C. Tsai (1974). " Soil-Structure Interaction : Continuum or Finite Element ?", Nuclear Engrg. and Design, Vol. 31, No. 2, pp. 151-167.

7. Jennings, P.C. (1970). " Distant Motions from a Building Vibration Test," Bull. Seism. Soc. Amer., Vol. 60, No. 6, pp. 2037-2043.

8. Longman, I.M. (1958). " On the Numerical Evaluation of Cauchy Principal Values of Integrals," Mathematical Tables and Other Aids to Computation, Vol. 12, pp. 205-207.

9. Love, A.E.H. (1927). " A Treatise on the Mathematical Theory of Elasticity," Dover 0-486-60174-9, New York.

10. Luco, J.E., H.L. Wong, and M.D. Trifunac (1975). " A Note on Response of Embedded Foundations," Earthquake Engrg. and Str. Dyn., (in press).

11. Luco, J.E., M.D. Trifunac, and F.E. Udwadia (1975). " An Experimental Study of Ground Deformations Caused by Soil-Structure Interaction," Proc., U.S. Nat. Conf. on Earthquake Engrg., Ann Arbor, Michigan.

12. Lysmer, J., and G. Waas (1972) . " Shear Waves in Plane Infinite Structures," Journal of Engrg. Mech. Div., A.S.C.E., Vol. 98, No. EM1, pp. 85-105.

13. Mow, C.C., and Y.H. Pao (1971). " The Diffraction of Elastic Waves and Stress Concentrations," RAND Report, R-482-PR.

14. Smythe, W.R. (1951). " The Capacitance of a Circular Annulus," Journal of Applied Physics , Vol. 22, No. 12, pp. 1499-1501.

15. Sneddon, I.N. (1966). " Mixed Boundary Value Problems in Potential Theory." North Holland Publishing Company, p 268.

16. Trifunac, M.D. (1972). " Comparison Between Ambient and Forced Vibration Experiments," Earthquake Engrg. and Str. Dyn., Vol. 1, No. 2, pp.133-150.

17. Wong, H.L., and P.C. Jennings (1975). " Topographic Effects on Strong Ground Motions," Bull. Seism. Soc. Amer., (in press).

APPENDIX A

A BIBLIOGRAPHY ON SOIL-STRUCTURE INTERACTION

A1. Sezawa, K., and K. Kanai (1935). " Decay in the Seismic Vibration of a Simple or Tall Structure by Dissipation of Their Energy into the Ground," Bull. Earth. Res. Inst., XIII, Part 3, pp. 164-168.

A2. Sezawa, K., and K. Kanai (1936). " Improved Theory of Energy Dissipation in Seismic Vibration of a Structure," Bull. Earth. Res. Inst., XIV, Part 2, pp. 164-168.

A3. Jacobsen, L.S. (1939). " Natural Periods of Uniform Cantilever Beams," Trans. A.S.C.E., Vol. 104, pp. 402-439.

A4. Kano, K. (1949). " Relation Between the Earthquake Damage of Non-Wooden Buildings and the Nature of the Ground," Bull. Earth. Res. Inst. Tokyo, Vol. 27, pp. 97-100.

A5. Suyehiro, K. (1932). " Engineering Seismology, Notes on the American Lectures," Proc. A.S.C.E., Vol. 58, No. 4, Part 2.

A6. Tanabashi, R., and H. Ishizaki (1953). " Earthquake Damages and Elastic Properties of the Ground," Bull. No. 4, Disaster Prevention Research Institute, Kyoto University, Japan.

A7. Merritt, R.G., and G.W. Housner (1954) " Effect of Foundation Compliance on Earthquake Stresses in Multistory Buildings," Bull. Seism. Soc. Amer., Vol. 44, No. 4.

A8. Housner, G.W. (1957). " Interaction of Buildings and Ground During an Earthquake," Bull. Seism. Soc. Amer., Vol. 47, No. 3, pp. 179-186.

A9. Thomson, W. (1960). " A Survey of Ground-Building Vibrations," Proc., 2nd World Conference on Earthquake Engineering, Japan, Vol. 2, pp. 833-846.

A10. Sandi, H. (1960). " A Theoretical Investigation of the Interaction Between Ground and Structure During Earthquake," Proc., 2nd World Conference on Earthquake Engineering, Japan, Vol. 2, pp. 1327-1343.

A11. Ishizaki, H., and N. Hatakeyama (1960). " Experimental and Numerical Studies on Vibrations of Buildings," Proc., 2nd World Conference on Earthquake Engineering, Japan, Vol. 2, pp. 1263-1284.

A12. Kobori, T., and R. Minai (1960). " Study of Unstationary Vibration of Building Structure with Plastic Deformation of Substructure," Proc., 2nd World Conference on Earthquake Engineering, Japan, Vol. 2, pp. 1085-1104.

A13. Sato, Y., and R. Yamaguchi (1960). " Vibration of a Building Upon an Elastic Foundation," Bull. Earth. Res. Inst. Tokyo, Vol. 38, pp. 369-383.

A14. Lycan, D., and N.M. Newmark (1961). " Effect of Structure and Foundation Interaction," Journal of the Engineering Mechanics Div., A.S.C.E., Vol. 87, No. EM5, pp. 1-32.

A15. Fleming, J.F., F.N. Screwvala, and R.L. Kondner (1965). " Foundation Superstructure Interaction under Earthquake Motion," Proc., 3rd World Conference on Earthquake Engineering, New Zealand, Vol. 1, pp. 122-130.

A16. Rosenberg, L.A. (1965). " On the Interaction Between Ground and Structure During Earthquakes," Bull. of the International Institute of Seismology and Earthquake Engineering, Vol. 2, pp. 29-36.

A17. Parmlee, R.A. (1967). " Building-Foundation Interaction Effects," Journal of the Engineering Mechanics Div., A.S.C.E., Vol. 93, No. Em2, pp. 131-152.

A18. Scavuzzo, R.J. (1967). " Foundation-Structure Interaction in the Analysis of Wave Motions," Bull. Seism. Soc. Amer., Vol. 57, No. 4, pp. 735-746.

A19. Tajimi, H. (1967). " Discussion: Building-Foundation Interaction Effects, Proc. Paper 5200," Journal of the Engineering Mechanics Div., A.S.C.E., Vol. 93, No. EM6, pp. 294-298.

A20. Kuroiwa, J.H. (1967). " Vibration Test of a Multi-Story Building," Earthquake Engineering Research Lab., California Institute of Technology, Pasadena, California.

A21. Whitman, R.V., and F.E. Richart Jr. (1967). " Design Procedures for Dynamically Loaded Foundations," Journal of the Soil Mechanics and Foundations Div., A.S.C.E., Vol. 93, No. SM6, pp.169-193.

A22. Jennings, P.C., and J.H. Kuroiwa (1968). " Vibration and Soil-Structure Interaction Tests of a Nine-Story Reinforced Concrete Building," Bull. Seism. Soc. Amer., Vol. 58, No. 3, pp. 891-916.

A23. Parmlee, R.A., Perelman, D.S., Lee, S.L., and Keer, L.M. (1968). " Seismic Response of Structure-Foundation Systems," Journal of the Engineering Mechanics Div., A.S.C.E., Vol. 94, No. EM6, pp. 1295-1315.

A24. Luco, J.E. (1969). " Dynamic Interaction of a Shear Wall with the Soil," Journal of the Engineering Mechanics Div., A.S.C.E., Vol. 95, No. EM2, pp. 333-346.

A25. Parmelee, R.A., D.S. Perelman, and S.L. Lee (1969). " Seismic Response of Multi-Story Structures on Flexible Foundations," Bull. Seism. Soc. Amer., Vol. 59, No. 3, pp. 1061-1070.

A26. Blume, J.A. (1969). " Response of High-Rise Buildings to Ground Motions from Underground Nuclear Detonations," Bull. Seism. Soc. Amer., Vol. 59, No. 6, pp. 2343-2370.

A27. Hradilek, P.J. (1970). " Dynamic Soil-Structure Interaction," M.S. Thesis, University of California, Los Angeles.

A28. Castellani, A. (1970). " Foundation Compliance Effects on Earthquake Response Spectra," Journal of Soil Mechanics and Foundation Div., A.S.C.E., Vol. 96, No. SM4, pp. 1335-1355.

A29. Hradilek, P.J., and J.E. Luco (1970). " Dynamic Soil-Structure Interaction," IDIEM, Technical Report No. 14, Saniago, Chile.

A30. Duke, C.M., J.E. Luco, A.R. Carriveau, P.J. Hradilek, R. Lastrico, and D. Ostrom (1970). " Strong Earthquake Motions and Site Conditions: Hollywood," Bull. Seism. Soc. Amer., Vol. 60, No. 4, pp. 1272-1289.

A31. Sarrazin, M.A. (1970). " Soil-Structure Interaction in Earthquake Engineering Design," M.I.T., Dept. Civil Engrg. Report R70-59.

A32. Bielak, J. (1971). " Earthquake Response of Building-Foundation System," Earthquake Engineering Research Lab. Report EERL 71-04, California Institute of Technology.

A33. Liu, S.C., and L.W. Fagel (1971). " Earthquake Interaction by Fast Fourier Transform," Journal of the Engineering Mechanics Div., A.S.C.E., Vol. 97, pp. 1223-1237.

A34. Chakravorty, M.K., M.F. Nelson, and R.V. Whitman (1971). " Approximate Analysis of 3-DOF Model for Soil-Structure Interaction," Report R71-11, Dept. of Civil Engineering, Massachusetts Institute of Technology, Cambridge.

A35. Protonotarios, J.N., R.V. Whitman, and M.F. Nelson (1971). " Soil-Structure Interaction: New York World's Fair Chimes Tower," Research Report R71-9, Dept. of Civil Engineering, Massachusetts Institute of Technology, Cambridge.

A36. Yamahara, H. (1971). " Practical Solutions for Soil-Structure Interaction Systems," Shimizu Technical Report No. 1, Shimizu Construction Company, Ltd., Tokyo, Japan.

A37. Kobori, T., R. Minai, and K. Kusakabe (1971). " Vibrational Characteristics of a Coupled Rigid Bodies System on an Elastic Ground," Reports of the Architectural Institute of Japan (Kiuki Sub-Division), Japan, pp. 13-16.

A38. Yuan, H.F., and R.E. Walker (1971). " The Investigation of a Simple Soil-Structure Interaction Model," Dynamic Waves in Civil Engineering, Howells, D.A., Heigh, I.P., and Taylor, C., ed's., Wiley-Interscience, London, England, pp. 247-266.

A39. Rainer, J.H. (1971). " Method of Analysis of Structure-Ground Interaction in Earthquakes," Technical Paper No. 340, Division of Building Research Council of Canada, Ottawa.

A40. Carr, A.J., and P.J. Moss (1971). " Elastic Soil-Structure Interaction," Bulletin of the New Zealand Society for Earthquake Engineering, Vol. 4, No. 1, pp. 258-269.

A41. Finn, W.D.L., and R.B. Reimer (1971). " Effect of Soil-Structure Interaction on Seismic Response," Earthquake Engineering, Proc. of the 3rd European Symposium on Earthquake Engineering, Bulgarian Academy of Sciences Press, Sofia, Bulgaria, pp. 243-251.

A42. Parmelee, R.A., and J.H. Wronkiewicz (1971). " Seismic Design of Soil-Structure Systems," Journal of the Structural Div., A.S.C.E., Vol. 97, No. ST10, pp. 2503-2517.

A43. Finn, W.D.L., J.J. Emery, and R.B. Reimer (1972). " The Effect of Foundation Soils on Seismic Response of Structures," Proc., 1st Canadian Conference on Earthquake Engineering, Vancouver, B.C., May 1971, Cherry, S., ed., University of British Columbia, Vancouver, Canada, pp. 128-141.

A44. Bielak, J. (1971). " Earthquake Response of Building-Foundation Systems," Memorias, III Congreso Nacional de Ingenieria Sismica, Sociedad Mexicana de Ingenieria Sismica, Mexico City, Mexico, Vol. 1, Paper No. 6.

A45. Matsushima, Y., and P.G. Carydis (1971). " Study on the Seismic Interaction Problem between Ground and Shear Structures," Bull. of the International Institute of Seismology and Earthquake Engineering, Vol. 8, pp. 237-252.

A46. Rukos, E.A., and E.L. Wilson (1971). " Earthquake Analysis of Interacting Ground-Structure Systems," SESM 71-9, Structural Engineering Lab., University of California, Berkeley.

A47. Sarrazin, M.A., J.M. Roesset, and R.V. Whitman (1972). " Dynamic-Soil Structure Interaction," Journal of the Structural Div., A.S.C.E., Vol. 98, No. ST7, pp. 1525-1544.

A48. Fagel, L.W., and S. Liu (1972). " Earthquake Interaction for Multistory Buildings," Journal of the Engineering Mechanics Div., A.S.C.E., Vol. 98, No. EM4, pp. 929-946.

A49. Trifunac, M.D. (1972). " Interaction of a Shear Wall with the Soil for Incident Plane SH-Waves," Bull. Seism. Soc. Amer., Vol. 62, No. 1, pp. 63-83.

A50. Serbanescu, G., and H. Sandi (1971). " Some Data on the Importance of Ground Compliance," Earthquake Engineering, Proc. of the 3rd European Symposium on Earthquake Engrg., Bulgarian Academy of Sciences Press, Sofia, Bulgaria, pp. 319-328.

A51. Kobori, T. (1971). " Random Vibrations of Structure-Foundation Interaction System," Proc., 3rd U.S. - Japan Joint Seminar on Stochastic Methods in Dynamical Problems, U.S. National Science Foundation and Japan Society for Promotion of Science, Kyoto, Japan.

A52. Kobori, T., R. Minai, and Y. Shiriozaki (1971). " Vibration of a Rigid Circular Disc on an Elastic Half Space Subjected to Plane Waves," Proc. of the 21st Japan National Congress for Applied Mechanics.

A53. Wood, J.H. (1972). " Analysis of the Earthquake Response of a Nine-Story Steel Frame Building During the San Fernando Earthquake," Report No. EERL 72-04, Earthquake Engineering Research Lab., California Institute of Technology, Pasadena, California.

A54. Whitman, R.V. (1972). " Dynamic Soil-Structure Interaction," Technical Paper T72-2, Dept. of Civil Engineering, Massachusetts Institute of Technology, Cambridge.

A55. Whitman, R.V. (1972). " Analysis of Soil-Structure Interaction, A State-of-the-Art Review," Professional Paper P72-3, Dept. of Civil Engineering, Massachusetts Institute of Technology, Cambridge, Massachusetts.

A56. Roesset, J.M., R.V. Whitman, and R. Dobry (1972). " Modal Analysis for Structures with Foundation Interaction," Professional Paper P72-7, Dept. of Civil Engineering, Massachusetts Institute of Technology, Cambridge.

A57. Sarrazin, M.A. (1972). " Dynamic Soil-Structure Interaction," Journal of the Structural Div., A.S.C.E., Vol. 98, No. ST7, pp. 1525-1544.

A58. Whitman, R.V., J.N. Protonotarios, and M.F. Nelson (1972). " Case Study of Soil-Structure Interaction," Technical Paper T72-2, School of Engineering, Massachusetts Institute of Technology, Cambridge.

A59. Minami, T. (1972). " Elastic-Plastic Earthquake Response of Soft-Building Systems," EERC-72-3, Earthquake Engineering Research Center, University of California, Berkeley.

A60. Matsushima, Y. (1972). " Structure-Soil Interaction for Finite-Element-Hysteretically Damped Systems," Transaction of the Architectural Institute of Japan, 199, pp. 25-33.

A61. Kobori, T., R. Minai, and T. Susuki (1972). " General Representations for the Vibrational Characteristics of a Ground-Structure Systems," Annuals, Disaster Prevention Research Institute, Kyoto University, Kyoto, pp. 139-169.

A62. Seed, H.B., and I.M. Idriss (1973). " Soil-Structure Interaction of Massive Embedded Structures During Earthquakes," Fifth World Conference on Earthquake Engineering, Rome, Italy, Paper No. 233, pp. 1881-1890.

A63. Parmelee, R.A., and R.J. Kudder (1973). " Seismic Soil-Structure Interaction of Embedded Buildings," Fifth World Conference on Earthquake Engineering, Rome, Italy, Paper No. 241a, pp. 1941-1950.

A64. Hradilek, P.J., A.R. Carriveau, G.R. Saragoni, and C.M. Duke (1973). " Evidence of Soil-Structure Interaction in Earthquakes," Fifth World Conference on Earthquake Engrg., Rome, Italy, Paper No. 258, pp. 2080-2083.

A65. Petrovski, J. (1973). " Dynamic Response of Embedded Foundation," Fifth World Conference on Earthquake Engrg., Rome, Italy.

A66. Novak, M. (1973). " The Effect of Embeddment on Vibration of Footings and Structures," Fifth World Conference on Earthquake Engineering, Rome, Italy, Paper No. 337, pp. 2658-2661.

A67. Parmelee, R.A., and J.H. Wronkiewicz (1973). " Dynamic Coefficents for Evaluating the Seismic Response of Soil-Structure Interaction Systems," Fifth World Conference on Earthquake Engineering, Rome, Italy, Paper No. 330, pp. 2606-2609.

A68. Jennings, P.C., and J. Bielak (1973). " Dynamics of Building-Soil Interaction," Bull. Seism. Soc. Amer., Vol. 63, No. 1, pp. 9-48.

A69. Luco, J.E., and L.A. Contesse (1973). " Dynamic Structure-Soil-Structure Interaction," Bull. Seism. Soc. Amer., Vol. 63, No. 4, pp. 1289-1303.

A70. Vaish, A.K., and A.K. Chopra (1973). " Earthquake Analysis of Structure-Foundation Systems," Report No. EERC 73-9, Earthquake Engineering Research Center, University of California, Berkeley.

A71. Crouse, C.B. (1973). " Engineering Studies of the San Fernando Earthquake," Report No. EERL 73-04, Earthquake Engineering Research Laboratory, California Institute of Technology, Pasadena, California.

A72. Agrawal, R.K. (1973)." Comparative Study for Soil-Structure Interaction Effect by the Soil Spring and Finite Element Model," Report No. SAD-082, Sargent and Lundy Engineers.

A73. Salmon, M.A., S.A. Thau, and W. Huang (1973). " Wave Diffraction by Rigid Foundations," Journal of the Engineering Mechanics Div., A.S.C.E., Vol. 99, No. EM4, Technical Notes, pp. 902-906.

A74. Iguchi, M. (1973). " Seismic Response with Consideration of both Phase Differences of Ground Motions and Soil-Structure Interaction," Proceedings of the Japan Earthquake Engineering Symposium, Tokyo, Japan.

A75. Roesset, J.M., R.V. Whitman, and R. Dobry (1973). " Model Analysis for Structures with Foundation Interaction," Journal of the Structural Div., A.S.C.E., Vol. 99, No. ST3, pp. 399-416.

A76. Tsai, N.C., D. Niehoff, M. Swatta, and A.H. Hadjian (1974). " The Use of Frequency-Independent Soil-Structure Interaction Parameters," Nuclear Engineering and Design.

A77. Tsai, N.C. (1974). " Modal Damping for Soil-Structure Interaction," Journal of the Engineering Mechanics Div., A.S.C.E., Vol. 100, No. EM2, pp. 323-341.

A78. Luco, J.E., and A.H. Hadjian (1974). " Two-Dimensional Approximations to the Three-Dimensional Soil-Structure Interaction Problem," Nuclear Engineering and Design, Vol. 31, No. 2, pp. 195-203.

A79. Luco, J.E., A.H. Hadjian, and H.D. Bos (1974). " The Dynamic Modeling of the Half Plane by Finite Elements," Nuclear Engineering and Design, Vol. 31, No. 2, pp.184-194.

A80. Hadjian, A.H., D. Niehoff, and J. Guss (1974). " Simplified Soil structure Interaction Analysis with Strain-Dependent Soil Properties," Nuclear Engineering and Design.

A81. Thau, S.A., A. Umek, and R. Rostamian (1974). " Seismic Motion of Buildings with Buried Foundations," Journal of Engineering Mechanics Div., A.S.C.E., Vol. 100, No. EM5, pp. 919-934.

A82. Veletsos, A.S., and B. Verbic (1974). " Basic Response Functions for Elastic Foundations," Journal of Engineering Mechanics Div., A.S.C.E., Vol. 100, No. EM2, pp 189-202.

A83. Chopra, A.K., and J.A. Gutierrez (1975). " Earthquake Response Analysis of Multi-Storey Building Including Foundation Interaction," Earthquake Engrg. and Str. Dyn., Vol. 3, pp. 65-79.

A84. Veletsos, A.S., and J.W. Meek (1975). " Dynamic Behavior of Building-Foundation Systems," Earthquake Engrg. and Str. Dyn., Vol. 3, pp. 121-138.

A85. Bielak, J. (1975) " Dynamic Behavior of Structures with Embedded Foundations," Earthquake Engrg. and Str. Dyn., Vol. 3, pp. 259-274.

SOIL-STRUCTURE INTERACTION FOR NUCLEAR POWER PLANTS

A86. Akino, K., and H. Tajimi (1965). "A Seismic Design and Dynamic Analysis of Nuclear Power Plants, Part I, Swaying Motion; Part II, Rocking Motion," Nuclear Structural Engineering, North Holland Publishing Company.

A87. Scavuzzo, R.J., J.L. Bayley, and D.D. Raftopoulos (1969). " Lateral Structure-Foundation Interaction of Nuclear Power Plants During Earthquake Loading," Technical Report No. 2, The Research Foundation, The University of Toledo.

A88. Scavuzzo, R.J., D.D. Raftopoulos, and J.L. bayley (1969). " Lateral Structure-Foundation Interaction of Nuclear Power Plants with Large Base Masses," Technical Report No. 3, The Research Foundation, The University of Toledo.

A89. Chiapetta, R. (1970). " Effect of Soil-Structure Interaction on the Response of Reactor Structures to Seismic Ground Motion," IIT Research Institute Report to the Research Foundation, The University of Toledo.

A90. Biggs, J.M., and R.V. Whitman (1970). " Soil-Structure Interaction in Nuclear Power Plants," Proc. 3rd Japan Earthquake Engineering Symposium, Tokyo, Japan.

A91. Isenberg, J. (1970). " Interaction Between Soil and Nuclear Reactor Foundations During Earthquakes," Report prepared for the Research Foundation of the University of Toledo.

A92. Scavuzzo, R.J. (1970). " Structure-Foundation Interaction of Nuclear Power Plants - Phase I Final Report," The Research Foundation, The University of Toledo.

A93. Scavuzzo, R.J., J.L. Bayley, and D.D. Raftopoulos (1971). "Lateral Structure Interaction with Seismic Waves," Journal of Applied Mechanics, Vol. 38, pp. 125-134.

A94. Constantino, C.J. (1971). " Analysis of Soil-Structure Interaction Effects under Seismic Excitation," First International Conference on Structural Mechanics in Reactor Technology, B.A.M., Berlin. Germany, and Commission of the European Communities, Brussels, Belgium, Vol. 4.

A95. Scavuzzo, R.J., and R.R. Little (1971). " The Influence of Seismic Pulse Time on Structure-Foundation Interactions," First International Conference on Structural Mechanics in Reactor Technology, B.A.M., Berlin, Germany and Commission of the European Communities, Belgium, Vol. 4.

A96. Lee, T.H., and D.A. Wesley (1971). " Soil-Foundation Interaction of Reactor Structures Subjected to Seismic Excitation," First International Conference on Structural Mechanics in Reactor Technology, B.A.M., Berlin, Germany and Commission of the European Communities, Brussels, Belgium, Vol.4.

A97. Whitman, R.V., J.T. Christian, and J.M. Biggs (1971). " Parametric Analysis of Soil-Structure Interaction for a Reactor Building," First International Conference on Structural Mechanics in Reactor Technology, B.A.M., Berlin, Germany and the Commission of the European Communities, Brussels, Belgium, Vol. 4.

A98. Lee, T.H., and D.A. Wesley (1971). " Soil-Structure Interaction Effects on the Seismic Response of Nuclear Power Plants," American Nuclear Society Transactions, 1971 Annual Meeting, Boston, pp. 268-269.

A99. Hadjian, A.H. (1971). " Earthquake Forces on Equipment in Nuclear Power Plants," A.S.C.E., Vol. 97, No. PO3, Proc. Paper 8240, pp. 649-666.

A100. Anderson, J.C. (1972). " Seismic Response Effects on Embedded Structures," Bull. Seism. Soc. Amer., Vol. 62, No. 1, pp. 177-194.

A101. Scavuzzo, R.J., D.D. Raftopoulos, and J.L. Bayley (1972). " Lateral Structure-Foundation Interaction of Structures with Base Masses," Bull. Seism. Soc. Amer., Vol. 62, No. 2, pp. 453-470.

A102. Isenberg, J., and S.A. Adham (1972). " Interaction of Soil and Power Plants in Earthquakes," Journal of the Power Div., A.S.C.E., pp. 273-291.

A103. Miller, C.A., and C.J. Constantino (1973). " Rocking Effects in a Nuclear Power Plant Subjected to a Seismic Disturbance," Fifth World Conference on Earthquake Engineering, Rome, Italy, Paper No. 312, pp. 2469-2474.

A104. Chu, S.L., P.K. Agrawal, and S. Singh (1973). " Finite Element Treatment of Soil-Structure Interaction Problem for Nuclear Power Plant under Seismic Excitation," Proc. 2nd International Conference on Structural Mechanics in Reactor Technology, Paper k 2/4, Berlin, Germany.

FINITE ELEMENT APPROACH

A105. Zienkiewicz, O.D., and Y.K. Cheung (1967). " The Finite Method in Structural and Continuum Mechanics, McGraw-Hill, New York.

A106. Lysmer, J., and R.L. Kuhlemeyer (1969). " Finite Dynamic Model for Infinite Media," Journal of the Engineering Mechanics Div., A.S.C.E., Vol. 95, No. EM4, pp. 859-877.

A107. Ghosh, S.V., and E. Wilson (1969). " Dynamic Analysis of Axisymmetric Structures under Arbitrary Loading," Report No. EERC69-10, College of Engineering, University of California, Berkeley.

A108. Isenberg, J. (1970). " Interaction Between Soil and Nuclear Reactor Foundations During Earthquakes," Report prepared for the Research Foundation of the University of Toledo.

A109. Wilson, E.L. (1972). " Solid SAP - A Static Analysis Program for Three-Dimensional Solid Structures," SESM, 71-19, University of California, Berkeley.

A110. Waas, G. (1972). " Analysis Method for Footing Vibrations through Layered Media," Ph.D. Thesis, University of California, Berkeley.

A111. Schnable, P.B., J.T. Lysmer, and H.B. Seed (1972). " SHAKE - A Computer Program for Earthquake Response Analysis of Horizontally Layered Sites," Report No. EERC 72-12, Earthquake Engineering Research Center, University of California, Berkeley.

A112. Kuhlemeyer, R.L., and J.T. Lysmer (1973). " Finite Element Method Accuracy for Wave Propagation Problems," Journal of the Soil Mechanics and Foundation Div., A.S.C.E., Technical Notes, Vol. 99, No. SM5, pp. 421-426.

A113. Lysmer, J.T., T. Udaka, H.B. Seed, and R. Hwang (1974). " A Computer Program for Complex Response Analysis of Soil-Structure Systems," Report No. EERC 74-4, Earthquake Engineering Research Center, University of California, Berkeley.

A114. Vaish, A.K., and A.K. Chopra (1974). " Earthquake Finite Element Analysis of Structure-Foundation Systems," Journal of the Engineering Mechanics Div., A.S.C.E., Vol. 100, No. EM6, pp. 1101-1116.

DYNAMIC RESPONSE OF FOUNDATIONS

I. RIGID CIRCULAR FOUNDATIONS

1.1 TORSIONAL VIBRATIONS

A115. Reissner, E. and Sagoci, H. F. (1944), "Forced Torsional Oscillations of an Elastic Half-space," J. Appl. Phys., Vol. 15, No. 9.

A116. Ufliand, Ia. S. (1961), "On Torsional Vibrations of Half-space," P.M.M., Vol. 25, No. 1.

A117. Collins, W. D. (1962), "The Forced Torsional Oscillations of an Elastic Half-space and an Elastic Stratum," Proc. London Math. Soc., Vol. 12, No. 46.

A118. Stallybrass, M. P. (1962), "A Variational Approach to a Class of Mixed Boundary-value Problems in the Forced Oscillations of an Elastic Medium," Proc. 4th U.S. Natl. Cong. Appl. Mech., p. 391.

A119. Robertson, I. A. (1976), "On a Proposed Determination of the Shear Modulus of an Isotropic Elastic Half-space by the Forced Torsional Oscillations of a Circular Disc," Appl. Sci. Res., Vol. 17, p. 305.

A120. Thomas, D. P. (1968), "A Note on the Torsional Oscillations of an Elastic Half-space," Int. J. Engng. Sci., Vol. 6, p. 565.

A121. Thomas, D. P. (1968), "Torsional Oscillations of an Elastic Half-space," J. Mech. Appl. Math., Vol. 21, p. 51.

1.2 VERTICAL VIBRATIONS

A122. Zakorko, V. N. and Rostovtsev, N. A. (1965), "Dynamic Contact Problem of Steady Vibrations of an Elastic Half-space," P.M.M., Vol. 29, p. 644.

A123. Lysmer, J. (1965), "Vertical Motion of Rigid Footing," Ph. D. Thesis, University of Michigan.

A124. Robertson, I. A. (1966), "Forced Vertical Vibration of a Rigid Circular Disc on a Semi-infinite Elastic Solid," Proc. Camb. Phil. Soc., A. Vol. 62, p. 547.

A125. Shah, P. M. (1968), "On the Dynamic Response of Foundation Systems," Ph. D. Thesis, Rice University, Houston, Texas.

1.3 ROCKING AND HORIZONTAL VIBRATIONS

A126. Zakorko, V. N. and Rostovtsev, N. A. (1965), "Dynamic Contact Problem of Steady Vibrations of an Elastic Half-space," P.M.M., Vol. 29, p. 644.

A127. Gladwell, G. M. L. (1968), "Forced Tangential and Rotatory Vibration of a Rigid Circular Disc on a Semi-infinite Solid," Int. J. Engng. Sci., Vol. 6, p. 591.

A128. Luco, J. E. and Westmann, R. A. (1971), "Dynamic Response of Circular Footings," Engineering Report No. 7113, School of Engineering and Applied Science, University of California, Los Angeles.

A129. Luco, J. E. and Westmann, R. A. (1971), "Dynamic Response of Circular Footings," Journal of the Engr. Mechs. Div., A.S.C.E., Vol. 97, No. EM5, Oct., pp. 1381-1395.

A130. Veletsos, A. S. and Wei, Y. T. (1971), "Lateral and Rocking Vibration of Footings," Report No. 8, Dept. of Civil Engr., Rice University, Houston, Texas.

A131. Veletsos, A. S. and Wei, Y. T. (1971), "Lateral and Rocking Vibration of Footings," Jour. of the Soil Mechs. and Foundation Div., A.S.C.E., Vol. 97, pp. 1227-1248.

1.4 WELDED CONTACT

A132. Spence, D. A. (1968), "Self Similar Solutions to Adhesive Contact Problems with Incremental Loading," Proc. Roy. Soc., A, Vol. 305, p. 55 (static).

A133. Gladwell, G. M. L. (1969), "A Contact Problem for a Circular Cylindrical Punch in Adhesive Contact with an Elastic Half-space: The Case of Rocking, and Translation Parallel to the Plan," Int. J. Engng. Sci., Vol. 7, p. 295 (static).

A134. Bielak, J. (1971), "Earthquake Response of Building-Foundation Systems," Report No. EERL 71-04, Earthquake Engineering Research Laboratory, California Institute of Technology.

1.5 VIBRATIONS ON A LAYERED MEDIUM

A135. Bycroft, G. N. (1956), "Forced Vibrations of a Rigid Circular Plate on a Semi-Infinite Elastic Space or on an Elastic Stratum," Phil. Trans., Royal Soc. of London, Vol. 248, pp. 327-368.

A136. Warburton, G. B. (1957), "Forced Vibrations of a Body on an Elastic Stratum," J. Appl. Mech., A.S.M.E., Vol. 24, pp. 55-58.

A137. Collins, W. D. (1962), "The Forced Torsional Oscillations of an Elastic Half-space and an Elastic Stratum," Proc. London Math. Soc., Vol. 12, No. 46.

A138. Paul, H. S. (1967), "Vibration of a Rigid Circular Disc on an Infinite Elastic Plate," J. of the Acoustical Soc. of Amer., Vol. 42, pp. 412-416.

A139. Kashio, J. (1970), "Steady State Response of a Circular Disc Resting on a Layered Medium," Ph.D. Thesis, Rice University.

A140. Wei, Y. (1971), "Steady State Response of Certain Foundation Systems," Ph.D. Thesis, Rice University.

A141. Bielak, J. and Martinez, B. (1974), "An Asymmetric Mixed Boundary-Value Problem of the Elastic Layer: Translation of a Rigid Circular Disc Parallel to the Contact Plane," (to be published) (static).

A142. Luco, J. E. (1974), "Impedance Functions for a Rigid Foundation on a Layered Medium," Nuclear Engineering and Design.

1.6 VIBRATIONS ON A VISCOELASTIC MEDIUM

A143. Kobori, T., Minai, R., Suzuki, T., and Kusakabe, K. (1968), "Dynamic Ground Compliance of Rectangular Foundation on a Semi-infinite Viscoelastic Medium, Annual Report, Disaster Prevention Research Institute of Kyoto University, No. 11A, pp. 349-367.

A144. Kobori, T., and Suzuki, T. (1970), "Foundation Vibrations on a Viscoelastic Multilayered Medium," Proc. Third Japan Earthquake Engineering Symposium, Tokyo, pp. 493-499.

A145. Veletsos, A. S., and Verbic, B. (1973), "Vibration of Viscoelastic Foundations," Earthquake Engng. and Str. Dyn., Vol. 2, pp. 87-102.

1.7 INTERACTION BETWEEN TWO CIRCULAR FOUNDATIONS

A146. MacCalden, P. B. (1969), "Transmission of Steady-State Vibrations Between Circular Footings," Ph.D. Thesis, University of California, Los Angeles.

A147. Warburton, G. B., Richardson, J. D., and Webster, J. J. (1971), "Forced Vibrations of Two Masses on an Elastic Half-space," Jour. Appl. Mech., A.S.M.E., Vol. 38, Series E, No. 1, February.

A148. MacCalden, P. B. and Mathiesen, R. B. (1973), "Coupled Response of Two Foundations," Proc. Fifth World Conf. on Earthquake Engr., Rome, Italy, Paper No. 238.

1.8 SOLUTIONS BASED ON ASSUMED STRESS DISTRIBUTIONS AND OTHERS

A149. Sung, T. Y. (1953), "Vibrations on Semi-infinite Solids due to Periodic Surface Loading," Symposium on Dynamic Testing of Soils, A.S.T.M., special tech. publ. No. 156.

A150. Quinlan, P. M. (1953), "The Elastic Theory of Soil Dynamics," Symposium on Dynamic Testing of Soils, A.S.T.M., special tech. publ. No. 156.

A151. Arnold, R. N., Bycroft, G. N., and Warburton, G. B. (1955), "Forced Vibration of a Body on an Infinite Elastic Solid," J.A.M., A.S.M.E., Vol. 22, No. 3.

A152. Bycroft, G. N. (1956), "Forced Vibration of a Rigid Circular Plate on a Semi-infinite Elastic Half-space and on Elastic Stratum," Phil. Trans. Roy. Soc. of London, A, Vol. 248, p. 248.

A153. Awojobi, A. O. and Grootenhuis, P. (1965), "Vibration of Rigid Bodies on Semi-infinite Elastic Media," Proc. Roy. Soc., A, Vol. 287, p. 27.

A154. Richart, F. E. and Whitman, R. V. (1967), "Comparison of Footing Vibration Tests with Theory," Jour. of Soil Mech. and Found. Div., A.S.C.E., Vol. 94, No. SM1.

A155. Awojobi, A. O. (1971), "Approximate Solution of High-Frequency-Factor Vibrations of Rigid Bodies on Elastic Media," Jour. Appl. Mech., A.S.M.E., Vol. 38, Series E, No. 1, March.

II. RIGID STRIP FOUNDATIONS

2.1 ANTI-PLANE VIBRATIONS

A156. Hradilek, P. J. (1970), "Dynamic Soil-Structure Interaction," M.S. Thesis, University of California, Los Angeles.

2.2 VERTICAL, ROCKING AND HORIZONTAL VIBRATIONS

A157. Karasudhi, P., Keer, L. M. and Lee, S. L. (1968), "Vibratory Motion of a Body on an Elastic Half Plane," J.A.M., A.S.M.E., Vol. 35, E, No. 4, p. 697.

A158. Luco, J. E. (1969, "Application of Singular Integral Equations to the Problem of Forced Vibrations of a Rigid Footing," Ph.D. Thesis, University of California, Los Angeles.

A159. Oien, M. A. (1971), "Steady Motion of a Rigid Strip Bonded to an Elastic Half-Space," J. Appl. Mech., Vol. 3, Series E, June, pp. 328-334.

A160. Luco, J. E. and Westmann, R. A. (1972), "Dynamic Response of a Rigid Footing Bonded to an Elastic Half-Space," J. of Appl. Mech., A.S.C.E., Vol. 39, Series E, No. 2, June, pp. 527-534.

III. RECTANGULAR FOUNDATIONS

A161. Kobori, T. (1962), "Dynamical Response of Rectangular Foundations on an Elastic Space," Proc. Japan Natl. Symp. on Earthquake Engng.

A162. Thomson, W. T. and Kobori, T. (1963), "Dynamical Compliance of Rectangular Foundations on an Elastic Half-Space," J.A.M., A.S.M.E., Vol. 30.

A163. Elorduy, J., Nieto, J. A. and Szekely, E. M. (1967), "Dynamic Response of Bases of Arbitrary Shape Subjected to Periodic Vertical Loading," Proc. Intl. Symp. on Wave Propagation and Dyn. Properties of Earth Materials.

A164. Kobori, T., Minai, R., Suzuki, T. and Kusakabe, K. (1966), "Dynamical Ground Compliance of Rectangular Foundations," Proc. of the 16th Japan Natl. Cong. for Appl. Mech.

A165. Chae, Y. S. (1969), "Vibration of Noncircular Foundations," J. Soil Mech. and Found. Div., A.S.C.E., Vol. 95, No. SM6.

A166. Sarrazin, M. A. (1970), "Soil-Structure Interaction in Earthquake Resistant Design," Research Report R70-59, Dept. of Civil Eng., Mass. Inst. of Tech., Sept.

A167. Kobori, T., Minai, R. and Kusakabe, K. (1971), "Vibrational Characteristics of a Coupled Rigid Bodies System on an Elastic Ground," Reports of the Architectural Institute of Japan (Kiuki Sub-Division), Japan, May, pp. 13-16.

IV. EMBEDDED FOUNDATIONS

4.1 ANTIPLANE VIBRATIONS

A168. Luco, J. E. (1969), "Dynamic Interaction of a Shear Wall with the Soil," J. Engr. Mech. Div., A.S.C.E., Vol. 95, EM2, April, pp. 333-346.

A169. Trifunac, M. D. (1972), "Interaction of a Shear Wall with the Soil for Incident Plane SH Waves," Bull. Seism. Soc. Amer., Vol. 62, No. 1, February, pp. 63-83.

A170. Luco, J. E. and Contesse, L. A. (1973), "Dynamic Structure-Soil-Structure Interaction," Bull. Seism. Soc. Amer., Vol. 63, No. 4, August 1973, pp. 1289-1303.

A171. Thau, S. A. and Umek, A. (1974), "Transient Response of a Buried Foundation to Antiplane Shear Waves," J. Appl. Mech. A.S.M.E. (in press).

A172. Wong, H. L. and Trifunac, M. D. (1974), "Interaction of a Shear Wall with the Soil for Incident Plane SH Waves: Elliptical Rigid Foundation," Bull. Seism. Soc. Amer., Vol. 64, No. 6, December, pp. 1825-1842.

A173. Wong, H. L. and Trifunac, M. D., "Two Dimensional, Antiplane, Building-Soil-Building Interaction for Two or More Buildings and for Incident Plane SH-Waves," Submitted to Bull. Seism. Soc. Amer.

4.2 TWO-DIMENSIONAL FOUNDATIONS

A174. Seed, H. B. and Idriss, I. M. (1973), "Soil-Structure Interaction of Massive Embedded Structures During Earthquakes," Proc. of the Fifth World Conf. on Earthquake Engr., Rome.

A175. Krizek, R. J., Gupta, D. C., Parmelee, R. A. (1972), "Coupled Sliding and Rocking of Embedded Foundations," J. Soil Mech. and Found. Div., A.S.C.E., Vol. 98, No. SM12, December, pp. 1347-1358.

A176. Parmelee, R. A. and Weesakul, W. (1972), "Soil-Structure Interaction of Embedded Buildings," Structural Dynamics Technical Report No. SD 72-1, Dept. of Civil Engr., Northwestern University, Evanston, Ill.

4.3 THREE-DIMENSIONAL FOUNDATIONS

A177. Baranov, V. A. (1967), "On the Calculation of Excited Vibrations of an Embedded Foundation," (in Russian), Voprosy Dynamiki i Prochnocti, No. 14, Polytechnical Institute of Riga, pp. 195-209.

A178. Novak, M. (1972), "Vibrations of Embedded Footings and Structure," A. S. C. E. National Structural Engineering Meeting, April, San Francisco, California.

A179. Novak, M. and Beredugo, Y. O. (1971), "The Effect of Embedment on Footing Vibrations," Proc. of the First Canadian Conf. on Earthquake Engr. Res., University of British Columbia, Vancouver, B. C., May, pp. 111-125.

A180. Beredugo, Y. O. and Novak, M. (1972), "Coupled Horizontal and Rocking Vibration of Embedded Footings," Canadian Geotechnical J., November, pp. 477-497.

A181. Novak, M. and Beredugo, Y. O. (1972), "Vertical Vibration of Embedded Footings," J. Soil Mech. and Found. Div., A. S. C. E., December.

A182. Novak, M., Sachs, K., "Torsional and Coupled Vibrations of Embedded Footings," Int. J. of Earthquake Engr. and Struct. Dynamics, J. Wiley and Sons (to appear).

A183. Novak, M. (1973), "The Effect of Embedment on Vibration of Footings and Structures," Proc. Fifth World Conf. on Earthquake Engr., Rome.

A184. Tajimi, H. (1964), "Dynamic Analysis of a Structure Embedded in an Elastic Stratum," Proc. Fourth World Conf. on Earthquake Engr., Santiago, Chile.

A185. Masao, T., and Tajimi, H. (1973), "Earthquake Response of Multi-Story Building Considering Surface Layer-Basement Interaction," Proc. Fifth World Conf. on Earthquake Engr., Rome.

A186. Yasui, Y. and Nakagawa, K. (1973), "Sway-Rocking Vibration of Rigid-Structure Embedded in an Elastic Stratum," Proc. Fifth World Conf. on Earthquake Engr., Rome.

A187. Abe, T. and Ang, A. H. S. (1973), "Seismic Response of Structures Buried Partially in a Multi-Layered Medium," Proc. Fifth World Conf. on Earthquake Engr., Rome.

A188. Kuhlemeyer, R. L. (1969, "Vertical Vibrations of Footings Embedded in Layered Media," PL. D. Thesis, University of California, Berkeley.

A189. Lysmer, J. and Kuhlemeyer, R. L. (1971), "Finite Dynamic Model for Infinite Media," J. Engr. Mech. Div., A. S. C. E., Vol. 95, No. EM4, August, 1969, pp. 959-977. Closure to Discussions, February, pp. 129-131.

A190. Waas, G. and Lysmer, J. (1972), "Vibrations of Footings Embedded in Layered Media," Proc. of the WES Symp. on Appl. of the Finite Element Method in Geotechnical Engr., U. S. Army Engineer Waterways Experiment Station, Vicksburg, Miss., May.

A191. Parmelee, R. A. (1973), "Designing for Seismic Soil-Structure Interaction," A. S. C. E. Natl. Struct. Engr. Meeting, April, San Francisco, California.

A192. Parmelee, R. A. and Kudder, R. J. (1973), "Seismic Soil-Structure Interaction of Embedded Buildings," Proc. Fifth World Conf. on Earthquake Engr., Rome.

APPENDIX B

In a three-dimensional elastic, homogeneous and isotropic medium, the governing equation for harmonic wave motion is

$$(\lambda + \mu)\underline{\nabla}(\nabla \cdot \underline{u}) + \mu\nabla^2\underline{u} + \rho\omega^2\underline{u} = 0 \qquad \text{(B-1)}$$

where λ and μ are the lame' constants and $\underline{u} = [u_1, u_2, u_3]$ is the displacement in the $[x_1, x_2, x_3]$ direction, respectively.

Using Fourier Transforms to obtain a solution for steady harmonic waves in a semi-infinite medium, the three components of the displacement, $\underline{u}$, and their Fourier Transforms, $\tilde{\underline{u}}$, are defined as:

$$[u_1, u_2, u_3] = \frac{1}{2\pi} \int_{-\infty}^{\infty} \int_{-\infty}^{\infty} [\tilde{u}_1, \tilde{u}_2, \tilde{u}_3]\, e^{i(\xi x_1 + \eta x_2)}\, d\xi\, d\eta \qquad \text{(B-2a)}$$

$$[\tilde{u}_1, \tilde{u}_2, \tilde{u}_3] = \frac{1}{2\pi} \int_{-\infty}^{\infty} \int_{-\infty}^{\infty} [u_1, u_2, u_3]\, e^{i(\xi x_1 + \eta x_2)}\, dx_1 dx_2 \qquad \text{(B-2b)}$$

Substituting equations (B-2b) into the Fourier Transform of equation (B-1), the solutions for the half space with positive x_3 have then the form,(A162)

$$[u_1, u_2, u_3] = \frac{A}{h^2}[i\xi, i\eta, \gamma_1]\, e^{-\gamma_1 x_3} + \left[B, C, -\frac{i(\xi D + \eta C)}{\gamma_2}\right] e^{-\gamma_2 x_3} \qquad \text{(B-3)}$$

where $\gamma_1^2 = \beta_s^2 + \alpha_s^2 - \omega^2/\alpha_s^2$, $\gamma_2^2 = \beta_s^2 + \alpha_s^2 - \omega^2/\beta_s^2$, and A, B, and C are the arbitrary constants which have to be determined by the boundary conditions at the surface where $x_3 = 0$.

To match stress boundary conditions, the Fourier Transform of the stress components on the negative x_3-face can be expressed in terms $\tilde{\underline{u}}$ as:

$$\tilde{\tau}_{13}|_{x_3=0} = \mu\left(\frac{\partial\tilde{u}_3}{\partial x_1} + \frac{\partial\tilde{u}_1}{\partial x_3}\right)|_{x_3=0} = -\mu\left[\frac{i2\gamma_1\xi}{h^2}A + \frac{(\xi^2+\gamma_2^2)}{\gamma_2}B + \frac{\xi_n}{\gamma_2}C\right] \qquad \text{(B-4a)}$$

$$\tilde{\tau}_{23}|_{x_3=0} = \mu\left(\frac{\partial\tilde{u}_3}{\partial x_2} + \frac{\partial\tilde{u}_2}{\partial x_3}\right)|_{x_3=0} = -\mu\left[\frac{i2\gamma_1\eta}{h^2}A + \frac{\xi_n}{\gamma_2}B + \frac{(\eta^2+\gamma_2^2)}{\gamma_2}C\right] \qquad \text{(B-4b)}$$

$$\tilde{\tau}_{33}|_{x_3=0} = \left[\lambda\sum_{j=1}^{3}\frac{\partial u_j}{\partial x_j} + 2\mu\frac{\partial\tilde{u}_3}{\partial x_3}\right]|_{x_3=0} = -\mu\left[\frac{A}{h^2}(2\gamma_2^2+k^2) - 2(\xi B+\eta C)\right] \qquad \text{(B-4c)}$$

The matrix representation of B-4 is therefore

$$-\mu\begin{bmatrix} i\frac{2\gamma_1\xi}{h^2} & \frac{(\xi^2+\gamma_2^2)}{\gamma_2} & \frac{\xi\eta}{\gamma_2} \\ i\frac{2\gamma_1\eta}{h^2} & \frac{\xi\eta}{\gamma_2} & \frac{(\eta^2+\gamma_2^2)}{\gamma_2} \\ \frac{(2\gamma_2^2+k^2)}{h^2} & -2i\xi & -2i\eta \end{bmatrix}\begin{bmatrix} A \\ B \\ C \end{bmatrix} = \begin{bmatrix} \tilde{\tau}_{13} \\ \tilde{\tau}_{23} \\ \tilde{\tau}_{33} \end{bmatrix}|_{x_3=0} \qquad \text{(B-5)}$$

in which the vector of the right hand side of equation (B-5) contains the Fourier Transforms of the stress boundary conditions. The determination of unknowns A, B, and C will lead to the determination of $\tilde{\underline{u}}$ and, hence, $\underline{u}$, by using equations (B-4) and (B-2a), respectively.

Uniformly Distributed Vertical Load over a Rectangular Area

Consider the case of a uniformly distributed vertical load over a rectangular area. The boundary conditions representing the compressive stress in the x_3-direction are

$$\tau_{13}|_{x_3=0} = \tau_{23}|_{x_3=0} = 0 \qquad \begin{matrix} -\infty \le x_1 \le \infty \\ -\infty \le x_2 \le \infty \end{matrix}$$

$$\tau_{33}|_{x_3=0} = \begin{cases} -T_3 = -\dfrac{P_3}{4bc} & \text{for } \begin{matrix} -b \le x_1 \le b \\ -c \le x_2 \le c \end{matrix} \\ 0 & \text{otherwise} \end{cases} \tag{B-6}$$

Therefore, the right hand side of (B-5) becomes

$$\begin{bmatrix} \tilde{\tau}_{13} \\ \tilde{\tau}_{23} \\ \tilde{\tau}_{33} \end{bmatrix}_{x_3=0} = -\frac{4T_3}{2\pi} \frac{\sin \xi b \sin \eta c}{\xi \eta} \begin{bmatrix} 0 \\ 0 \\ 1 \end{bmatrix}. \tag{B-7}$$

Applying Cramer's Rule, the constants are

$$\begin{bmatrix} A \\ B \\ C \end{bmatrix}_V = \frac{4T_3}{2\pi\mu} \frac{\sin \xi b \sin \eta c}{\xi \eta F(\xi, \eta)} \begin{bmatrix} h^2[2(\xi^2 + \eta^2) - k^2] \\ -i2\gamma_1\gamma_2\xi \\ -i2\gamma_1\gamma_2\eta \end{bmatrix} \tag{B-8}$$

where $F(\xi, \eta) = [2(\xi^2 + \eta^2) - k^2]^2 - 4\gamma_1\gamma_2(\xi^2 + \eta^2)$ is the Rayleigh determinant and $h = \omega/\alpha_s$ and $k = \omega/\beta_s$ are the wave numbers.

Substituting (B-8) into (B-3),

$$\begin{bmatrix} \tilde{u}_1 \\ \tilde{u}_2 \\ \tilde{u}_3 \end{bmatrix}_v = \frac{4T_3}{2\pi\mu}\left(\frac{\sin\xi b \sin\eta c}{\xi\eta F(\xi,\eta)}\right) \begin{bmatrix} i\xi[(\gamma_1-\gamma_2)^2+h^2] \\ i\eta[(\gamma_1-\gamma_2)^2+h^2] \\ -\gamma_1 k^2 \end{bmatrix} , \tag{B-9}$$

by (B-2a) and the substitution, $T_3 = P_3/4bc$, we have

$$\begin{bmatrix} u_1(x_1,x_2,0) \\ u_2(x_1,x_2,0) \\ u_3(x_1,x_2,0) \end{bmatrix}_v = \frac{P_3}{4\mu\pi^2 bc}\int_{-\infty}^{\infty}\int_{-\infty}^{\infty} \begin{bmatrix} i\xi[(\gamma_1-\gamma_2)^2+h^2] \\ i\eta[(\gamma_1-\gamma_2)^2+h^2] \\ -\gamma_1 k^2 \end{bmatrix} \frac{\sin\xi b \sin\eta c}{\xi\eta F(\xi,\eta)} e^{-i(\xi x_1+\eta x_2)}\, d\xi\, d\eta \tag{B-10}$$

Uniformly Distributed Horizontal Load Over a Rectangular Area

The boundary conditions for the case where the uniform load is applied tangentially in the x_1-direction are

$$\tau_{13}|_{x_3=0} = \begin{cases} -T_1 = -\dfrac{P_1}{4bc}\ ; & -b \le x_1 \le b \\ & -c \le x_2 \le c \\ 0\ , & \text{otherwise} \end{cases} \tag{B-11}$$

$$\tau_{23}|_{x_3=0} = \tau_{33}|_{x_3=0} = 0\ ; \qquad -\infty \le x_1 \le \infty \quad -\infty \le x_2 \le \infty\ .$$

Hence,

$$\begin{bmatrix} \tilde{\tau}_{13} \\ \tilde{\tau}_{23} \\ \tilde{\tau}_{33} \end{bmatrix}_{x_3=0} = -\frac{4T_1}{2\pi}\,\frac{\sin\xi b \sin\eta c}{\xi\eta} \begin{bmatrix} 1 \\ 0 \\ 0 \end{bmatrix} \tag{B-12}$$

Substituting (B-12) into (B-5) yields

$$\begin{bmatrix} A \\ B \\ C \end{bmatrix}_H = -\frac{4T_1}{2\pi\mu} \frac{\sin \xi b \sin \eta c}{\xi \eta F(\xi,\eta)} \begin{bmatrix} 2i\xi\gamma_2 h^2 \\ \frac{1}{\gamma_2}\{[2(\xi^2+\eta^2)-k^2][\xi^2+2\eta^2-k^2]-4\gamma_1\gamma_2\eta^2\} \\ -\frac{\xi\eta}{\gamma_2}\{[2(\xi^2+\eta^2)-k^2]-4\gamma_1\gamma_2\} \end{bmatrix}. \tag{B-13}$$

Hence, by (B-3)

$$\begin{bmatrix} \tilde{u}_1 \\ \tilde{u}_2 \\ \tilde{u}_3 \end{bmatrix}_H = \frac{4T_1}{2\pi\mu} \frac{\sin \xi b \sin \eta c}{\xi\eta} \begin{bmatrix} \frac{1}{\gamma_2} - \frac{\xi^2\{[2(\eta^2+\xi^2)-k^2]+2\gamma_2^2-4\gamma_1\gamma_2\}}{\gamma_2 F(\xi,\eta)} \\ -\frac{\xi\eta\{[2(\xi^2+\eta^2)-k^2]+2\gamma_2^2-4\gamma_1\gamma_2\}}{\gamma_2 F(\xi,\eta)} \\ -\frac{i\xi[(\gamma_1-\gamma_2)^2+h^2]}{F(\xi,\eta)} \end{bmatrix}. \tag{B-14}$$

Applying the inverse Fourier transformation of (B-2a) and letting $T_1 = \frac{P_1}{4bc}$,

$$\begin{bmatrix} u_1(x_1,x_2,0) \\ u_2(x_1,x_2,0) \\ u_3(x_1,x_2,0) \end{bmatrix}_H = \frac{P_1}{4\mu\pi^2 bc} \int_{-\infty}^{\infty}\int_{-\infty}^{\infty} \begin{bmatrix} \frac{1}{\gamma_2} - \frac{\xi^2\{[2(\eta^2+\xi^2)-k^2]+2\gamma_2^2-4\gamma_1\gamma_2\}}{\gamma_2 F(\xi,\eta)} \\ -\frac{\xi\eta\{[2(\xi^2+\eta^2)-k^2]+2\gamma_2^2-4\gamma_1\gamma_2\}}{\gamma_2 F(\xi,\eta)} \\ -\frac{i\xi[(\gamma_1-\gamma_2)^2+h^2]}{F(\xi,\eta)} \end{bmatrix} \frac{\sin\eta c \sin\xi b}{\eta\xi} \times$$

$$\times\ e^{-i(\xi x_1+\eta x_2)}\, d\xi d\eta \tag{B-15}$$

Coordinate Transformation

Since the odd part of the integrands of (B-10) and (B-15) vanishes after integration, the remaining even part can be expressed as double integrals with limits $\xi, \eta = 0 \rightarrow \infty$. A further transformation of (ξ,η) into polar coordinates (z, θ) will result in just one infinite integral with the other one finite.

Let

$$\begin{cases} \xi = kz \cos\theta \\ \eta = kz \sin\theta \end{cases} ; \qquad \begin{matrix} z = 0 \rightarrow \infty \\ \theta = 0 \rightarrow \frac{\pi}{2} \end{matrix} \tag{B-16}$$

then

$$d\xi d\eta = k^2 z dz d\theta ,$$

and

$$F(\xi,\eta) = F(z) = (2z^2 - 1)^2 - 4(z^2 - 1)^{\frac{1}{2}}(z^2 - n^2)^{\frac{1}{2}}z^2 . \tag{B-17}$$

The next step is to substitute (B-16) and (B-17) in (B-10) and (B-15) which results in the following expressions:

Vertical Excitation

$$\left\{\begin{array}{l} u_1(x_1, x_2, 0) = \dfrac{P_3}{\mu c} \displaystyle\int_0^{\frac{\pi}{2}} \int_0^{\infty} \dfrac{[(2z^2 - 1) - 2\sqrt{z^2-n^2)(z^2-1)}\,]}{F(z) \sin\theta} \Psi \sin(zkx_1 \cos\theta) \cos(zkx_2 \sin\theta) dz d\theta \\ u_2(x_1, x_2, 0) = -\dfrac{P_3}{\mu c} \displaystyle\int_0^{\frac{\pi}{2}} \int_0^{\infty} \dfrac{[(2z^2 - 1) - 2\sqrt{(z^2-n^2)(z^2-1)}\,]}{F(z) \cos\theta} \Psi \sin(zkx_1 \cos\theta) \sin(zkx_2 \sin\theta) dz d\theta \\ u_3(x_1, x_2, 0) = -\dfrac{P_3}{\mu c} \displaystyle\int_0^{\frac{\pi}{2}} \int_0^{\infty} \dfrac{\sqrt{z^2-n^2}}{zF(z) \cos\theta \sin\theta} \Psi \cos(zkx_1 \cos\theta) \cos(zkx_2 \sin\theta) dz d\theta \end{array}\right\} \quad (B\text{-}18)$$

Horizontal Excitation

$$\left\{\begin{array}{l} u_1 = \dfrac{P_1}{\mu c} \displaystyle\int_0^{\frac{\pi}{2}} \int_0^{\infty} \left[\dfrac{\sin^2\theta}{z\sqrt{z^2-1}} - \dfrac{\sqrt{z^2-1}\cos^2\theta}{zF(z)}\right] \dfrac{\Psi}{\sin\theta \cos\theta} \cos(zkx_1 \cos\theta) \cos(zkx_2 \sin\theta) dz d\theta \\ u_2 = \dfrac{P_1}{\mu c} \displaystyle\int_0^{\frac{\pi}{2}} \int_0^{\infty} \left[\dfrac{1}{z\sqrt{z^2-1}} + \dfrac{\sqrt{z^2-1}}{zF(z)}\right] \Psi \sin(zkx_1 \cos\theta) \sin(zkx_2 \sin\theta) dz d\theta \\ u_3 = -\dfrac{P_1}{\mu c} \displaystyle\int_0^{\frac{\pi}{2}} \int_0^{\infty} \dfrac{[(2z^2-1) - 2\sqrt{(z^2-n^2)(z^2-1)}\,]}{F(z) \sin\theta} \Psi \sin(zkx_1 \cos\theta) \cos(zkx_2 \sin\theta) dz d\theta \end{array}\right\} \quad (B\text{-}19)$$

where $\Psi = \dfrac{1}{\pi^2 kb} \sin(zkb \cos\theta) \sin(zkc \sin\theta)$.